HEINRICH HEINE
UNIVERSITÄT DÜSSELDORF

Regulation of energy-dependent quenching (qE) of excess light by the thylakoid transmembrane electric field ($\Delta\psi$) as a dynamic component of the chloroplast proton motive force (*pmf*)

Inaugural Dissertation

for attaining the title of Doctor (PhD)
in the Faculty of Mathematics and Natural Sciences
at Heinrich Heine University Düsseldorf

Presented by

Lazar Pavlovic

From Užice, Serbia

Düsseldorf, 2015

iGRAD*plant*
International
Graduate
Program
for Plant Science

From the Institute of Plant Biochemistry,
Heinrich Heine University Düsseldorf

Printed with permission from the Faculty of Mathematics and Natural Sciences,
Heinrich Heine University Düsseldorf

Supervisor: Prof. Dr. Peter Jahns
Co-Supervisor: Prof. Dr. Laura E. Rose

Date of Oral Examination:

Посебно посвећено мојој најдражој и најмилијој породици, заувек.

Table of Contents

1.1 Introduction

1.1.1 Primary light-driven photochemical reactions

Photosynthesis, the process by which photoautotrophic organisms like algae, cyanobacteria, and plants convert radiant energy into biologically active sugars and oxygen as a by-product is one of the most important phenomena to have emerged in the evolution of life on earth (Dau and Zaharieva, 2009). The overall process can be broadly subdivided into the light-harvesting and subsequent carbon-assimilatory reactions, or formerly the dark reactions. Protein and lipid complexes and co-factors that make up the thylakoid membrane system of chloroplasts are arranged in such a way that key biochemical reactions have been fine-tuned by evolution to perform efficiently under natural conditions. Efficient photosynthesis in plants and other photoautotrophs involves optimal use of absorbed photonic energy under limiting light conditions. More specifically, there is a rapid femto to picosecond transfer of energy among photon excited pigment molecules, largely chlorophyll (Chl) *a* and *b*, in the light-harvesting antenna complexes of photosystems I (PSI) and II (PSII), namely LHCI and LHCII, respectively, toward their respective reaction centres (RC's) (Witt, 1979; Baker *et al*., 2007; Dau and Zaharieva, 2009). The oxidation of PSI and PSII RC's drives linear electron flow from water oxidized on the lumenal side of PSII and coupled proton (H^+) influx via the Q cycle in the adjacent cytochrome b_6f complex to $NADP^+$ at PSI via the mobile electron carriers plastocyanin (PC) and ferredoxin (Fd) as part of the light reactions (Figure 1.1). This generates an electrochemical potential consisting of a proton gradient (ΔpH) as well as an electric field ($\Delta\psi$) across the thylakoid membrane in accordance with Mitchell's chemiosmotic hypothesis (Mitchell, 1961). Together they constitute the so-called proton motive force (*pmf*), which drives endergonic ATP synthesis via the reversible endergonic-exergonic reactions of the chloroplast (C)F_0-(C)F_1 ATP synthase. Energy and reducing power stored in resulting ATP and NADPH molecules, respectively, are subsequently used in the Calvin-Benson cycle as needed for fixing and reducing atmospheric carbon dioxide (CO_2).

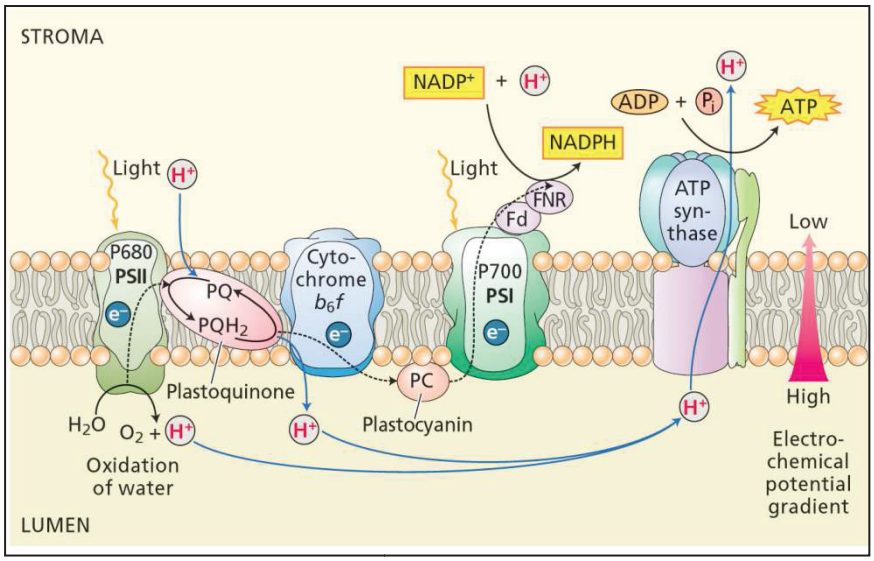

Figure 1.1 – Schematic model of photosynthetic electron and proton transport (from Taiz and Zeiger, 2002). Excitation of photosystem I (PSI) and II (PSII) leads to oxidation of their reaction cores, which is responsible for establishing charge separation within the two photosystems as electrons are rapidly shuttled via critical complexes in the thylakoid membrane from water oxidized at PSII to NADPH at PSI. Protons are released into the lumen following water oxidation at PSII and PQH_2 oxidation at cytochrome b_6f, generating an electrochemical potential difference or proton motive force (*pmf*) across the membrane that is required for ATP synthesis. As a consequence, proton translocation is coupled to or driven by electron transfer reactions at four critical points as part of the 'Mitchellian' chemiosmotic energy storage system (Baker *et al*., 2007).

Application of 3-(3,4-dichlorophenyl)-1,1-dimethylurea (DCMU), which selectively blocks electron flow from water oxidized at PSII to the plastoquinone (PQ) binding site at cytochrome b_6f, has enabled more detailed studies of photosynthetic electron transport, particularly cyclic electron transport, as DCMU has no effect on PSI or other photosynthetic reactions (Huber and Edwards, 1976; Metz *et al*., 1986; Hosler and Yocum, 1987). Such studies have greatly improved collective understanding of overall electron, but also proton transfer reactions of photosynthesis and the key complexes and co-factors involved. However, the regulation of these two circuits of photosynthesis is not fully clear and will be discussed in more detail in 4.2 and 4.3.

1.1.2 Sensing and acclimation to excess light

All photoautotrophic organisms periodically absorb light at levels that exceed capacity for efficient utilization during light-harvesting reactions of photosynthesis, leading to photo-oxidative stress. Such excess light (EL) conditions vary with the native environmental conditions over a wide range of light intensities. Intra-cellular free radicals, reactive oxygen species (ROS), such as the highly reactive superoxide radical ($^1O_2^*$), and other reactive intermediates and by-products accumulate and compromise the structure and function of proteins, lipids, and DNA within cells (Apel and Hirt, 2004; Baier and Dietz, 2005; Li *et al*., 2009). With prolonged exposure, photo-oxidative damage manifests itself phenotypically in the form of microscopic programmed cell death and macroscopic chlorosis and dead tissue zones or lesions. Consequently, photosynthetic organisms have evolved various forms of protective mechanisms that minimize or prevent the effects of photo-oxidation. Higher vascular plants in particular have evolved an intricate and dynamic suite of photoprotective mechanisms for directly and indirectly sensing EL (Li *et al*., 2009). Various plant and algal species can directly sense high incoming photon fluxes via several classes of photoreceptors, which include phototropins, neochromes, and rhodopsins. Phototropins and neochromes are involved in chloroplast movement in cells (Wada *et al*., 2003; Suetsugu *et al*., 2005), one of various strategies of EL avoidance and prevention of oxidative stress. In contrast, rhodopsins play a critical role in phototaxis and photophobic movement, as deduced from studies of the green alga *Chlamydomonas reinhardtii* (Govorunova *et al*., 2004). As part of a complex and not fully understood signal transduction cascade, plants can indirectly sense EL through resulting biochemical and metabolic changes involving signals that mediate photoprotective and photoacclimatory responses. For example, upon saturation of the electron transport chain following the absorption of EL, the PQ and thiol pools are significantly reduced as various ROS are produced (Oelze *et al*., 2008). These ROS are scavenged and detoxified as part of the plant antioxidant defense system. ROS themselves, in particular hydrogen peroxide, also serve various signaling functions (Asada, 2006). Additionally, there is an accumulation of protons in the thylakoid lumen as proton production exceeds consumption or conductance by the ATP synthase, the activity of which becomes down regulated (Kanazawa and Kramer, 2002; Takizawa *et al*., 2008). A decrease in the thylakoid lumen pH triggers various regulatory processes that include dissipation of excess absorbed light energy as heat. This dissipation process, called non-photochemical quenching (NPQ), protects the photosynthetic apparatus from photo-oxidation during short-term fluctuations in light levels and to a certain

extent during long-term exposure. Thus, photoautotrophic organisms in general minimize photo-oxidative damage by: (1) reducing light absorption; (2) scavenging and detoxifying reactive intermediates and by-products; and (3) dissipating excess light energy as heat.

1.1.3 Non-photochemical quenching (NPQ)

Quenching of excess excitation energy differs mechanistically to some degree across the plant kingdom, which becomes evident when one traces the evolution of photosynthetic organisms across aquatic and terrestrial environments. Despite these differences, the critical pigment and protein complexes, co-factors, and other components involved in the overall quenching process have been greatly conserved. For example, the carotenoid pigments *β*-carotene and lutein deactivate excited triplet chlorophyll ($^3Chl^*$) and $^1O_2{}^*$ molecules and dissipate heat in the RC's and antenna proteins, respectively, by forming triplet carotenoid complexes (Pogson *et al*., 1996; Niyogi *et al*., 1997; Jahns and Holzwarth, 2012). In so doing, they prevent or minimize the formation of activated molecular oxygen.

Pioneering studies utilizing Chl *a* fluorescence in cyanobacteria and green algae (Papageorgiou and Govindjee, 1968a, b), intact thylakoids and chloroplasts (Murata and Sugahara, 1969; Wraight and Crofts, 1970; Krause *et al*., 1982), and leaves of common spinach (Krause, 1973) have shown that a small fraction of light energy absorbed by the LHC's is re-emitted back into space as Chl *a* fluorescence. The majority of this fluorescence originates from the PSII antennae at normal physiological (room) temperatures (Krause and Jahns, 2003). It is well known that the primary photochemical reactions compete directly for photon energy with both the radiationless deactivation of excited singlet $^1Chl^*$ molecules and the emission of fluorescence (Krause and Jahns, 2003, 2004). As such, photosynthetic processes approximately influence directly or indirectly fluorescence emission. Consequently, the extent and kinetics of Chl fluorescence provide valuable information concerning the state and activity of both photochemical and non-photochemical reactions. The development of refined techniques to record and analyze Chl fluorescence has led to profound interpretations of fluorescence phenomena studied both *in vitro* (in isolated thylakoids, chloroplasts, and PSII particles) and *in vivo* (in intact leaves of vascular plants as well as photosynthetic micro-organisms). As a result, fluorescence has become a powerful, widely used non-invasive tool in plant science. The development of 'pulse-amplitude-modulation' (PAM) fluorometry allowed for the application of repetitive saturating light pulses during the dark relaxation phase of fluorescence quenching and thus greater resolution

of additional components that constitute NPQ (Schreiber *et al*., 1986; Krause and Jahns, 2003). PAM fluorometers differ technically from non-modulated fluorometers, which have been optimized for analyses of fast fluorescence induction transients in dark-adapted leaves (Strasser *et al*., 1995). The severe shortcomings of non-modulated fluorometry have been addressed by PAM fluorometry (Krause and Jahns, 2003). Such limitations include extrinsic light interference with fluorescence recording and poor resolution of quenching processes *in vivo*. In parallel with the development of PAM systems, ultra sensitive 'pump and probe' and 'fast-repetition-rate' fluorometers were developed to measure Chl *a* fluorescence (Kolber *et al*., 1998), among other signals. They were later adopted in studies beyond initial assessments of fluorescence phenomena in aquatic ecosystems (i.e., Falkowski and Kolber, 1995).

Based on these early technical studies, it is now well known that the deactivation or quenching of excited Chl *a* molecules in the LHC can result from a non-photochemical process that predicates the buildup of a rapidly inducible and reversible 'high-energy state' (Krause and Jahns, 2003, 2004). In terrestrial plants, this major short-term (several minutes) energy-dependent (qE) component of NPQ observed under saturating light conditions is strongly dependent upon the establishment of: (1) an initial high transthylakoid ΔpH or low lumen pH (< 6.2); (2) PSII-associated PsbS protein-mediated conformational changes of the Chl *a*/*b*-binding (CAB) LHCII antenna complexes; and (3) the conversion of the carotenoid violaxanthin (V_X) to zeaxanthin (Z_X) via antheraxanthin (A_X) as part of the xanthophyll cycle and subsequent binding of Z_X to specific sites in the antennae (Figure 1.2). Current understanding supports the notion that carboxylic residues of pigment-binding PSII antenna protein complexes, particularly the *psbS*-encoded PSII subunit PsbS or CP22, are protonated on the lumenal side. In this way, the PsbS protein acts as a sensor of the lumen pH. In combination with the binding of Z_X and A_X to both inner minor (CP24/26/29) and peripheral major (LHCIIb) LHCII complexes, these processes are believed to induce allosteric changes in the organization of LHCII complexes, which taken together are required for and contribute synergistically to the generation of maximal qE.

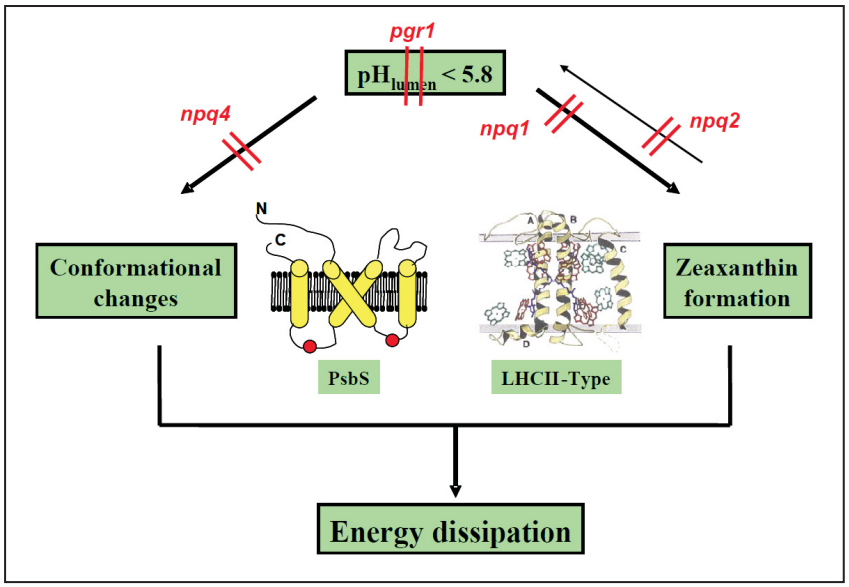

Figure 1.2 – Schematic model of the rapidly inducible and reversible pH-regulated energy-dependent (qE) dissipation of excess light energy. A reduction in the lumen pH (below ~ 6) leads to a high transthylakoid ΔpH that induces PsbS-mediated conformational changes in the antenna complexes of PSII (LHCII) as well as formation of zeaxanthin via the xanthophyll cycle and its subsequent binding to specific sites in the LHCII complex. These processes synergistically contribute to qE-type energy dissipation according to a photo-physical mechanism that is not fully understood.

In addition to qE, three other components of NPQ were identified: qT, qZ, and qI. State-transition quenching, qT, is a comparatively minor component of NPQ that is physiologically relevant for optimizing photosynthesis under low, limiting light conditions, particularly in environments of fluctuating light flux and quality (Bennett *et al*., 1980; Allen *et al*., 1981). It involves the redistribution of excitation energy between PSI and PSII. Imbalances in the distribution of excitation energy lead to state transitions, whereby phosphorylation of the major LHCII complexes causes detachment of phosphorylated LHCII, its movement from the grana to the stromal lamellae, and finally attachment to PSI. This is manifested by a decrease in the PSII absorption cross-section and quenching of Chl fluorescence. Although it is debated whether excitation energy absorbed by phosphorylated LHCII complexes is transferred to PSI, it is known that the redox state of PQ and/or the cytochrome b_6f complex regulate LHCII phosphorylation. The Z_X-dependent quenching component, qZ, has been identified recently based on the kinetic correlation of NPQ induction and Z_X formation as well as of NPQ relaxation and Z_X epoxidation (Nilkens *et al*., 2010). qZ is generated under saturating light conditions along with Z_X formation in 15 to 30 min and relaxes in the dark (or under low light) concomitant with Z_X epoxidation in 30 to 60 min. Once formed in high light, qZ is maintained in the dark in the absence of a low lumen pH and by that allows a rapid reactivation of qE during periods of fluctuating low and high light conditions. Based on its kinetic properties, this component has originally been ascribed to either qT or qI processes.

While detailed quenching analysis of the *Arabidopsis* mutant *stn7*, which is deficient in state transitions, showed that qT does not contribute to NPQ under saturating light conditions in terrestrial plants, likely via control by qE due to a high ΔpH (Oxborough *et al*., 1987; Walters and Horton, 1991), the rapidly relaxing portion of qI is likely to be identical with qZ (Nilkens *et al*., 2010). Photoinhibitory quenching, qI, which is the major component of NPQ in the long-term ($t_{1/2}$ > 30 min) following the relaxation of qE and qZ after the light-dark transition, is related to photoinhibition of PSII (Walters and Horton, 1993). It manifests itself as increased thermal dissipation at PSII (Demmig and Björkman, 1987), as in qE and qZ. The extent of qI depends on the photosynthetically active radiation (PAR) applied, the length of exposure, genotype, and acclimation state of the plant. Nevertheless, a consistent decrease in the potential efficiency of PSII, expressed as F_V/F_M, with time is always observed. Several distinct phases have been observed in low light with respect to the relaxation kinetics of qI that suggest that at least three different mechanisms or components contribute to qI formation, some of which are still debated (Leitsch *et al*., 1994). For instance, the accumulation of inactive D1 proteins in the PSII reaction core, which are consecutively 'marked' for degradation so that proteolysis occurs at the same rate as the synthesis of newly replaced D1, represents the slow phase (several hours) component of qI (Aro *et al*., 1992; Leitsch *et al*., 1994; Thiele *et al*., 1996). It is probably the last line of defense against EL stress. In contrast, permanently high levels of Z_X and A_X (Jahns *et al*., 2000), due partially to a high ΔpH maintained in the dark or low light by ATP hydrolysis (Gilmore, 1997) in high-light acclimated plants with a large persistent pool of high-turnover xanthophyll pigments (Krause *et al*., 1995; Streb *et al*., 1997), may offer significant qE-type photoprotection. This represents the fast phase of qI (Thiele *et al*., 1996; Gilmore, 1997; Jahns *et al*., 2000). Prolonged exposure to EL may maintain such quenching even after the ΔpH has relaxed, assuming that the Z_X and A_X remain bound to sites in the LHCII complex other than those required for qE and dissociate slowly enough to allow for epoxidation and qI reversion. This type of quenching is likely to be identical with the above qZ component. Whether D1 turnover is related to xanthophyll cycle activity in qI *in vivo* is unclear.

NPQ and its constituent regulatory factors and components have been extensively studied to date. However, many questions still remain open. For instance, where is/are the quenching center(s) in qE and by what photophysical mechanism is the excess energy quenched? Is more than one quenching mechanism active in the context of qE and qI? Despite long-standing debate, there is considerable evidence that the site of qE quenching in higher plants

occurs in the CAB antennae proteins, which contain the xanthophyll pigments. Binding studies of *N,N´*-dicyclohexylcarbodiimide (DCCD), which supposedly binds carboxylic residues on nearly all PSI and PSII CAB proteins (Jahns and Junge, 1990) and thus acts as a suppressor of sites of lumen pH sensing and regulation (Walters *et al*., 1996), support a role of minor antenna proteins given reductions in qE (Ruban *et al*., 1992). Studies using plants lacking either Lhcb1/2 (Andersson *et al*., 2003), Lhcb4/5 (Andersson *et al*., 2001) or Lhcb6 (Kovacs *et al*., 2006) showed that only a lack of Lhcb6 leads to a strong reduction of qE, while in all other cases the organization of the PSII antenna is mainly affected. Thus, among all PSII antenna proteins, Lhcb6 seems to be the most critical subunit for qE quenching, particularly in Z_X-dependent quenching processes (Passarini *et al*., 2009). Studies of *Arabidopsis* mutants lacking the *psbS* gene, but otherwise possessing a normal pigment and protein composition and functioning xanthophyll cycle, have underscored the importance of the PsbS protein in qE formation given a drastic reduction in qE capacity in *npq4* (Li *et al*., 2000) or *psbs-1.3* (Graßes *et al*., 2002). Such studies have concluded that the PsbS plays an intrinsic role in qE formation by altering the conformation of LHCII protein-pigment complexes. However, it is uncertain whether protonation of PsbS induces quenching or if the PsbS protein contains a quenching site and thus acts directly as a quencher. In contrast, studies of *Chlamydomonas* have shown that qE formation requires preceding acclimation to high light and is positively dependent on the expression of the LHCSR3 (NPQ4) or LI818 protein (Elrad *et al*., 2002), which functionally resembles the PsbS protein and is present in many photosynthetic eukaryotes except red algae and vascular plants (Koziol *et al*., 2007). However, in *Chlamydomonas*, qE formation is independent of the PsbS, which is encoded by two genes. However, *PSBS* transcripts, but not the PsbS protein have been observed only upon nitrogen starvation (Miller *et al*., 2010) and after transfer from low to higher light intensities (Mettler *et al*., 2014), leaving the role of PsbS in *C. reinhardtii* unclear.

Phenotypic analyses of *C. reinhardtii* and *A. thaliana* mutants defective in xanthophyll cycle activity have highlighted the central role of Z_X in qE (Niyogi *et al*., 1997, 1998). A relatively large pool of Z_X occupying all of the specific binding sites in the antennae is required for maximal qE formation (Krause and Jahns, 2004). *Arabidopsis* mutants lacking V_X de-epoxidase (V_XDE), so-called *npq1* mutants, and thus deficient in Z_X synthesis show greatly reduced NPQ (Niyogi *et al*., 1998). However, mutants of the back-reaction catalyzed by Z_X epoxidase (Z_XE), namely *npq2* (also called *aba1*), show normal or slightly reduced NPQ, generated at a noticeably greater rate, despite containing permanently high Z_X levels. Thus,

the presence of Z_X alone in the absence of EL is not necessary for qE induction (Noctor *et al*., 1991). Indeed, V_XDE activity inhibited by the reductant dithiothreitol (DTT) has led to the identification of a Z_X-independent component of NPQ (Demmig-Adams *et al*., 1990). Further studies of the *npq1* mutant have suggested the possibility of an additional Z_X-independent component of qE that accounts for the residual qE observed previously under a low lumen pH (Demmig-Adams *et al*., 1990; Thiele and Krause, 1994). Although it is unclear whether this Z_X-independent component has a significant role in the presence of an active xanthophyll cycle under *in vivo* conditions, substantial Z_X-independent quenching may occur when the lumen pH and Z_X as well as A_X levels are low at the onset of strong illumination *in vivo* (Horton and Ruban, 1992). However, it appears that the Z_X-dependent quenching, which originates from different quenching sites compared to Z_X-independent quenching (Holzwarth *et al*., 2009), predominates under steady-state photosynthesis. Alternatively, A_X can act as a substitute for Z_X in the quenching process, which has been shown in the prasinophycean alga *Mantionella squamata* (Gilmore and Yamamoto, 2001). Little Z_X is synthesized, even under strong light conditions, as Ax is mainly accumulated in this alga (Goss *et al*., 1998). This has been attributed to the altered pH-dependence of V_XDE in *Mantionella* in comparison to higher plants (Frommolt *et al*., 2001). Therefore, different xanthophylls may be involved in qE-type quenching, and in vascular plants, Z_X, A_X, and probably lutein are needed for maximal NPQ formation.

Current understanding of qE-related energy dissipation therefore proposes two alternative hypotheses concerning the possible mechanisms of qE-type quenching. One hypothesis suggests that the ΔpH- and Z_X-induced conformation changes of the LHCII antennae lead to the interaction between Chl molecules and thus deactivation of excited singlet chlorophyll ($^1Chl^*$) molecules via so-called 'concentration quenching' (Horton *et al*., 1999). More specifically, the interaction between Chl-binding domains within the same rather than different LHCII subunits leads to quenching in isolated LHCII complexes (Horton *et al*., 2000). The aggregation of LHCII complexes upon Z_X binding is now considered a secondary effect in the context of qE formation. In contrast, alternative hypotheses postulate a direct function of Z_X in qE-type quenching. Originally, it has been proposed that a singlet-singlet energy transfer from $^1Chl^*$ to Z_X is possible due to the collective binding of Z_X and subsequent structural changes in LHCII (Frank *et al*., 1994; Owens, 1994). However, given that the difference between the excited singlet energy states of Chl and Z_X is relatively small, the probability of energy transfer is low. More recently, ultrafast transient absorption

spectroscopy applied to isolated thylakoids and/or isolated/recombinant antenna proteins provided evidence that the formation of a $Chl^{+}Z_X^{-}$ radical pair might be the molecular basis of qE (Holt *et al*., 2005; Ahn *et al*., 2008). At present, both quenching mechanisms, not necessarily mutually exclusive, related either to a direct or indirect function of Z_X, are possible based on all existing data. In fact, recent time-resolved fluorescence measurements applied to intact leaves provided evidence that two different quenching sites are active under *in vivo* conditions (Holzwarth *et al*., 2009). Indeed qE may arise heterogeneously, such that radical Z_X formation in part may directly contribute to qE-type quenching. Additional work on purified LHCII and *in vivo* in *Arabidopsis* supports the transfer of excess energy from Chl *a* to an excited carotenoid at an energetically lower state as the primary mechanism of qE-related quenching (Ruban *et al*., 2007). Femtosecond transient absorption spectroscopy showed that ΔpH-induced LHCII conformational changes facilitate energy transfer to one of two LHCII-bound lutein molecules (lutein 1), which acts a direct quencher of excitation energy. Thus, concentration-type quenching involving the population of excited carotenoid states to include that of excited Z_X, A_X, and lutein offer a molecular basis for qE *in vivo*.

In addition to the ΔpH, the xanthophyll cycle, and the antenna proteins, a possible role of $\Delta\psi$ in qE regulation has been proposed, but remains somewhat unclear to date. The ΔpH serves various crucial functions in both the light reactions of photosynthesis and qE regulation (Kramer *et al*., 1999). It establishes the *pmf* required for ATP synthesis under non-saturating light conditions as well as the qE-promoting protonation of carboxylic residues of a defined pK_a value under EL conditions. In addition, the ΔpH regulates electron transport through PSII and the cytochrome b_6f complex. Consequently, it serves as a central regulatory feedback mechanism of photosynthesis, and the $\Delta\psi$ may serve as a crucial activating factor for ΔpH-dependent qE as simply being an extension of this regulatory mechanism that can be fine-tuned in response to rapid physiological changes.

1.1.4 The Electrochromic Shift (ECS)

A better understanding of the proton circuitry of photosynthesis would reveal how qE is regulated, particularly by changes in parsing of chloroplast *pmf* into the $\Delta\psi$ and ΔpH *in vivo*. Probing the *pmf in vivo* is important because existing knowledge concerning the topology, kinetics, and thermodynamics of the electron and proton circuitry has been based on so-called 'pulse-poise' approaches that monitor transient processes returning to equilibrium from high energy states induced by brief pulses of light (Sacksteder and Kramer, 2000). Such approaches include pump and probe spectroscopy and have been used to monitor absorbance changes at 515 nm, which strictly result from a transient electrochromic shift (ECS) of Chl and carotenoid pigment absorption spectra induced by an electric field (Witt, 1971; de Grooth *et al*., 1980). Indeed, chromatophores of *Rhodopseudomonas sphaeroides* and spinach chloroplasts as well as other photosynthetic organisms are known to show electrochromic absorbance changes that are linearly dependent on the light-induced membrane potential. This involves an interaction between $\Delta\psi$ and the polarizability of pigment molecules that induces a small red shift of the Chl and carotenoid absorption bands in the Soret region, proportional to the square of the strength or magnitude of the light-induced $\Delta\psi$. These absorbance changes at 515 nm may also reflect charge and field formation in the antenna pigments away from the PSII core (Delrieu and Rosengard, 1993). Based on these findings, it was proposed that these pigments sustain a permanent dipole moment imposed by the local environment due to permanent $\Delta\psi$ formation, which must be preferentially oriented towards the outside of the thylakoid membrane in the direction of the light-induced $\Delta\psi$ to account for the red shift (de Grooth *et al*., 1980). The permanent $\Delta\psi$ must also be larger than the light-induced $\Delta\psi$ to account for the linear dependence of absorbance changes on $\Delta\psi$.

Flash-induced absorbance changes at 515 nm typically follow biphasic kinetics in intact dark-adapted leaves or chloroplasts (Figure 1.3), similar to that observed in algae (Horváth *et al*., 1979). The initial rapid absorbance increase following a brief saturating turnover-flash has been related to cytochrome b_6f and PC-mediated delocalized $\Delta\psi$ formation in intact chloroplasts (Horváth *et al*., 1979; Peters *et al*., 1984). The subsequent slow 20 ms long rise and eventual decay in dark-adapted greening chloroplasts suspended in low salt media has been related to proton-translocating Q cycle activity at cytochrome b_6f (Bulychev and Vredenberg, 1976; Peters *et al*., 1984). This slow absorbance increase and eventual decay following a saturating flash can be abolished by valinomycin supplemented by high salt

concentrations or prolonged illumination, which induce $\Delta\psi$-dissipating counterion fluxes (Bulychev and Vredenberg, 1976; Horváth *et al*., 1979). In contrast, the rate and magnitude of this increase of the slow phase can be enhanced by nigericin, a higher pH (Horváth *et al*., 1979) or higher temperatures (Shimizu and Nishimura, 1977; Horváth *et al*., 1979) of the external medium. This is attributed to increased transthylakoid proton flux mediated by nigericin as well as increased pH and temperature of the medium.

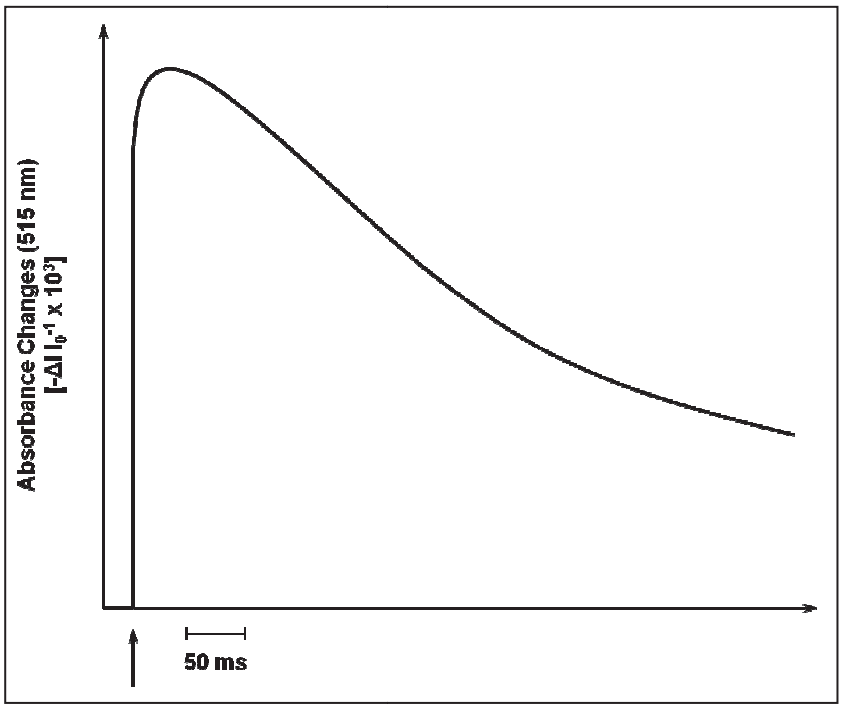

Figure 1.3 – Kinetics of absorbance changes at 515 nm following a single saturating (xenon) flash of light (vertical inset arrow). Axes are scaled approximately for illustration purposes only.

While extremely powerful and accurate in terms of characterizing single partial reactions, the pulse-poise approach is limited to artificially induced reaction states not typically observed at steady state under normal physiological conditions *in vivo*. Steady-state conditions greatly simplify kinetic modeling of natural physiological processes, the majority of which likely occur under such conditions, by virtue of a lack of changing intermediate concentrations or states during the course of measurement (Sacksteder and Kramer, 2000). However, characterization of steady-state processes is often limited to measurements of overall flux, such as of O_2 and CO_2, because of the difficulties of measuring such changes over long periods of time needed to reach steady state.

As the *pmf per se* lacks concrete detectable signals, existing means of probing the proton circuitry *in vivo* are limited to indirect measurements of *pmf* effects on other processes (Avenson *et al*., 2005). Thus, an alternative, more direct and by far the least invasive method

of probing the proton circuit, compared for instance to using coupled electron flux as a proxy of changes in the *pmf*, involves monitoring the effects of proton flux on the $\Delta\psi$. This is readily measured via the ECS, which is assessed specifically using the dark-interval relaxation kinetics (DIRK) approach, as described previously and reviewed elsewhere (i.e., Sacksteder and Kramer, 2000; Avenson *et al*., 2005). This approach relies on perturbing the steady-state balance of proton flux across the thylakoid membrane during photochemical and competing non-photochemical reactions in the light by rapidly shutting off the actinic light (Avenson *et al*., 2005; Takizawa *et al*., 2007). Analysis of ECS kinetics during dark relaxation (Figure 1.4) provides crucial information about steady-state *pmf*-related processes.

Briefly, net proton flux into the lumen ceases ~ 100 ms after the light to dark transition, which is characterized by net proton efflux into the stroma via the ATP synthase as the *pmf* equilibrates along the free energy gradient of ATP formation (ΔG_{ATP}) (Avenson *et al*., 2005). This is reflected by rapid relaxation of the steady-state ECS signal below the dark baseline on the order of tens of milliseconds, which follows a pseudo-first-order exponential decay (Figure 1.4a) in accordance with Ohm's law (Avenson *et al*., 2004; Avenson *et al*., 2005). The ΔG_{ATP}, estimated at 45 kJ mol^{-1}, dictates dark *pmf* formation, which will therefore offset any estimates of the light-induced *pmf*. Estimation of the net light-induced *pmf*, ($\Delta pmf_{light\text{-}dark}$) is proportional to the amplitude of this exponential decay of the ECS signal (ECS_t) during the light-dark transition (Figure 1.4a), which will therefore change in proportion to any differences in the magnitude of the *pmf* present in the light- and dark-adapted states. A linear relationship between ECS_t and the light-induced *pmf* is thus obtained (Avenson *et al*., 2005). This assumes that the light-induced *pmf* is generated exclusively by linear electron flow, although contribution from cyclic electron flow under certain conditions can be substantial. It also assumes a constant proton/electron ratio and proportional turnover of Fd- or possibly NADPH dehydrogenase-dependent cyclic electron flow. Rapid decay of the ECS signal below the dark baseline occurs as a result of an 'inverted' $\Delta\psi$ transiently generated by the largely ATP synthase-driven efflux of protons from the lumen into the stroma (Avenson *et al*., 2004; Avenson *et al*., 2005; Johnson and Ruban, 2014).

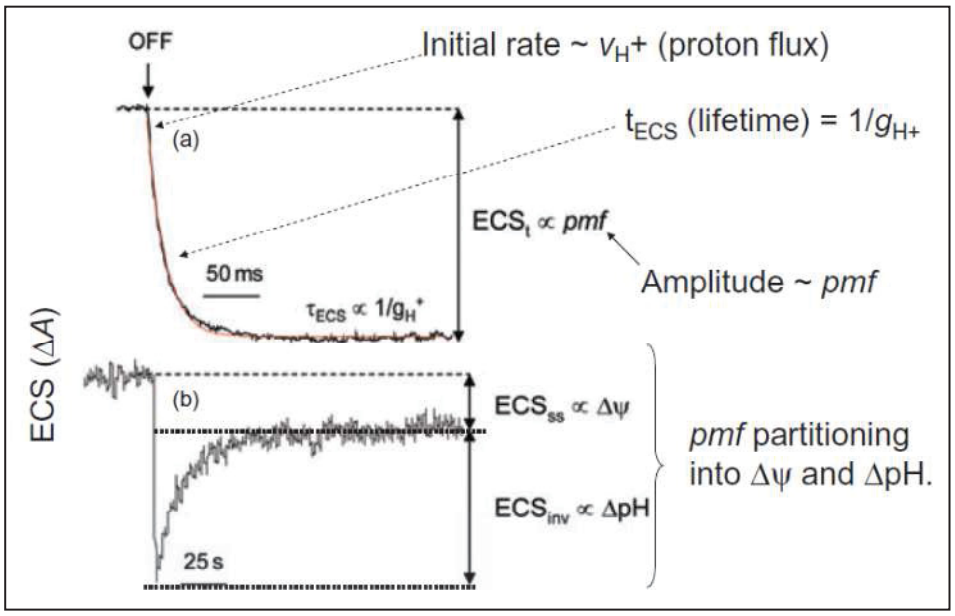

Figure 1.4 – Dark-interval relaxation kinetics (DIRK) of the electrochromic shift (ECS) at 515 nm following a period of continuous illumination (denoted by 'OFF') (from Baker *et al*., 2007). Perturbation of steady-state conditions during the light-dark transition leads to multiphase decay of the ECS signal, which can be analyzed using the DIRK approach to yield critical information about the proton circuit of photosynthesis. The initial rate of decay of the ECS signal to a quasi-stable state on the order of tens to hundreds of milliseconds during the dark interval (a), termed v_H^+, is roughly proportional to largely ATP synthase-driven proton efflux. This generates a transient negative undershoot of the ECS signal below the baseline in the dark-adapted state and thus an 'inverted' $\Delta\psi$ in relation to the $\Delta\psi$ generated in the light. The maximum amplitude of this decay from the steady state in the light to the quasi-stable state in the dark is proportional to the total chloroplast *pmf* established in the light, while the inverse of the time constant or lifetime for ECS decay, denoted τ_{ECS}, reflects proton conductivity through the ATP synthase, termed g_H^+. The subsequent increase in the ECS signal back to the dark baseline on the order of seconds (b) is mediated by $\Delta\psi$-collapsing counterion movement across the thylakoid membrane. Relaxation of the ΔpH, estimated from the inverse portion of the ECS signal (ECS_{inv}), as well as the $\Delta\psi$, estimated from the difference in the inverse and steady-state ECS (ECS_{ss}) signals, established in the light and their relative partitioning of the *pmf* can thus be visualized.

The transient undershoot of the ECS signal below the dark baseline (Figure 1.4b) is similar to that documented in early direct measurements of membrane potential in intact *Peperomia* chloroplasts after prolonged periods of illumination (Vredenberg and Tonk, 1975; Bulychev *et al*., 1980). The $\Delta\psi$ is positive in the direction of net proton movement (stromal side in the light) and is inverted (lumenal side in the dark) in relation to the $\Delta\psi$ rapidly generated at the onset of illumination reflected by the rapid millisecond rise in the ECS signal during the dark-light transition (Cruz *et al*., 2001; Avenson *et al*., 2005). The extent of the inverted $\Delta\psi$, which essentially represents the total light-induced *pmf* initially during the light-dark transition, is limited by an energetically opposing proton diffusion potential. This means that the inverted $\Delta\psi$ will cease to increase when it exceeds energetically the difference in the proton diffusion potential across the membrane (Cruz *et al*., 2001; Avenson *et al*., 2005). In the absence of active ion translocation mediated in part by *KEA3* (Armbruster *et al*., 2014) and *TPK3* (Carraretto *et al*., 2013), movement of counterions like potassium (K^+) along the

transmembrane potential gradient proceeding on the order of tens of seconds at a 1000-fold slower rate compared to that of protons ultimately collapses the inverted $\Delta\psi$, particularly when the chloroplast ionic strength is high. Increasing $\Delta\psi$-collapsing counterion movement is reflected by a subsequent slow rise of the ECS signal back to the dark baseline level on the order of tens of seconds is related to (Sacksteder *et al*., 2000; Avenson *et al*., 2005; Johnson and Ruban, 2014). The light-induced ΔpH fraction of the *pmf* is then proportional to the inverted portion of the ECS signal (ECS_{inv}), which relaxes over tens of seconds. The difference between these amplitudes is related to the contribution of $\Delta\psi$ to the light-induced *pmf* at steady state (ECS_{ss}). Thus, decay of the light-induced $\Delta\psi$ occurs rapidly initially and precedes that of the ΔpH during the light-dark transition and any differences in the $\Delta\psi$ present in the light and dark are reflected in changes in the ECS. The relative contribution of the $\Delta\psi$ and ΔpH to the *pmf* established in the light can thus be estimated.

Certain limitations to the ECS approach must however be taken into consideration. In particular, longer-term (i.e., pH-induced light scattering) processes can interfere with and affect the resulting signal (Sacksteder *et al*., 2000; Avenson *et al*., 2004; Avenson *et al*., 2005). Consequently, absorbance changes at 515 nm induced by a rapid saturating pulse of light can be used to estimate rapid changes in the ECS signal over a total trace time of 1 s in the absence of contaminating signals related for instance to cytochrome b_6f oxidation as well as xanthophyll conversion (Sacksteder *et al*., 2000; Avenson *et al*., 2004). Given significant light-scattering effects over prolonged periods of illumination, absorbance changes at 505, 520, and 535 nm can be measured near-simultaneously and subsequently deconvoluted to correct for these effects and obtain more accurate estimates of ECS-related parameters (Avenson *et al*., 2004). These approaches to controlling for long-term processes are also important when measuring different species or mutant lines given possible differences in pigment shifts reflected by the ECS signal (Avenson *et al*., 2005).

1.1.5 An Integrated Approach to Studying Light Reactions

Studies based on Chl fluorescence, single-turnover pulse and continuous illumination spectroscopy, and other biophysical approaches have therefore significantly improved our understanding of NPQ and its constituent regulatory components. Characterization of these key regulatory factors and components can also be accomplished through *in vitro* application of specific inhibitors or uncouplers. They have been traditionally used to probe electron transport, ΔpH and $\Delta\psi$ formation across the thylakoid membrane, and xanthophyll cycle activity, among other critical regulatory components of NPQ and general light-harvesting reactions. Various molecular and genetic approaches involving the isolation and characterization of various photosynthetic and NPQ-related mutants of *Arabidopsis*, *Chlamydomonas*, and other species have also provided compelling evidence for the role and significance of the ΔpH, the PsbS protein, the xanthophyll cycle, and other integrated factors and components regulating NPQ and photosynthesis as a whole. Future studies integrating biophysical, biochemical, and molecular approaches that extend beyond current limitations, including the availability of genomic resources (i.e., stable mutant lines) and technical hardware limitations, will ultimately unravel the exact mechanistic underpinnings of photoprotection and photosynthesis down to the individual gene level.

1.2 Aims and Objectives

The aims of the proposed work are to examine in detail (a) the importance of $\Delta\psi$ in qE regulation in established model C_3 plants, spinach and *A. thaliana*; (b) the dynamics of *pmf* partitioning in relation to NPQ, electron transport, xanthophyll conversion in Wt and select mutants of *A. thaliana*, and (c) the role of K^+/H^+ antiport during photosynthetic acclimation to fluctuating light in *kea3* of *A. thaliana*. It is hypothesized that the electron transport-driven transthylakoid $\Delta\psi$ precedes the formation of a ΔpH and may contribute to qE regulation during early light activation of photosynthesis.

Initial work will involve analyses of $\Delta\psi$ and ΔpH in isolated thylakoids and leaves of common spinach and *A. thaliana*. Comparisons of the extent and kinetics of NPQ, $\Delta\psi$ and ΔpH partitioning of the chloroplast *pmf* in the presence of different types and concentrations of channel-forming ionophores that uncouple the $\Delta\psi$ and/or ΔpH will be studied using PAM spectrofluorometry. The general action of each ionophore will be confirmed by monitoring light-induced absorbance changes at 515 nm using pump and probe and PAM spectrophotometry. These and other spectroscopic methods currently being investigated and developed will be complemented by biochemical characterization of xanthophyll cycle conversion as well as spectroscopic analyses of select *Arabidopsis* mutants defective in crucial components of photochemical and NPQ reactions.

In the long term, this work will provide further insight into key regulatory processes that influence light-harvesting and downstream carbon fixation reactions of photosynthesis. Combined with the tools and techniques established, this will significantly contribute to current and future studies aimed at better understanding photoprotective responses to light and other abiotic stresses as part of a more integrated and holistic systems-based approach. This is particularly important given the pivotal role of photosynthesis in global carbon sequestration and climate regulation amidst changing environmental conditions and imposed stresses (Sage, 2004). From a practical standpoint, a better understanding of photosynthesis will aid international efforts to improve crop breeding and ultimately yields in some of the world's most productive C_3 and C_4 crops like wheat and maize, respectively, in order to meet growing global food and energy demand (Hibberd *et al*., 2008). This includes improved regulation of ion transport activity involved in modulating the switch between photosynthesis and photoprotection under fluctuating light conditions (Armbruster *et al*., 2014).

2. Materials and Methods

2.1 Chemicals Used

Various chemicals and compounds used to produce necessary stock solutions and media required within the framework of this thesis have been obtained from AppliChem GmbH, Germany, Carl Roth GmbH + Co. KG, Germany, Fisher Scientific GmbH, Germany, J.T. Baker B.V., the Netherlands, Sigma-Aldrich Chemie GmbH, Germany, VWR International GmbH, Germany.

2.2 Plant Growth Conditions

Common spinach, *Spinacia oleracea* L., was grown on C400 soil (Stender AG, Germany) pre-mixed with Cocopor® and Nitrophoska Perfect 15-5-20 (+2+20) fertilizer (EuroChem Agro GmbH, Germany) in the greenhouse under natural light conditions supplemented by 400 W high pressure sodium lamps (Philips International B.V., the Netherlands) for up to 8 weeks over a 8/16 h day/night cycle.

Arabidopsis thaliana L. wild-type (Wt) Columbia (Col-0) and Wassilewskija (Ws) seeds and those of a direct Wt descendant of Col-1 (Col-gl1) were stratified in 0.1 % agarose for 48 h at 4 °C to synchronize germination. Seeds were subsequently sown on soil (BP-Substrate 3, Klasmann-Deilmann GmbH, Germany) pre-mixed with Lizetan® (Bayer CropScience Deutschland GmbH, Germany) according to manufacturer instructions. In addition to Wt, various mutants grown under the same conditions are summarized in Table 2.1.

Table 2.1 – Overview of mutant lines used.

Genotype	Background	Mutation	Source	Reference
pgr5	Col-gl1	Cyclic electron transport	T. Shikanai (Japan)	Munekage *et al*., 2002
pgrl1ab #273	Col-0	Cyclic electron transport	SALK_052933.54.00.x (SALK), D. Leister (Germany)	Dalcorso *et al*., 2008
pgr1	Col-0	Cytochrome b_6f complex	SALK_019871C (SALK), T. Shikanai (Japan)	Munekage *et al*., 2001
L17	Col-0	PsbS overexpression	K.K. Niyogi (USA)	Li et *al*., 2002
npq4 (psbs-1.3)	Col-0	PsbS-deficiency	D. Leister (Germany)	Graßes *et al*., 2002
npq2 (aba1-6)	Col-0	Zeaxanthin epoxidase	N3772 (NASC)	Niyogi *et al*., 1998
npq1-2	Col-0	Violaxanthin de-epoxidase	N3771 (NASC)	Niyogi *et al*., 1998
kea3-1	Col-0	Potassium/proton antiport	N416305 (NASC), U. Armbruster (USA)	Grossman *et al*., 2010
kea3-2	Ws	Potassium/proton antiport	FLAG_493C01 (INRA), U. Armbruster (USA)	Grossman *et al*., 2010

All lines and their respective Wt backgrounds were grown under custom-built 8 x 58 W fluorescent light arrays (Siteco GmbH, Germany) for up to 6 weeks at 100 μmol quanta m^{-2} s^{-1} over a 10/14 h day/night cycle and a constant day/night temperature of 23 °C.

2.3 Preparation of Plant Material

Active, coupled thylakoids were isolated from mature 6-8-week-old spinach plants dark-adapted overnight at 4 °C prior to experimental use. Intact leaves were detached from mature 4-6-week-old *Arabidopsis* plants dark-adapted overnight at room temperature (23 °C).

2.3.1 Isolation of Intact Thylakoids in Spinach

Isolation of intact thylakoids was carried out at all times in the dark on ice at 4 °C using ca. 20 g of dark-adapted leaves with detached petioles washed thoroughly in 1X distilled water and pre-cooled at 4 °C for 30 min. All isolation media (pH adjusted at 4 °C, where applicable) and equipment were pre-cooled to 4 °C. Leaf material was rapidly homogenized once at maximum speed in a Warring blender for 5 s in 100 mL of isolation medium, pH 7.6, to which was freshly added 0.1 % (w/v) bovine serum albumin and 330 mg L^{-1} sodium ascorbate (Table 2.3.1.1). Homogenate was carefully squeezed through four layers of gauze,

one layer of 20 μm nylon mesh, and finally two layers of gauze. Total homogenate volume was equally allotted between two 50 mL Falcon centrifuge tubes, which were centrifuged at 4 °C for 3 min at 1010 *g*. The resulting supernatant was carefully discarded and the pellet was carefully resuspended with 2 mL of shock medium (Table 2.2). An additional 8 mL of shock medium was added and the suspension was incubated for 10-15 s on ice before 5 mL of resuspension medium, pH 7.6, was added (Table 2.2). Following centrifugation at 4 °C for 5 min at 1010 *g*, the supernatant was discarded and 1 mL of pre-mixed equal parts shock and resuspension media was added to resuspend the pellet. An additional 3 mL of the same mixture was added.

Table 2.2 – Media for thylakoid isolation in spinach.

Isolation Medium pH 7.6	Shock Medium	Resuspension Medium pH 7.6
1 mM $MgCl_2$	5 mM $MgCl_2$	5 mM $MgCl_2$
1 mM $MnCl_2$		10 mM NaCl
10 mM NaCl		2 mM KH_2PO_4
330 mM Sorbitol		80 mM HEPES/NaOH
HEPES/NaOH (pH 7.6)		660 mM Sorbitol
5 mM EGTA		5 mM $MgCl_2$
5 mM EDTA		

The reaction or measuring medium (pH adjusted at room temperature) prepared for various *in vitro* spectroscopic and biochemical assays contained: 0.33 M sucrose, 40 mM HEPES/NaOH (pH 8.0), 5 mM $MgCl_2$, 10 mM NaCl, 50 mM KCl, 20 mM sodium ascorbate, and 20 μM of the electron acceptor methyl viologen. Finally, the chlorophyll *a* and *b* content of the thylakoid suspension was determined (see below).

2.3.2 Chlorophyll *a* and *b* Content Determination

An aliquot (2.5-10 μL) of the thylakoid suspension was dissolved in the corresponding volume (990-997.5 μL) of 80 % aqueous acetone and centrifuged for 2 min at 10,000 *g*. The chlorophyll concentration (mg mL^{-1}) of the supernatant was determined according to Arnon (1949) using the extinction coefficients of chlorophyll *a* and *b* at 645 and 663 nm:

$$c_{Chl}\left[mg\ mL^{-1}\right] = \left[\frac{(E_{645} \times 20.2) + (E_{663} \times 8.02)}{1000}\right] x \frac{Volume_{total}}{Volume_{sample}}$$

The final concentration of Chl in all thylakoid preparations for all further spectroscopic and biochemical assays was set to 30 μg Chl mL^{-1}.

2.3.3 Preparation of Leaf Material for *in vivo* Assays

Detached leaves wrapped at the petioles with fine tissue paper dipped in water were consistently measured and maintained under ambient air conditions (23 °C, ~ 394 ppm CO_2) during all spectroscopic assays.

2.4 Pulse-Amplitude-Modulation (PAM) Fluorometry

The development of PAM fluorometry (Schreiber *et al*., 1986) has enabled versatile and user-friendly study of various biochemical and photophysical processes to include NPQ, P700 oxidation and chloroplast *pmf* formation under *in vivo* and/or *in vitro* conditions.

2.4.1 Chlorophyll *a* Fluorescence and P700 Oxidation Measurements

The dynamics of non-photochemical quenching (NPQ) were derived from measurements of maximal Chl fluorescence quenching using PAM fluorometry and the saturation pulse method (Schreiber, 2004), provided by the modular DUAL-PAM-100 spectrofluorometry system (Heinz Walz GmbH, Germany). Measurements were performed in detached leaves, held in place by a supplied leaf cuvette, and isolated thylakoids constantly stirred in 2 mL of reaction medium added to a 10 mm quart cuvette supplied with the PAM system. Pulse-modulated (1-100 kHz) measuring light originating from a light emitting diode (7 μmol quanta m^{-2} s^{-1}, 620 nm DUAL-DR) was used to induce fluorescence detected at wavelengths over 700 nm. Continuous, non-modulated red actinic light (λ = 635 nm) at intensities of 53-1287 μmol quanta m^{-2} s^{-1} was applied for 10-20 min prior to 5-10 min of dark relaxation, where specified. Concurrently, saturating pulses (200 ms duration, 6000 μmol quanta m^{-2} s^{-1}) were applied every 10, 20, and 60 s during illumination as well as every 20 and 60 s during the subsequent dark period. The induction and relaxation kinetics of fluorescence quenching related to competing primary photochemical quenching (qP) and NPQ reactions were thus monitored by measuring the ground and maximal fluorescence yields in the dark- (F_0, F_M) and light- (F_{0s}, F_{ms}) adapted states as well as during dark relaxation ($F_{0'}$, $F_{M'}$) (Figure 2.1).

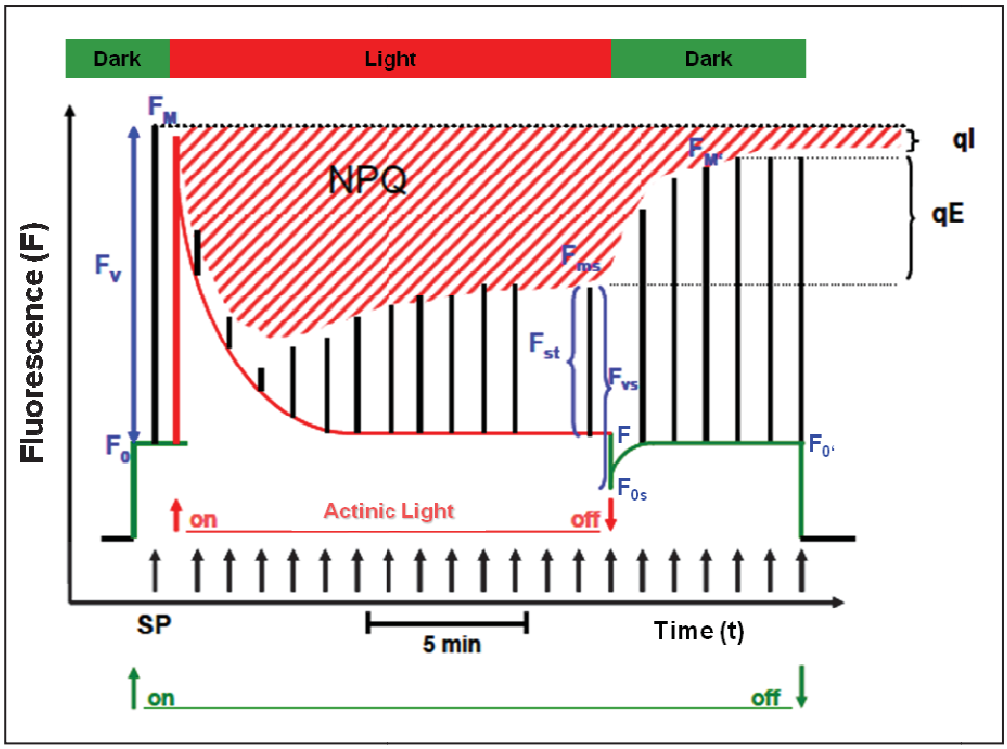

Figure 2.1 - Time-resolved analyses of chlorophyll *a* fluorescence signals and derived parameters, as recorded with a modulation fluorometer. Total fluorescence yield, denoted by F, at time t is measured in the presence and absence of continuous actinic light turned on and off, as indicated by the corresponding arrows. Weak modulated measuring light (green line) and additional saturating pulses (SP) are applied in order to determine the initial and maximal fluorescence in the dark- and light-adapted states, F_0 and F_M and F_{0s} and F_{ms} respectively. Calculation of photochemical (qP) and non-photochemical quenching in relation to maximal (qN_{SV}) or variable (qN_C) fluorescence as well as other parameters proceed by comparing light and subsequent dark-relaxation phase fluorescence signals: $F_V = F_M - F_0$; $F_{vs} = F_{ms} - F_{0s}$; $F_{st} = F_{ms} - F$; $qP = F_{st}/F_{vs}$; $qN_{SV} = F_M/F_{ms} - 1$; $qN_C = 1 - F_{vs}/F_V$.

Relevant quenching coefficients and parameters can be obtained as follows:

$$\text{qP (photochemical quenching)} = \frac{F_{st}}{F_{vs}}$$

$$\text{qE}_{SV}\ (\Delta\text{pH-dependent quenching}) = \frac{F_M}{F_{ms}} - \frac{F_M}{F_{M'}}$$

$$\text{qI}_{SV}\ (\text{photoinhibitory quenching}) = \frac{F_M}{F_{M'}} - 1$$

$$\text{NPQ (non-photochemical quenching)} = \frac{F_M}{F_{ms}} - 1$$

Thus: $$\mathbf{NPQ = qE_{SV} + qI_{SV}}$$

Using the same approach, simultaneous measurement of the redox state of the PSI RC chlorophyll, P700, was carried out by monitoring absorbance changes in the near-infrared region, peaking at 810 to 840 nm (Klughammer and Schreiber, 2008). This provides critical information relating to the energy conversion efficiency in PSI, including the PSI quantum yield, as in PSII monitored via Chl fluorescence. Simultaneous quenching of 1 μM 9-aminoacridine (9-AA), dissolved in 20 % (v/v) aqueous ethanol, was used to monitor changes in the lumen pH and thus the ΔpH under *in vitro* conditions using pulse-modulated UV-A excitation light at 365 nm (Schreiber and Klughammer, 2009). 9-AA is a fluorescent indicator of lumen pH in its protonated form with peak excitation at ~ 400 nm. The ΔpH is calculated according to Schuldiner *et al*. (1972) by comparing stable values of ground-state and steady-state fluorescence yields of dark-light and light-dark transitions, F_0 and F respectively, prior to, during, and following 10 min of actinic illumination at 825 μmol quanta m^{-2} s^{-1}. Key parameters related to the strength and composition of the actinic and measuring light as well as the saturating pulses (Table 2.3) were defined so as to minimize non-specific optical effects on the appropriate signals during the course of each measurement.

Table 2.3 – Main parameter settings in the dual channel fluorescence and P700 oxidation/9-aminoacridine (9-AA) fluorescence measuring modes.

<table>
<tr><th>Measuring Mode</th><th>Measuring Light</th><th>Actinic Light</th><th>Slow Kinetics</th><th>Saturating Pulse</th><th>Photo-multiplier Settings (9-AA only)</th></tr>
<tr><td>Single/Dual Channel</td><td>Fluo: 3 (7 μmol quanta m^{-2} s^{-1})</td><td>5 (53 μmol quanta m^{-2} s^{-1})</td><td>Rate: 1-20 ms</td><td>Intensity: 6 (6000 μmol quanta m^{-2} s^{-1})</td><td>Coarse: 3-4 (varies by simple)</td></tr>
<tr><td>Detector 1: DB</td><td rowspan="8">P700/9-AA-
Fluo: 6</td><td>10 (216 μmol quanta m^{-2} s^{-1})</td><td rowspan="8">Points: varies (Slow Kinetics Trigger run-time-dependent)</td><td>Width: 200 ms</td><td rowspan="8">Fine: 4-10 (varies by sample)</td></tr>
<tr><td>Detector 2: N.C. (Single Channel) DP700 / DNADPH (Dual Channel)</td><td>15 (660 μmol quanta m^{-2} s^{-1})</td><td>P700 SP-Evaluation – Interval Delay: 5 μs Width: 30 ms</td></tr>
<tr><td>Analysis Mode: SP-Analysis</td><td>18 (1287 μmol quanta m^{-2} s^{-1})</td><td rowspan="5">Acquisition – Points: 16000 Rate: 100 μs</td></tr>
<tr><td>Fluo Gain: 1 (Low)</td><td rowspan="4">Far Red Light: 5 (value 64)</td></tr>
<tr><td>Fluo Damping: 1 ms (High)</td></tr>
<tr><td>P700/NADPH-Fluo Gain: 5 (High)</td></tr>
<tr><td>P700/NADPH Fluo Damping: 1 ms (High)</td></tr>
</table>

2.4.2 Measurements of the Electrochromic Shift (ECS)

The P515/535 accessory emitter-detector module of the DUAL-PAM-100 system was used to monitor changes in the electrochromic absorbance shift (ECS) at 515 nm and thus the $\Delta\psi$ and ΔpH in relation to the *pmf in vivo* (Schreiber and Klughammer, 2008). Intact dark-adapted leaves were continuously illuminated between 1 s and 20 min with red actinic light at 53-1287 μmol quanta m^{-2} s^{-1}, followed by 5 min of dark relaxation to assess the dynamics of *pmf* partitioning in Wt and corresponding mutant lines. An in-program script was generated for select illumination periods to obtain a high resolution (1 ms) ECS signal of the final 330 s of real time measurement, which includes the full 5 min dark relaxation period. All ECS signals were normalized to the amplitude of the rapid (microsecond) rise in the 515 nm absorbance signal established following a single 50 μs pulse applied to independently measured dark-adapted leaves from all lines. This accounts for any differences in leaf thickness, chloroplast density, and other optical properties between leaves within and between lines. As a result, rapid changes in the ECS signal can be estimated in the absence of overlapping signals to include cytochrome b_6f oxidation and xanthophyll conversion (Sacksteder *et al*., 2000; Avenson *et al*., 2004). Although deconvolution of individual overlapping absorbance changes was not carried out due to technical limitations, flash-normalized ECS measurements of *npq1* and *pgr1* mutants deficient in Z_X and ΔpH formation, respectively, thus offer an alternative means of controlling for xanthophyll activity and pH-dependent cytochrome b_6f activity. The absolute magnitudes, measured in volts and convertible to $-\Delta I\ I_0^{-1}$ via a built-in calibration routine, of the $\Delta\psi$, ΔpH, *pmf*, and by extension the derived lumen pH were quantified from the raw light-off or DIRK analysis of the P515 signal according to Takizawa *et al*. (2007). Relevant parameter settings concerning ECS measurements are summarized in Table 2.4.

Table 2.4 – Main parameter settings in the dual beam P515/535 measuring mode.

<table>
<tr><th>Measuring Mode</th><th>Measuring Light</th><th>Actinic Light</th><th>Slow Kinetics</th><th>Fast Kinetics</th><th>Fast Trigger</th></tr>
<tr><td>Dual Channel: I(535nm) + P515</td><td>I(535nm): 3 (7 μmol quanta m^{-2} s^{-1})</td><td rowspan="11">See Table 2.3</td><td rowspan="11">See Table 2.3</td><td>MT: 6 (6000 μmol quanta m^{-2} s^{-1})</td><td>P515_ST50μs.FTM</td></tr>
<tr><td>Detector 1: DP515/535</td><td rowspan="10">P515: 12
Intensity step</td><td>Acquistion –
Points: 128000
Rate: 2.5 μs
Time: 320 ms</td><td>Zero Time Shift: 64000 μs</td></tr>
<tr><td>Detector 2: N.C.</td><td>Target Averages: 10</td><td>S & H Off - Trigger On: 0 μs
Trigger Off: 100 μs</td></tr>
<tr><td>Analysis Mode: SP-Analysis/Fast Acquisition</td><td rowspan="2">Auto ML ON</td><td rowspan="9">ST –
Trigger On: 50 μs
Trigger Off: 100 μs</td></tr>
<tr><td>I(535nm) Gain: 1 (Low)</td><td rowspan="8">Clock: On 10 s</td></tr>
<tr><td>I(535nm) Damping: 1 ms (High)</td></tr>
<tr><td>P515 Gain: 5 (High)</td></tr>
<tr><td>P515 Damping: 1 ms (High) in SP-Analysis mode</td></tr>
<tr><td>P515 Damping: 10 μs (Low) in Fast Acquisition mode</td></tr>
</table>

2.5 Pump and Probe Spectroscopy

Pump and probe systems can rapidly generate one or a series of precisely defined single-turnover pulses or continuous actinic light, which can be supplied by internal or external sources, manipulated optically via specific interference and cut-off filters, and detected at specific wavelengths (i.e., pertaining to the blue, red and/or far-red regions). The actinic light excites and saturates PSII to induce both photosynthesis and fluorescence emission. As a result, one can easily study NPQ processes via Chl fluorescence as well as various processes related to electron and proton transport down to a time resolution of 10 μs (Joliot and Joliot, 2005). The latter in particular can be studied, as has been done in this work using the JTS-10 Joliot-type pump and probe spectrometer (Bio-Logic SAS, France). Standard applications of the JTS-10 system include monitoring transthylakoid pH variations (i.e., as transient flash-induced absorbance changes at ~ 560 nm of the hydrophilic stromal pH-indicator phenol red), changes in $\Delta\psi$ at 515 nm, and cyclic and linear electron flow under *in vivo* and in some cases under strictly *in vitro* conditions. In this work, the JTS-10 system was used primarily to measure changes in $\Delta\psi$ at 515 nm in 1 mL spinach thylakoid suspensions following application of a 50 μs xenon pulse of white light every 10 s, averaged 5 times for each measurement according to the parameter settings outlined in Table 2.5.

Table 2.5 – JTS-10 parameter settings used in measurements of changes in $\Delta\psi$ at 515 nm.

<table>
<tr><th>LED Control</th><th>Sequence</th><th>Light Source</th><th>Filters</th></tr>
<tr><td>Actinic II (I-J): 940 μmol quanta m^{-2} s^{-1}</td><td>Xenon flash (A, auxiliary)-based sequence: varies</td><td rowspan="2">Xenon Flash Lamp (Auxiliary Unit)</td><td rowspan="2">BG39 (reference detector)</td></tr>
<tr><td>Detector: White Light</td><td>Repeat: 5X</td></tr>
<tr><td rowspan="4">Sensitivity: 5.7</td><td>Delay: 10 s</td><td rowspan="2">Pulse Duration: 10 μs (full width at half maximum)</td><td rowspan="2">520 nm (interference filter), 10 μs (full width at half maximum)</td></tr>
<tr><td>Average Cycles</td></tr>
<tr><td>No Correction of Kinetics (ΔI/I)</td><td rowspan="2">Flash Number: ∞</td><td rowspan="2">Detector(s) Sensitivity: Max./Mid.</td></tr>
<tr><td>Photodiode Response: 4 μs</td></tr>
</table>

2.6 Pigment Analyses

Pigment composition was characterized using reversed-phase high-performance liquid chromatography (RP-HPLC), as described 2.6.3. This approach operates under high pressure and requires relatively little working material. Pigments are separated via a *reversed-phase* column and eluted by specific solvents through diminishing column polarity, as described previously (Gilmore und Yamamoto, 1991; Färber *et al*., 1997).

2.6.1 Preparation of Isolated Thylakoid Samples in Spinach

Spinach thylakoid suspensions (200 μL) of a given ionic strength in the reaction medium containing 30 μg Chl mL^{-1} were illuminated for 10 min at 825 μmol quanta m^{-2} s^{-1} with red actinic light in the presence or absence of either 2 μM nigericin, 2 μM gramicidin, or 10 nM valinomycin added prior to illumination in all cases. Dark-adapted and illuminated samples were dissolved in 800 μL 100 % absolute acetone. Samples were finally vortexed (Labinco B.V., the Netherlands) and filtered through a 0.20 μm PTFE-membrane filter (Sartorius Stedim Biotech GmbH, Germany).

2.6.2 Preparation of Leaf Samples in Wt *Arabidopsis*

Dark-adapted *Arabidopsis* Col-0 leaf discs were placed in open petri dishes half-filled with water and cooled by a fan to minimize water loss due to leaf transpiration during illumination with white light under a single 600 W incandescent bulb light array (Hortilux Schréder B.V., the Netherlands). Samples were illuminated for 10, 60, 180, 600, and 1200 s at 53-1287 μmol quanta m^{-2} s^{-1}, immediately shock frozen in liquid nitrogen, and thereafter mechanically homogenized for 30 s using a bead mill (Retsch GmbH, Germany) before being dissolved in 1 mL of 100 % absolute acetone. Remaining unbroken tissue and cell debris was vortexed and separated from solution via filtration through a 0.20 μm PTFE-membrane filter.

2.6.3 Pigment Separation via Reversed-Phase Chromatography

Filtered samples were loaded into a Merck-Hitachi L-7200 Autosampler (Hitachi High-Technologies Corporation, Japan) for UV-VIS detection-based reversed-phase chromatography. The system consists of various components listed in Table 2.6.

Table 2.6 – RP-HPLC system components required for pigment separation.

Component	Manufacturer
D-7000 Interface Module	Merck/Hitachi, Germany
L-7200 Autosampler	Merck/Hitachi, Germany
L-7100 Pump A	Merck/Hitachi, Germany
L-7420 UV/VIS Detector	Merck/Hitachi, Germany
Syringe Loading Sample Injector 7125 – 100 μL Sample Loop	Rheodyne Inc., USA
Peltier Sample Cooler for the L-7200	Merck/Hitachi, Germany
L-7614 Bubble Trap	Merck, Germany
LiChroCART 250-4 Column	Merck, Germany
LiChroCART 4-4 Column Filter	Merck, Germany

LiChrospher® 100 RP-18 sorbent with a spherical silica particle size of 5 μm served as the active column and column filter component. Pressurized liquid containing 20 μL of the sample and a mixture of specific solvents (Table 2.7) is passed through the column as pigments are eluted by these solvents.

Table 2.7 – Elution solvents (HPLC grade) of the RP-HPLC system. Tris/HCl buffer, stored at 4 °C, was filtered prior to use (0.20 μm pore size).

Solvent A		Solvent B	
87 % (v/v)	Acetonitrile	80 % (v/v)	Methanol
10 % (v/v)	Methanol	20 % (v/v)	n-Hexane
3 % (v/v)	Tris/HCl pH 8.0		

Separation and elution of pigments at a flow rate of 2 mL min^{-1} proceeds according to a defined program (Table 2.8).

Table 2.8 – RP-HPLC elution program.

Time [min]	Solvent
0-9	100 % Solvent A
9-12.5	Linear gradient to 100 % Solvent B
12.5-18	100 % Solvent B
18-19	Linear gradient to 100 % Solvent A
19-23	100 % Solvent A

Pigments are eluted by polarity and thus retention time on the column and detected photometrically at 440 nm. A photometric calibration series and corresponding conversion factors of pure pigment standards (Table 2.9) allows quantification of pigment content.

Table 2.9 – Pigment retention times (± 1 min) and conversion factors. *Values applicable to experimental work on spinach; ** values applicable to all experimental work on *Arabidopsis*.

Pigment	Time [min]	Conversion Factor
Neoxanthin	3.2	2920*, 2561**
Violaxanthin	4.2	3375*, 3133**
Antheraxanthin	6.3	3006*, 2738**
Lutein	9.3	2877*, 2919**
Zeaxanthin	10.3	1980*, 2452**
Chlorophyll *b*	13.3	842*, 965**
Chlorophyll *a*	13.9	1056*, 894**
β-Carotene	16.8	2595*, 2625**

2.7 Computer Analyses

Statistical analyses as well as curve fitting were carried out using Prism 5.01 (GraphPad Software Inc., USA) software. Statistical significance was assessed using the Student's *t*-test based on the critical cut-off alpha level, α, of 0.05. Graphing was performed using GraFit 5.0.11 (Erithacus Software Limited, USA) software and primary data input and processing was handled in Microsoft Office Excel 2007-2013 (Microsoft Corporation, USA).

3. Results

The first part of this work concerns the spectroscopic characterization of the role of $\Delta\psi$ in qE formation *in vitro* in spinach, a common model system in bioenergetic studies. The second part of the work in *A. thaliana* involves investigation of qE regulation in terms of (1) changes in *pmf* partitioning over a range of intensities and (2) transthylakoid K^+/H^+ antiport.

3.1 Probing the Contribution of $\Delta\psi$ to early qE Activation in Spinach

It is widely accepted that both the $\Delta\psi$ and ΔpH are required to drive ATP synthesis and that the ΔpH is critical early on for establishing qE-type thermal dissipation, as introduced in 1.1.1. However, the role of $\Delta\psi$ in this short-term energy-dependent component of quenching in higher plants remains unclear. Although it is clear that charge separation within the photosystems establishes the linear flow of electrons from PSII to PSI and to some extent cyclic electron flow, leading to a transmembrane potential difference (Witt, 1979; Baker *et al*., 2007; Dau and Zaharieva, 2009), it is unclear when and to what extent the $\Delta\psi$ is involved in qE. Consequently, qE-related phenomena probed by the actions of three channel-forming ionophores or uncouplers that inhibit $\Delta\psi$ and/or ΔpH formation (Table 3.1) were studied spectroscopically in active, intact thylakoids of dark-adapted spinach.

Table 3.1 – Overview of ionophores used.

Ionophore	Chemical Properties	Biological Action	Concentration [μM]	Reference
Valinomycin	Dodecadepsipeptide antibiotic; highly selective for K^+ over Na^+ as a K^+-specific transporter	Abolishes only $\Delta\psi$	0.01	Cammann, 1985; Rose and Jenkins, 2007
Nigericin	By-product antibiotic; H^+, K^+, Pb^{2+} ionophore, but commonly as H^+ and K^+ antiporter	Abolishes only ΔpH	2	Graven *et al*., 1966
Gramicidin	Heterogeneous antibiotic; linear pentadecapeptides with alternating L- and D-amino acids	Abolishes $\Delta\psi$ and ΔpH	2	Burkhart *et al*., 1999

This aspect of the work seeks to better understand the dynamics of qE induction and relaxation in the presence of the above ionophores, particularly valinomycin. The action of each ionophore has been studied and confirmed over a range of concentrations using PAM fluorometry and pump and probe spectroscopy. The questions addressed by the work are:

(a) What is the role of $\Delta\psi$ in qE regulation under *in vitro* conditions?
(b) Are there concentration and/or time-dependent effects of ionophore treatment?

3.1.1 Characterization of NPQ in its Dependence on the Transthylakoid ΔpH

Maximal Chl fluorescence quenching monitored in isolated spinach thylakoids provides a means of measuring NPQ formation and downregulation in its dependence on lumen acidification and consequent ΔpH formation. Ionophores were applied prior to or 5 min after the onset of continuous illumination, in the case of valinomycin, in order to probe possible time-dependence of uncoupler action and consequent impacts on NPQ. Changes in the ΔpH *in vitro* between light- and dark-adapted states in the presence and absence of ionophores can be estimated from simultaneous measurements of 9-AA fluorescence quenching. Kinetics of NPQ formation and 9-AA fluorescence quenching were monitored simultaneously using PAM fluorometry during 10 min of continuous illumination of thylakoid suspensions with actinic light at 825 μmol quanta m^{-2} s^{-1}, followed by 5 min of dark relaxation (Figure 3.1). A sufficiently low concentration of 9-AA (1 μM; Table 2.3) was used to minimize disruptive effects on simultaneous *in vitro* measurements of Chl fluorescence quenching.

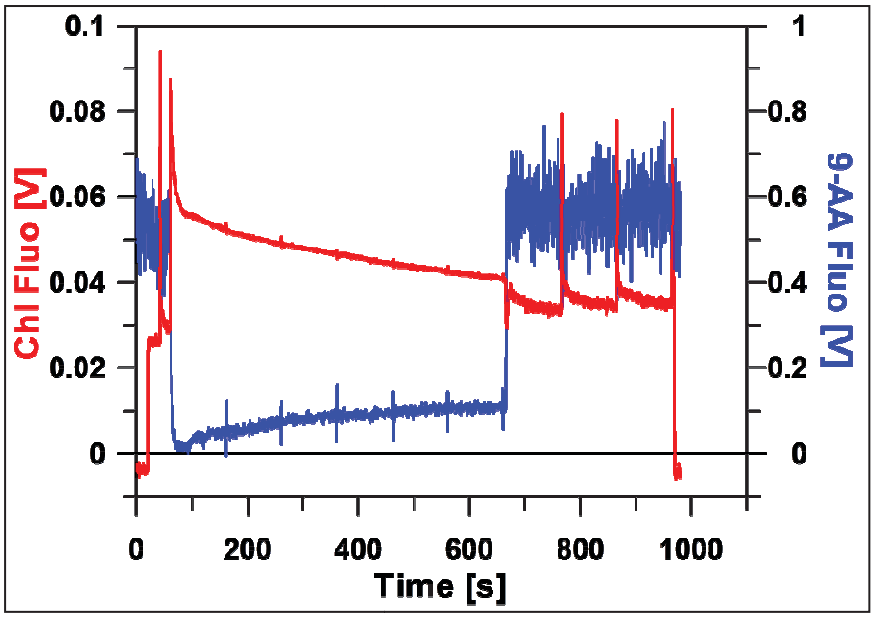

Figure 3.1 – Measurements of chlorophyll (Chl) *a* and 9-aminoacridine (9-AA) fluorescence quenching. Real-time PAM-based measurements were performed on isolated thylakoids from dark-adapted spinach leaves. Suspensions containing 1 μM 9-AA were illuminated for 10 min with red actinic light at 825 μmol quanta m^{-2} s^{-1} following a 1 min pre-illumination (dark baseline) period. Relaxation kinetics of Chl and 9-AA fluorescence were monitored during the subsequent 5 min dark period. Traces of Chl and 9-AA fluorescence show the starting point for Chl fluorescence measurements and the maximal extent of 9-AA quenching in the light.

Chl fluorescence kinetics probed by ionophores show that gramicidin and nigericin, both of which are known to collapse the transthylakoid ΔpH, clearly increased fluorescence yield and reduced quenching in the light (Figure 3.2A). In contrast, addition of valinomycin had no appreciable effect on Chl fluorescence yield and quenching in the light (Figure 3.2B).

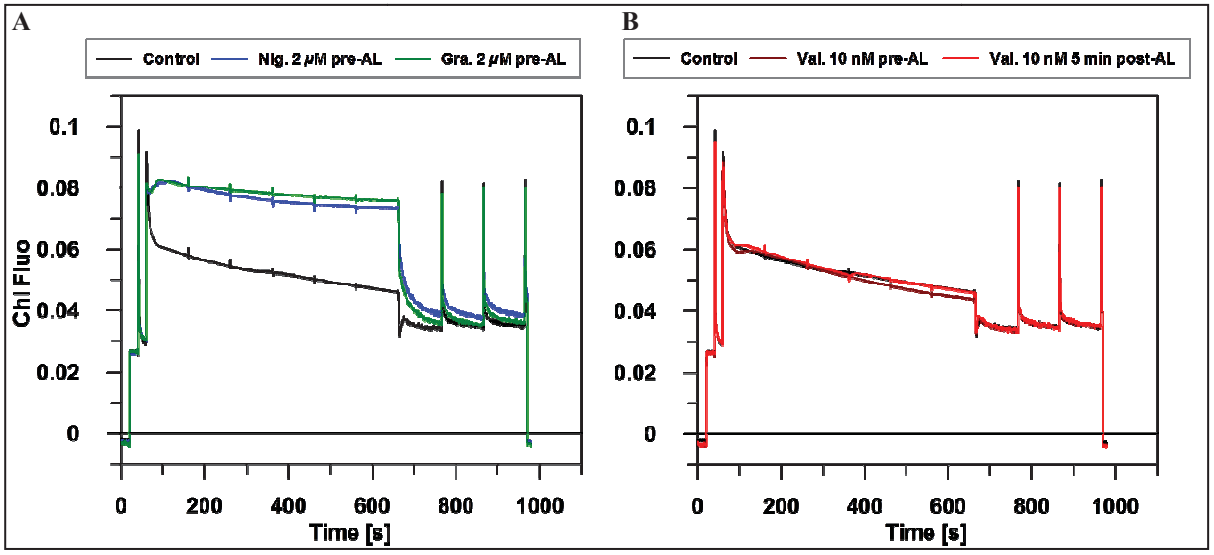

Figure 3.2 – Kinetics of maximal chlorophyll (Chl) fluorescence quenching in isolated spinach thylakoids. Chl fluorescence was monitored during 10 min of continuous actinic illumination at 825 μmol quanta m^{-2} s^{-1} and 5 min of dark relaxation in dark-adapted thylakoids. Thylakoid suspensions were (A) untreated (Control) or treated with 2 μM of nigericin (Nig.) or gramicidin (Gra.) prior to illumination with red actinic light (AL) and (B) 10 nM of valinomycin (Val.) prior to illumination or 5 min after the onset of illumination. Curves represent averages of at least three replicates from two or more independent experiments.

NPQ data thus show a clear, significant reduction (~ 82-85 %) in NPQ *in vitro* in the presence of 2 μM nigericin (Nig.) or gramicidin (Gra.) in comparison to negative controls, which show a maximum NPQ of ~ 1.1 (Figure 3.3A). Abolishment of the ΔpH by gramicidin and nigericin is reflected by reduced pH-dependent qE formation, as there is little to no relaxation of NPQ in the dark. In contrast, addition of 10 nM valinomycin (Val.) in the presence of 50 mM KCl prior to or 5 min after the onset of illumination had no significant effect on NPQ kinetics (Figure 3.3B). Likewise, the magnitude and rate of NPQ relaxation to include qE remained unchanged. On the basis of previous *in vitro* studies and preliminary supporting work, thylakoids were suspended in moderately concentrated K^+ media. This is because K^+-specific transthylakoid conductance is required for collapse of the $\Delta\psi$ selectively mediated by low concentrations of valinomycin (Table 3.1). Monovalent cations (i.e., K^+) and divalent cations (i.e., Mg^{2+}) have competing roles in regulating grana stacking and thus PSII to PSI excitation energy spillover as a function of their valence-dependent half-concentration effectiveness (Murata, 1969; Murata *et al*., 1970; Krause, 1974). Minimizing confounding effects on thylakoid structure and energy balance therefore necessitates that sufficient concentrations of dissolved cations are supplied *in vitro*. Thus, application of low nanomolar concentrations of valinomycin with KCl had no obvious effect on NPQ, regardless of when valinomycin is applied. This suggests that the $\Delta\psi$ collapsed by valinomycin has no impact on qE formation. However, higher concentrations of valinomycin (i.e., 2 μM) applied prior to and early on during illumination have been shown to reduce maximal NPQ (data not shown) and may reflect unspecific uncoupling effects of valinomycin on the proton gradient under these conditions (Telfer and Barber, 1974).

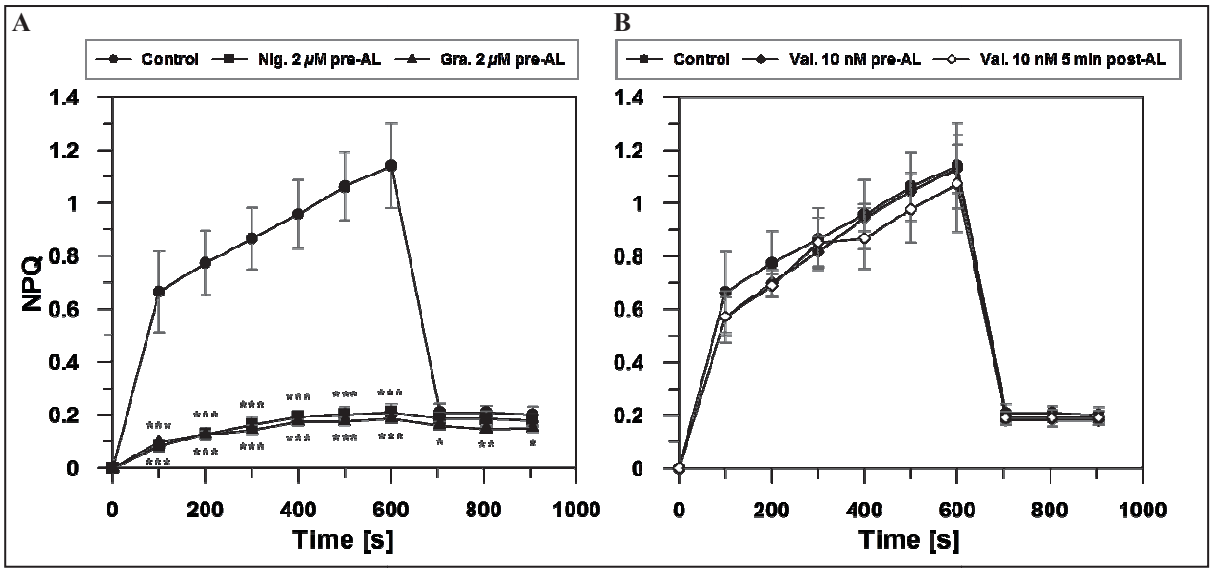

Figure 3.3 – Kinetics of non-photochemical quenching (NPQ) derived from measurements of maximal chlorophyll fluorescence quenching in isolated spinach thylakoids. NPQ was monitored for 10 min at 825 μmol quanta m^{-2} s^{-1} and 5 min of dark relaxation in dark-adapted thylakoids. Thylakoid suspensions were (A) untreated (Control) or treated with 2 μM of nigericin (Nig.) or gramicidin (Gra.) prior to illumination with red actinic light (AL) and (B) 10 nM of valinomycin (Val.) prior to illumination or 5 min after the onset of illumination. Curves represent mean values ± standard deviation (SD) of at least three replicates from two or more independent experiments. Asterisks indicate statistical significance (*P < 0.05, **P < 0.01, ***P < 0.001, α = 0.05, Student's t-test).

In addition to measurements of Chl fluorescence, simultaneous measurement of 9-AA fluorescence quenching as an indication of ΔpH formation has enabled characterization of the impact of various ionophores on the ΔpH. Although background fluorescence of thylakoid membranes in the absence of 9-AA can vary by preparation as well as on a sample-to-sample basis, it is assumed to be negligible for simplification of *in vitro* estimations of the ΔpH according to Schuldiner *et al*. (1972). Fluorescence quenching in the dark-light transition in controls occurred on the order of tens of seconds (Figure 3.4A-B). The rate of ΔpH-induced quenching was comparatively slower than the recovery of fluorescence in the light-dark transition, which reflects rapid continued proton efflux through the ATP synthase. The ΔpH in controls during these dark-light and light-dark transitions is estimated at 2.98 and 2.84 pH units, respectively, and thus a highly acidic lumen *in vitro* (pH ≈ 5). This assumes a constant stromal pH of ~ 8.0 dictated by the external measuring medium. Review of previous work in isolated thylakoids has shown that the ΔpH increases to ~ 3 pH units when the stromal pH increases to ~ 7.8 in the light (Kramer *et al*., 1999; Kramer *et al*., 2003).

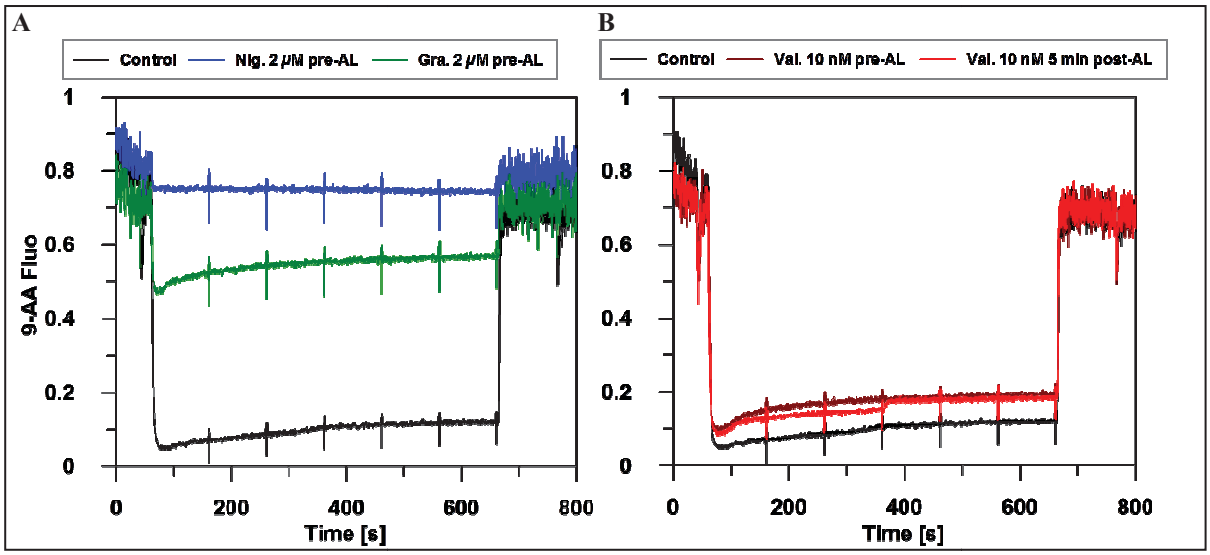

Figure 3.4 – Kinetics of 9-AA fluorescence quenching measured simultaneously with chlorophyll fluorescence in isolated spinach thylakoids. 9-AA fluorescence was monitored during 10 min of actinic illumination at 825 μmol quanta m^{-2} s^{-1} with a preceding and ensuing 1 min dark period in dark-adapted spinach thylakoids (A) untreated (Control) or treated with 2 μM of nigericin (Nig.) or gramicidin (Gra.) prior to illumination with red actinic light (AL) and (B) 10 nM of valinomycin (Val.) prior to illumination or 5 min after the onset of illumination. Curves represent averages of at least three replicates from two or more independent experiments.

Addition of 2 μM of ΔpH-abolishing nigericin or gramicidin prior to illumination led to a ~ 60 and 100 % reduction in the degree of 9-AA quenching, respectively, relative to controls (Figure 3.4). This corresponds to a significant decline in the ΔpH by 0.76 and 0.78 pH units ($P < 0.01$) in the presence of gramicidin during the dark-light and light-dark transitions, respectively, compared to controls. The ΔpH declined equally significantly by 1.24 and 1.32 pH units ($P < 0.01$) in the presence of nigericin during these respective transitions, and this decline in the ΔpH is more pronounced in the presence of nigericin compared to gramicidin. While complete or near-complete recovery of 9-AA fluorescence to the dark-adapted state level was observed in the presence of these ΔpH-abolishing ionophores (Figure 3.4A), the estimated ΔpH did not decline in proportion to the degree of 9-AA quenching in the light. This highlights overestimation of the ΔpH and would explain a low lumen pH in controls and limits the accuracy of these ΔpH estimations when background 9-AA fluorescence is assumed negligible. In contrast, there was a minor, though insignificant reduction in 9-AA quenching and thus the ΔpH in the presence of 10 nM valinomycin added prior to or 5 min into illumination compared to controls. This may be at least partially attributed to variable background 9-AA fluorescence. Biaudet and Havaux (1987) have also shown that a low concentration (50 nM) of valinomycin applied to dark-adapted spinach thylakoids has a negligible effect on 9-AA fluorescence quenching and thus ΔpH in the presence of 50 mM KCl and 5 mM $MgCl_2$. This indicates that valinomycin at low nanomolar concentrations has

no impact on the ΔpH, regardless of the time point of application. However, higher concentrations of valinomycin (2 μM) applied to isolated thylakoids under the same conditions have been shown to clearly reduce 9-AA quenching and thus the ΔpH (data not shown), again highlighting possible unspecific proton-uncoupling effects of valinomycin.

3.1.2 Pump and Probe Spectroscopic Characterization of the Transthylakoid Δψ

Absorbance changes peaking at 515 nm offer insight into the light-induced Δψ formation. Absorbance changes were measured for 300 ms in isolated spinach thylakoids following a single high-intensity pulse of white light applied five times sequentially every 10 s. Application of selective Δψ-abolishing ionophores like valinomycin can be used to study and confirm the action of these ionophores that alter the strength or magnitude of Δψ via membrane conductivity. For instance, valinomycin reduced the amplitude of the rapid increase in the 515 nm signal, related to the magnitude of the light-induced Δψ, and accelerated decay of the signal (Figure 3.5B). Application of gramicidin, which is known to abolish the Δψ in addition to the ΔpH, led to a more pronounced reduction in the amplitude of the increase in and subsequent decay of the signal. The decay of the 515 nm signal in controls follows a one-phase exponential decay (Figure 3.5A-B). In contrast, a two-phase decay is observed in the presence of valinomycin as well as nigericin, such that the signal decays rapidly initially over several milliseconds and slowly thereafter over several tens of milliseconds (Figure 3.5A-B). One-phase exponential decay was fitted for calculation of half-decay times ($T_{1/2}$) for comparison of the effects of uncouplers on the rate of rapid initial 515 nm decay, related specifically to changes in Δψ.

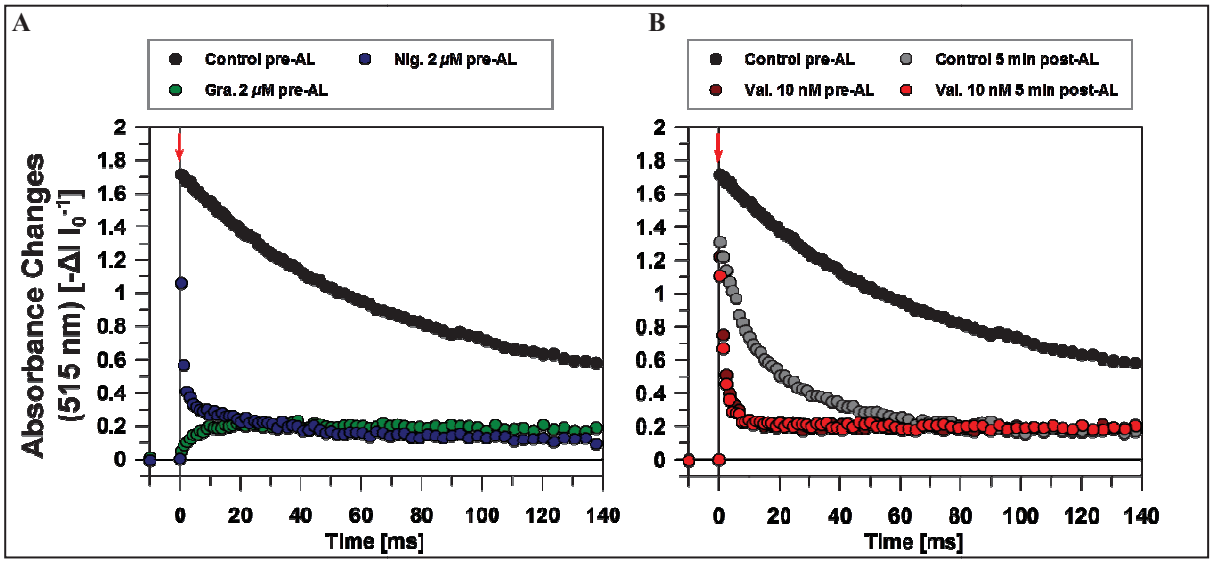

Figure 3.5 – Kinetics of absorbance changes at 515 nm following a single saturating flash of light (red inset arrows). Absorbance changes were monitored for a total of 300 ms following a 50 μs pulse of white light applied five times every 10 s to dark-adapted spinach thylakoids that were (A) untreated (Control) or treated with 2 μM of nigericin (Nig.) or gramicidin (Gra.) and (B) 10 nM of valinomycin (Val.) prior to or 5 min after the onset of illumination and compared against corresponding dark-adapted (pre-AL) or illuminated (5 min post-AL) controls. Curves represent averages of at least three replicates from two or more independent experiments.

Quantitative analysis of 515 nm absorbance kinetics shows that the amplitude of the rapid rise in the 515 nm signal, related to the magnitude of light-induced $\Delta\psi$, was significantly reduced by ~ 30 % upon addition of 10 nM of valinomycin to dark-adapted thylakoids compared to controls (Table 3.2). Collapse of the $\Delta\psi$ due to increased transmembrane K^+ conductivity facilitated by valinomycin significantly reduced the amplitude of the single-phase decay of the 515 nm signal (Table 3.2). Continuous illumination for 5 min led to a significant increase and decrease in the amplitude of the rapid and slow phases of signal decay, respectively, in valinomycin-treated thylakoids. This is due to valinomycin-mediated $\Delta\psi$ collapse compounded by light-activated $\Delta\psi$-dissipating ion fluxes. In contrast, 2 μM of gramicidin completely reduced the amplitude of the 515 nm signal, which showed no exponential decay as the $\Delta\psi$ collapsed (Table 3.2). However, addition of 2 μM of nigericin significantly reduced the amplitude of the rapid increase in the signal as well as the amplitude of slow decay following a saturating pulse by ~ 40 and 80 %, respectively, compared to corresponding controls (Table 3.2). The latter is associated with a ~ 3-fold increase in the rapid phase of signal decay. This contradicts with the specificity of nigericin for collapsing exclusively the ΔpH. Nigericin may have unspecific disruptive effects on the $\Delta\psi$ at such high concentrations *in vitro*.

Table 3.2 – Amplitudes, expressed in -ΔI I_0^{-1}, of the rapid rise (induction) and subsequent decay and associated half-decay times ($t_{1/2}$), in milliseconds (ms), of absorbance changes at 515 nm following a 50 μs pulse of white light in isolated spinach thylakoids. One- and two-phase exponential decay functions were fitted to determine amplitudes of rapid and slowly decaying phases of the 515 nm signal, as described in 2.5. Values represent means ± standard deviation (SD) of at least three replicates from two or more independent experiments. Statistical significance relative to corresponding column (negative) controls is indicated by asterisks (*$P < 0.05$; **$P < 0.01$; ***$P < 0.001$, $\alpha = 0.05$, Student's t-test); n.s. denotes not significant.

	Amplitude [-ΔI I_0^{-1}]				Half-Decay Time ($T_{1/2}$) [ms]
	Induction	One-Phase Decay	Two-Phase Decay		One-Phase Decay
			Fast	Slow	
Control pre-AL	1.71 ± 0.06	1.43 ± 0.07	0.38 ± 0.16	1.03 ± 0.13	34.61 ± 8.32
Control 5 min post-AL	1.31 ± 0.05 ***	-	0.79 ± 0.04 **	0.43 ± 0.06 ***	5.72 ± 0.71
Nigericin 2 μM pre-AL	1.06 ± 0.25 ***	-	0.75 ± 0.15 *	0.19 ± 0.08 ***	0.66 ± 0.43 *
Gramicidin 2 μM pre-AL	0.00 ± 0.00 ***	-	-	-	-
Valinomycin 10 nM pre-AL	1.22 ± 0.03 ***	0.99 ± 0.00 ***	-	-	1.03 ± 0.13 n.s.
Valinomycin 10 nM 5 min post-AL	1.10 ± 0.06 **	-	0.88 ± 0.04 *	0.04 ± 0.00 ***	1.02 ± 0.16 **

Addition of nigericin markedly increased the rate of decay of the 515 nm signal decay (Table 3.2), consistent with a reduction in the corresponding half-decay time ($T_{1/2}$), due possibly to unspecific effects of nigericin on membrane conductivity via the ΔpH. Gramicidin completely eliminated the decay of the 515 nm signal by abolishing both the $\Delta\psi$ and ΔpH (Table 3.2). Thus, relevant half-decay times could not be calculated. Addition of 10 nM of valinomycin significantly accelerated the decay and thus decreased $T_{1/2}$ by more than 30-fold compared to negative controls (Table 3.2). Continuous illumination for 5 min significantly reduced the amplitude of the signal in controls as well as in valinomycin-treated samples (Table 3.2). A clear reduction in $T_{1/2}$ was also observed in the presence of valinomycin added after 5 min of illumination. Similar reductive effects on the amplitude and rate of 515 nm decay relative to negative controls were observed in the absence of KCl, but were less pronounced compared to corresponding treatments with 50 mM KCl ($P < 0.05$; data not shown). Negative EtOH injection controls showed no impacts on 515 nm kinetics.

Reductions in the flash-induced rise in and subsequent decay of the 515 nm signal in the presence of valinomycin and KCl underscore the specificity of valinomycin for abolishing

the transthylakoid $\Delta\psi$ at low nanomolar concentrations. These findings support previous reports of valinomycin-probed $\Delta\psi$ formation across the thylakoid membrane, assessed as absorbance changes at 515 nm. For instance, early work of Junge and Schmid (1971) has clearly shown that 11 nM of valinomycin in the presence of 10 mM KCl accelerates the decay of 515 nm signal in isolated chloroplasts. This confirms that valinomycin abolishes the light-induced $\Delta\psi$ by selectively increasing thylakoid membrane conductivity for K^+ ions.

3.1.3 pH-Dependent Xanthophyll Cycle Activity Probed by Ionophores

Pigment content and composition of spinach thylakoids were characterized using RP-HPLC analysis. In particular, the conversion of V_X to Z_X catalyzed by V_XDE, assessed from the de-epoxidation state (DEPS) of the total V_X, A_X, and Z_X (VAZ) pool probed by ionophores, is important because it offers and insight into underlying changes in the lumen pH and thus ΔpH, which is required for NPQ formation. All ionophores were added to dark-adapted thylakoids prior to illumination for 10 min with actinic light at 825 μmol quanta m^{-2} s^{-1}.

Analysis of pigment data shows a significant increase in DEPS of the VAZ pool after 10 min of illumination by ~ 26-fold, respectively, in controls (Table 3.3). Pigment analyses in isolated thylakoids thus highlight a marked decrease in DEPS in the presence of gramicidin (Table 3.3). This is consistent with the role of gramicidin in abolishing the ΔpH as a crucial pre-requisite for pH-dependent Z_X formation and subsequent NPQ formation. Similarly, nigericin exclusively abolished the transthylakoid ΔpH and raised the lumen pH above the minimum threshold required to activate V_XDE bound to the lumenal side of the thylakoid membrane, thus reducing DEPS in saturating light.

Table 3.3 – Pigment composition in dark-adapted and illuminated spinach thylakoids. Pigment content and composition was evaluated using RP-HPLC, as described in 2.6.1. DEPS, expressed in %, denotes the de-epoxidation state of xanthophyll pigments zeaxanthin (Z_X) and antheraxanthin (A_X) formed from violaxanthin (V_X), in relation to the total xanthophyll pigment pool (VAZ), where DEPS = $[Z_X + (0.5 \times A_X)]$/VAZ and VAZ refers to V_X, A_X, Z_X. Values represent mean values ± standard deviation (SD) of three replicates. Asterisks separated by commas indicate statistical significance for corresponding within-treatment (column) comparisons, followed by between-treatment (row) comparisons relative to corresponding (negative) row controls (**P < 0.01, ***P < 0.001, α = 0.05, Student's t-test); n.s. denotes not significant.

	Duration of Illumination [min]	**Control**	**Nigericin 2 μM**	**Gramicidin 2 μM**	**Valinomycin 10 nM**
DEPS	0	1.86 ± 0.12	1.88 ± 0.17 n.s.	2.07 ± 0.10 n.s.	2.05 ± 0.11 n.s.
	10	49.23 ± 1.19 ***	6.31 ± 0.18 ***, ***	14.24 ± 1.66 **, ***	7.70 ± 0.25 ***, ***

In contrast, the strong reductive effect of valinomycin on DEPS (Table 3.3) is difficult to reconcile with the supposedly specific $\Delta\psi$-abolishing action of valinomycin at low concentrations, which does not affect NPQ or 9-AA quenching. It is possible that valinomycin may somehow interact with and perturb V_XDE binding to the thylakoid membrane. This may limit Z_X formation and in turn NPQ, assuming NPQ formation is Z_X-dependent. However, an expected reduction in NPQ was not observed under these conditions.

3.2 Variable *pmf* Partitioning in qE Regulation in *Arabidopsis*

The role of $\Delta\psi$ in qE regulation has thus far been examined under *in vitro* conditions in spinach, a well-established model system for studies of chloroplast bioenergetics. To gain further insight into the role of $\Delta\psi$, a crucial parameter of the *pmf*, in qE regulation, the dynamics of *pmf* partitioning into the $\Delta\psi$ and ΔpH in relation to NPQ and electron transport at low and higher intensities were characterized spectroscopically in Wt and select mutants of *A. thaliana*. Finally, the role of H^+/K^+ antiport in photosynthetic acclimation to fluctuating light was studied in *kea3* using various spectroscopic, biochemical, and molecular approaches (see appended manuscript).

3.2.1 Dynamics of *pmf* Partitioning *in vivo* in *Arabidopsis*

The transthylakoid ΔpH as an extension of the *pmf* is known to play a central regulatory role in both photochemical and non-photochemical reactions. However, it is uncertain to what extent partitioning of the *pmf* influences pH-regulated processes like qE. The aim of this part of the work is to first characterize the kinetics of NPQ and electron transport. It is then of particular interest to examine previously uncharacterized dynamics of *pmf* partitioning in relation to these kinetics in Wt and select mutant lines of *Arabidopsis* under the same conditions. Partitioning of the *pmf* during initial light exposure gives further insight into key processes critical to early light activation of qE towards stable qE at steady state. NPQ, electron transport, xanthophyll conversion, and *pmf* partitioning were thus characterized over a wide range of illumination periods (1-1200 s) and light intensities (~ 50-1200 μmol quanta m^{-2} s^{-1}) in Wt. Mutants deficient in PsbS (*npq4*), cytochrome b_6f (*pgr1*), xanthophyll conversion (*npq1, npq2*), and cyclic electron transport (*pgr5, pgrl1ab*) were exposed to the same periods of low and high light (~ 50 and 700 μmol quanta m^{-2} s^{-1}).

To summarize briefly, this aspect of the work seeks to determine:

(a) To what extent do the $\Delta\psi$ and ΔpH contribute to light-induced *pmf* partitioning in relation to qE over the same range of illumination periods and intensities?

(b) The role of $\Delta\psi$ in during early activation of qE *in vivo* in Wt and mutants exposed to limiting and more saturating light.

3.2.2.1 NPQ, Linear Electron Transport, and P700 Oxidation *in vivo*

Detached leaves of Wt Col-0 *Arabidopsis* were used to simultaneously measure quenching of maximal chlorophyll fluorescence and thus NPQ, the electron transport rate through PSII (ETR), and P700 oxidation inferred from donor-side limitation-based PSI quantum yield (Φ_I), as described in 2.4.1 and shown in Figure 2.1 using the DUAL-PAM-100 system. Kinetics were monitored during 20 min of actinic illumination at 53-1287 μmol quanta m^{-2} s^{-1}, followed by 10 min of dark relaxation (Figure 3.6).

Classical intensity-dependent induction and relaxation kinetics of NPQ were observed (Figure 3.6A-B). A clear increase in steady-state NPQ from ~ 0.20 at 53 μmol quanta m^{-2} s^{-1} to ~ 2.20 was observed in Wt after 20 min of continuous illumination at 1287 μmol quanta m^{-2} s^{-1} ($P < 0.001$) (Figure 3.6A). Formation of NPQ during the initial 30-50 s of illumination was similar across all intensities and continued to increase thereafter at higher intensities (Figure 3.6B). However, a peak transient NPQ of ~ 0.50 was established after ~ 50-60 s at 53 μmol quanta m^{-2} s^{-1}, which declined within 200 s to a minimal steady-state level during illumination at 53 μmol quanta m^{-2} s^{-1}. This is a well-known phenomenon that reflects most notably underlying transient lumen acidification and ΔpH formation driven by linear as well as cyclic electron flow (Munekage *et al*., 2002; Kalituho *et al*., 2007). The involvement of fundamental light-regulated processes like lumen acidification during early NPQ formation, as implicated in transient NPQ formation in low light, warrants further study of *pmf* partitioning into the ΔpH and $\Delta\psi$ under these conditions. The relative contribution of $\Delta\psi$ to *pmf* partitioning is of particular interest under these conditions in terms of a hypothesized role of $\Delta\psi$ in early qE activation to include transient NPQ formation.

At intensities above 100 μmol quanta m^{-2} s^{-1}, stable ΔpH formation contributes to longer-term PsbS-mediated conformational changes of LHCII and Z_X accumulation in LHCII, which synergistically contribute to stable NPQ formation. These rapid, short-term and slower, longer-term processes are reflected in the rapid and slow phases of NPQ induction and relaxation observed at more saturating intensities above ~ 200 μmol quanta m^{-2} s^{-1} (Figure 3.6A). Thus, increasing photoinhibition was observed at intensities above ~ 700 μmol quanta m^{-2} s^{-1}, consistent with an increasing qI fraction observed during NPQ relaxation in the dark.

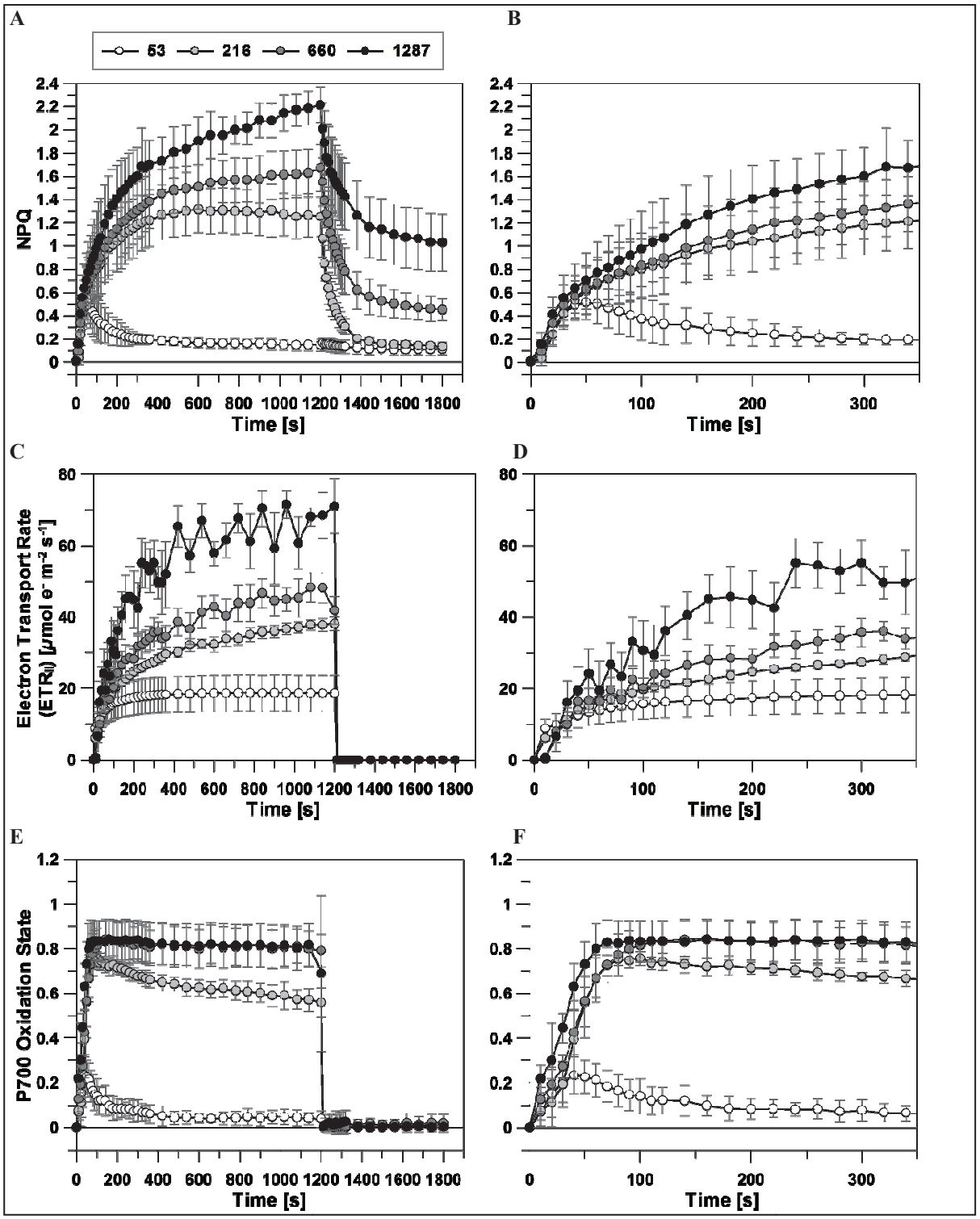

Figure 3.6 – Kinetics of (A-B) non-photochemical quenching (NPQ), (C-D) linear electron transport at PSII (ETR_{II}), and (E-F) the P700 oxidation state derived from measurements of PSI quantum yield based on donor-side limitation *in vivo* in *Arabidopsis*. Kinetics were monitored simultaneously during 20 min of actinic illumination at 53-1287 μmol quanta m^{-2} s^{-1} and 10 min of dark relaxation in detached Col-0 leaves. Light intensity values in the legend are expressed in μmol quanta m^{-2} s^{-1}. Curves represent mean values ± standard deviation (SD) of at least four replicates from two or more independent experiments.

The relative rate of linear electron transport through PSII based on the effective quantum yield of electron transport at PSII derived from *in vivo* measurements of chlorophyll fluorescence at a given intensity (Genty *et al*., 1989) depends on the incident PAR absorbed by PSII (Krause and Jahns, 2003). Induction of electron transport increased in an intensity-dependent manner as PSII RC's are rapidly flooded with electrons in the light, leading to saturation or near-saturation of ETR at steady state (Figure 3.6C-D). By virtue of its derivation based in part on the incident PAR, ETR is zero in the dark. Observed ETR values are in line with those previously reported (i.e., Nilkens *et al*., 2010). However, relative differences in ETR are more informative in the context of this work. While linear electron transport proceeds alongside coupled NPQ formation, ETR and NPQ induction kinetics, at least in low light, are not closely intercorrelated.

Cyclic electron transport is derived from the PSI quantum yield of NPQ in electron-limited RC's (donor-side limitation), which represents one of three complementary quantum yields of energy conversion in PSI (Kramer *et al*., 2004). The P700 signal ranges from its minimal oxidation state (0) during complete P700 reduction in the dark and increases to a given maximal state (≤ 1) during oxidation in the light (Figure 3.6E). In contrast to linear electron transport, changes in P700 oxidation (Figure 3.6E) influenced by linear electron transport correlate relatively closely with NPQ formation (Figure 3.6A) and are therefore particularly informative of changes in NPQ over a range of intensities. Indeed, initial peak transient P700 oxidation at 53 μmol quanta m^{-2} s^{-1} (~ 0.25; Figure 3.6F) fits with transient NPQ formation under these conditions. This reflects transient limitation of electron transfer on the acceptor-side of PSI in low light (Klughammer and Schreiber, 2008; Schreiber and Klughammer, 2008) as well as downstream ATP synthesis and CO_2 fixation during the Calvin-Benson cycle (Avenson *et al*., 2005). At higher intensities above 100 μmol quanta m^{-2} s^{-1}, electron transfer on the donor-side of PSI becomes increasingly limited (Klughammer and Schreiber, 2008), consistent with increasing P700 oxidation (Figure 3.6E).

3.2.2.2 ECS-based Characterization of the Dynamics of *pmf* Partitioning *in vivo*

Measurements of the ECS peaking at 515 nm enabled more detailed study of *pmf* partitioning into the ΔpH and Δψ. This is particularly important during early light-induced NPQ formation because it will clarify the hypothesized role of Δψ in early qE regulation *in vivo*, at least under specific conditions to include low light. The resulting work will give further insight into qE regulation mediated by changes in *pmf* partitioning, as proposed by Cruz *et al*. (2001). The ECS was monitored for 1-1200 s of actinic illumination at 53-1287 μmol quanta m^{-2} s^{-1}, followed by 5 min of dark relaxation in detached leaves of Col-0 *Arabidopsis*. The dynamics of Δψ and ΔpH contributions to the light-induced *pmf*, lumen pH, and proton conductance (g_H^+) through the ATP synthase were derived from key DIRK parameters, as described in 2.4.2 and shown in Figure 2.2.

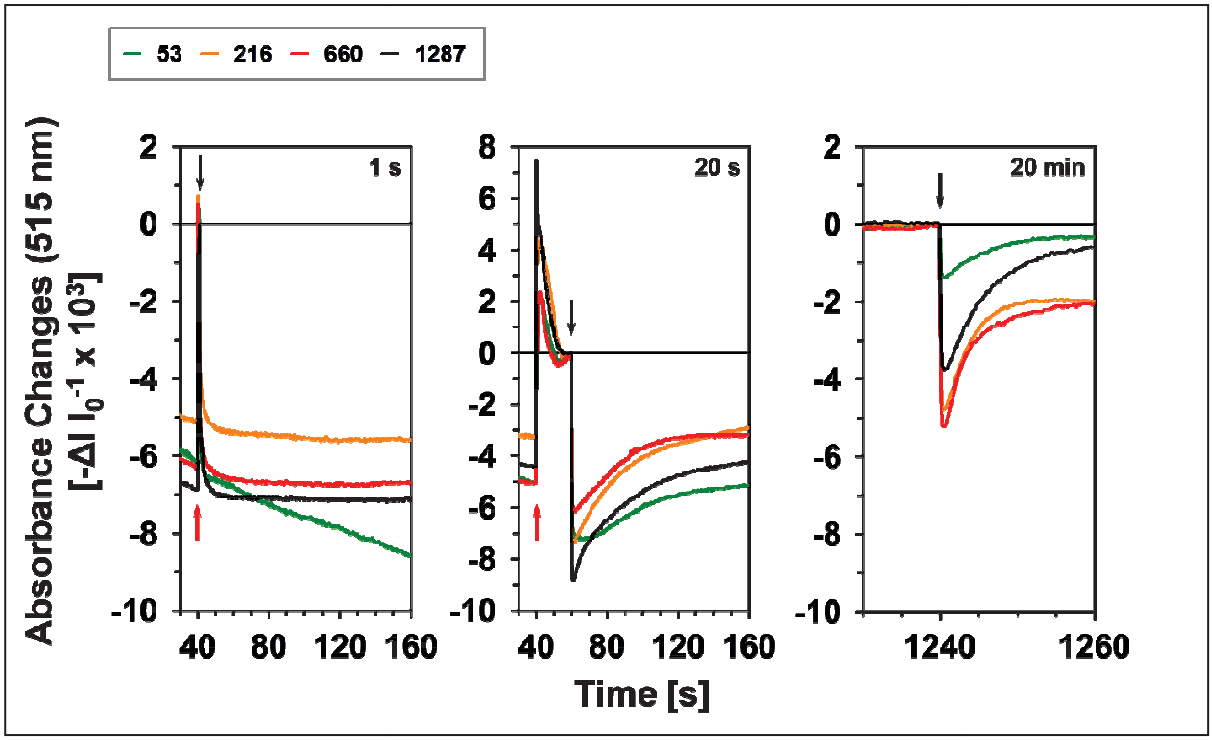

Figure 3.7 – The electrochromic shift (ECS) at 515 nm *in vivo* in *Arabidopsis*. Changes in the ECS signal during and after 1 and 20 s as well as after 20 min of actinic illumination at 53-1287 μmol quanta m^{-2} s^{-1} were measured in detached Col-0 leaves. Inset red and black arrows represent the onset and end of the illumination period. Absorbance changes were always normalized to the light off point. Light intensity values in the legend are expressed in μmol quanta m^{-2} s^{-1}. Curves represent single exemplary traces for illustration purposes only.

Characteristic changes in the ECS with prolonged illumination at low and higher intensities are clearly shown by raw representative traces (Figure 3.7). Analyses of such kinetics during the light-off (DIRK) phase clearly show that the amplitude of the rapidly decaying ECS signal following illumination (ECS_t) declines progressively with prolonged illumination at all intensities, particularly low light. The amplitude of this decay is related to the total *pmf*

established in the light (Cruz *et al*., 2001; Takizawa *et al*., 2007). It is assumed that the light-induced *pmf* is established largely by linear electron flow (Avenson *et al*., 2005), while cyclic electron flow is more important in *pmf* formation in low ambient CO_2 for instance. Concomitantly, a proportionate increase in the amplitude of the inverse portion of the decaying DIRK ECS signal (ECS_{inv}) below the baseline in the dark was observed. The amplitude of this decay has been related to the ΔpH fraction of the light-induced *pmf* that is consumed by continued proton efflux through the ATP synthase in the dark. Concomitantly, the relative contribution of the $\Delta\psi$ to the *pmf*, estimated as the difference between these two amplitudes, declines rapidly with prolonged illumination at all intensities from an all $\Delta\psi$-stored *pmf* after brief (i.e., 1 s) periods of illumination (Figure 3.7). The $\Delta\psi$ is progressively dissipated by light-activated counterion fluxes across the thylakoid membrane with prolonged illumination (i.e., 20 s or 20 min). Indeed, the relative ΔpH contribution to the *pmf* established within seconds of illumination in low and particularly high light is substantial.

The extent of the ECS signal is normalized to the amplitude of a 50 μs flash-induced absorbance change at 515 nm, which corresponds to one charge separation per photosystem and is defined as ECS-Unit. Analysis of DIRK ECS kinetics highlight a substantial transient increase in the total *pmf* within 60 s of illumination at all intensities (Figure 3.8B), which decreases thereafter to a lower steady-state level within 20 min (Figure 3.8A), particularly in low light. This transient ECS_t behaviour correlates with a transient increase in NPQ peaking after ~ 50 s in low light, but does not correlate as strongly with changes in NPQ at higher intensities. ECS_t is thus a good indicator of changes in NPQ formation in low light in particular. Notably, the total *pmf* was generally higher after 60 s leading to steady state at 216-1287 μmol quanta m^{-2} s^{-1} compared to 53 μmol quanta m^{-2} s^{-1} ($P < 0.05$; Figure 3.8A). This intensity effect on ECS_t is consistent with previous reports of an increasing steady-state ECS_t with increasing intensity in ambient air (Takizawa *et al*., 2007). However, the steady-state ECS_t is somewhat higher at 53-216 μmol quanta m^{-2} s^{-1} (Figure 3.8A) compared to previous estimates at comparable intensities in ambient air (Takizawa *et al*., 2007).

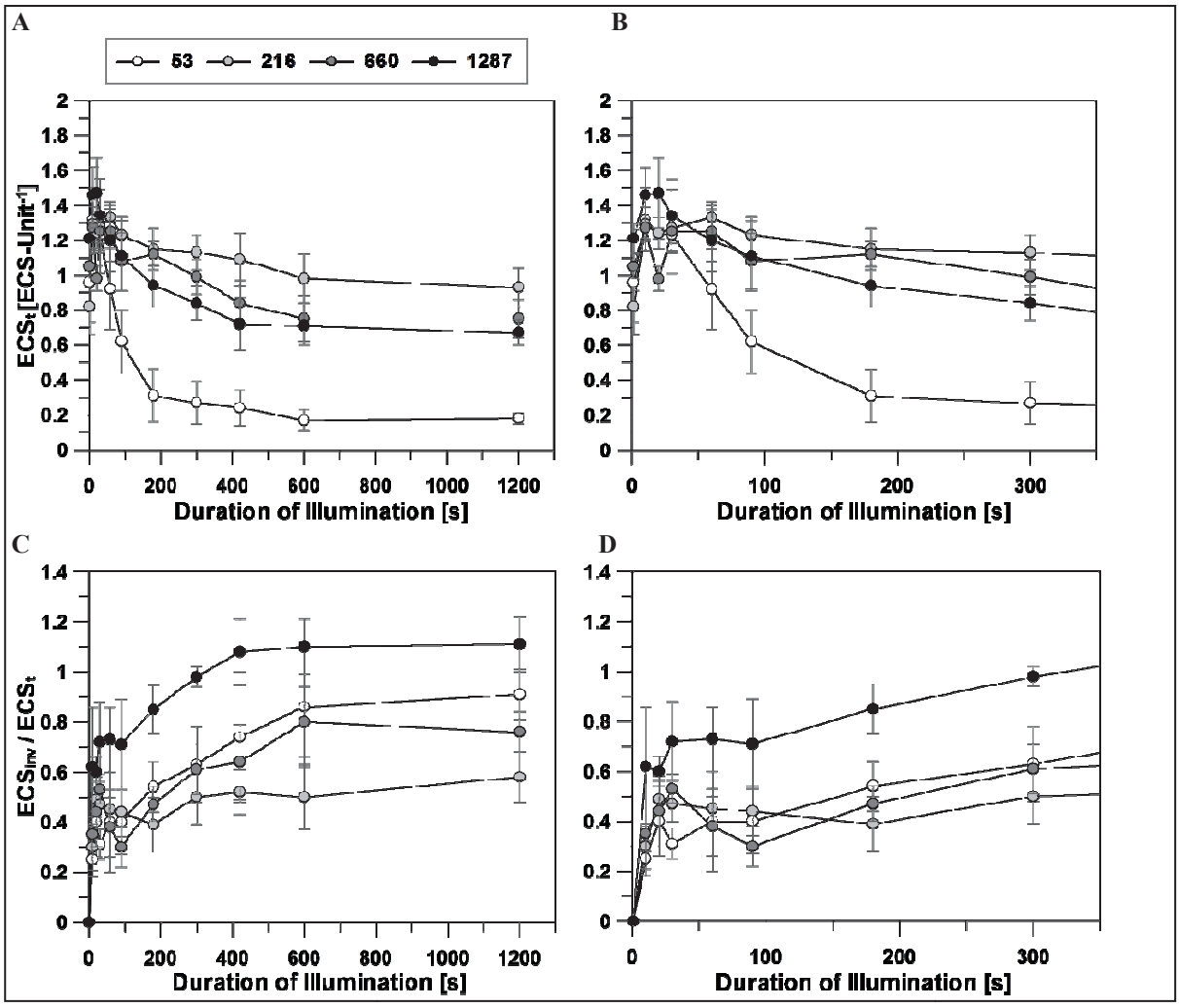

Figure 3.8 – Dynamics of proton motive force (*pmf*) formation and partitioning in the light *in vivo* in *Arabidopsis* derived from changes in the dark-interval relaxation kinetics (DIRK) of the electrochromic shift (ECS) at 515 nm. DIRK ECS analysis yields the (A-B) magnitude of the light-induced *pmf*, estimated from the flash-normalized amplitude of the rapid decay of the ECS signal during the light-dark transition (ECS_t), and (C-D) the relative contribution of the ΔpH fraction, estimated from the flash-normalized inverse portion of the DIRK ECS signal (ECS_{inv}), to the total *pmf* (ECS_{inv} / ECS_t). DIRK parameters were quantified in detached Col-0 leaves during 5 min of dark relaxation after 1-1200 s of actinic illumination at 53-1287 μmol quanta m^{-2} s^{-1}. Light intensity values in the legend are expressed in μmol quanta m^{-2} s^{-1}. Curves represent mean values ± standard deviation (SD) of at least four replicates from two or more independent experiments.

Quantification of the amplitude of the inverse portion of the DIRK ECS signal (ECS_{inv}), related to the ΔpH fraction of the total light-induced *pmf*, in relation to ECS_t highlights the dynamic nature of *pmf* partitioning during prolonged illumination at various intensities. In particular, there is a rapid early transient increase in the estimated ΔpH contribution to the *pmf* (Figure 3.8D). This coincides with the transient increase in the early light-induced *pmf* at all intensities. The relative ΔpH contribution to the *pmf* continues to increase thereafter at a slower rate to a final intensity-dependent steady-state level (Figure 3.8C). This relative ΔpH contribution is similar at 53-660 μmol quanta m^{-2} s^{-1}, particularly during the initial ~ 20 s of illumination, but is generally higher early on and during prolonged illumination at 1287 μmol

quanta m^{-2} s^{-1} compared to lower intensities (Figure 3.8D). Strikingly, the dynamics of *pmf* partitioning in low light correlate poorly with transient NPQ formation in low light, but correlate more clearly with NPQ formation at higher intensities.

Analysis of steady-state *pmf* partitioning indicates a higher (~ 75-80 %; Figure 3.8C) than previously reported (~ 50 %) contribution of the ΔpH to the steady-state *pmf* observed above 400 μmol quanta m^{-2} s^{-1} under ambient air conditions *in vivo* in *Arabidopsis* (Takizawa *et al*., 2007). However, detached leaves enclosed in the measuring cuvette may have been limited in atmospheric CO_2 exchange. Thus low CO_2 levels may explain the generally higher estimates of the relative ΔpH contribution to the *pmf* at all intensities under low CO_2 conditions, as reported previously (Takizawa *et al*., 2007). However, a steady-state *pmf* stored in excess of 100 % as the ΔpH at 1287 μmol quanta m^{-2} s^{-1} (Figure 3.8C) is not possible and may not be solely explained by low CO_2 availability. Rather, an overshoot of the slowly decaying DIRK ECS signal at steady state was observed in certain cases, where the amplitude of ECS_{inv} is greater than that of ECS_t, thus skewing overall estimates of the relative ΔpH contribution to *pmf*. However, such cases were not excluded because they may not necessarily be outliers for any particular reason. Nevertheless, existing data indicates that ~ 40 % of the *pmf* is stored as the ΔpH during the initial 60 s of illumination at 53-660 μmol quanta m^{-2} s^{-1} (Figure 3.8D). This suggests that ~ 60 % of the *pmf* can be stored as the $\Delta\psi$ under these conditions. Such a substantial $\Delta\psi$ contribution to the *pmf* is consistent with previous reports of a persistent $\Delta\psi$ contribution to the *pmf* over a range of conditions (i.e., Cruz *et al*., 2001; Takizawa *et al*., 2007). It is possible that the formation of a proportionately higher $\Delta\psi$ fraction of the *pmf* may significantly contribute to early qE formation during light activation of photosynthesis, as originally hypothesized. However, this remains to be confirmed in future *in vivo* study of qE regulation via changes in *pmf* partitioning.

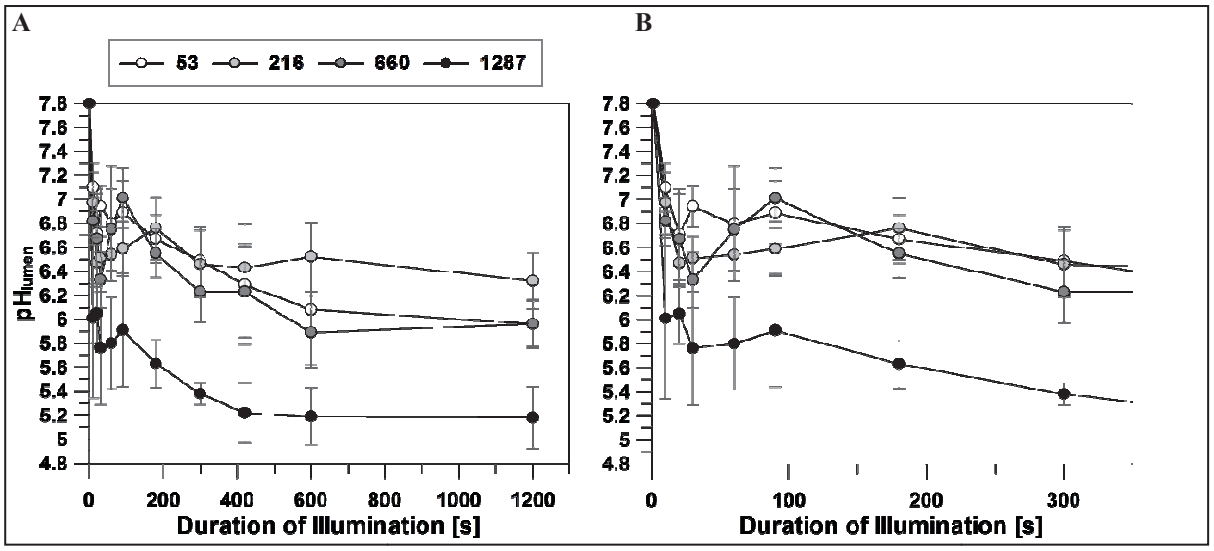

Figure 3.9 – Changes in the lumen pH *in vivo* in *Arabidopsis* derived from changes in the dark-interval relaxation kinetics (DIRK) of the electrochromic shift (ECS) at 515 nm. The lumen pH was derived according to Takizawa *et al*. (2007). Changes in the lumen pH were assessed in detached Col-0 leaves during the 5 min dark relaxation interval after (A) 1-1200 s of actinic illumination at 53-1287 μmol quanta m^{-2} s^{-1}, with an emphasis on the initial (B) 1-300 s of illumination. Light intensity values in the legend are expressed in μmol quanta m^{-2} s^{-1}. Curves represent mean values ± standard deviation (SD) of at least four replicates from two or more independent experiments.

Changes in the lumen pH in the light *in vivo*, derived from key DIRK ECS parameters according to Takizawa *et al*. (2007), offer a clear overview of lumenal processes related to qE regulation at the proton level. Lumen acidification follows changes in the relative contribution of the ΔpH to the total *pmf*. The rapid decline in the lumen pH (Figure 3.9B) leading to increasing ΔpH formation in relation to the total *pmf* is comparable during the initial ~ 30 s as well as after 180 s at 53-660 μmol quanta m^{-2} s^{-1}. However, a more pronounced decline in the lumen pH was observed already after 10 s leading to steady state at 1287 μmol quanta m^{-2} s^{-1} ($P < 0.01$; Figure 3.9A). This is consistent with an increased ΔpH contribution to the *pmf* under these conditions, although the extent of NPQ formed during the initial ~ 30-50 s is similar across all intensities. This indicates that NPQ induction is delayed in relation to lumen acidification on the order of tens of seconds. Furthermore, increasing lumen acidification to a comparable degree after 180 s at 53-660 μmol quanta m^{-2} s^{-1} does not account for declining transient NPQ after ~ 60 s at 53 μmol quanta m^{-2} s^{-1}.

Steady-state estimates of the lumen pH *in vivo* range from ~ 5.2 to 6.4, assuming a stromal pH of 7.8. These estimates are ~ 1 pH unit lower overall than what has been reported previously under comparable ambient conditions *in vivo* in *Arabidopsis* (Takizawa *et al*., 2007) and may in large part arise from limited CO_2 availability in the measuring cuvette. Indeed, a steady-state lumen pH of < 6.0 was estimated *in vivo* at > 400 μmol quanta m^{-2} s^{-1}

under low ambient CO_2 conditions, assuming a stromal pH of 7.6 (Takizawa *et al*., 2007). However, a highly acidic lumen at the lowest and particularly the highest intensity, though consistent with a largely if not all ΔpH-stored steady-state *pmf*, is difficult to reconcile with previous reports and may not be exclusively attributed to limited CO_2 availability. Other possibilities are discussed in 4.3.1. Regardless, it is thus clear that the dynamics of light-induced lumen acidification are not clearly correlated with observed changes in NPQ formation under certain conditions (i.e., limiting light).

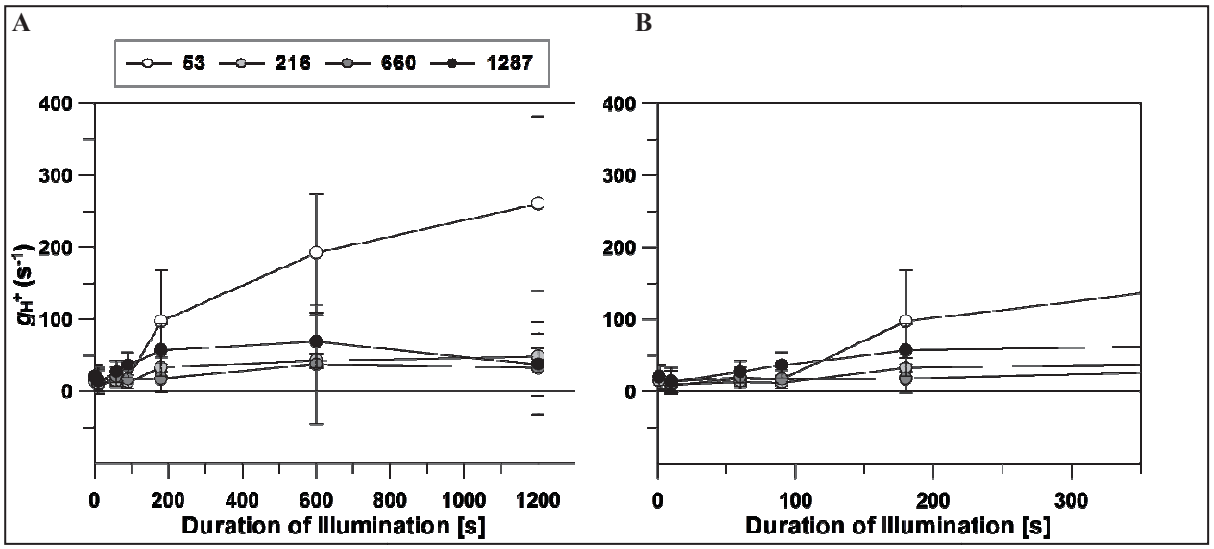

Figure 3.10 – Dynamics of proton conductance (g_H^+) through the ATP synthase *in vivo* in *Arabidopsis* derived from changes in the dark-interval relaxation kinetics (DIRK) of the electrochromic shift (ECS) at 515 nm. Proton conductance was calculated as the inverse of the time (s) required for the amplitude of the 515 nm ECS signal (ECS_t) to decay to $1/\tau$, where τ = e, or ~ 40% of its initial value during the dark relaxation phase (Kanazawa and Kramer, 2002). Changes in g_H^+ were assessed in detached Col-0 leaves during the 5 min dark relaxation interval after (A) 1-1200 s of actinic illumination at 53-1287 μmol quanta m^{-2} s^{-1}, with an emphasis on the initial (B) 1-300 s of illumination. Light intensity values in the legend are expressed in μmol quanta m^{-2} s^{-1}. Curves represent mean values ± standard deviation (SD) of at least three replicates from two or more independent experiments.

The establishment of a ΔpH due to lumen acidification during actinic illumination drives proton conductance (g_H^+), largely modulated by the ATP synthase (Kanazawa and Kramer, 2002). Changes in g_H^+ are therefore important to understanding changes in the ΔpH *in vivo*. g_H^+ is shown to increase from ~ 15-17 s^{-1} after 1 s of illumination to ~ 260 s^{-1} after 20 min at 53 and as low as and ~ 40 s^{-1} after 20 min at 216-1287 μmol quanta m^{-2} s^{-1} ($P < 0.05$; Figure 3.10A-B). This ~5-7-fold difference in steady-state g_H^+ between low and higher intensities is more pronounced compared to previous reports of a reduction in steady-state g_H^+ from ~ 85 s^{-1} at 45 μmol quanta m^{-2} s^{-1} to ~ 55 s^{-1} at 800 μmol quanta m^{-2} s^{-1} *in vivo* in ambient air (Kanazawa and Kramer, 2002). Clearly, a reduced steady-state g_H^+ at higher, more saturating intensities cannot be solely explained by the downregulatory effect of higher, more saturating

intensities on the linear electron transport chain and coupled ATP synthase activity driven by proton efflux. Rather, such a large difference in steady-state g_H^+ may be reconciled by increased noise of the decaying DIRK ECS signal, as shown most clearly after prolonged illumination in low light. Accurate curve fitting of ECS decay and estimation of the time constant for ECS decay can thus vary greatly, as reflected by high sample variation under these conditions. This may explain such a high g_H^+ at steady state in low light.

Limited CO_2 availability during ECS measurements, which may have contributed to an increased ΔpH fraction and thus more pronounced lumen acidification at steady state (Figures 3.8C and 3.9A), can further limit g_H^+ in addition to the effect of light intensity. Indeed, a substantially reduced g_H^+ was observed over a range of intensities *in vivo* in *Arabidopsis* under low compared to ambient CO_2 conditions (Kanazawa and Kramer, 2002). This discrepancy is particularly evident at lower intensities. However, a substantially higher steady-state g_H^+ was observed in low light (Figure 3.10A) compared to previous steady-state estimates of g_H^+ in low light *in vivo* under low CO_2 conditions (Kanazawa and Kramer, 2002). This indicates a minor, if any effect of CO_2 availability on g_H^+, such that CO_2 levels may not have been severely limited during prolonged measurements. Nevertheless, increasing g_H^+ after 90 s in low light reflects increasing thioredoxin-dependent light-activated ATP synthase activity (Nikkanen and Rintamäki, 2014). This correlates with a reduction in transient NPQ after ~ 60 s in low light. Sustained reductions in g_H^+ during prolonged illumination in high light are consistent with increasing NPQ formation in more saturating light. ECS analyses of g_H^+ thus indicate that light-induced changes in g_H^+ generally correlate with observed kinetics of NPQ induction in limiting and saturating light.

3.2.2.3 Characterization of pH-Dependent Changes in Xanthophyll Cycle Activity

To assess changes in xanthophyll cycle conversion, specifically lumen pH-dependent Z_X formation, with respect to qE formation, the DEPS of the total VAZ pool was assessed in Wt over a comparable time and intensity range as that used to study NPQ. The DEPS, reflecting the levels of de-epoxidized Z_X and A_X, is a critical measure underlying changes in lumen pH. Pigment content was characterized in detached Wt leaves illuminated for 10-1200 s at ~ 50-1200 μmol quanta m^{-2} s^{-1}. Analysis of pigment data highlights a clear, intensity-dependent increase in DEPS with prolonged illumination, particularly after 20 min of illumination at 660 and 1287 μmol quanta m^{-2} s^{-1} ($P < 0.01$) compared to 53 μmol quanta m^{-2} s^{-1} (Figure 3.11). DEPS increased sharply during the initial 60 s of illumination at higher intensities, particularly at 660 μmol quanta m^{-2} s^{-1} ($P < 0.001$). This is consistent with the rapid increase in the ΔpH contribution to the light-induced *pmf* and thus lumen acidification under these conditions, particularly at higher intensities. However, DEPS showed a delayed increase during the initial 60 s at 53 μmol quanta m^{-2} s^{-1}. This reflects delayed early V_XDE activation.

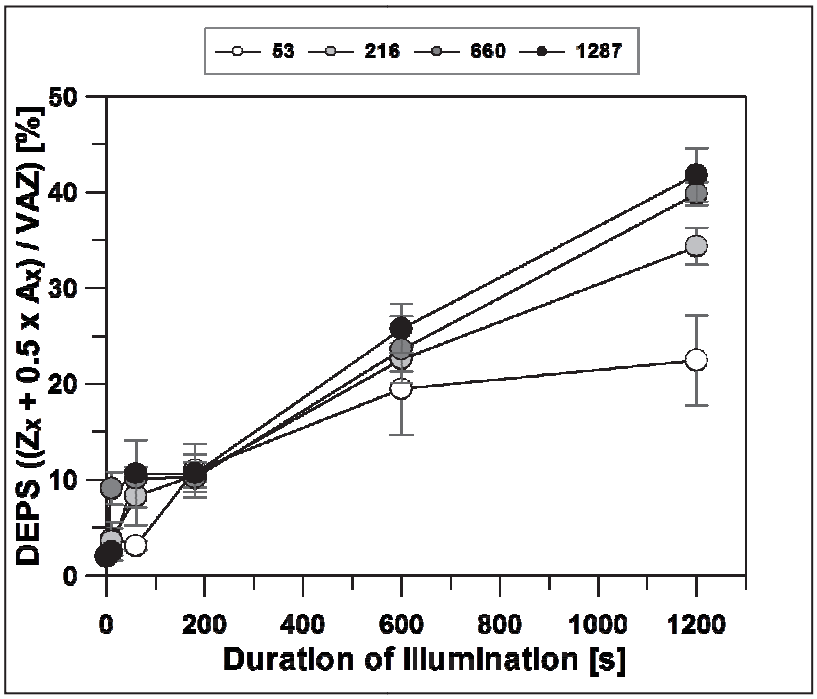

Figure 3.11 – The de-epoxidation state (DEPS) *in vivo* in *Arabidopsis*. DEPS is derived from the total xanthophyll pigment pool consisting of violaxanthin (V_X), antheraxanthin (A_X), and zeaxanthin (Z_X), denoted as VAZ. Pigment content was evaluated in dark-adapted and illuminated homogenized Col-0 leaves using RP-HPLC, as described in 2.6.2. DEPS = $[Z_X + (0.5 \times A_X)]$/VAZ. Light intensity values in the legend are expressed in μmol quanta m^{-2} s^{-1}. Curves represent means ± standard deviation (SD) of at least three replicates from two or more independent experiments.

Lumen acidification promotes accumulation of Z_X required for stable qE formation in more saturating light. DEPS data in support of ECS data highlight the independence between early NPQ formation and pH-dependent Z_X accumulation, as a lower lumen pH is required for qE compared to V_XDE activation (Takizawa *et al*., 2007). Rather, other underlying processes in addition to rapid early lumen acidification are comparatively more important in early qE regulation, particularly under limiting light conditions. Existing findings underscore the importance of, but not exclusive dependence on lumen acidification and Z_X in modulating qE responses, particularly during early light activation of photosynthesis.

3.2.2.4 NPQ and Electron Transport *in vivo* in *Arabidopsis* Mutants

The kinetics of NPQ and linear and cyclic electron transport were thus far examined in detail in Wt *Arabidopsis* over a range of intensities. The dynamics of *pmf* partitioning under corresponding light conditions have been characterized in relation to the induction kinetics of NPQ and electron transport in Wt. To gain further insight into light-dependent processes involved in qE regulation, it is important to examine the kinetics of NPQ and electron transport impacted by defects in cyclic electron transport, cytochrome b_6f, PsbS, and xanthophyll cycle activities. This is critical to further understanding the impacts of mutant-specific changes in cyclic and linear electron transport and coupled energy dissipation as well as xanthophyll conversion on *pmf* partitioning. It is then important to assess the role of $\Delta\psi$ during early qE-activation, taking into account these individual mutant-specific defects. Thus, NPQ and cyclic electron transport around PSI inferred from the P700 oxidation state were measured simultaneously using the DUAL-PAM-100 system. Kinetics were monitored in detached Wt and mutant leaves for 1-1200 s of actinic illumination at 53 and 660 μmol quanta m^{-2} s^{-1}, followed by 10 min of dark relaxation.

Analysis of NPQ kinetics in Wt and various mutant lines highlights well-known intensity-dependent formation and relaxation of NPQ as well as differences in NPQ kinetics characteristic to various mutant lines relative to their corresponding Wt backgrounds. Impaired cyclic electron transport around PSI in both *pgr5* and *pgrl1ab #273* (Munekage *et al*., 2002; DalCorso *et al*., 2008) is reflected by reduced peak transient NPQ formation in both lines established after ~ 50-60 s of illumination at 53 μmol quanta m^{-2} s^{-1} (~ 0.20-0.30; $P < 0.05$; Figures 3.12B and 3.12D) compared to Wt (~ 0.50; Figures 3.12A and 3.12C). Initial NPQ formation in high light was somewhat reduced in both lines, which also showed minor reductions in maximal steady-state NPQ in high light compared to Wt, consistent with previous reports (i.e., DalCorso *et al*., 2008). Relaxation of NPQ in low light appears to be slightly delayed in *pgr5* and *pgrl1ab #273* compared to Wt, such that NPQ relaxes to a slightly higher level in the dark following illumination in both mutants (Figures 3.12B and 3.12D). Overall, these findings underscore the contribution of lumen acidification to NPQ formation, particularly in low light, due to proton influx at cytochrome b_6f mediated in part by *PGR5*- and *PGRL1*-dependent cyclic electron transport (DalCorso *et al*., 2008).

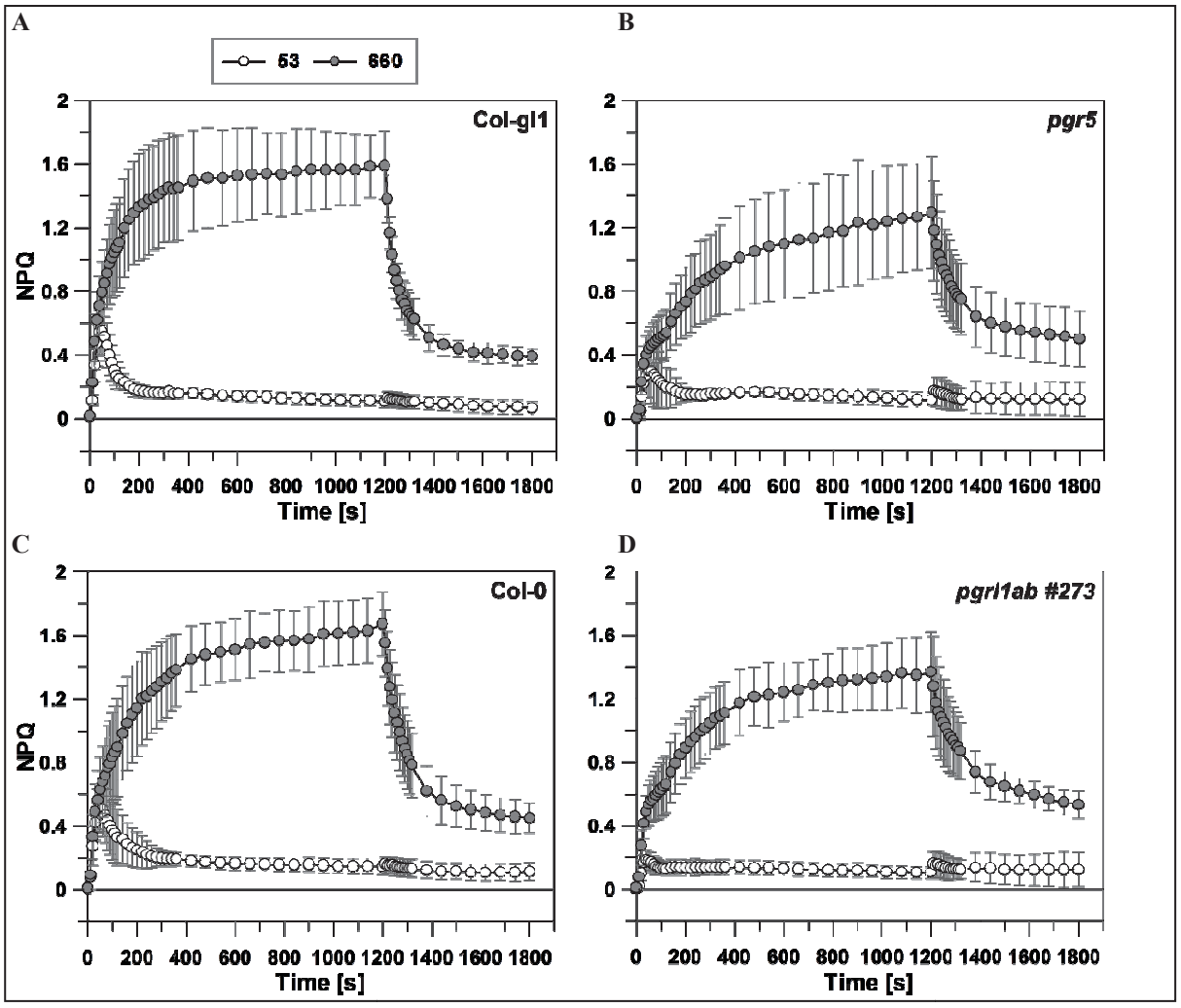

Figure 3.12 – Kinetics of non-photochemical quenching (NPQ) *in vivo* in *Arabidopsis*. Kinetics were monitored during 20 min of actinic illumination at 53 and 660 μmol quanta m^{-2} s^{-1} and 10 min of dark relaxation in detached leaves of (A) Col-gl1, (B) *pgr5*, (C) Col-0, and (D) *pgrl1ab #273*. Light intensity values in the legend are expressed in μmol quanta m^{-2} s^{-1}. Curves represent mean values ± standard deviation (SD) of at least four replicates from two or more independent experiments.

Well-known NPQ induction and relaxation kinetics are also displayed by the *pgr1*, *L17*, and *npq* mutant lines of *Arabidopsis* (Figure 3.13B-E) studied previously over a range of conditions (Niyogi *et al*., 1998; Kalituho *et al*., 2007; Nilkens *et al*., 2010). A defect in cytochrome b_6f limits ΔpH formation in *pgr1* (Munekage *et al*., 2001). The importance of the ΔpH in NPQ in low and high light is consistent with a lack of transient NPQ formation at 53 μmol quanta m^{-2} s^{-1} as well as a slow increase in and reduced steady-state NPQ in *pgr1* at 660 μmol quanta m^{-2} s^{-1} ($P < 0.001$; Figure 3.13B). Overexpression of PsbS, crucial to the qE response, in *L17* is thus reflected by increased peak transient NPQ formation in low light (~ 0.70; $P < 0.05$; Figure 3.13C). NPQ established rapidly in high light in *L17* is ~ 2-fold higher at steady state compared to Wt ($P < 0.001$; Figure 3.13C), as shown before (Li *et al*., 2002; Nilkens *et al*., 2010). In contrast, the PsbS-deficient *npq4* mutant (Li *et al*., 2000) displayed a

lack of transient NPQ formation in low light and reduced steady-state NPQ in high light ($P < 0.001$; Figure 3.13D). This highlights the importance of the PsbS to transient and stable NPQ formation in low and high light, respectively (Kalituho *et al*., 2007; Nilkens *et al*., 2010).

In addition to the ΔpH and PsbS, it is equally important to consider the contribution of Z_X to NPQ formation in low and high light. Sustained accumulation of Z_X due to impaired Z_XE activity in *npq2* (Niyogi *et al*., 1998) corresponds to enhanced peak transient NPQ in low light in *npq2* (~ 0.80; $P < 0.01$). This highlights the importance of Z_X accumulation in LHCII in transient NPQ formation in low light (Kalituho *et al*., 2007). As a consequence, NPQ was more rapidly established initially in high light in *npq2* (Figure 3.13E). However, steady-state NPQ in high light was markedly decreased in *npq2* (~ 1.30; $P < 0.001$; Figure 3.13E) compared to Wt (~ 1.60; Figure 3.13A), as shown previously (Nilkens *et al*., 2010). This may be due to permanent accumulation of Z_X even in the dark, which may limit qE capacity in the light. NPQ relaxed more slowly in *npq2* after high as well as low light illumination (Figure 3.13E), as reported previously in *npq2* following high light exposure (Johnson *et al*., 2009). Conversely, impaired V_XDE activity and thus limited Z_X formation displayed by *npq1* (Niyogi *et al*., 1998) leads to a reduction in peak transient NPQ in low light (~ 0.35; $P < 0.01$; Figure 3.13F). Steady-state NPQ formation in high light is thus reduced in *npq1* ($P < 0.001$), consistent with previous findings (Niyogi *et al*., 1998; Kalituho *et al*., 2007), despite more rapid initial NPQ induction in high light and subsequent NPQ relaxation in the dark compared to Wt. This underscores the importance of Z_X formation in transient and longer-term NPQ formation in low and high light, respectively, predominantly controlled by the ΔpH and PsbS activity.

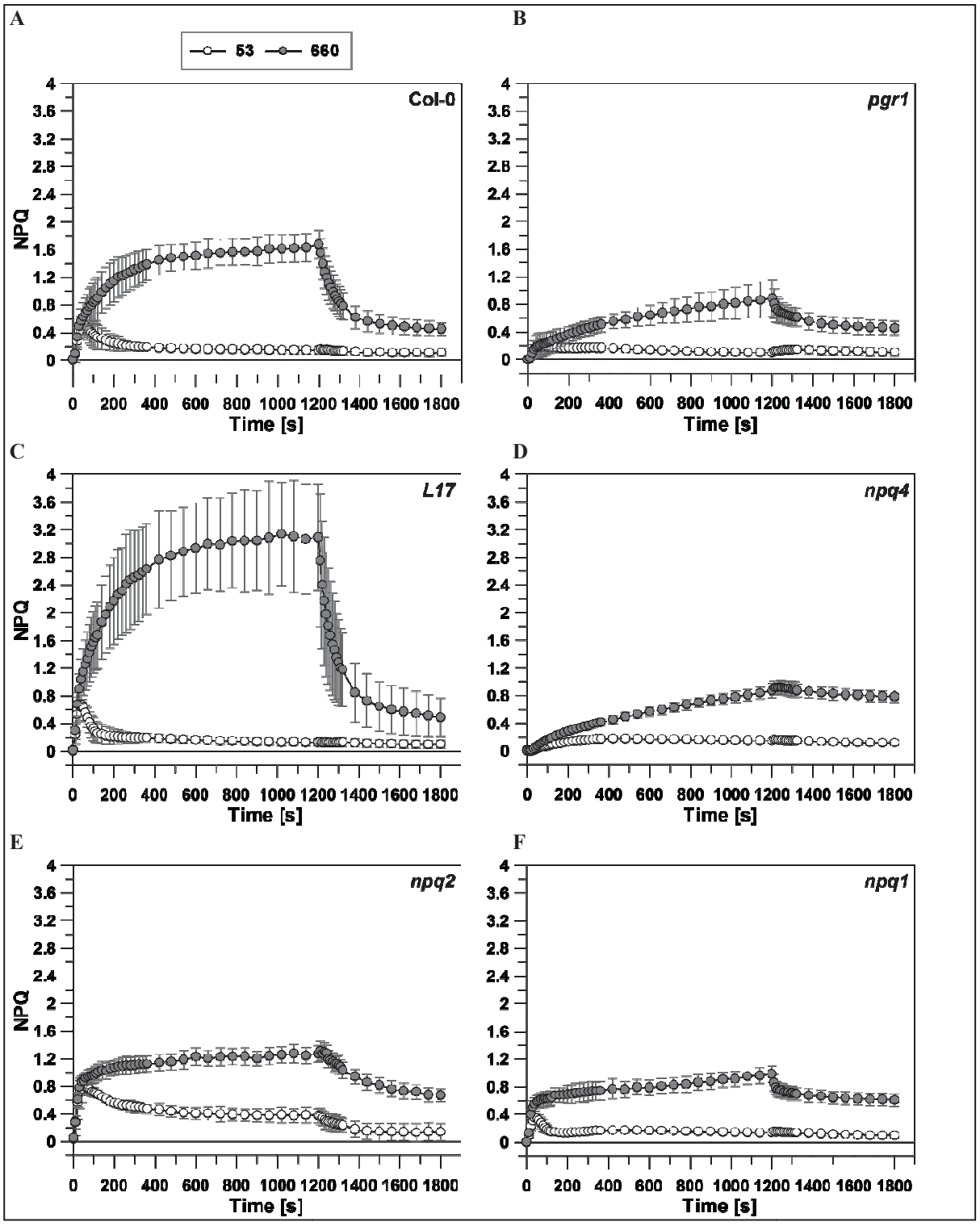

Figure 3.13 – Kinetics of non-photochemical quenching (NPQ) *in vivo* in *Arabidopsis*. Kinetics were monitored during 20 min of actinic illumination at 53 and 660 μmol quanta m^{-2} s^{-1} and 10 min of dark relaxation in detached leaves of (A) Col-0, (B) *pgr1*, (C) *L17*, (D) *npq4*, (E) *npq2*, and (F) *npq1*. Light intensity values in the legend are expressed in μmol quanta m^{-2} s^{-1}. Curves represent mean values ± standard deviation (SD) of at least four replicates from two or more independent experiments.

P700 oxidation as an indirect measure of cyclic electron transport around PSI that closely follows changes in NPQ provides important information concerning NPQ regulation by electron transport in select mutants of *Arabidopsis*. While certain mutant lines do not show any characteristic differences in P700 oxidation compared to Wt, others show unique differences that are informative of early light-regulated processes involved in qE, particularly in low light. Most notably, impaired cyclic electron transport in *pgr5* and *pgrl1ab #273* is reflected by a sustained increase in P700 oxidation at 53 μmol quanta m^{-2} s^{-1} in both lines (Figures 3.14B and 3.14D) compared to Wt (Figures 3.14A and 3.14C). This is due to impaired cyclic electron flow arising from impaired recovery of permanently reduced PSI acceptor sites even in the dark (DalCorso *et al*., 2008). This confirms the observed reduced peak transient NPQ formed in low light in *pgr5* and *pgrl1ab #273* and thus the importance of cyclic electron transport in lumen acidification and transient NPQ formation in low light. As electron transfer on the donor side of PSI is increasingly limited above 100 μmol quanta m^{-2} s^{-1}, sustained reduction of PSI acceptor sites due to impaired cyclic electron transport leads to slow P700 oxidation in high light in *pgrl1ab #273*. In contrast, *pgr5* showed rapid initial P700 oxidation in high light. Regardless, both mutants showed markedly reduced P700 oxidation in high light ($P < 0.001$; Figures 3.14B and 3.14D), as reported previously (Munekage *et al*., 2002; DalCorso *et al*., 2008). Accompanying reductions in linear electron transport in *pgr5* and *pgrl1ab #273* in high light ($P < 0.05$; data not shown; DalCorso *et al*., 2008) may reflect a reduced contribution of cyclic electron flow to linear electron flow-driven proton translocation at cytochrome b_6f.

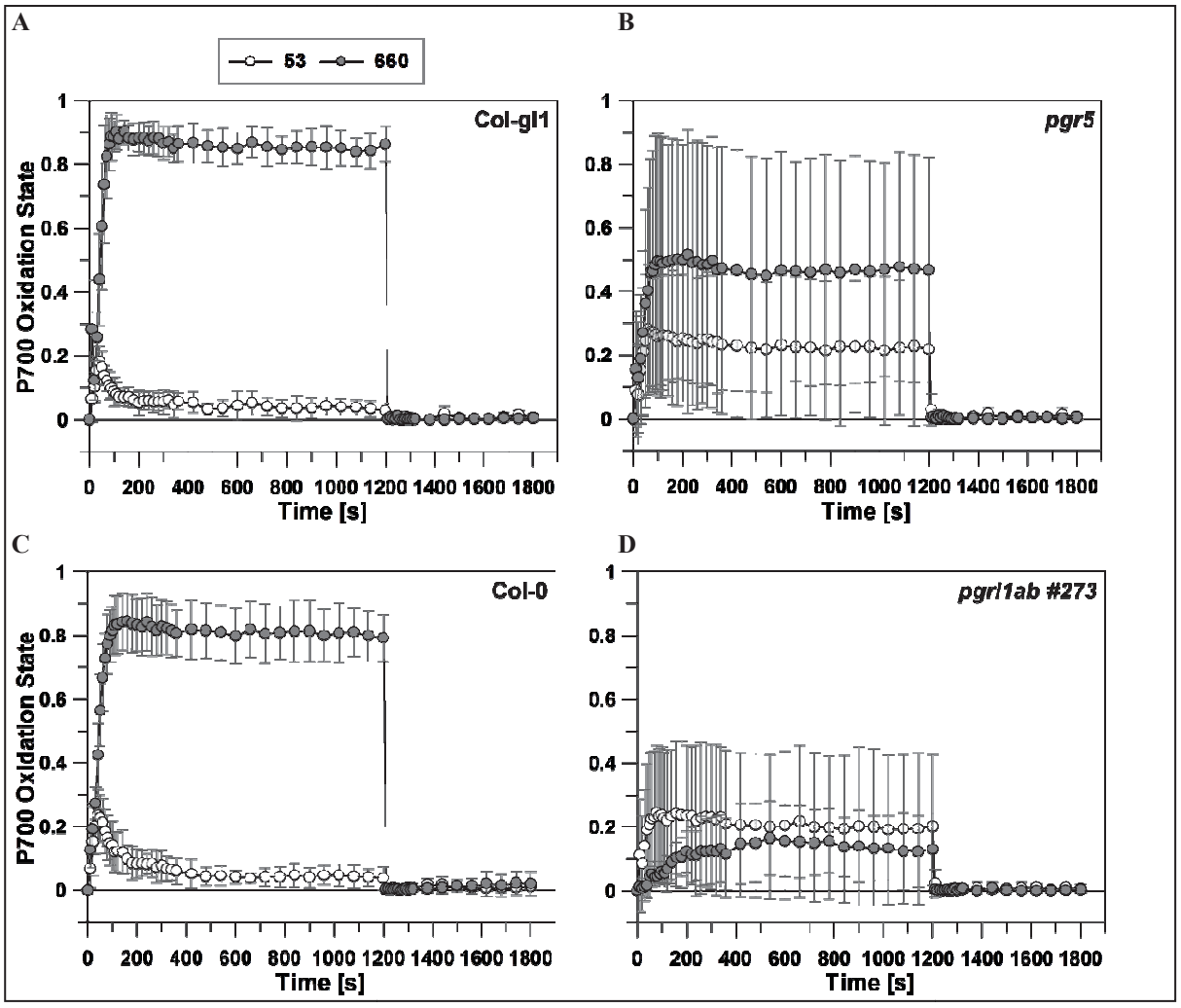

Figure 3.14 – Kinetics of the P700 oxidation state derived from measurements of PSI quantum yield based on donor-side limitation *in vivo* in *Arabidopsis*. Kinetics were monitored during 20 min of actinic illumination at 53 and 660 μmol quanta m^{-2} s^{-1} and 10 min of dark relaxation in detached leaves of (A) Col-gl1, (B) *pgr5*, (C) Col-0, and (D) *pgrl1ab #273*. Light intensity values in the legend are expressed in μmol quanta m^{-2} s^{-1}. Curves represent mean values ± standard deviation (SD) of at least four replicates from at least two independent experiments.

The cytochome b_6f-deficient *pgr1* mutant displayed increased peak transient P700 oxidation in low light (~ 0.35; $P < 0.05$; Figure 3.15B) compared to Wt (~ 0.25; Figure 3.15A). This may be due to increased PSI acceptor-side limitation and thus reduced cyclic electron transport arising from a defect in cytochrome b_6f. As cyclic electron flux has been implicated in transient NPQ formation in low light, these findings are consistent with reduced peak transient NPQ in low light in *pgr1*. Reduced linear electron flow at cytochrome b_6f in *pgr1* in high light ($P < 0.05$; data not shown), as shown previously by Munekage *et al*. (2001), would exacerbate PSI donor-side limitation of electron flow in high light. This would raise the steady-state P700 oxidation level observed in high light in *pgr1* ($P < 0.05$; Figure 3.15B). Linear and cyclic electron transport is thus limited by cytochrome b_6f activity (Munekage *et al*., 2001), which regulates the ΔpH and thus qE.

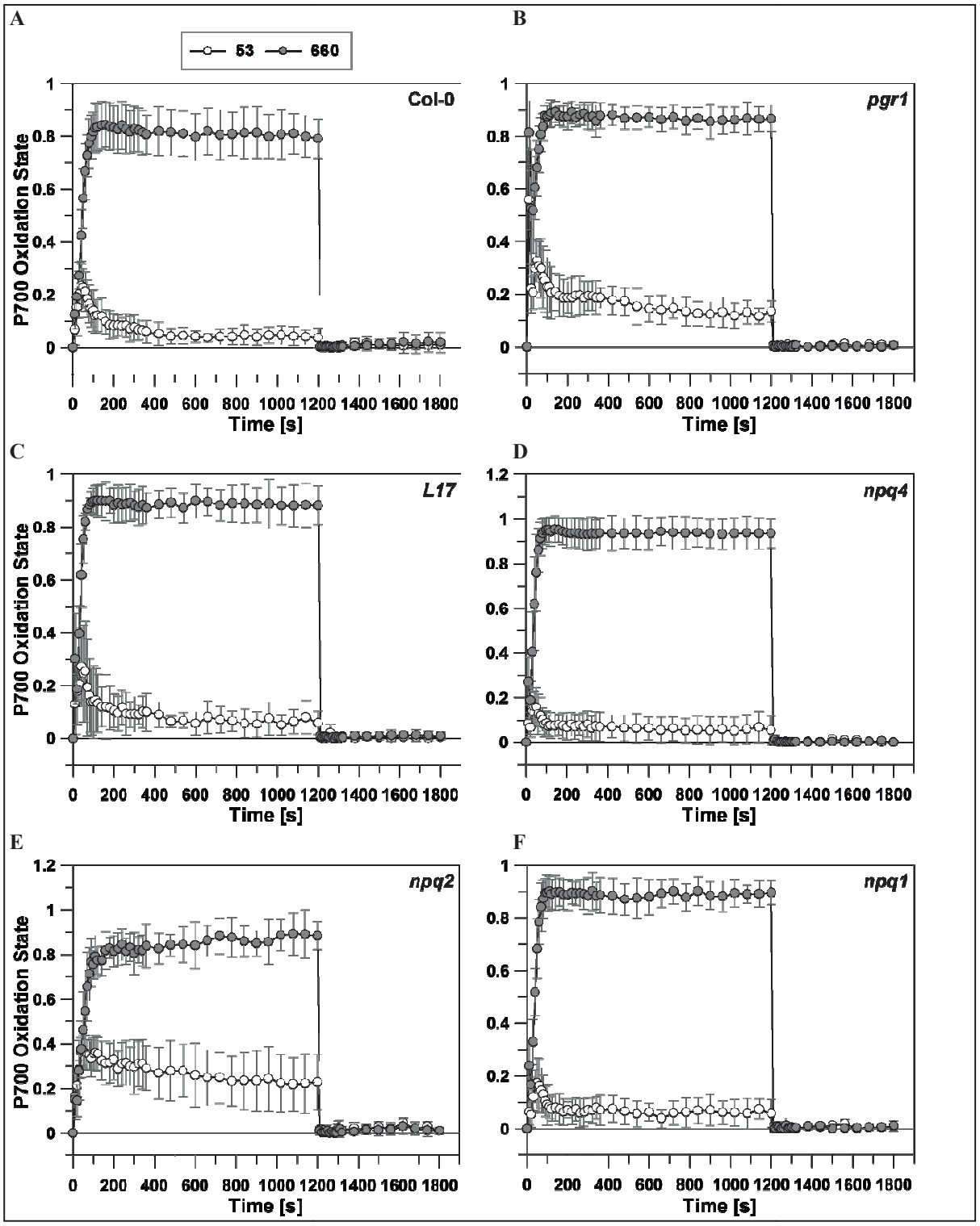

Figure 3.15 – Kinetics of the P700 oxidation state derived from measurements of PSI quantum yield based on donor-side limitation *in vivo* in *Arabidopsis*. Kinetics were monitored during 20 min of actinic illumination at 53 and 660 μmol quanta m^{-2} s^{-1} and 10 min of dark relaxation in detached leaves of (A) Col-0, (B) *pgr1*, (C) *L17*, (D) *npq4*, (E) *npq2*, and (F) *npq1*. Light intensity values in the legend are expressed in μmol quanta m^{-2} s^{-1}. Curves represent mean values ± standard deviation (SD) of at least four replicates from two or more independent experiments.

In addition to *pgr1*, *npq2* showed clearly altered P700 oxidation kinetics compared to Wt. Permanent accumulation of Z_X in *npq2* is also characterized by increased P700 oxidation in low light in *npq2* (~ 0.35; $P < 0.01$, Figure 3.15E) compared to Wt (Figure 3.15A). This corresponds to increased peak transient NPQ in low light in *npq2* and reflects reduced cyclic electron transport due to reduced or inefficient early linear electron transport limited by sustained Z_X-dominated quenching in low light in *npq2* (Kalituho *et al*., 2007). An enhanced rate of linear electron transport was observed at steady state in high light in *npq2* ($P < 0.01$; data not shown), as reported previously (Nilkens *et al*., 2010). This may exacerbate limitation of PSI donor-side electron transfer, which would contribute to increased steady-state P700 oxidation, as observed in high light in *npq2* (~ 0.90; $P < 0.05$; Figure 3.15E) compared to Wt (~ 0.80; Figure 3.15A). Slightly higher peak transient and steady-state P700 oxidation was observed in low and high light, respectively, in *L17* compared to Wt (Figure 3.15C), but may not necessarily be relevant owing to the high degree of sample variation (SD). A minor reduction in peak transient P700 oxidation was observed however in *npq1* compared to Wt (Figure 3.15F), reflecting transiently increased cyclic electron transport in *npq1*. Increased steady-state P700 oxidation in high light in *npq1* may be attributed to a minor reduction in steady-state linear electron transport in high light in *npq1* (data not shown). However, the PsbS-deficient *npq4* mutant showed a minor reduction in peak transient P700 oxidation in low light (~ 0.18; $P < 0.05$; Figure 3.15D). This corresponds to a reduced NPQ in low light in *npq4* due to a lack of PsbS. In contrast, increased steady-state P700 oxidation in high light in *npq4* ($P < 0.05$; Figure 3.15D) may be attributed to reduced steady-state linear electron transport in high light in *npq4* ($P < 0.05$; data not shown). Thus, it is clear that defects in Z_XE and PsbS activities in *npq2* and *npq4*, respectively, affect linear and in turn cyclic electron transport. Changes in cyclic electron transport influence NPQ, particularly in low light, given the close phenomenological similarity between P700 oxidation and NPQ kinetics.

3.2.2.5 Dynamics of *pmf* Partitioning *in vivo* in *Arabidopsis* Mutants

The aim of this aspect of the work is to characterize possible differences in previously uncharacterized dynamics of *pmf* partitioning between Wt and mutant lines over a range of illumination periods in low and high light and to relate those differences to mutant-specific kinetics of NPQ and electron transport. This will offer further insight into the regulation of qE responses influenced by changes in *pmf* partitioning, as proposed by Cruz *et al*. (2001), as well as clarify the role of $\Delta\psi$ in early qE regulation.

Absorbance changes at 515 nm were monitored for 1-1200 s of actinic illumination at 53 and 660 μmol quanta m^{-2} s^{-1}, followed by 5 min of dark relaxation in detached leaves of Wt and mutants of *Arabidopsis*. Analyses of ECS signal kinetics during the dark-light and light-dark transitions yields valuable information concerning above all progressive changes in partitioning of the light-induced *pmf* into the $\Delta\psi$ and ΔpH and derived changes in the lumen pH. This is clearly demonstrated by exemplary raw traces of the ECS measured at 515 nm using the DUAL-PAM-100 system (Figure 3.16A-C). These traces show the progression of changes in ECS kinetics over a range of illumination periods in low and high light, particularly during the initial 1-3 min of illumination corresponding to transient formation and decline in NPQ and P700 oxidation in low light. The dynamics of DIRK ECS kinetics for *L17* and *npq1* after 1-3 min of illumination, particularly in high light, are shown for comparison against Wt. Most strikingly, a substantial *pmf*, consisting largely of the $\Delta\psi$, was established after 1 min of illumination in high light in *L17* (Figure 3.16B) and *npq1* (Figure 3.16C). Slow relaxation of the ECS signal during the dark relaxation phase following illumination was observed in both mutants, particularly *L17*, under these conditions. In contrast, a comparatively more rapid rate of ECS relaxation was observed in both mutants, particularly *npq1*, after 3 min of illumination in high light. Such kinetics of early light-induced *pmf* partitioning may be characteristic to these mutants and are particularly important in subsequent analyses of the role of $\Delta\psi$ in early qE regulation.

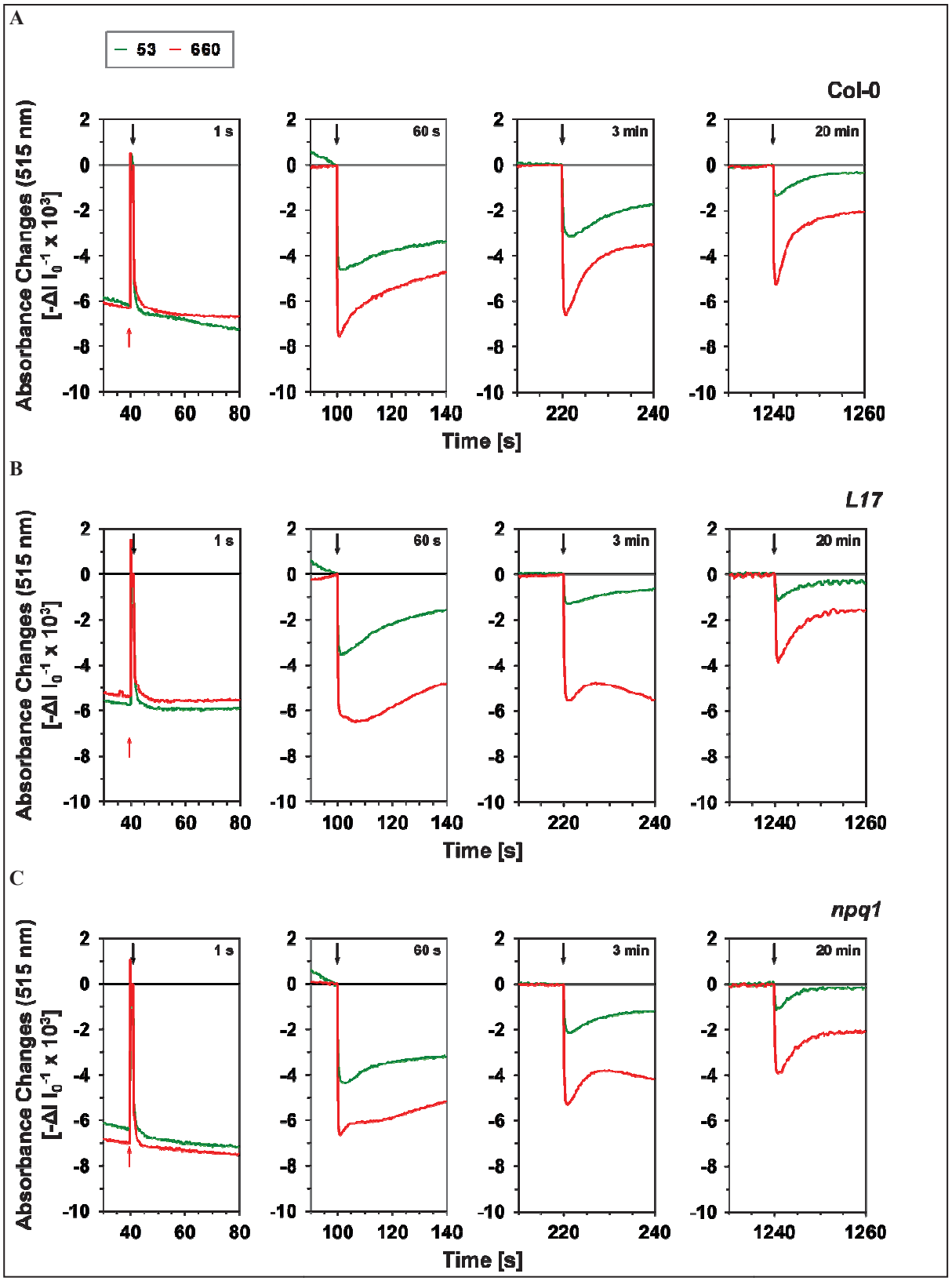

Figure 3.16 – The electrochromic shift (ECS) at 515 nm *in vivo* in *Arabidopsis*. Changes in the ECS signal during and after 1 s and after 1, 3, and 20 min of actinic illumination at 53-1287 μmol quanta m^{-2} s^{-1} were measured in detached leaves of (A) Col-0, (B) *L17*, and (C) *npq1*. Inset red and black arrows represent the onset and completion of the illumination period. Absorbance changes were always normalized to the light off point. Light intensity values in the legend are expressed in μmol quanta m^{-2} s^{-1}. Curves represent single exemplary traces for illustration purposes only.

Quantification of the total amplitude of the DIRK ECS signal (ECS_t), related to the magnitude of the *pmf* established in the light (Cruz *et al*., 2001; Takizawa *et al*., 2007), highlights important differences in *pmf* formation in the light between Wt and specific mutant lines. Most notably, a more rapid decline in the total *pmf* established after 60 s of illumination at 53 μmol quanta m^{-2} s^{-1} was observed particularly in *pgrl1ab #273* (Figure 3.17B) and to a lesser extent in *pgr5* (Figure 3.17D) compared to the respective Wt. This correlates with a reduction in early peak transient NPQ and increased P700 oxidation in low light characteristic to the cyclic electron transport-deficient mutants *pgr5* and *pgrl1ab #273*. A reduced *pmf* established after 20 min of steady-state illumination at 660 μmol quanta m^{-2} s^{-1} was also observed in both *pgr5* and *pgrl1ab #273* ($P < 0.05$; Figures 3.17B and 3.17D). This is attributed to steady-state reductions in linear electron transport in high light in *pgr5* and *pgrl1ab #273* (DalCorso *et al*., 2008), impacted by a reduced contribution of *PGR5*- and *PGRL1*-mediated cyclic electron transport to linear electron transport-coupled ΔpH formation (Avenson *et al*., 2005; Shikanai, 2014). This will then reduce the *pmf*, as observed at steady state in high light in *pgr5* in particular, and may explain the minor reductions in steady-state NPQ in high light in *pgr5* and *pgrl1ab #273*. Thus, reduced *pmf* formation in low and high light reflects reductions in peak transient and steady-state NPQ in low and high light, respectively, in these mutants.

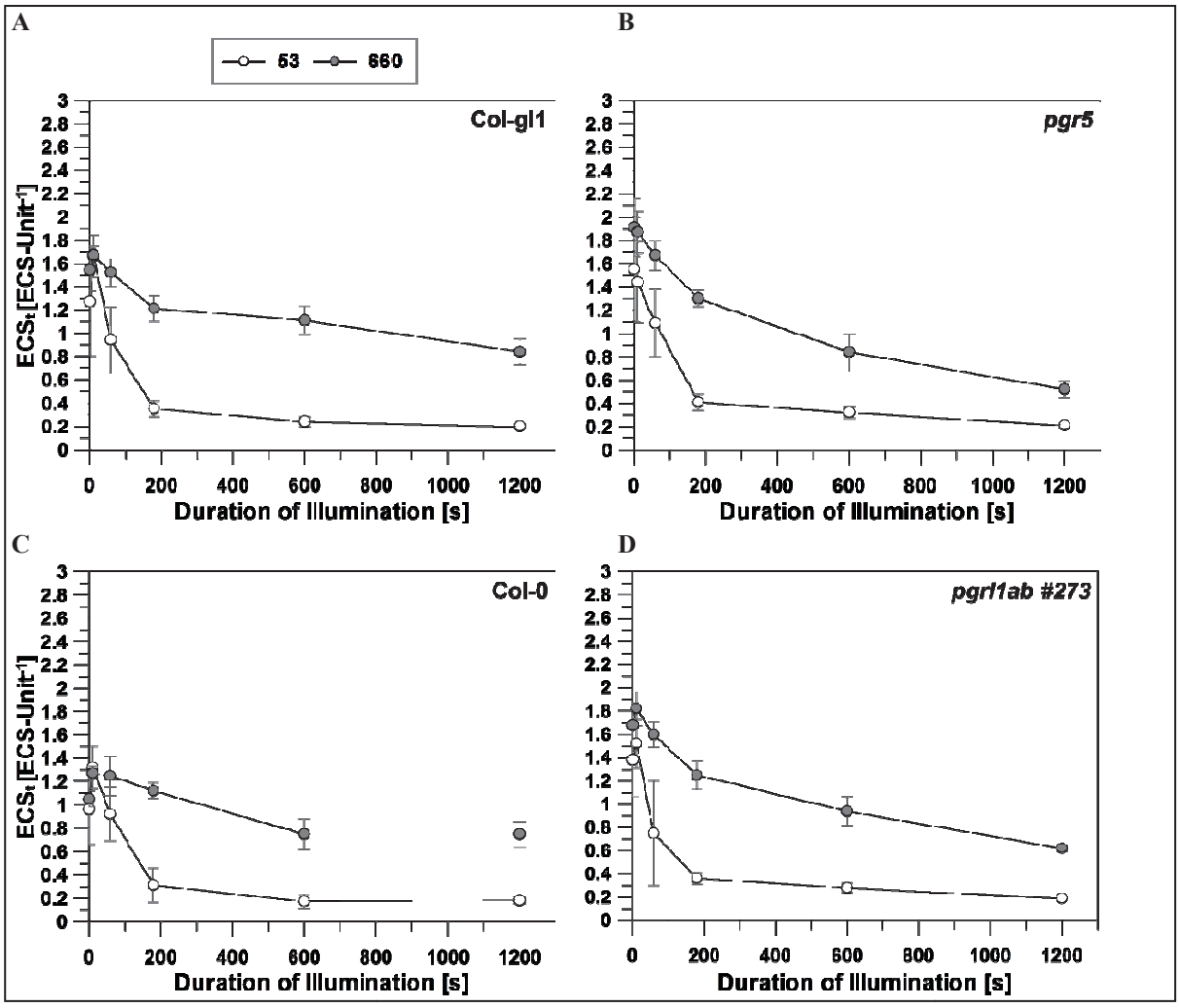

Figure 3.17 – Dynamics of proton motive force (*pmf*) formation in the light *in vivo* in *Arabidopsis* derived from changes in the dark-interval relaxation kinetics (DIRK) of the electrochromic shift (ECS) at 515 nm. The light-induced *pmf*, proportional to the flash-normalized amplitude of the rapid decay of the DIRK ECS signal during the light-dark transition (ECS_t), was quantified in detached leaves of (A) Col-gl1, (B) *pgr5*, (C) Col-0, and (D) *pgrl1ab #273* during 5 min of dark relaxation after 1-1200 s of actinic illumination at 53 and 660 μmol quanta m^{-2} s^{-1}. Light intensity values in the legend are expressed in μmol quanta m^{-2} s^{-1}. Curves represent mean values ± standard deviation (SD) of at least four replicates from two or more independent experiments.

The cytochrome b_6f-impaired *pgr1* mutant showed a more rapid reduction in the total *pmf* established within seconds in low light (Figure 3.18B) compared to Wt (Figure 3.18A). Similarly, the total *pmf* declined rapidly within seconds of illumination in high light, such that a reduced steady-state *pmf* was observed in high light in *pgr1* ($P < 0.001$, Figure 3.18A). Altered pH-dependence of PQH_2 oxidation due to a defect in cytochrome b_6f in *pgr1* limits linear electron transport, which would limit the extent of the *pmf* established in low and high light in *pgr1*. This is consistent with reduced NPQ formation in low and high light in *pgr1*.

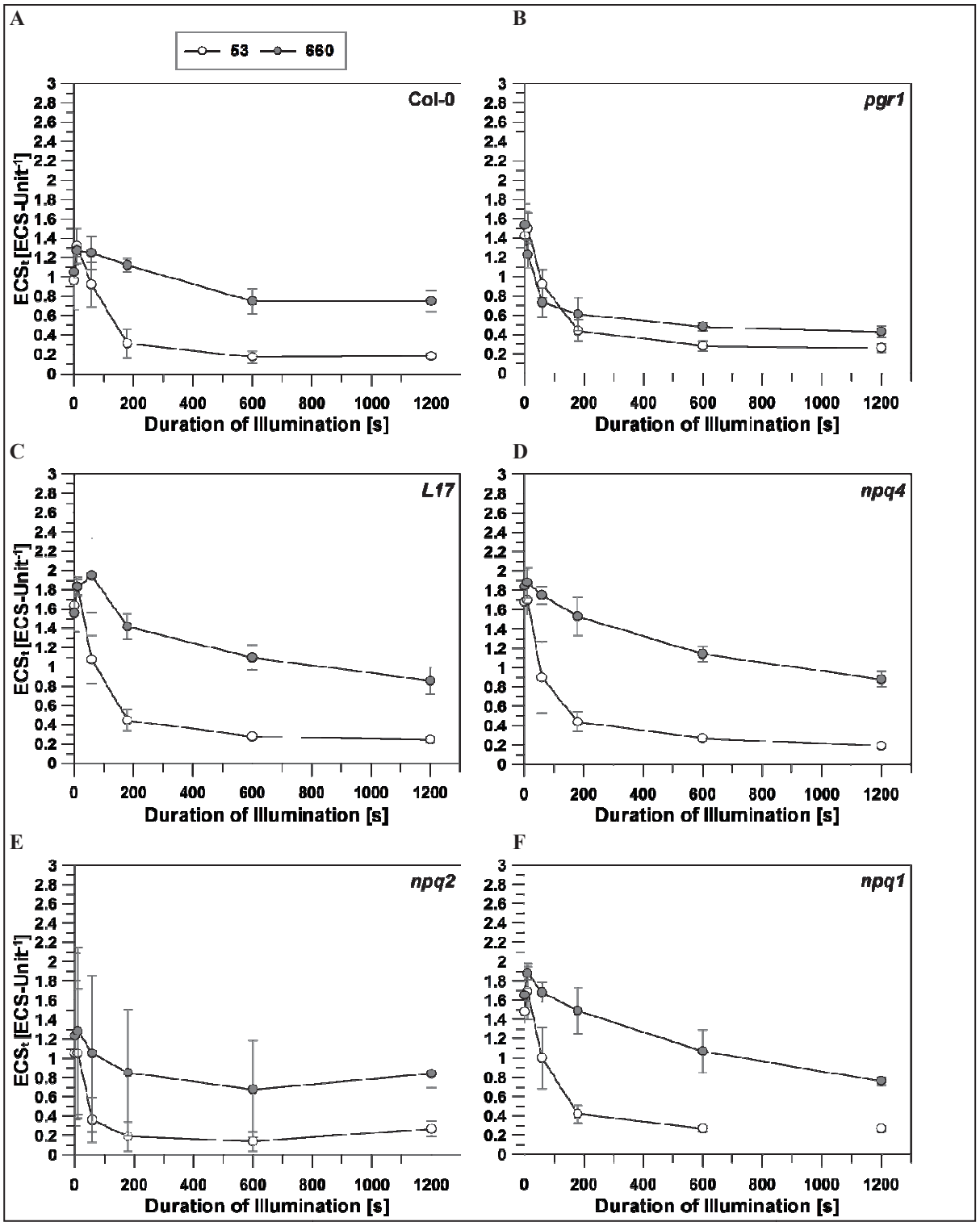

Figure 3.18 – Dynamics of proton motive force (*pmf*) formation in the light *in vivo* in *Arabidopsis* derived from changes in the dark-interval relaxation kinetics (DIRK) of the electrochromic shift (ECS) at 515 nm. The light-induced *pmf*, proportional to the flash-normalized amplitude of the rapid decay of the DIRK ECS signal during the light-dark transition (ECS_t), was quantified in detached leaves of (A) Col-0, (B) *pgr1*, (C) *L17*, (D) *npq4*, (E) *npq2*, and (F) *npq1* during 5 min of dark relaxation after 1-1200 s of actinic illumination at 53 and 660 μmol quanta m^{-2} s^{-1}. Light intensity values in the legend are expressed in μmol quanta m^{-2} s^{-1}. Curves represent mean values ± standard deviation (SD) of at least four replicates from two or more independent experiments.

The total light-induced *pmf* is markedly higher during the initial seconds during early illumination in low and high light in *L17* ($P < 0.01$; Figure 3.18C) compared to Wt (Figure 3.18A). A higher *pmf* sustained with prolonged illumination leading to steady state in low and high light was observed in *L17* compared to Wt. This contrasts with severely reduced NPQ in low and high light in *L17* and may not necessarily be relevant, as Col-0 showed a generally reduced *pmf* compared to most genotypes to include Col-gl1. An increased *pmf* in low and high light in *L17* corroborates enhanced peak transient and maximal NPQ formation in low and high light, respectively, due to PsbS overexpression in *L17*. This is supported by a previously observed increase in linear electron transport in *L17* in high light (Nilkens *et al*., 2010), which largely contributes to light-induced *pmf* formation. Impaired V_XDE activity leading to sustained accumulation of V_X in *npq1* is also characterized by a higher total *pmf*, particularly during the initial 60 s ($P < 0.001$) to 180 s ($P < 0.05$) of high light exposure compared to Wt (Figure 3.18F). This suggests that early qE quenching influenced largely by the PsbS in *L17* and *npq1* may contribute to rapid early light-induced *pmf* formation.

The PsbS-deficient *npq4* mutant displayed a higher total *pmf* within seconds of low light exposure as well as after 10 and 20 min of low light illumination ($P < 0.01$; Figure 3.18D) compared to Wt. This was also the case during early and prolonged illumination (up to 10 min) in high light in *npq4* ($P < 0.05$). Contrastingly, NPQ formation was severely reduced in low and high light in *npq4*. The Z_XE-deficient *npq2* mutant in comparison to the other mutants displayed a more rapid decline in the total *pmf* in low light given reduced ECS_t after 60 s of illumination in low light ($P < 0.001$; Figure 3.18E). This may be due to a minor reduction in initial linear electron transport in low light in *npq2* (Kalituho *et al*., 2007). Taken together, it is clear that the total light-induced *pmf*, estimated from ECS_t, is generally a good indicator of NPQ formation in low and high light.

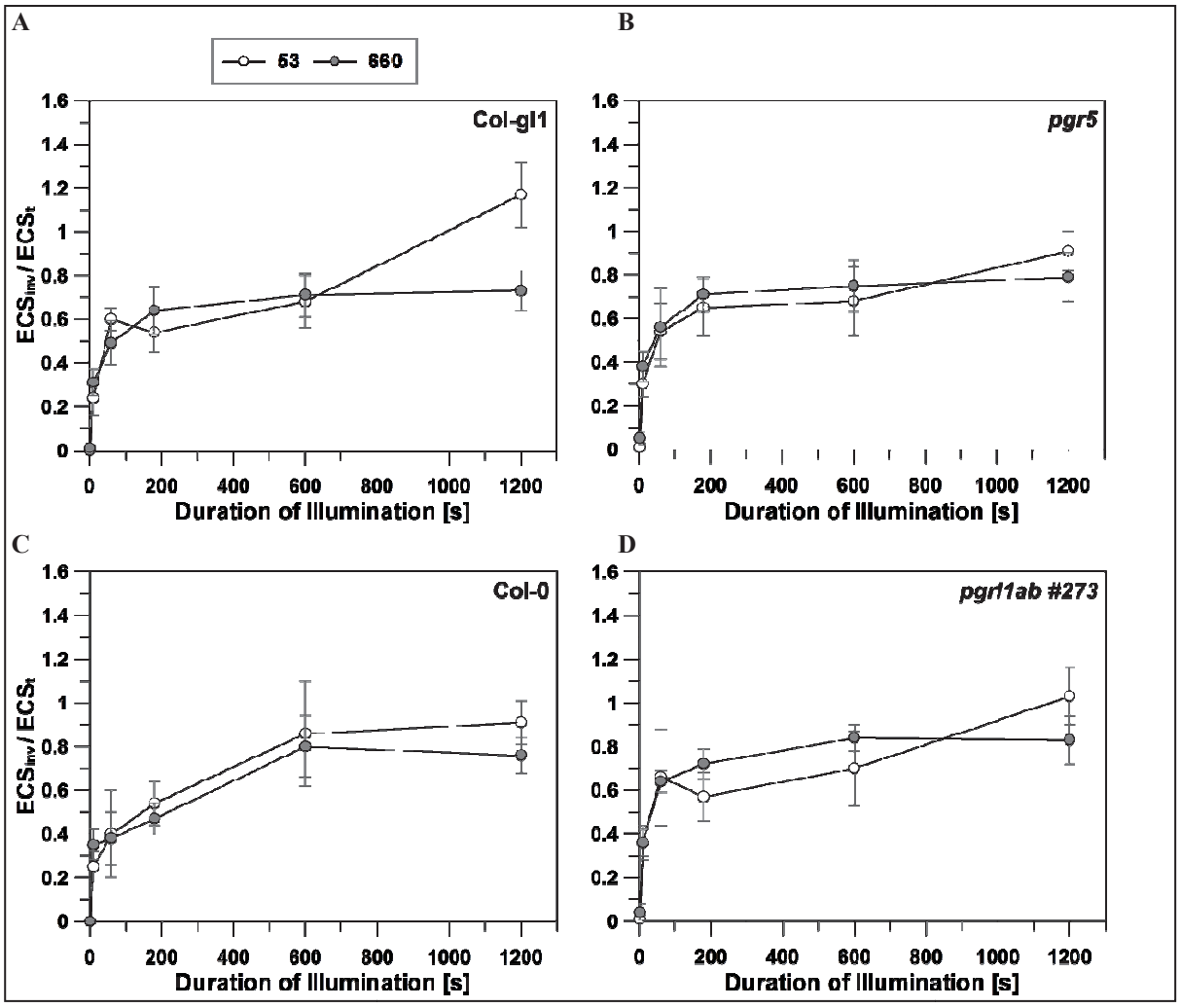

Figure 3.19 – Dynamics of proton motive force (*pmf*) partitioning in the light *in vivo* in *Arabidopsis* derived from changes in dark-interval relaxation kinetics (DIRK) of the electrochromic shift (ECS) at 515 nm. The relative contribution of the ΔpH fraction, estimated from the flash-normalized inverse portion of the DIRK ECS signal (ECS_{inv}), to the total light-induced *pmf* (ECS_{inv} / ECS_t) was quantified in detached leaves of (A) Col-gl1, (B) *pgr5*, (C) Col-0, and (D) *pgrl1ab #273* during 5 min of dark relaxation after 1-1200 s of actinic illumination at 53 and 660 μmol quanta m^{-2} s^{-1}. Light intensity values in the legend are expressed in μmol quanta m^{-2} s^{-1}. Curves represent mean values ± standard deviation (SD) of at least four replicates from two or more independent experiments.

Estimates of the amplitude of the inverse portion of the decaying DIRK ECS signal (ECS_{inv}) in relation to the amplitude of the total DIRK ECS signal (ECS_t) provide an overview of changes in the relative ΔpH contribution to the light-induced *pmf* with prolonged illumination. Clearly, *pmf* partitioning into an increasing relative ΔpH fraction is generally comparable with prolonged illumination in low and high light in *pgr5* (Figure 3.19B). Such dynamics do not differ noticeably from those of Col-gl1 (Figure 3.19A), although *pgr5* showed a slightly reduced ΔpH contribution to the *pmf* after 60 s of illumination in low light compared to Wt. This corresponds to a reduction in the total *pmf* (ECS_t) and peak transient NPQ under these conditions. A reduced relative ΔpH contribution in *pgr5* supports a general reduction in the ΔpH dissipated by continued proton efflux via the ATP synthase in the

absence of commensurate *PGR5*-mediated proton influx at cytochrome b_6f (Avenson *et al*., 2005; Shikanai, 2014). In contrast, the *pgrl1ab #273* mutant displayed an increased relative ΔpH contribution to the total *pmf* established within 60 and 180 s of illumination in low and high light (~ 0.60-0.70; $P < 0.05$; Figure 3.19D) compared to Col-0 (Figure 3.19C). However, a high degree of variation in the estimated relative ΔpH contribution after 60 s in low light in *pgrl1ab #273* questions these differences in early *pmf* partitioning in low light between *pgrl1ab #273* and Wt. Early *pmf* partitioning into an increased ΔpH fraction in low light in *pgrl1ab #273* is not consistent with reduced early peak transient NPQ in low light in *pgrl1ab #273*. Furthermore, a reduced ΔpH contribution to early *pmf* formation in high light in *pgrl1ab #273* is not consistent with a general reduction in the ΔpH predicted on the basis of reduced proton efflux via the ATP synthase in the absence of balancing *PGRL1*-mediated proton influx. One can therefore conclude that the impacts of impaired cyclic electron transport on *pmf* partitioning are not fully reflected by kinetics of NPQ formation affected by impaired cyclic electron transport. This is particularly evident during early activation of qE, suggesting that changes in the total *pmf* give a better indication of changes in qE responses when cyclic electron transport is impaired.

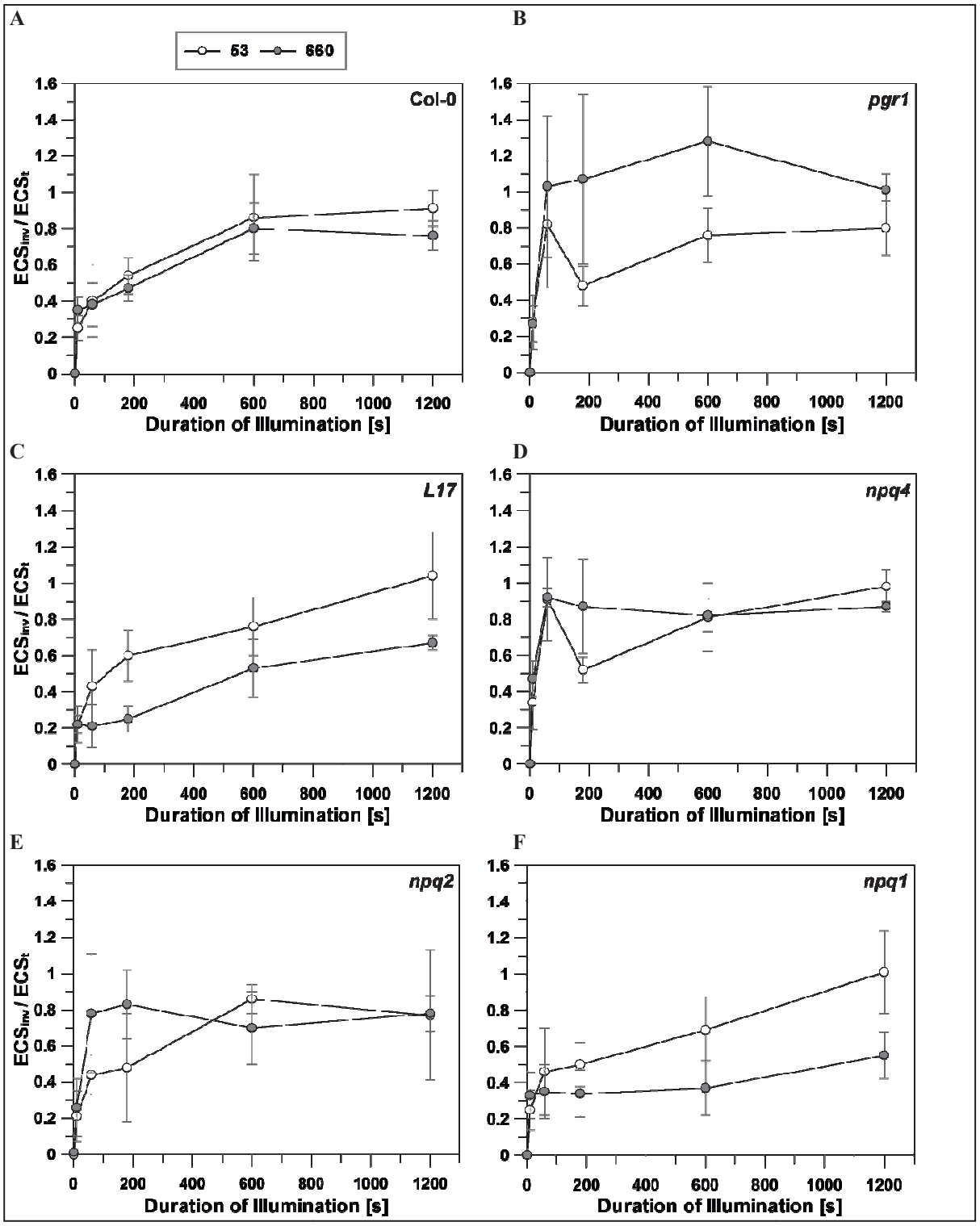

Figure 3.20 – Dynamics of proton motive force (*pmf*) partitioning in the light *in vivo* in *Arabidopsis* derived from changes in dark-interval relaxation kinetics (DIRK) of the electrochromic shift (ECS) at 515 nm. The relative contribution of the ΔpH fraction, estimated from the flash-normalized inverse portion of the DIRK ECS signal (ECS_{inv}), to the total light-induced *pmf* (ECS_{inv} / ECS_t) was quantified in detached leaves of (A) Col-0, (B) *pgr1*, (C) *L17*, (D) *npq4*, (E) *npq2*, and (F) *npq1* during 5 min of dark relaxation after 1-1200 s of actinic illumination at 53 and 660 μmol quanta m^{-2} s^{-1}. Light intensity values in the legend are expressed in μmol quanta m^{-2} s^{-1}. Curves represent mean values ± standard deviation (SD) of at least four replicates from two or more independent experiments.

It is also important to examine the dynamics of *pmf* partitioning into the ΔpH and Δψ in the absence of sufficient ΔpH formation (*pgr1*) required to generate maximal transient and steady-state NPQ in low and high light, respectively. DIRK ECS analysis shows a rapidly increasing ΔpH fraction of the *pmf* in low and particularly high light in *pgr1* (Figure 3.20B) compared to Wt. As such, an increased ΔpH contribution to the *pmf* was observed after 60 s of illumination in low light in *pgr1* (~ 0.80; $P < 0.01$; Figure 3.20B) compared to Wt (~ 0.40; Figure 3.20A), while NPQ was reduced in low light in *pgr1* compared to Wt. Despite high sample variation, *pgr1* also displayed a clearly increased relative ΔpH contribution to the *pmf* after 60 s of high light illumination leading to steady state (> 1; $P < 0.05$). The observed rapid increase in the relative ΔpH fraction of the *pmf* in *pgr1* thus accompanies a rapid reduction in the total *pmf* during early illumination in low and high light in *pgr1* (Figure 3.18B).

Further DIRK ECS analysis importantly reveals a reduced relative ΔpH contribution to the *pmf* formed after 60-180 s of high light illumination in *L17* (~ 0.20; $P < 0.05$; Figure 3.20C) compared to Wt. This is reflected by slower relaxation of the DIRK ECS signal and an increased total *pmf* in *L17* after 60 s of high light illumination (Figure 3.16B). Similarly, the V_XDE-impaired *npq1* mutant displayed a minor reduction in the relative ΔpH contribution to the *pmf* formed after 60-180 s of high light illumination (~ 0.35; Figure 3.20F) compared to Wt, but to a lesser extent than *L17*. This is also reflected by a minor delay in relaxation of the DIRK ECS signal in *npq1* after 60 s in high light (Figure 3.16C), which then relaxed more rapidly after 60-180 s of illumination in high light. These reductions in the relative ΔpH contribution to the *pmf* established within 60 s of illumination in high light, particularly in the presence of excess PsbS in *L17*, highlight a relatively higher Δψ contribution (> 60 %) to the early light-induced *pmf*.

As *pgr1*, the PsbS-deficient *npq4* mutant most notably showed a markedly increased relative ΔpH contribution to the total *pmf* established after 60 s of low and high light illumination ($P < 0.001$; Figure 3.20D). An enhanced ΔpH contribution in low light may be driven to some extent by transiently increased cyclic electron transport, inferred from reduced peak transient P700 oxidation in low light in *npq4* (Figure 3.15D). In contrast, an enhanced relative ΔpH contribution to the *pmf* established initially in high light in *npq4* may be accommodated by an increase in the extent of light-induced *pmf* formation observed in *npq4* in high light (Figure 3.18D). Strikingly, permanent accumulation of Z_X in the Z_XE-impaired *npq2* mutant is reflected by a rapid increase in the relative ΔpH contribution to the total *pmf*, peaking after

60-180 s of illumination in high light ($P < 0.05$). This may contribute to rapid initial NPQ formation observed in high light in *npq2*. A low ΔpH contribution to the *pmf* thus consisting primarily of the $\Delta\psi$ (≥ 50 %) was observed during the initial 60-180 s of illumination in low light in *npq2*. This corresponds to a reduced total *pmf* (ECS_t) and increased transient NPQ after 60-180 s of illumination in low light in *npq2* compared to Wt. Taken together, mutant-specific differences in *pmf* formation and partitioning are clearly related to well-known changes in qE responses in low and high light, as shown most clearly in *L17* and *npq1*.

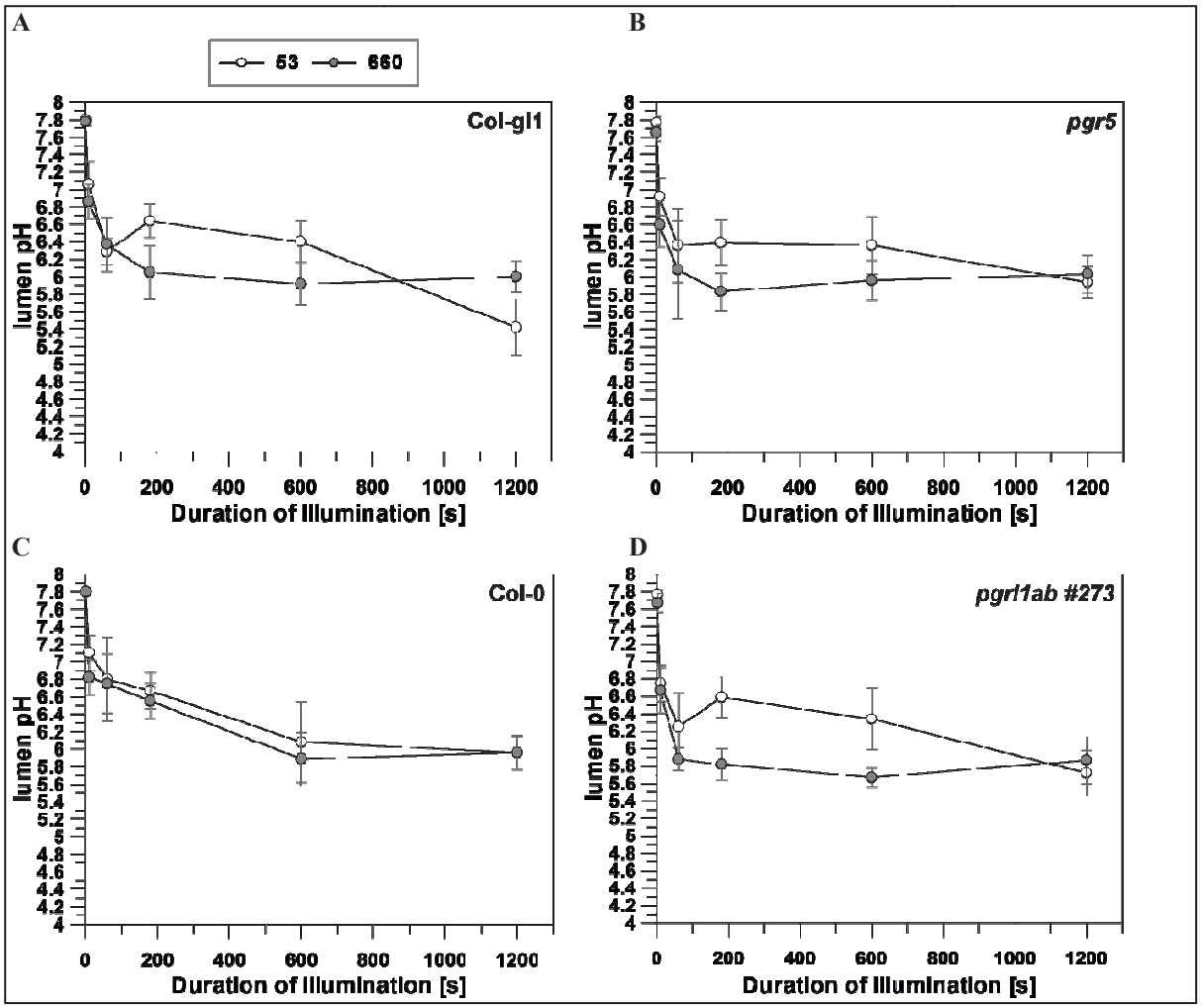

Figure 3.21 – Changes in lumen pH *in vivo* in *Arabidopsis* derived from the dark-interval relaxation kinetics (DIRK) of the electrochromic shift (ECS) at 515 nm. The lumen pH was derived according to Takizawa *et al*. (2007). Changes in lumen pH were assessed in detached leaves of (A) Col-gl1, (B) *pgr5*, (C) Col-0, and (D) *pgrl1ab #273* during the 5 min dark relaxation interval after 1-1200 s of actinic illumination at 53 and 660 μmol quanta m^{-2} s^{-1}. Light intensity values in the legend are expressed in μmol quanta m^{-2} s^{-1}. Curves represent mean values ± standard deviation (SD) of at least four replicates from at two or more independent experiments.

Finally, estimation of the lumen pH *in vivo* corroborates *pmf* partitioning data and underscores differences in lumen acidification in various mutants in relation to qE formation during early and prolonged illumination in low and high light. The cyclic electron transport-

impaired *pgr5* is characterized by slightly delayed lumen acidification during the initial 60 s at 53 μmol quanta m^{-2} s^{-1} (Figure 3.21B) compared to Col-gl1 (Figure 3.21A). This confirms the observed increase in the relative ΔpH contribution to the *pmf* in low light in *pgr5* compared to Wt. In contrast, more rapid initial lumen acidification in low and high light in *pgrl1ab #273* is characterized by a markedly reduced lumen pH after 60-180 s at 53 and 660 μmol quanta m^{-2} s^{-1} ($P < 0.05$; Figure 3.21D) compared to Col-0 (Figure 3.21C). This corroborates the increased relative contribution of the ΔpH to the *pmf* established early on in low and high light in *pgrl1ab #273*. However, this is not consistent with reduced peak transient NPQ formation in low light and delayed NPQ induction in high light in *pgrl1ab #273*. This suggests that the impacts of impaired cyclic electron transport on the dynamics of lumen acidification like *pmf* partitioning are not clearly correlated with NPQ formation in low and high light affected by impaired cyclic electron transport.

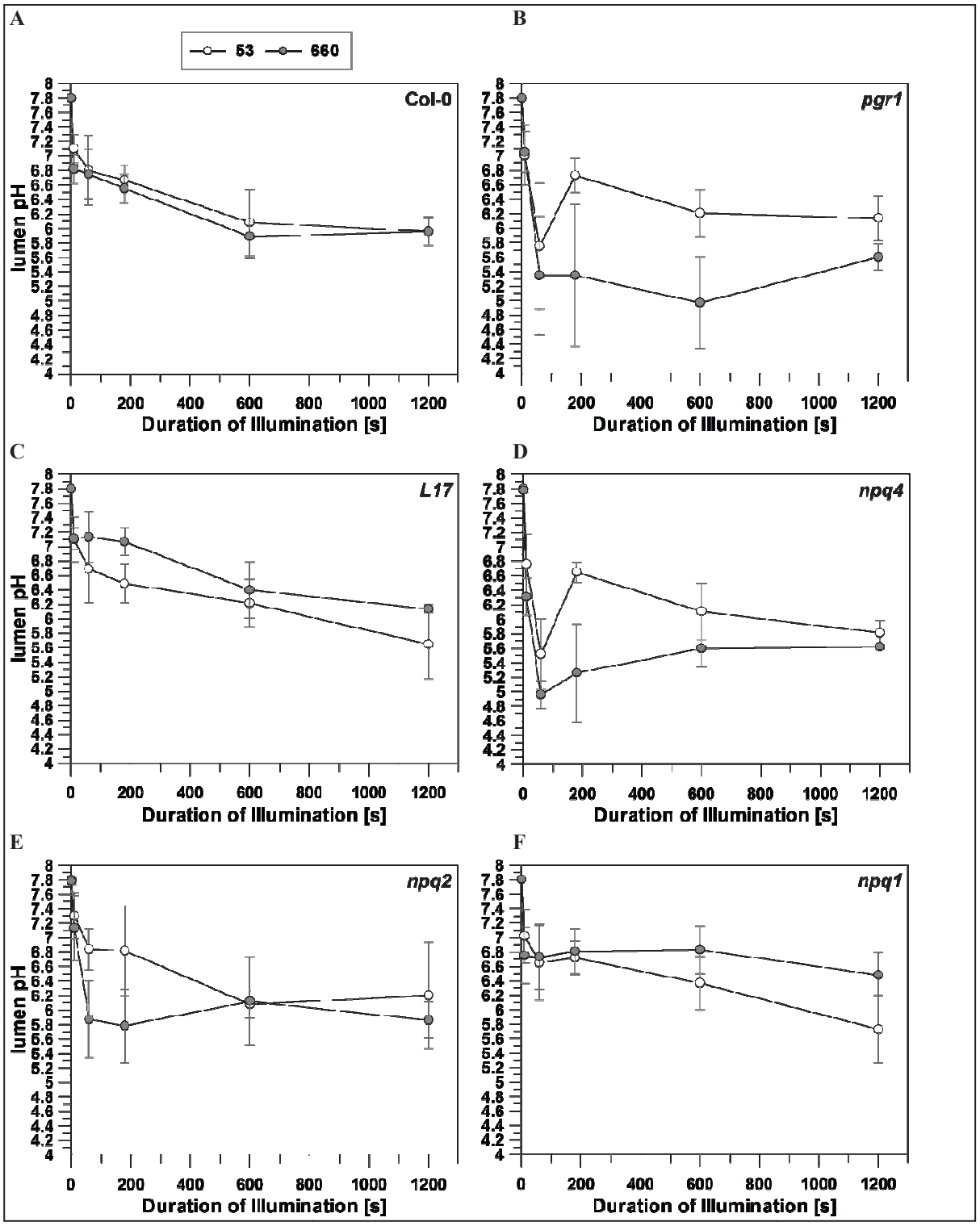

Figure 3.22 – Changes in lumen pH *in vivo* in *Arabidopsis* derived from the dark-interval relaxation kinetics (DIRK) of the electrochromic shift (ECS) at 515 nm. The lumen pH was derived according to Takizawa *et al*. (2007). Changes in lumen pH were assessed in detached leaves of (A) Col-0, (B) *pgr1*, (C) *L17*, (D) *npq4*, (E) *npq2*, and (F) *npq1* during the 5 min dark relaxation interval after 1-1200 s of actinic illumination at 53 and 660 μmol quanta m^{-2} s^{-1}. Light intensity values in the legend are expressed in μmol quanta m^{-2} s^{-1}. Curves represent mean values ± standard deviation (SD) of at least four replicates from at two or more independent experiments.

Increasing lumen acidification with prolonged illumination at low and high intensities is generally observed in Wt and mutants alike, though in some exceptions more pronounced lumen acidification in low compared to high light is evident. The *pgr1* mutant displayed a more rapid initial decline in lumen pH in both low and high light ($P < 0.01$; Figure 3.22B) compared to Wt (Figure 3.22A). Rapid initial lumen acidification is consistent with an increased relative fraction of the *pmf* stored as the ΔpH during initial illumination in low light. However, rapid lumen acidification thus gives no indication of limited ΔpH formation and reduced NPQ formation limited by impaired cytochrome b_6f activity in *pgr1*. Thus, light-induced *pmf* formation, estimated from ECS_t, correlates more closely with NPQ formation than *pmf* partitioning or lumen acidification in low and high light in *pgr1*. Like *pgr1*, the PsbS-deficient *npq4* mutant displayed more rapid initial lumen acidification in low and high light compared to Wt ($P < 0.01$; Figure 3.22D). This is consistent with an increased relative ΔpH contribution to the *pmf* established during initial low and high light illumination, as shown above, in spite of a drastically reduced and delayed induction of NPQ in low and high light in *npq4*. The Z_XE-impaired *npq2* mutant also showed a clear early decline in the lumen pH after 60 and 180 s of high light exposure ($P < 0.05$; Figure 3.22E), but less pronounced than that observed in *npq4*. This is also consistent with a more rapid initial decline in the total *pmf* and increased relative ΔpH contribution to the *pmf* during early high light exposure in *npq2* paralleling increased peak transient NPQ formation in low light in *npq2*.

Delayed early lumen acidification in high light was clearly observed in the PsbS-overexpression *L17* line, reflected by a higher lumen pH during the initial 180 s of illumination in high light ($P < 0.01$; Figure 3.22C). This was also observed in the V_XDE-deficient *npq1* mutant, but to a lesser extent. Delayed lumen acidification reflects the initial lag in recovery of DIRK ECS decay in high light in *L17* (Figure 3.16B) and *npq1* (Figure 3.16C), characterized by a reduced relative ΔpH contribution to the *pmf*, consisting largely of $\Delta\psi$, established initially in high light. Consistent with previous analyses of the dynamics of *pmf* partitioning in Wt, *L17*, and *npq1*, this underscores the importance of PsbS in addition to lumen acidification during early activation of qE. The role of $\Delta\psi$ during early light activation of qE is supported by a largely $\Delta\psi$-stored *pmf* during early light activation of qE in *L17* and *npq1*. Overall, changes in the dynamics of lumen acidification (i.e., inefficient lumen acidification) will affect efficient energy dissipation driven largely by qE in the short-term. This will have direct impacts on energy allocation towards efficient photosynthesis, which becomes increasingly limited at more saturating light intensities.

3.2.2 Defining Ion Antiport-Mediated qE Regulation in Fluctuating Light

It is well established that the transthylakoid ΔpH is central to the regulation of qE under EL conditions. However, natural light conditions can fluctuate by several orders of magnitude within seconds due to cloud or canopy shading (Pearcy, 1990; Reinhard *et al*., 2010). This necessitates rapid switching between a photoprotective state in high or excess light and an efficient light-harvesting state under limiting light conditions to maximize light use efficiency. Understanding the molecular factors and mechanisms underpinning these rapid light-regulated responses to include downregulation of qE in limiting light is therefore critical to improving crop yields, while more broadly revealing fundamental principles of robust energy conversion systems.

Ion channels have significant physiological roles in functioning plant and other photosynthetic systems (Mäser *et al*., 2001; Marmagne *et al*., 2007; Kunz *et al*., 2014). However, poor understanding of their molecular identity limited by the small number of genes identified, particularly anion channel-encoding genes, has hampered some of the progress in this field (Marmagne *et al*., 2007). Cation/proton antiporters in the thylakoid membrane may be involved in regulating the dynamics of qE. The search for cation/proton antiporters transcriptionally co-regulated with photosynthesis-related genes in the model plant *Arabidopsis thaliana* led to the identification of the K^+ Efflux Antiporter 3 (*KEA3*), which has been recently characterized in the manuscript below by Armbruster *et al*. (2014). *KEA3* is one of six genes belonging to the putative K^+/H^+ antiporter *KEA* or monovalent cation:proton antiporter family 2 (*CPA2*) family that have been identified in *Arabidopsis* to date (Mäser *et al*., 2001).

– Manuscript –

Ion antiport accelerates photosynthetic acclimation in fluctuating light environments

nature COMMUNICATIONS

ARTICLE

Received 3 Jun 2014 | Accepted 1 Oct 2014 | Published 13 Nov 2014

DOI: 10.1038/ncomms6439 OPEN

Ion antiport accelerates photosynthetic acclimation in fluctuating light environments

Ute Armbruster[1], L. Ruby Carrillo[2], Kees Venema[3], Lazar Pavlovic[4], Elisabeth Schmidtmann[1], Ari Kornfeld[5], Peter Jahns[4], Joseph A. Berry[5], David M. Kramer[2] & Martin C. Jonikas[1]

Many photosynthetic organisms globally, including crops, forests and algae, must grow in environments where the availability of light energy fluctuates dramatically. How photosynthesis maintains high efficiency despite such fluctuations in its energy source remains poorly understood. Here we show that *Arabidopsis thaliana* K^+ efflux antiporter (KEA3) is critical for high photosynthetic efficiency under fluctuating light. On a shift from dark to low light, or high to low light, *kea3* mutants show prolonged dissipation of absorbed light energy as heat. KEA3 localizes to the thylakoid membrane, and allows proton efflux from the thylakoid lumen by proton/potassium antiport. KEA3's activity accelerates the downregulation of pH-dependent energy dissipation after transitions to low light, leading to faster recovery of high photosystem II quantum efficiency and increased CO_2 assimilation. Our results reveal a mechanism that increases the efficiency of photosynthesis under fluctuating light.

[1] Department of Plant Biology, Carnegie Institution for Science, 260 Panama Street, Stanford, California 94305, USA. [2] Plant Research Laboratory, Michigan State University, R106 Plant Biology Building, East Lansing, Michigan 48824-1312, USA. [3] Dpto de Bioquímica, Biología Celular y Molecular de Plantas, Estación Experimental del Zaidín, Consejo Superior de Investigaciones Científicas, c/. Profesor Albareda 1, 18008 Granada, Spain. [4] Biochemie der Pflanzen, Heinrich-Heine-Universität Düsseldorf, Universitätsstraße 1, 40225 Düsseldorf, Germany. [5] Department of Global Ecology, Carnegie Institution for Science, 260 Panama Street, Stanford, California 94305, USA. Correspondence and requests for materials should be addressed to U.A. (email: ute.armbruster78@gmail.com) or to M.C.J. (email: mjonikas@carnegiescience.edu).

Efficient conversion of energy is a critical challenge for all organisms. Energy in the environment is available either as chemical potential or light. Uniquely, the energy available as light can undergo extreme fluctuations in amplitude on short time scales. Photon flux can change 100-fold within seconds, for example, due to shade from clouds or leaves moving in the wind[1,2]. Understanding the mechanisms that underlie efficient photosynthesis in fluctuating light can open doors to increased crop yields, and more broadly can reveal fundamental principles of robust energy conversion systems.

The light reactions of photosynthesis produce NADPH and ATP to power carbon fixation. Light-harvesting antennae absorb photons and transfer their energy to the photosystems, which pump electrons from water to NADPH. This process is coupled to proton translocation across the thylakoid membrane into the thylakoid lumen, which drives ATP synthesis[3,4]. Under high light, the high proton concentration in the thylakoid lumen activates energy-dependent quenching (qE), a mechanism that dissipates absorbed light energy in the PSII antenna as heat[5]. qE is thus part of a negative feedback loop that decreases energy transfer to PSII by up to 75% in response to excess light[6–8].

To maximize yields under continuously changing light intensities, the PSII antenna must rapidly alternate between dissipation of excess absorbed energy under high light, and efficient harvesting of photons for photosynthesis under limiting light[9]. On transition from high to limiting light, the qE energy dissipation mechanism is downregulated to increase the energy available to PSII. However, this downregulation occurs on a timescale of minutes, producing an extended period where heat dissipation of light energy starves the photosystems of excitation energy. Simulations predict that the slow downregulation of heat dissipation mechanisms can reduce the photosynthetic efficiency by ~10% in crop canopies[10]. The design principles that determine the kinetics of qE downregulation remain unknown[11], motivating a search for molecular factors that affect its dynamics.

Here we show that ion antiport activity across the thylakoid membrane accelerates photosynthetic acclimation after a change in light intensity from dark to low light, or from high to low light. In the model plant *Arabidopsis thaliana* (hereafter '*Arabidopsis*'), K^+ efflux antiporter 3 (KEA3) is localized in the thylakoid membrane and mediates H^+/K^+ antiport. After each transition to low light, KEA3 allows proton efflux from the lumen, which accelerates the downregulation of pH-dependent energy quenching, and transiently increases photosystem II quantum efficiency and CO_2 fixation. Our findings demonstrate that a K^+/H^+ antiport activity mediated by KEA3 increases photosynthetic efficiency under fluctuating light conditions.

Results

KEA3 is co-regulated with photosynthesis-related genes. The previously established regulation of qE by thylakoid pH[5] led us to hypothesize that proton/cation antiporters in the thylakoid membrane could regulate the dynamics of qE. We therefore searched for proton/cation antiporters in *Arabidopsis* that were transcriptionally co-regulated with photosynthesis-related genes. The expression of *KEA3* was strongly correlated with genes annotated with the gene ontology (GO) term 'photosynthesis' (Supplementary Fig. 1a, $P<10^{-12}$, Mann–Whitney *U*-test). Conversely, the most significantly enriched GO term among the 100 genes whose expression was most highly correlated with *KEA3* was 'photosynthesis' ($P<10^{-41}$). KEA3 is highly conserved among photosynthetic eukaryotes (Supplementary Fig. 1b).

KEA3 is localized in the thylakoid membrane. Two splice forms of *KEA3* are annotated in *Arabidopsis*: *KEA3.1* and *KEA3.2*. Both

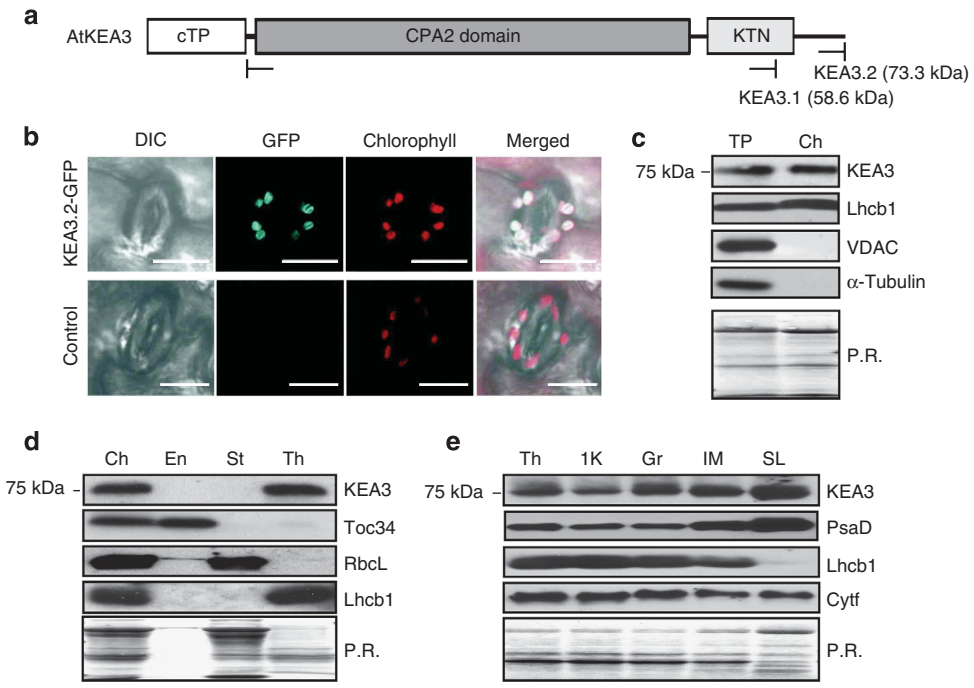

Figure 1 | KEA3 localizes to the thylakoid stromal lamellae. (**a**) KEA3.2 has an amino-terminal chloroplast-targeting peptide, a cation/proton exchanger (CPA2) domain and a putative KTN domain. (**b**) Differential interference contrast, GFP and chlorophyll fluorescence were imaged in leaf guard cells from *Arabidopsis* WT plants and *kea3-1* plants transformed with *KEA3.2-GFP*. Scale bar, 10 μm. (**c**–**e**) KEA3 abundance was measured by western blot in: (**c**) Total protein (TP) and chloroplast (Ch) protein extracts; (**d**) Ch subfractionated into envelope (En), stroma (St) and thylakoids (Th); (**e**) Th separated into the fraction pelleted by 1,000*g* (1K), grana (Gr), intermediate membranes (IM) and stromal lamellae (SL). (**c**–**e**) Ponceau red (P.R.) stains of membranes after protein transfer before immunodetection are shown as loading controls.

encode a predicted chloroplast transit peptide and a cation/H^+ antiporter (CPA2) domain (Fig. 1a, Supplementary Fig. 2a). *KEA3.2* additionally encodes a carboxyl-terminal (C-terminal) K^+ transport/nucleotide-binding (KTN) domain, which is truncated in *KEA3.1*. Size analyses of the endogenous KEA3 protein and tagged versions of both isoforms indicate that KEA3.2 is the major protein isoform in leaves (Supplementary Fig. 2). Recently, C-terminal fluorescent protein fusions of KEA3.1 and KEA3.2 were localized to the chloroplast and the Golgi, respectively[12,13]. In contrast to previous work, we observed KEA3.2-green fluorescent protein (GFP) in the chloroplast (Fig. 1b). We confirmed the localization of the endogenous KEA3 to the chloroplast in wild-type (WT) leaves by western blot of total and chloroplast protein extracts (Fig. 1c, Supplementary Fig. 3a). Subfractionation of WT chloroplasts demonstrated that endogenous KEA3 is located in the thylakoid membrane and is enriched in the stromal lamellae (Fig. 1d,e, Supplementary Fig. 3b,c).

KEA3 accelerates photosynthetic acclimation to low light. We analysed the phenotypes of two *kea3* mutant alleles, *kea3-1* and *kea3-2* (Supplementary Fig. 2). These mutants displayed no measurable defects in growth, leaf colouration or protein composition of the photosynthetic apparatus (Supplementary Fig. 4). To characterize potential defects in regulation of photosynthesis, we performed chlorophyll fluorescence measurements across various light conditions. We observed a striking perturbation of the kinetics of non-photochemical energy quenching (NPQ) on a shift from dark to low-light conditions. In flowering plants, a shift from a dark-acclimated state to light-limiting conditions causes a transient rise in NPQ, which is attributed to qE[14]. The *kea3* mutants displayed a higher maximum NPQ and a delay in its peak and relaxation (Fig. 2a, Supplementary Fig. 5a). This *kea3* phenotype was complemented by expressing a KEA3.2-GFP fusion protein that accumulated at levels similar to the native protein (Fig. 2a, Supplementary Fig. 6). Remarkably, plants overexpressing the amino-terminal part of KEA3 containing the chloroplast transit peptide and CPA2 domains (*oeKEA3*$_{CPA2}$) showed accelerated qE relaxation kinetics. When shifted from dark to higher light intensities, *kea3* mutants displayed WT-like induction kinetics of NPQ (Supplementary Fig. 5c,e).

The transient nature of the additional NPQ observed on a shift to low light suggested that qE was perturbed in *kea3*. qE is known to be modulated by the luminal pH and zeaxanthin, and normal qE kinetics require the protein PsbS[14]. *kea3psbs* double mutants exhibited the same NPQ kinetics as *psbs* single mutants (Fig. 2b, Supplementary Fig. 7a), indicating that PsbS is required for the additional NPQ observed in *kea3*. Double mutants of *kea3* with *npq1* (lacking zeaxanthin) and *npq2* (overaccumulating zeaxanthin) revealed that the NPQ phenotype was modulated by levels of zeaxanthin (Supplementary Fig. 7b,c). Application of high concentrations of nigericin, which inhibit qE[15], to leaves, abolished the rapid component of NPQ in both WT and *kea3* (Supplementary Fig. 8a). Thus, the additional NPQ observed in *kea3* shows the key characteristics of qE.

The transient increase in NPQ was accompanied by lower PSII quantum yield (Φ_{II}) in *kea3* ($P<0.004$, Student's *t*-test, Fig. 2c), indicating decreased linear electron flow through PSII. This decrease in Φ_{II} was PsbS dependent (Supplementary Fig. 7e), suggesting that it was caused by an increase in qE. In *oeKEA3*$_{CPA2}$, Φ_{II} was transiently higher than in WT (Fig. 2c). We conclude that KEA3 accelerates qE relaxation, allowing more absorbed light energy to be used to drive electron flow through PSII.

KEA3 likely mediates K^+/H^+ antiport. To gain insights into the identity of the cations transported by the CPA2 domain of

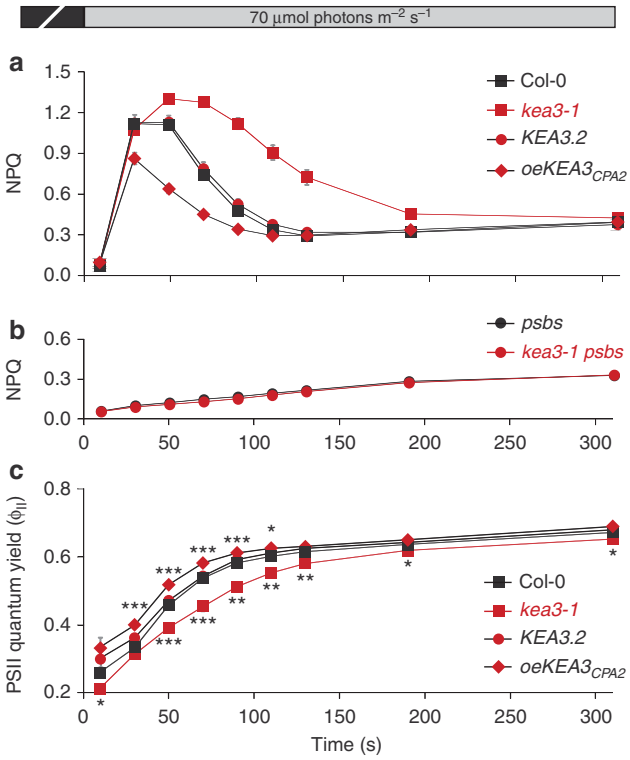

Figure 2 | KEA3 accelerates qE relaxation on transition from dark to low light. (**a**) NPQ induction in detached leaves of 3-week-old Col-0, *kea3-1* and *kea3-1* expressing *KEA3.2-GFP* (*KEA3.2*) or overexpressing *KEA3*$_{CPA2}$*-GFP* (*oeKEA3*$_{CPA2}$) was measured at 70 µmol photons m^{-2} s^{-1} after 30 min dark incubation. (**b**) The extra NPQ in *kea3* mutants requires PsbS. NPQ induction in detached leaves of 2-week-old *psbs* and *kea3-1 psbs* mutant plants was measured as in **a**. (**c**) The higher transient NPQ in *kea3* decreases the PSII quantum yield (Φ_{II}), and *oeKEA3*$_{CPA2}$ show transiently increased Φ_{II}. Φ_{II} was calculated from the same experiment as **a**. Asterisks indicate time points where *kea3-1* or *oeKEA3*$_{CPA2}$ differ significantly from WT (*$0.01<P<0.04$, **$0.001<P<0.01$, ***$P<0.001$, Student's *t*-test). (**a**–**c**) Error bars represent s.e.m. ($n=6$).

KEA3, we used phylogenetics. KEA3 shows more sequence homology to experimentally validated K^+/H^+ antiporters AtKEA2 (ref. 16) and EcKefC[17] than to Na^+/H^+ antiporters EcNhaA and TtNapA (Fig. 3a). Comparison of two amino acid residues critical for Na^+/H^+ binding in Na^+/H^+ antiporters of the CPA2 family[18,19] indicates that presence of an Aspartate–Aspartate motif strictly correlates with Na^+/H^+ antiport activity, while conversion of the first residue to Asparagine or Glutamine correlates with K^+/H^+ antiport activity[16,17,20] (Fig. 3b). Like AtKEA2 and EcKefC, KEA3 has a Glutamine–Aspartate motif. Finally, the presence of the K^+ transport-related KTN domain in KEA3 further supports a K^+/H^+ antiporter activity[21,22].

We reasoned that if KEA3 is a K^+/H^+ antiporter, low concentrations of the small molecule electroneutral K^+/H^+ antiporter nigericin might rescue the *kea3* phenotype. Strikingly, infiltration of leaves with 0.03 µM nigericin fully rescued the qE phenotype (Fig. 3c, Supplementary Fig. 8a). This result strongly suggests that KEA3 accelerates the qE relaxation by electroneutral K^+/H^+ antiport.

KEA3 decreases the ΔpH component of the proton motive force. If KEA3 is a K^+/H^+ antiporter, it could alter the proton concentration (ΔpH) and/or electric potential (Δψ) components

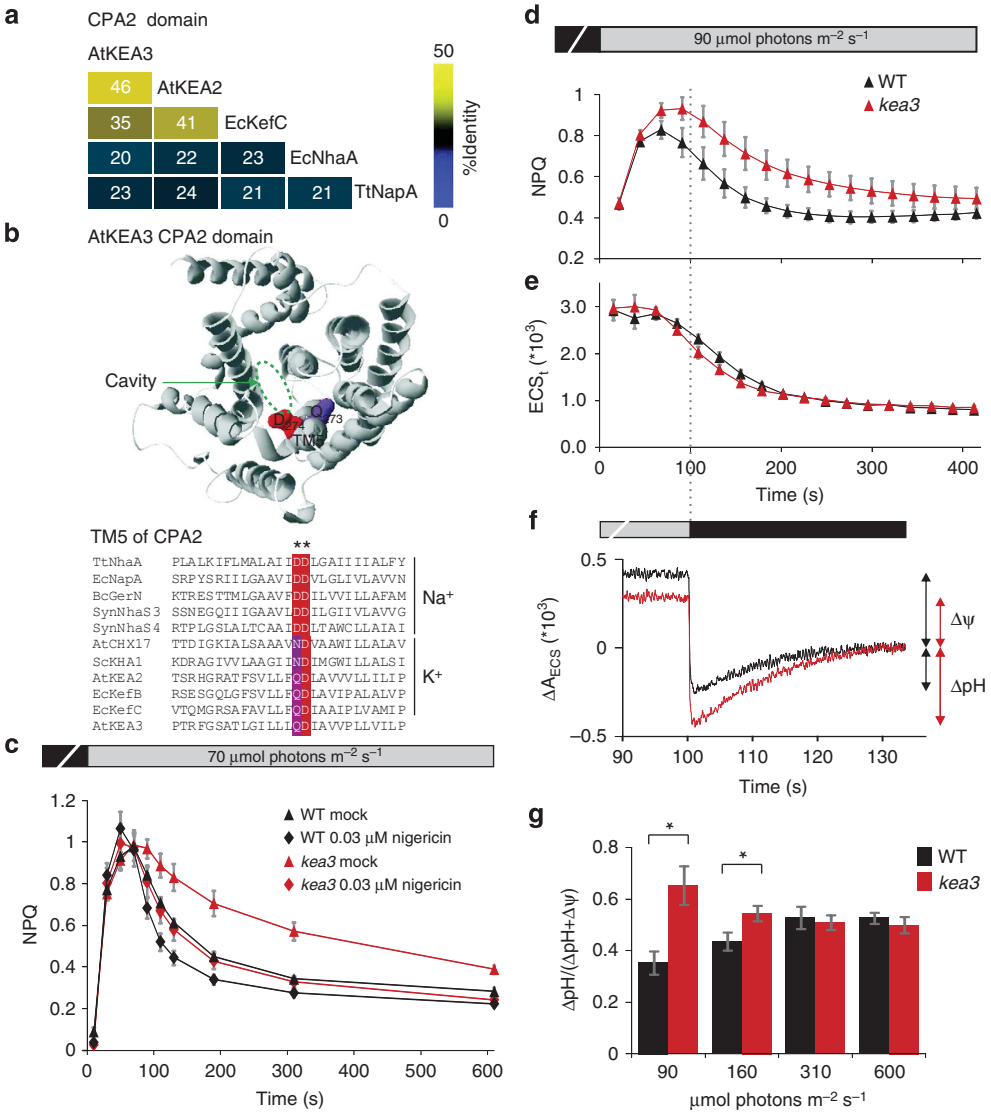

Figure 3 | KEA3 regulates the composition of the p.m.f. by mediating potassium/proton antiport. (**a**) The CPA2 domain of KEA3 is homologous to that of known K^+/H^+ antiporters. A percent identity matrix is shown for *Arabidopsis* KEA2 and KEA3, *E. coli* KefC and NhaA and *T. thermophilus* NapA. (**b**) The locations of two key substrate-binding amino acid residues in TM5 of the CPA2 domain[19] are shown on a model of KEA3. (**c**) Low levels of Nigericin complement the *kea3* NPQ phenotype. NPQ induction on transition from dark to 70 µmol m^{-2} s^{-1} light was measured in WT (Ws) and *kea3-2* leaves incubated in water (mock) or 0.03 µM nigericin. (**d**,**e**) p.m.f. kinetics in *kea3* mutants are largely unaffected. NPQ and ECS_t (which reports the magnitude of the p.m.f.) were measured near-simultaneously in WT (Ws) and *kea3-2* by Chl fluorescence and dark-induced relaxation kinetics, respectively, in single leaves during a transition from dark to 90 µmol m^{-2} s^{-1}. (**f**) After 100 s of low light, *kea3* mutants show increased ΔpH and decreased Δψ. Full ECS decay kinetics were recorded after 100 s of low light (90 µmol m^{-2} s^{-1}) to measure ΔpH and Δψ in WT (Col-0) and *kea3-1*. The average of six independent measurements per genotype was plotted as a moving average with interval 5 (see also Supplementary Fig. 9). (**g**) The experiment in **f** was repeated at different light intensities, and the fraction of the p.m.f. contributed by ΔpH was plotted. Asterisks indicate where WT and *kea3* differ significantly (*$P<0.04$, Student's *t*-test). (**c**–**e**,**g**) Error bars represent s.e.m. ($n=6$).

of the proton motive force (p.m.f.). We performed near-simultaneous measurements of NPQ as a readout of ΔpH, and of the magnitude of the carotenoid electrochromic shift (ECS_t)[23] as a readout of total p.m.f. (ΔpH + Δψ), during the transition from dark to low light (Fig. 3d,e). The dynamics of the p.m.f. were largely unchanged in *kea3*, but the ratio of NPQ to ECS_t was higher than in WT, suggesting that KEA3 transiently decreases the contribution of ΔpH to the proton motive force.

We measured both ΔpH and Δψ after 100 s illumination by turning off the light and observing the extended kinetics of the ECS[24]. These measurements indicated that after 100 s of low light, the ΔpH is greater in *kea3* than in WT ($P<0.04$, Student's *t*-test, Fig. 3f,g, Supplementary Fig. 8b), consistent with the observed increased NPQ in *kea3* at this time point (Figs 2a and 3d, Supplementary Fig. 5a). This difference was not present at higher light intensities. These data further support the idea that KEA3 decreases the contribution of ΔpH and increases the contribution of Δψ to p.m.f.

KEA3 accelerates acclimation from high to low light. Transitions from high to low light are common in many growth environments, including crop canopies[1]. We therefore asked whether KEA3 influences the dynamics of photosynthesis during transitions from high to low light. After a sudden shift from high to low light, NPQ in WT *Arabidopsis* plants decayed over ~80 s

to a new, lower level (Fig. 4a,b, Supplementary Fig. 9a). Strikingly, NPQ decayed more slowly in *kea3*, while high and low light NPQ values were comparable to WT. The half time of the NPQ decay in *kea3* was twice as long as that in WT (Col-0: 24.8 ± 1.4 s, *kea3-1*: 47.6 ± 3.0 s, $P = 4.1 \times 10^{-5}$; Ws: 25.9 ± 1.4 s, *kea3-2*: 51.8 ± 2.0 s $P = 1.8 \times 10^{-6}$ (± s.e.m., Student's *t*-test)). These data suggest that KEA3 plays a key role in accelerating the decay of NPQ during transitions from excess to limiting light conditions.

We observed decreased Φ_{II} in *kea3* ($P < 0.02$, Student's *t*-test) over a similar time interval to the NPQ defect (Fig. 4c, Supplementary Fig. 9b). As during transition from dark to low light (Fig. 2a,c), these data suggest that the slower relaxation of NPQ in *kea3* results in a transient decrease in linear electron flow relative to WT.

We measured CO_2 assimilation during the same transition. While CO_2 assimilation rates of *kea3* and WT plants were similar under steady-state high and low light, *kea3* exhibited a period of lower CO_2 assimilation than WT immediately after a transition from high to low light (Fig. 4d,e, $P < 0.007$, Supplementary Fig. 9c,d, $P < 0.04$). We conclude that following a high- to low-light transition, KEA3 accelerates the downregulation of qE, thus allowing a larger fraction of the absorbed light energy to drive linear electron flow and CO_2 fixation.

KEA3 improves photosynthetic efficiency in fluctuating light. To investigate the role of KEA3 under continuously fluctuating light, we exposed plants to alternating cycles of 140 s at high light and 100 s at low light. *kea3* mutants consistently showed slower NPQ relaxation and Φ_{II} recovery than WT after each transition (Fig. 4f,g and Supplementary Fig. 10). These phenotypes were present regardless of whether the fluctuations were preceded by 10 min of high light or 10 min of low light, suggesting that KEA3's function is not extensively affected by preceding light conditions. NPQ and Φ_{II} in *kea3* reached WT levels after the fluctuations stopped, further supporting the role of KEA3 specifically in light transitions. We conclude that KEA3 improves photosynthetic efficiency under continuously fluctuating light.

Discussion

Our data are consistent with the following intriguing model: (i) The dynamics of qE relaxation are dictated by the dynamics of the thylakoid luminal pH. (ii) After a sudden transition to low light, the ATP synthase alone cannot sustain sufficient proton efflux to enable rapid downregulation of qE. (iii) KEA3 overcomes this limitation by providing an additional route for proton efflux, thereby accelerating qE relaxation and increasing photosynthetic yield. KEA3's electroneutral activity would provide two advantages for proton efflux over a simple proton channel: (i) it retains the $\Delta\psi$ component of the p.m.f. and (ii) it can rapidly mediate a large flux because its activity does not generate an opposing electric field.

We note that the combined activities of KEA3 and the recently identified thylakoid potassium channel TPK3 (ref. 25) would dissipate the p.m.f. We thus anticipate that under most conditions, the activities of these two proteins are tightly regulated to minimize waste of energy. However, under some conditions causing harmful excess ΔpH[26], KEA3 and TPK3 together may form a safety valve to allow dissipation of p.m.f.

Intriguingly, the KTN domain of KEA3 could regulate KEA3 activity in response to the redox state of the stroma. In *E. coli*, NADH binds to the KefC KTN domain and represses KefC activity[17]. The observation that the *kea3* phenotype is specific to transitions to low light suggests that KEA3 might similarly be repressed by NADPH (or alternatively, activated by NADP).

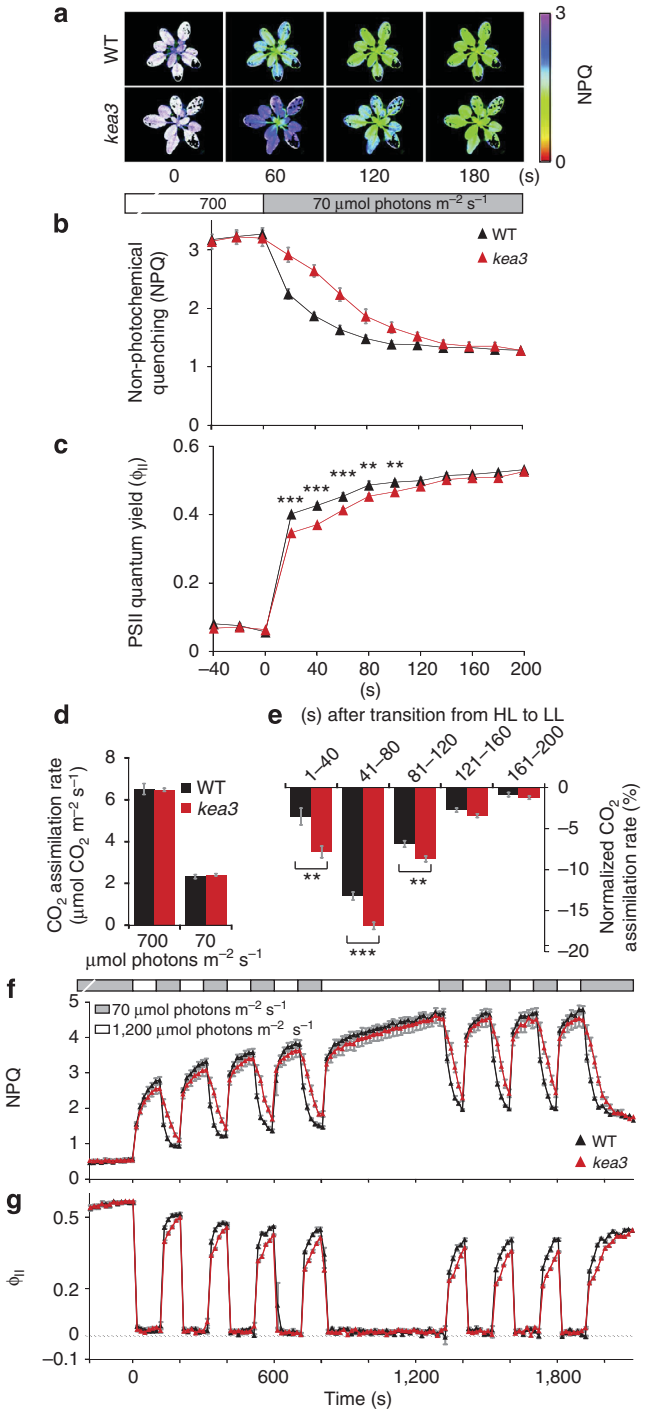

Figure 4 | KEA3 regulates the dynamics of photosynthesis during transitions from high to low light. (**a**,**b**) NPQ relaxation on transition from high to low light is delayed in *kea3* (*kea3-2*) as compared with WT (Ws). (**c**) Φ_{II} is decreased during transition from high to low light. Φ_{II} was calculated from the same measurement as in **a**,**b**. (**d**) WT (Ws) and *kea3* (*kea3-2*) show similar CO_2 assimilation rates during steady-state high (HL, 700 µmol photons m^{-2} s^{-1}) and low light (LL, 70 µmol photons m^{-2} s^{-1}). (**e**) The normalized CO_2 assimilation rate (shown as a percentage of the difference between HL and LL) is decreased in *kea3* (*kea3-2*). (**f**) In fluctuating light, NPQ relaxation is delayed after each transition from high to low light in *kea3-2*. (**g**) Φ_{II} is decreased in *kea3-2* during each transition from high to low light. Φ_{II} was calculated from the same measurement as in (**f**). (**c**,**e**) Asterisks represent significantly lower values in *kea3-2* (**$0.001 < P < 0.01$, ***$P < 0.001$, Student's *t*-test). (**b**–**g**) Error bars represent s.e.m. (**b**–**e**: $n = 7$; **f**,**g**: $n = 4$).

KEA3 could thus be a key component of a feedback loop, which detects an oxidized stroma and facilitates reduction of oxidized PSI electron acceptors by downregulating qE.

Our work demonstrates that the kinetics of qE decay influence photosynthetic efficiency. Our discovery that plants have a built-in machinery to accelerate these kinetics makes KEA3 a new target for efforts to improve crop productivity. Excitingly, overexpression of the KEA3 CPA2 domain produces a transient increase in the relative CO_2 assimilation rate after transition from high to low light (Supplementary Fig. 9). However, the over-expression of the CPA2 domain appears to also result in undesirable photodamage in high light. It is possible that improved regulation of KEA3 would overcome this limitation. Thus, the future investigation of KEA3 should yield both fascinating insights into the core logic of photosynthesis regulation, as well as keys to possible enhancements in crop yields.

Methods

Plant material, propagation and growth conditions. The *kea3-1* mutant (Gabi_170G09) in the Col-0 genetic background originates from the GABI-KAT collection[27]. The *kea3-2* mutant (FLAG_493_C01) in the Wassilewskija (Ws) genetic background originates from the FLAGdb/FST T-DNA collection[28]. The *aba1* mutant (Salk_059469) in the Col-0 genetic background originates from the SALK T-DNA collection[29]. The *npq1* and *psbs* mutants have been described previously[7,8].

Plants expressing *KEA3.1* and *KEA3.2* with a C-terminal HA tag were generated by introducing the *KEA3* coding regions (for primers, see Supplementary Table 1) into the Gateway plant expression vector pJCV55 (ref. 30) downstream of a Cauliflower mosaic virus 35S promoter. Constructs for expressing KEA3.02 and $KEA3_{CPA2}$ with a C-terminal eGFP tag were generated in a similar manner, but with vector pB7FWG2. Flowers of *kea3-1* mutant plants were transformed with the *KEA3* constructs by floral dip[31]. The plants were then transferred to the greenhouse and seeds were collected after 3 weeks. Individual transgenic plants were selected on the basis of their resistance to kanamycin (pJCV55) or Basta (pB7FWG2) on sterile 1% agar media containing 1 × MS nutrients (PhytoTechnology Laboratories) and 0.05 g l^{-01} MES, adjusted to pH 5.7 with KOH. Before transfer to soil, Kanamycin- and Basta-resistant plants were additionally screened for red fluorescent protein and GFP expression, respectively, using an M165 FC fluorescence microscope (Leica) to verify expression of the transgene (the T-DNA deriving from pJCV55 carries an additional red fluorescent protein-encoding gene). The presence of the *KEA3* transgene in transformants was confirmed by PCR and its expression was confirmed by protein immunoblot analyses.

WT and mutant *Arabidopsis* plants were grown on soil under controlled conditions in the greenhouse (matted daylight supplemented with high pressure sodium 400 W lamps, ~100 µmol photons $m^{-2} s^{-1}$ on leaf surfaces, 14/10 h light/dark cycle, constant temperature of 20 °C) or in growth chambers (10 h light, 22 °C/14 h dark, 23 °C, with a light intensity of 100 µmol photons $m^{-2} s^{-1}$).

Nucleic acid analysis. *Arabidopsis* DNA was extracted using RedExtract-N-Amp (Sigma). T-DNA insertion junction sites were recovered by PCR using combinations of insertion- and gene-specific primers (see Supplementary Table 1), and then sequenced. For reverse transcriptase-PCR (RT–PCR) analysis and cDNA synthesis, RNA was extracted from leaves using the RNeasy plant mini kit (Qiagen) according to the manufacturer's instructions.

The cDNA for cloning purposes was synthesized using Superscript III (Invitrogen). RT–PCR was performed with SuperScript III One-Step RT–PCR System (Invitrogen) and gene-specific primers (see Supplementary Table 1), both according to the manufacturer's instructions.

Fluorescence measurements. Room temperature Chl *a* fluorescence of whole leaves of 2–3-week-old *Arabidopsis* plants was measured using an imaging chlorophyll fluorometer (Open FluorCam 800-O/1010; Photon Systems Instruments) or the Dual-PAM 100 (Walz). NPQ during dark-to-light transitions was determined using the FluorCam by acclimating plants for 30 min to dark, followed by 5–10 min at indicated light intensities of red light. To measure Fm and Fm′, white light pulses (4,000 µmol photons $m^{-2} s^{-1}$, duration 800 ms) were applied. NPQ induction and relaxation during dark to 50, 220 and 660 µmol photons $m^{-2} s^{-1}$ transitions were monitored using the Dual-PAM by applying red actinic light and white light pulses (4,000 µmol photons $m^{-2} s^{-1}$, duration 800 ms) at 20 s intervals. NPQ was calculated as $(Fm - Fm')/Fm'$ and Φ_{II} as $(Fm - Fs)/Fm$.

NPQ relaxation half times were calculated as follows. A steady-state low light average NPQ value was subtracted from the first five data points during the NPQ relaxation period. The binary logarithm of these values was taken, and a linear fitting was performed to obtain a slope *s*. $t_{1/2}$ was calculated as $t_{1/2}(NPQ) = 1/-s$.

For nigericin rescue experiments, plants were dark adapted for 30 min. Then, leaves were pressed against sand paper to facilitate nigericin uptake and incubated in indicated concentrations of nigericin for 3 h in the dark before measuring NPQ during dark-to-light transitions at 70 µmol photons $m^{-2} s^{-1}$.

ECS measurements. Near-simultaneous ECS and fluorescence measurements as well as p.m.f. partitioning analysis were performed on a custom made spectrophotometer/chlorophyll fluorometer chamber with non-focusing optics using three different wavelengths (505, 520 and 535 nm) for deconvoluted ECS measurements[23,32]. Leaves were dark adapted for 30 min before the actinic light of 90 µmol photons $m^{-2} s^{-1}$ was turned on. Each dark interval relaxation kinetic measurement was made by turning off the actinic light for 200 ms. p.m.f. parsing traces were obtained by turning off the actinic light at 100 s. The ECS steady-state ($\Delta\psi$) and ECS inverse (ΔpH) were extracted from these traces as described previously[24,33].

CO_2 assimilation measurements. Plants were grown in 50 ml Falcon tubes with a pierced bottom filled with Sunshine Mix 4 potting mix, placed in a dish containing 1–3 cm of water, under 100 µmol $m^{-2} s^{-1}$ fluorescent light. For measurement, the Falcon tubes were inserted using a foam gasket into a LI-COR 6400-17 Whole Plant Arabidopsis Chamber. The chamber was placed under a Walz MAXI IMAGING-PAM with blue actinic LEDs, which ran the light programs and was used to simultaneously record chlorophyll fluorescence data. CO_2 assimilation was measured with a reference CO_2 concentration of 400 µmol mol^{-1} and a 500 µmol s^{-1} flow rate, averaging and recording data over 2 s intervals. The steady-state assimilation rates under high and low light were obtained for each plant by averaging the assimilation rate over the intervals (− 40 to 0 s) and (+ 560 to + 600 s), respectively, and normalizing the assimilation rate by the rosette area measured from IMAGING-PAM images with ImageJ. The transient CO_2 assimilation was calculated as follows. For each plant, the data was normalized so that steady-state high light assimilation rate was 1, and the steady-state low light assimilation rate was 0. The average normalized assimilation rate in each time interval was then calculated for each plant.

Leaf pigment analysis. Pigments were analysed by reverse-phase high-performance liquid chromatography[34]. For pigment extraction, leaf discs were frozen in liquid nitrogen and disrupted with beads in microcentrifuge tubes in the presence of acetone. After a short centrifugation, pigment extracts were filtered through a membrane filter (pore size 0.2 µm) and either used directly for high-performance liquid chromatography analysis or stored for up to 2 days at − 20 °C.

Computational analysis. *Arabidopsis KEA3.1* and *KEA3.2* (*At4g04850.1* and.*2*) DNA and protein sequences were retrieved from TAIR (The Arabidopsis Information Resource; www.arabidopsis.org). Subcellular localization signals were analysed by SUBA3 (http://suba.plantenergy.uwa.edu.au/), which combines predictions from up to 22 prediction programs[35], and by ChloroP (http://www.cbs.dtu.dk/services/ChloroP)[36].

For sequence comparisons, homologues of the *Arabidopsis* KEA3 protein (AtKEA3, Uniprot: Q9M0Z3) were identified by BLAST. Percent identity matrices were calculated for the CPA2 (Pfam00999) domains of *E. coli* NhaA (EcNhaA, P13738), *T. thermophilus* NapA (TtNapA, Q72IM4), *E. coli* KefC (EcKefC, P03819), AtKEA3, *Arabidopsis* KEA2 (AtKEA2, Q65272) and homologous AtKEA3 sequences from *Oryza sativa* (O.s., Q2QM48), *Physcomitrella patens* (P.p., A9SSR0) and *Chlamydomonas reinhardtii* (C.r., A8ISE8) by using ClustalOmega (http://www.ebi.ac.uk/Tools/msa/clustalo/). For the homologous KEA3 sequences, an identity matrix was also calculated for the KTN domain (Pfam02254). To generate the KEA3 three-dimensional model, the TtNapA protein was used as a template by the Phyre2 server (http://www.sbg.bio.ic.ac.uk/~phyre2/)[37]. Sequence comparison of TM5 of the CPA2 domain of AtKEA3, EcNhaA, EcKefB (P45522) EcKefC, TtNapA, *Bacillus cereus* GerN (BcGerN, Q9KI10), Synechocystis NhaS3 (Q55190) and NhaS4 (Q5N3F5), *Arabidopsis* AtCHX17 (Q9SUQ7), AtKEA2 and *Saccharomyces cerevisiae* KHA1 (P40309) were performed using ClustalOmega.

KEA3 co-expression analysis was performed by determining Pearson correlation coefficients of all *Arabidopsis* genes with *KEA3* using the GeneCAT database (http://genecat.mpg.de). All genes in the database whose identifiers contained 'At' were used in this analysis. The 100 genes with the highest correlation values were analysed for the enrichment of specific GO terms by using AmiGO (amigo.geneontology.org/cgi-bin/amigo/term_enrichment,[38]).

Protein isolation, PAGE and immunoblot analyses. Total protein was isolated from leaves using the protein extraction buffer and corresponding protocol from Agrisera. Thylakoid membranes were isolated from leaves at 4 °C by shredding leaf tissue in 0.1 M Tricine/KOH pH 7.9, 400 mM Sorbitol, protease inhibitor cocktail (Sigma) using a Waring blender and filtering the homogenate through two layers of miracloth. The flow-through was centrifuged at 1,000*g* for 5 min. The resulting pellet was resuspended and incubated in 20 mM Hepes/KOH pH 7.6, 10 mM EDTA for 30 min to break remaining intact chloroplasts. Thylakoid membranes were then extracted by a centrifugation at 10,000*g* for 10 min. For SDS-

polyacrylamide gel electrophoresis, proteins were fractionated on Tris-glycine gels (Bio-Rad). For Blue Native polyacrylamide gel electrophoresis, thylakoid membranes were solubilized with 0.7% β-*n*-dodecyl-D-maltoside (w/v) and separated by Blue Native gels (Invitrogen)[39]. For protein blot analysis, proteins were transferred to a nitrocellulose membrane, blocked with 5% (w/v) nonfat dry milk and hybridized with the antibodies indicated in the figure legends and text. Antibodies (except for α-KEA3, α-GFP and α-HA) were purchased from Agrisera. All antibodies were diluted in 50 mM Tris, 150 mM NaCl, 0.1% (v/v) Tween 20 and 5% (w/v) nonfat dry milk before use (α-Tubulin (AS10680) 1:3,000, VDAC (AS07212) 1:10,000, Lhcb1 (AS01004) 1:10,000, RbcL (AS03037) 1:20,000, TOC34 (AS07238) 1:2,000, PsaD (AS09461) 1:5,000, Cytf (AS08306) 1:10,000, CP47 (AS04038) 1:10,000 and PsbS (AS03032) 1:5,000. α-GFP (Invitrogen, A-6455) was diluted 1:2,000 and α-HA (Sigma, H6908) 1:2,500. Uncropped scans of the western blots are shown in Supplementary Fig. 3. AtpB and PsbS signals were quantified by densitometric analysis of western bands using NIH ImageJ software and associated plug-ins (http://imagej.nih.gov/ij/).

For immunolocalization of KEA3, an antibody against the specific peptide sequence NQLGRKAADFLDERLDPGE (present in both KEA3.1 and KEA3.2 isoforms) was generated in rabbits by Yenzym and a dilution of 1:100 in 50 mM Tris, 150 mM NaCl, 0.01% (v/v) and 5% (w/v) nonfat dry milk was used for hybridization.

Determination of KEA3 localization. Leaves of Col-0 or *kea3-1* plants expressing *KEA3.2-GFP* were analysed using a Leica SP5 AOBS Point Scanning Confocal Microscope. GFP and chlorophyll autofluorescence (Chl) were excited at 488 nm and signals were collected at 660–736 nm (Chl) and 495–515 nm (GFP).

Arabidopsis chloroplasts were isolated by a two-step Percoll gradient centrifugation[40]. The homogenized leaf tissue was applied to a two-step Percoll gradient and intact chloroplasts were collected from the interphase. For chloroplast fractionation, chloroplasts were hypotonically lysed in 10 mM Tris/HCl, pH 8.0 and 1 mM EDTA, pH 8.0, at a chlorophyll concentration of 2 mg ml^{-1}, and loaded onto a three-step Sucrose gradient[41]. After centrifugation (30,000*g*; 4 °C, 1 h), the upper phase (containing the stroma), the upper interphase (with the envelope membranes) and the pellet (thylakoids) were collected and the proteins were precipitated[42].

Thylakoid fractionation was performed according to Kyle *et al.*[43] with minor modifications. Thylakoid membranes at 0.4 mg chlorophyll ml^{-1} in 15 mM Tricin/KOH pH7.8, 0.1 M Sorbitol, 15 mM NaCl, 5 mM $MgCl_2$ were treated with 0.15% digitonin (w/v) for 1 min and then diluted 10-fold with the same buffer. Samples were then centrifuged at 1,000; 10,000; 40,000; and 150,000*g* to yield the different fractions.

References

1. Pearcy, R. W. Sunflecks and photosynthesis in plant canopies. *Annu. Rev. Plant Physiol. Plant Mol. Biol.* **41,** 421–453 (1990).
2. Reinhard, K., Smith, W. K. & Carter, G. A. Clouds and cloud immersion alter photosynthetic light quality in a temperate mountain cloud forest. *Botany* **88,** 462–470 (2010).
3. Kramer, D. M., Cruz, J. A. & Kanazawa, A. Balancing the central roles of the thylakoid proton gradient. *Trends Plant. Sci.* **8,** 27–32 (2003).
4. Allen, J. Photosynthesis of ATP-electrons, proton pumps, rotors, and poise. *Cell* **110,** 273–276 (2002).
5. Müller, P., Li, X. P. & Niyogi, K. K. Non-photochemical quenching. A response to excess light energy. *Plant Physiol.* **125,** 1558–1566 (2001).
6. Demmig-Adams, B. *et al.* Using chlorophyll fluorescence to assess the fraction of absorbed light allocated to thermal dissipation of excess excitation. *Physiol. Plant.* **98,** 253–264 (1996).
7. Li, X. P. *et al.* A pigment-binding protein essential for regulation of photosynthetic light harvesting. *Nature* **403,** 391–395 (2000).
8. Niyogi, K. K., Grossman, A. R. & Björkman, O. *Arabidopsis* mutants define a central role for the xanthophyll cycle in the regulation of photosynthetic energy conversion. *Plant Cell* **10,** 1121–1134 (1998).
9. Demmig-Adams, B., Cohu, C. M., Muller, O. & Adams, 3rd W. W. Modulation of photosynthetic energy conversion efficiency in nature: from seconds to seasons. *Photosynth. Res.* **113,** 75–88 (2012).
10. Zhu, X. G., Ort, D. R., Whitmarsh, J. & Long, S. P. The slow reversibility of photosystem II thermal energy dissipation on transfer from high to low light may cause large losses in carbon gain by crop canopies: a theoretical analysis. *J. Exp. Bot.* **55,** 1167–1175 (2004).
11. Zaks, J., Amarnath, K., Kramer, D. M., Niyogi, K. K. & Fleming, G. R. A kinetic model of rapidly reversible nonphotochemical quenching. *Proc. Natl Acad. Sci. USA* **109,** 15757–15762 (2012).
12. Kunz, H. H. *et al.* Plastidial transporters KEA1, -2, and -3 are essential for chloroplast osmoregulation, integrity, and pH regulation in *Arabidopsis*. *Proc. Natl Acad. Sci. USA* **111,** 7480–7485 (2014).
13. Zheng, S., Pan, T., Fan, L. & Qiu, Q. S. A novel AtKEA gene family, homolog of bacterial K^+/H^+ antiporters, plays potential roles in K^+ homeostasis and osmotic adjustment in *Arabidopsis*. *PLoS ONE* **8,** e81463 (2013).
14. Kalituho, L., Beran, K. C. & Jahns, P. The transiently generated nonphotochemical quenching of excitation energy in *Arabidopsis* leaves is modulated by zeaxanthin. *Plant Physiol.* **143,** 1861–1870 (2007).
15. Brooks, M. D., Sylak-Glassman, E. J., Fleming, G. R. & Niyogi, K. K. A thioredoxin-like/beta-propeller protein maintains the efficiency of light harvesting in *Arabidopsis*. *Proc. Natl Acad. Sci. USA* **110,** E2733–E2740 (2013).
16. Aranda-Sicilia, M. N. *et al.* *Arabidopsis* KEA2, a homolog of bacterial KefC, encodes a K(+)/H(+) antiporter with a chloroplast transit peptide. *Biochim. Biophys. Acta* **1818,** 2362–2371 (2012).
17. Fujisawa, M., Ito, M. & Krulwich, T. A. Three two-component transporters with channel-like properties have monovalent cation/proton antiport activity. *Proc. Natl Acad. Sci. USA* **104,** 13289–13294 (2007).
18. Arkin, I. T. *et al.* Mechanism of Na^+/H^+ antiporting. *Science* **317,** 799–803 (2007).
19. Lee, C. *et al.* A two-domain elevator mechanism for sodium/proton antiport. *Nature* **501,** 573–577 (2013).
20. Maresova, L. & Sychrova, H. *Arabidopsis thaliana* CHX17 gene complements the kha1 deletion phenotypes in Saccharomyces cerevisiae. *Yeast* **23,** 1167–1171 (2006).
21. Chanroj, S. *et al.* Conserved and diversified gene families of monovalent cation/H^+ antiporters from algae to flowering plants. *Front. Plant Sci.* **3,** 25 (2012).
22. Roosild, T. P., Miller, S., Booth, I. R. & Choe, S. A mechanism of regulating transmembrane potassium flux through a ligand-mediated conformational switch. *Cell* **109,** 781–791 (2002).
23. Sacksteder, C. A. & Kramer, D. M. Dark-interval relaxation kinetics (DIRK) of absorbance changes as a quantitative probe of steady-state electron transfer. *Photosynth. Res.* **66,** 145–158 (2000).
24. Cruz, J. A., Sacksteder, C. A., Kanazawa, A. & Kramer, D. M. Contribution of electric field (Δφ) to steady-state transthylakoid proton motive force (pmf) *in vitro* and *in vivo*. control of pmf parsing into Δφ and ΔpH by ionic strength. *Biochemistry* **40,** 1226–1237 (2001).
25. Carraretto, L. *et al.* A thylakoid-located two-pore K^+ channel controls photosynthetic light utilization in plants. *Science* **342,** 114–118 (2013).
26. Kramer, D., Sacksteder, C. & Cruz, J. How acidic is the lumen? *Photosynth. Res.* **60,** 151–163 (1999).
27. Rosso, M. G. *et al.* An *Arabidopsis thaliana* T-DNA mutagenized population (GABI-Kat) for flanking sequence tag-based reverse genetics. *Plant Mol. Biol.* **53,** 247–259 (2003).
28. Samson, F. *et al.* FLAGdb/FST: a database of mapped flanking insertion sites (FSTs) of *Arabidopsis thaliana* T-DNA transformants. *Nucleic Acids Res.* **30,** 94–97 (2002).
29. Alonso, J. M. *et al.* Genome-wide insertional mutagenesis of *Arabidopsis thaliana*. *Science* **301,** 653–657 (2003).
30. Karimi, M., Inze, D. & Depicker, A. GATEWAY vectors for *Agrobacterium*-mediated plant transformation. *Trends Plant Sci.* **7,** 193–195 (2002).
31. Clough, S. J. & Bent, A. F. Floral dip: a simplified method for *Agrobacterium*-mediated transformation of *Arabidopsis thaliana*. *Plant J.* **16,** 735–743 (1998).
32. Sacksteder, C. A., Kanazawa, A., Jacoby, M. E. & Kramer, D. M. The proton to electron stoichiometry of steady-state photosynthesis in living plants: a proton-pumping Q cycle is continuously engaged. *Proc. Natl Acad. Sci. USA* **97,** 14283–14288 (2000).
33. Takizawa, K., Cruz, J. A., Kanazawa, A. & Kramer, D. M. The thylakoid proton motive force *in vivo*. Quantitative, non-invasive probes, energetics, and regulatory consequences of light-induced pmf. *Biochim. Biophys. Acta* **1767,** 1233–1244 (2007).
34. Färber, A., Young, A. J., Ruban, A. V., Horton, P. & Jahns, P. Dynamics of xanthophyll-cycle activity in different antenna subcomplexes in the photosynthetic membranes of higher plants. *Plant Physiol.* **115,** 1609–1618 (1997).
35. Tanz, S. K. *et al.* SUBA3: a database for integrating experimentation and prediction to define the SUBcellular location of proteins in *Arabidopsis*. *Nucleic Acids Res.* **41,** D1185–D1191 (2013).
36. Emanuelsson, O., Nielsen, H. & von Heijne, G. ChloroP, a neural network-based method for predicting chloroplast transit peptides and their cleavage sites. *Protein Sci.* **8,** 978–984 (1999).
37. Kelley, L. A. & Sternberg, M. J. Protein structure prediction on the Web: a case study using the Phyre server. *Nat. Protoc.* **4,** 363–371 (2009).
38. Boyle, E. I. *et al.* GO::TermFinder—open source software for accessing Gene Ontology information and finding significantly enriched gene ontology terms associated with a list of genes. *Bioinformatics* **20,** 3710–3715 (2004).
39. Peng, L., Shimizu, H. & Shikanai, T. The chloroplast NAD(P)H dehydrogenase complex interacts with photosystem I in *Arabidopsis*. *J. Biol. Chem.* **283,** 34873–34879 (2008).
40. Kunst, L. Preparation of physiologically active chloroplasts from *Arabidopsis*. *Methods Mol. Biol.* **82,** 43–48 (1998).
41. Li, H. M., Moore, T. & Keegstra, K. Targeting of proteins to the outer envelope membrane uses a different pathway than transport into chloroplasts. *Plant Cell* **3,** 709–717 (1991).

42. Wessel, D. & Flügge, U. I. A method for the quantitative recovery of protein in dilute solution in the presence of detergents and lipids. *Anal. Biochem.* **138,** 141–143 (1984).
43. Kyle, D. J., Staehelin, L. A. & Arntzen, C. J. Lateral mobility of the light-harvesting complex in chloroplast membranes controls excitation energy distribution in higher plants. *Arch. Biochem. Biophys.* **222,** 527–541 (1983).

Acknowledgements

We thank Luke Mackinder for fluorescence microscopy assistance; Jose Dinneny and Lina Duan for *Arabidopsis* growth and genotyping assistance; Krishna Niyogi for providing *psbs* mutant seeds, plant growth space and Imaging-PAM; and David Ehrhardt, Virginia Walbot, Trinna Cuellar, Xiaobo Li, Luke Mackinder, Leif Pallesen, Ru Zhang, Robert Jinkerson, Wolf Frommer, Jonathan Weissman and Peter Walter for feedback on this manuscript. This project was funded by the Carnegie Institution for Science, by ERDF-cofinanced grants from the Ministry of Economy and Competitiveness (BIO2012-33655) and Junta de Andalucia (CVI-7558) to K.V., the Natural Sciences and Engineering Research Council of Canada (NSERC) PGS-D3 scholarship to L.P. and Deutsche Forschungsgemeinschaft grants (JA 665/10-1 and GRK 1525 to P.J.; AR 808/1-1 to U.A.).

Author contributions

U.A. and M.C.J. conceived the study; U.A., P.J., K.V., D.M.K. and M.C.J. designed the experiments; U.A. performed KEA3 localization, generation and analysis of double mutants; U.A. and E.S were responsible for the generation of *KEA3-GFP* expressing plants; U.A. performed the analysis; U.A. and L.P. performed Chl *a* fluorescence measurements; L.R.C. performed simultaneous Chl *a* fluorescence and ECS measurements, parsing experiments; U.A., M.C.J., A.K. and J.A.B. performed simultaneous Chl *a* fluorescence and gas exchange measurements; L.P. performed the pigment analysis; U.A. and K.V. performed the phylogenetic analyses; U.A. and M.C.J. wrote the paper.

Additional information

Supplementary Information accompanies this paper at http://www.nature.com/naturecommunications

Competing financial interests: The Carnegie Institution for Science has submitted a patent form on behalf of U.A. and M.J. on aspects of the findings.

Reprints and permission information is available online at http://npg.nature.com/reprintsandpermissions/

How to cite this article: Armbruster, U. *et al.* Ion antiport accelerates photosynthetic acclimation in fluctuating light environments. *Nat. Commun.* 5:5439 doi: 10.1038/ncomms6439 (2014).

Supplemental Data

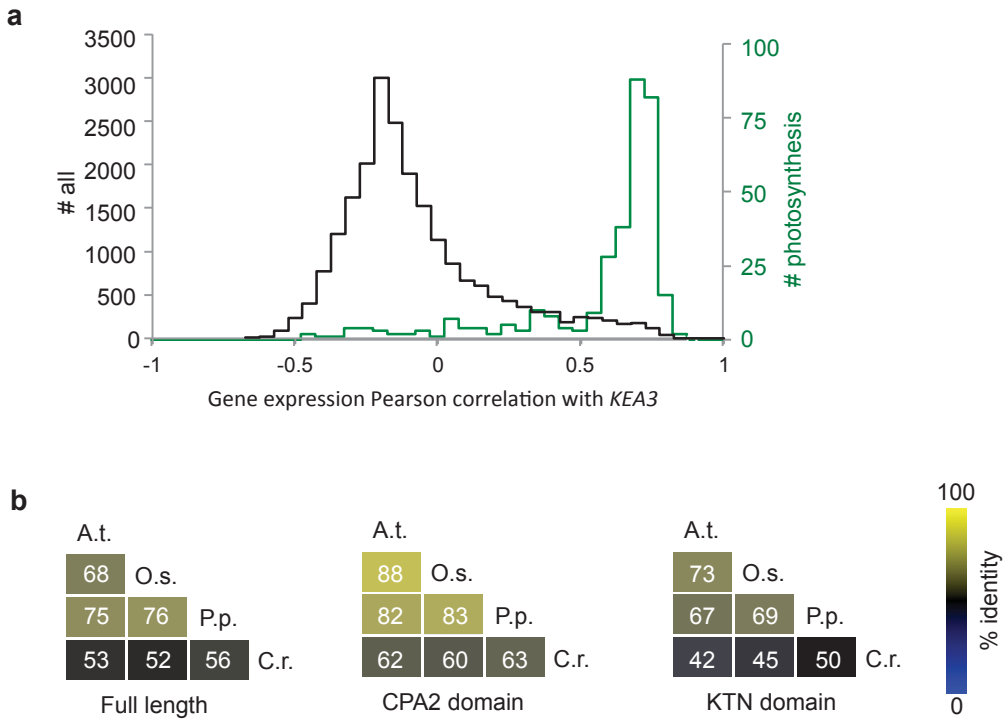

Supplementary Figure 1 | *KEA3* is transcriptionally co-regulated with genes involved in photosynthesis and is highly conserved in photosynthetic eukaryotes. a, We looked for enrichment of GO terms among the 100 genes whose expression was most highly correlated with *KEA3*. The most highly enriched GO terms were "photosynthesis" (GO:0015979; $p=10^{-41}$), “phosphate containing compound metabolic process” (GO:0006796, $p=10^{-38}$; this set includes most photosynthesis genes), "pentose phosphate shunt" (GO:0006098) and "NADPH regeneration" (GO:0006740, both $p= 10^{-38}$). Pearson correlation coefficients of *KEA3* with all genes (black) and genes belonging to the GO category “photosynthesis” (green) are plotted. **b,** The conservation of KEA3 proteins and its CPA2 and KTN domains was analyzed by sequence comparisons from *Arabidopsis thaliana* KEA3 and homologous proteins from the monocot *Oryza sativa*, the moss *Physcomitrella patens* and the green alga *Chlamydomonas reinhardtii*. This shows that especially the CPA2 domain is conserved. A percent identity matrix is shown.

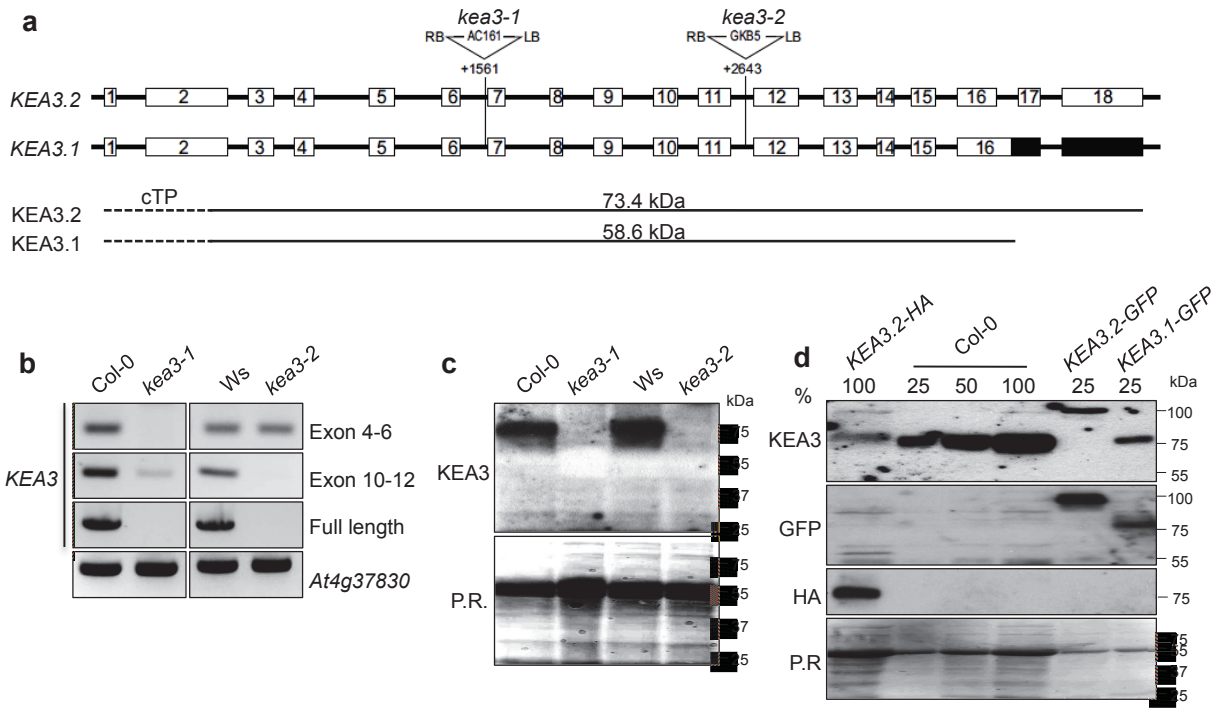

Supplementary Figure 2 | *kea3* mutants lack KEA3, and the major KEA3 isoform is KEA3.2. a, Two different *KEA3* splice forms are annotated in the TAIR database. The translated exons of the two splice forms identified by RT-PCR are depicted as open numbered boxes, un-translated regions as black boxes and introns as connecting black lines. Site and orientation of the T-DNA insertions of the two mutant *kea3* alleles employed in this work are provided. These sites have been confirmed by sequencing of the flanking regions. The sizes of the two mature KEA3 isoforms are shown below. **b,** RT-PCR analysis was performed on total leaf RNA from WT and mutant plants with *KEA3*-specific primers and primers to the unrelated gene *AT4G37830* as positive control using 40 PCR amplification cycles. **c,** Protein blot analysis was performed on total leaf extract from WT and mutant plants using a custom KEA3 antibody derived against the epitope NQLGRKAADFLDERLDPGE present in both isoforms. Ponceau Red (P.R.) was used to stain the membrane to visualize loading and transfer of total leaf protein. Only one KEA3 isoform was detected, which ran at the size of the 75 kDa marker band and was absent in both mutants. **d,** *kea3-1* T1 plants transformed with either *KEA3.1-HA* or *KEA3.2-HA* were selected for resistance to kanamycin and high expression of RFP, a second selection marker encoded by the T-DNA. Twenty independent mutants of each genotype were analyzed for expression of KEA3 and HA protein by Western blot. KEA3 and HA were not detected in plants transformed with *KEA3.1-HA*, suggesting that either the KEA3.1-HA protein or transcript was not stable. The native KEA3 ran only slightly lower than KEA3.2-HA, closer to the expected size of KEA3.2 of 73.4 kDa than to the expected size of KEA3.1 of 58.6 kDa. A KEA3.1-GFP fusion protein ran at similar size as the native KEA3 (the GFP-tag adds 28.2 kDa).

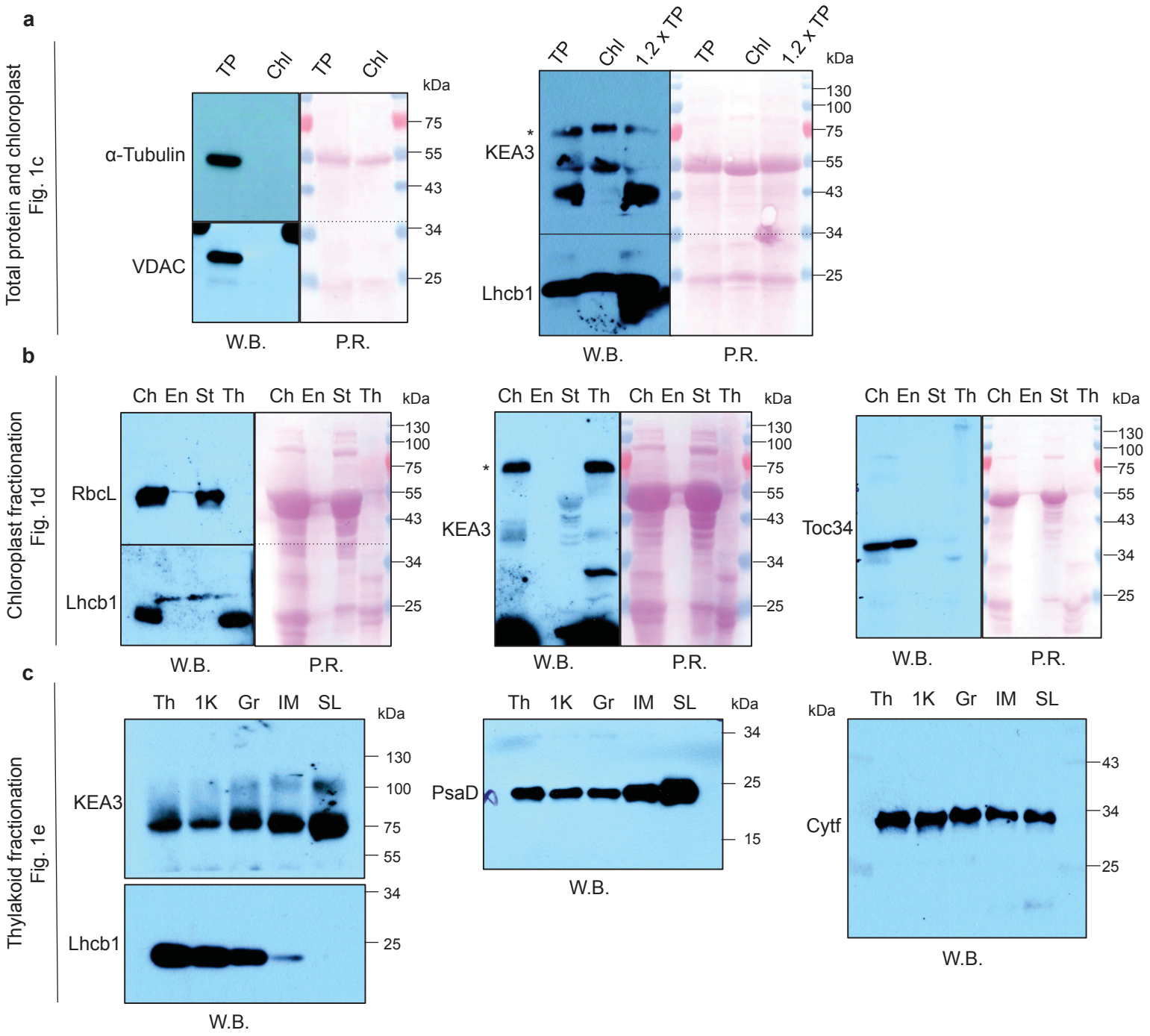

Supplementary Figure 3 | KEA3 localizes to the thylakoid stromal lamellae. **a,b,c,** Uncropped versions of the westernblots shown in Fig. 1. After transfer of proteins from SDS-PAGEs to nitrocellulose sheets, the membranes were stained with Ponceau red (P.R.) and probed with the indicated antibodies. Signals of the westernblots (W.B.) were detected using ECL and X-ray films. For **a** and **b** corresponding W.B. and P.R. are shown for each blot. Cutting of membranes prior to antibody hybridization is indicated with a dashed line. A representative P.R. for W.B. shown in **c** is presented in Figure 1e. **a, b,** Asterisks (*) indicate the specific KEA3.2 band at 75 kDa.

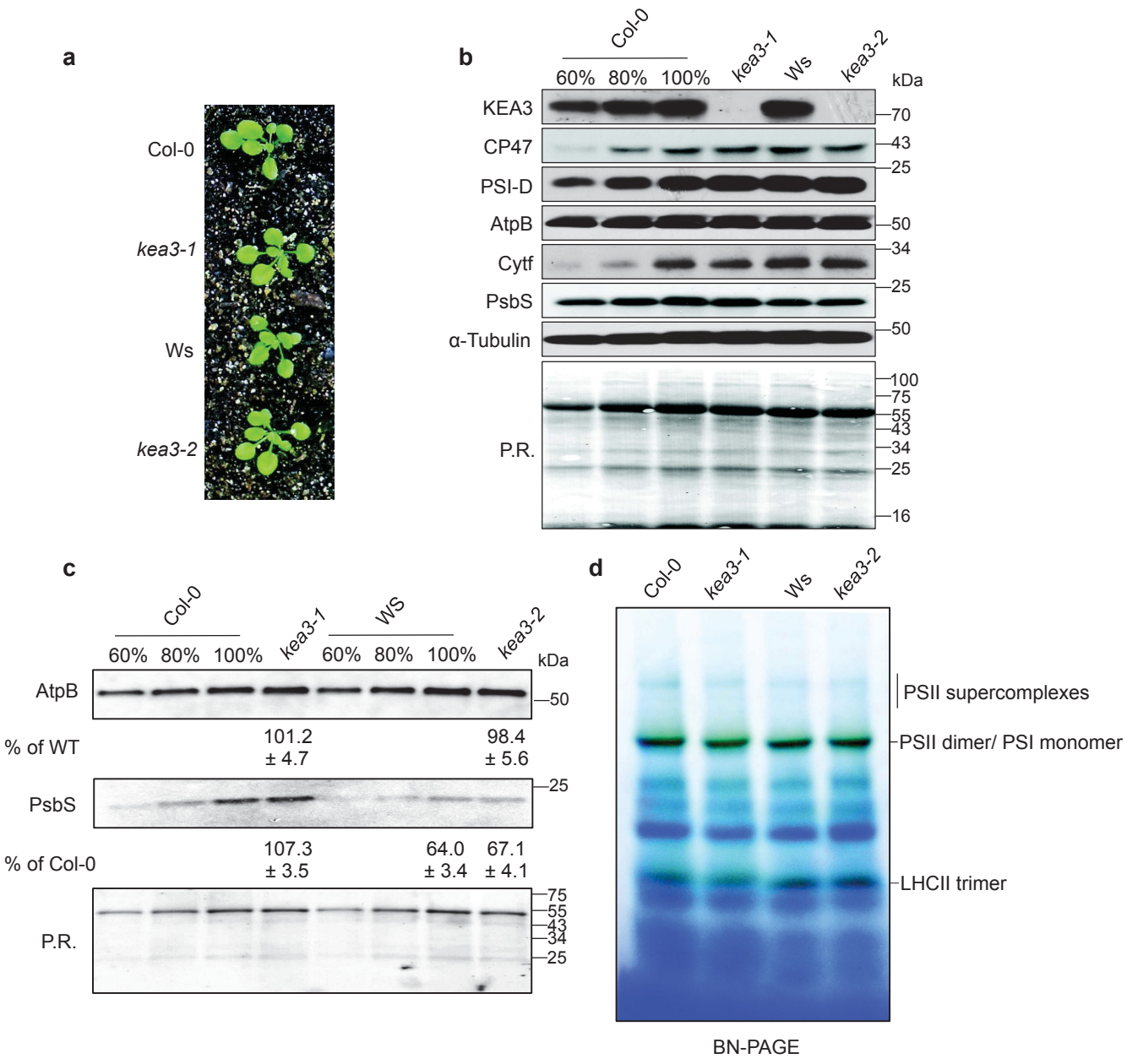

Supplementary Figure 4 | Growth, pigmentation and levels of photosynthetic complexes appear unchanged in *kea3* mutants. a, 17-day old *kea3* mutant (*kea3-1*, *kea3-2*) and corresponding WT (Col-0, Ws) plants were imaged. **b**, Total leaf proteins were separated by SDS-PAGE, transferred to nitrocellulose membranes and probed with antibodies against specific subunits of thylakoid photosynthetic complexes (CP47, PSII; PSI-D, PSI; AtpB, ATP-synthase; Cytf, Cyt b_6f complex) and PsbS. As controls, a ponceau-red (P.R.) stained membrane after protein transfer and a hybridization against the cytoplasmic α-tubulin subunit are shown. **c,** Total leaf extract was prepared as in b and membranes were probed with antibodies against AtpB and PsbS. Relative protein levels in each sample were obtained by normalizing AtpB and PsbS signals to the signal of the P.R stained membrane. A standard curve was calculated from the signals of the WT dilutions and protein levels were calculated according to the equation of the standard curve. Indicated relative protein levels (AtpB % of the corresponding WT; PsbS % of Col-0) correspond to mean values ± s.e.m. of two biological and three technical replicates. **d,** Thylakoids were isolated, complexes were solubilized with 0.7 % n-dodecyl-β-D-maltoside and proteins were separated by Blue-native (BN)-PAGE.

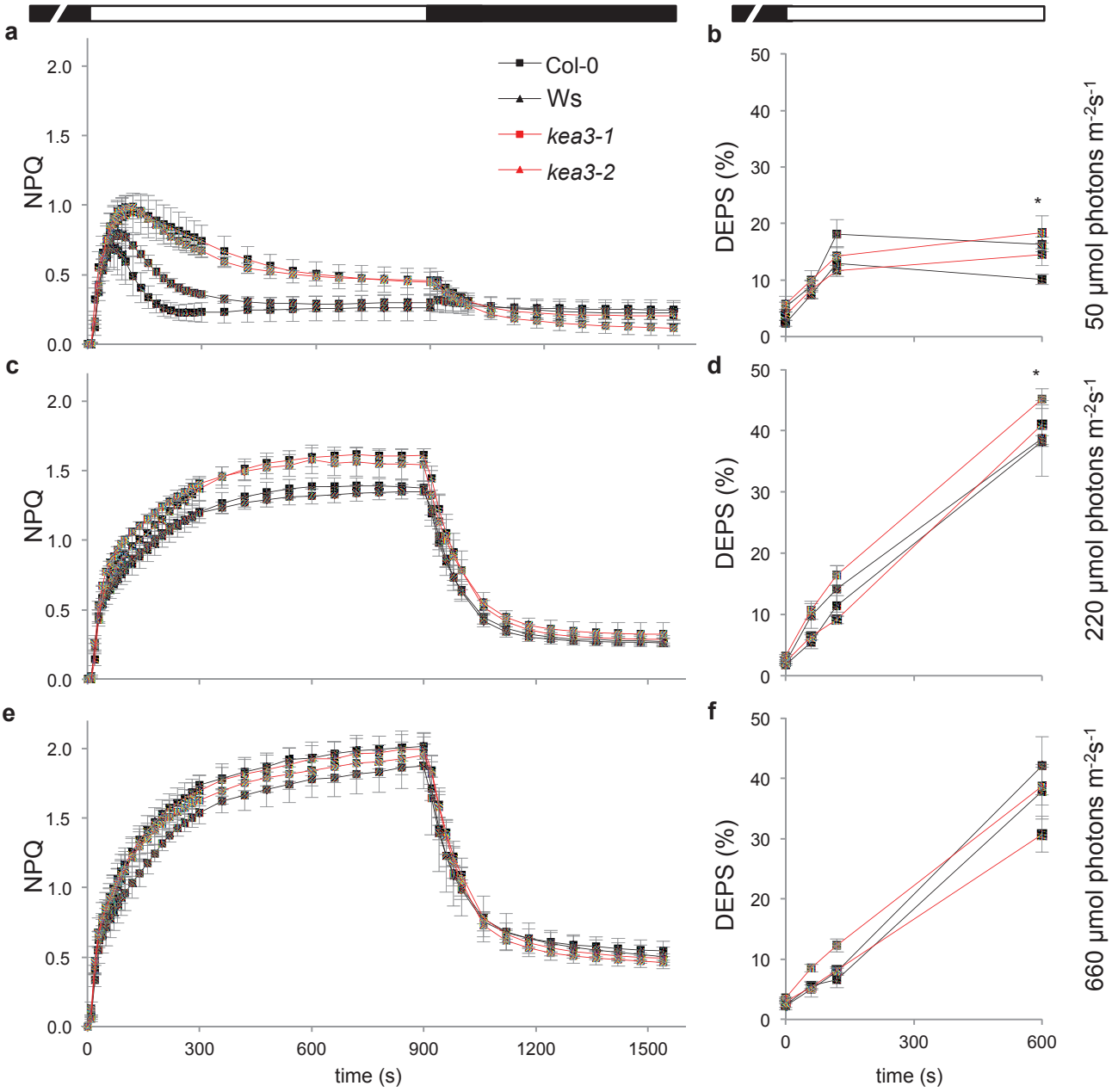

Supplementary Figure 5 | The *kea3* NPQ phenotype is specific for induction at low light intensities and correlates with increased DEPS levels after 10 min. NPQ induction and de-epoxidation state (DEPS, expressed as percentage of the sum of violaxanthin + antheraxanthin + zeaxanthin) were measured by Dual-PAM and HPLC, respectively, in four-week-old wild-type (Col-0, Ws) and mutant (*kea3-1* and *kea3-2*) plants. Leaves were dark-acclimated for 30 min before illumination at light intensities of 50 µmol photons $m^{-2}s^{-1}$ (**a**,**b**), 220 µmol photons $m^{-2}s^{-1}$ (**c,d**), and 660 µmol photons $m^{-2}s^{-1}$ (**e,f**), for 15 min followed by a 12 min dark relaxation period. Mean values ± s.e.m. of four (NPQ) and 12 (DEPS) independent experiments are shown. During the transition from dark to low light Col-0 shows a higher NPQ response than Ws. This is most likely due differences in the qE machinery and/or in the rate of cyclic electron transport around PSI between the two ecotypes , e.g. PsbS levels are lower in Ws (Supplementary Data Figure 3c). Lower luminal pH in the *kea3* mutants would be expected to increase activation of the violaxanthin de-epoxidase, increasing the de-epoxidation state (DEPS) of the xanthophyll antennae pigments (*24*). Consistent with this, a slight increase ($p<0.05$, ANOVA) in the de-epoxidation state (DEPS) of the xanthophyll pigments was found in *kea3* mutants after 10 min of illumination with 50 and 220 µmol photons $m^{-2}s^{-1}$. (**b,d**) Asterisks (*) indicate a difference between both mutants and their corresponding mutants at a given time point with $p<0.05$, Student's *t*-test.

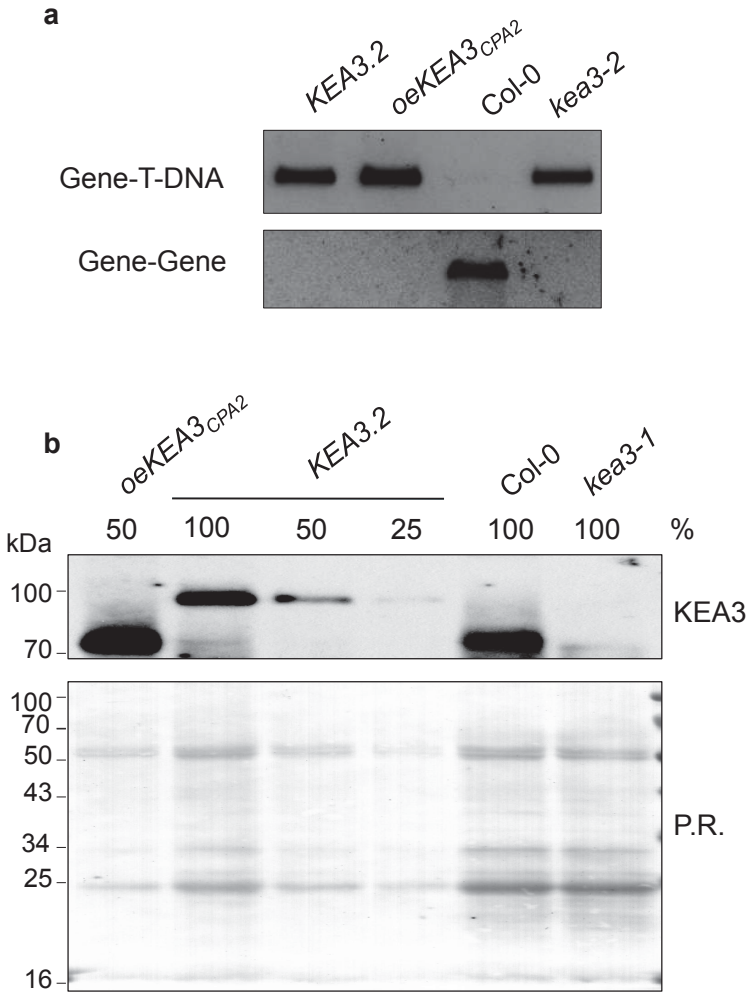

Supplementary Figure 6 | KEA3-GFP is expressed at similar levels to the native KEA3, while KEA3$_{CPA2}$-GFP is overexpressed. Twenty-five *kea3-1* plants transformed with pB7FWG2 containing the *KEA3.2* sequence were selected for GFP fluorescence and subsequently analyzed for fusion protein levels with the KEA3 antibody. The plant with highest KEA3.2-GFP levels (*KEA3.2*) was used for localization and complementation analysis. Of two *kea3-1* plants transformed with pB7FWG2 containing the *KEA3$_{CPA2}$* fragment and selected accordingly, one was expressing the fusion protein (oeKEA3$_{CPA2}$). **a,** DNA from *KEA3.2* and *oeKEA3$_{CPA2}$* was analyzed with primers spanning the *kea3* T-DNA insertion site (Gene-Gene) and a T-DNA left border primer with adjacent gene primer (Gene-T-DNA). DNA from Col-0 and *kea3-1* was used as control. **b,** Thylakoid proteins from *KEA3.2*, *oeKEA3$_{CPA2}$*, Col-0 and *kea3-1* were hybridized with KEA3 antibodies. Ponceau Red (P.R.) stain of the membrane prior to the immunodetection is shown as a second loading and protein transfer control. In *KEA3.2* the fusion protein is present at near-WT levels, and in *oeKEA3$_{CPA2}$* it is overexpressed more than two-fold.

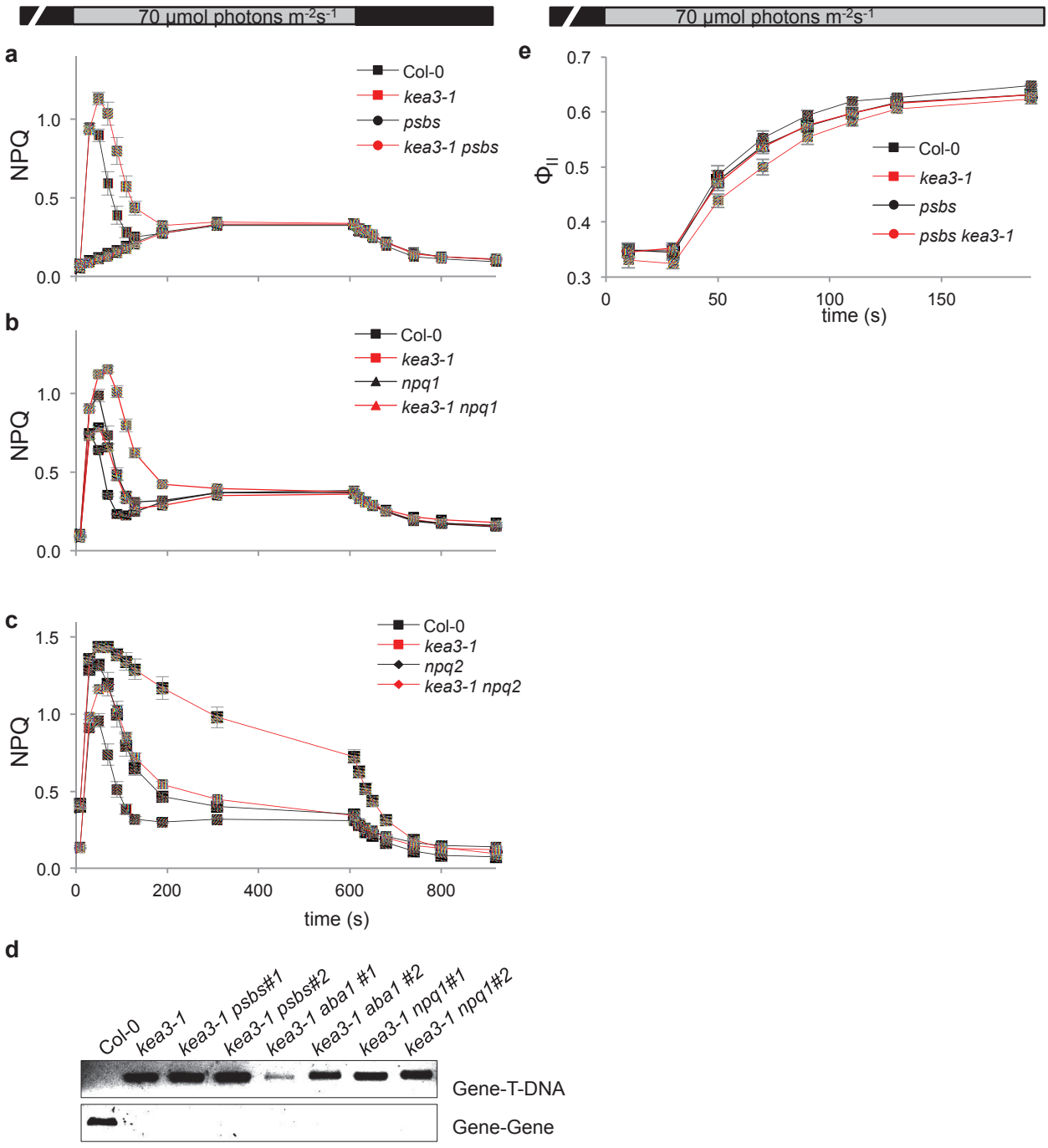

Supplementary Figure 7 | The transient NPQ phenotype in *kea3* is PsbS-dependent and modulated by zeaxanthin; the transient decrease in Φ_{II} observed in *kea3* is PsbS dependent. (**a**,**b**,**c**) NPQ induction in detached leaves of two-week-old plants was measured as in Fig 2A. Error bars represent s.e.m. (n = 6). **d,** Two independent double mutant lines were analyzed for (a,b,c). PCR confirms that all were double mutants with *kea3-1*. **e,** Φ_{II} was calculated from the same experiment as in (a).

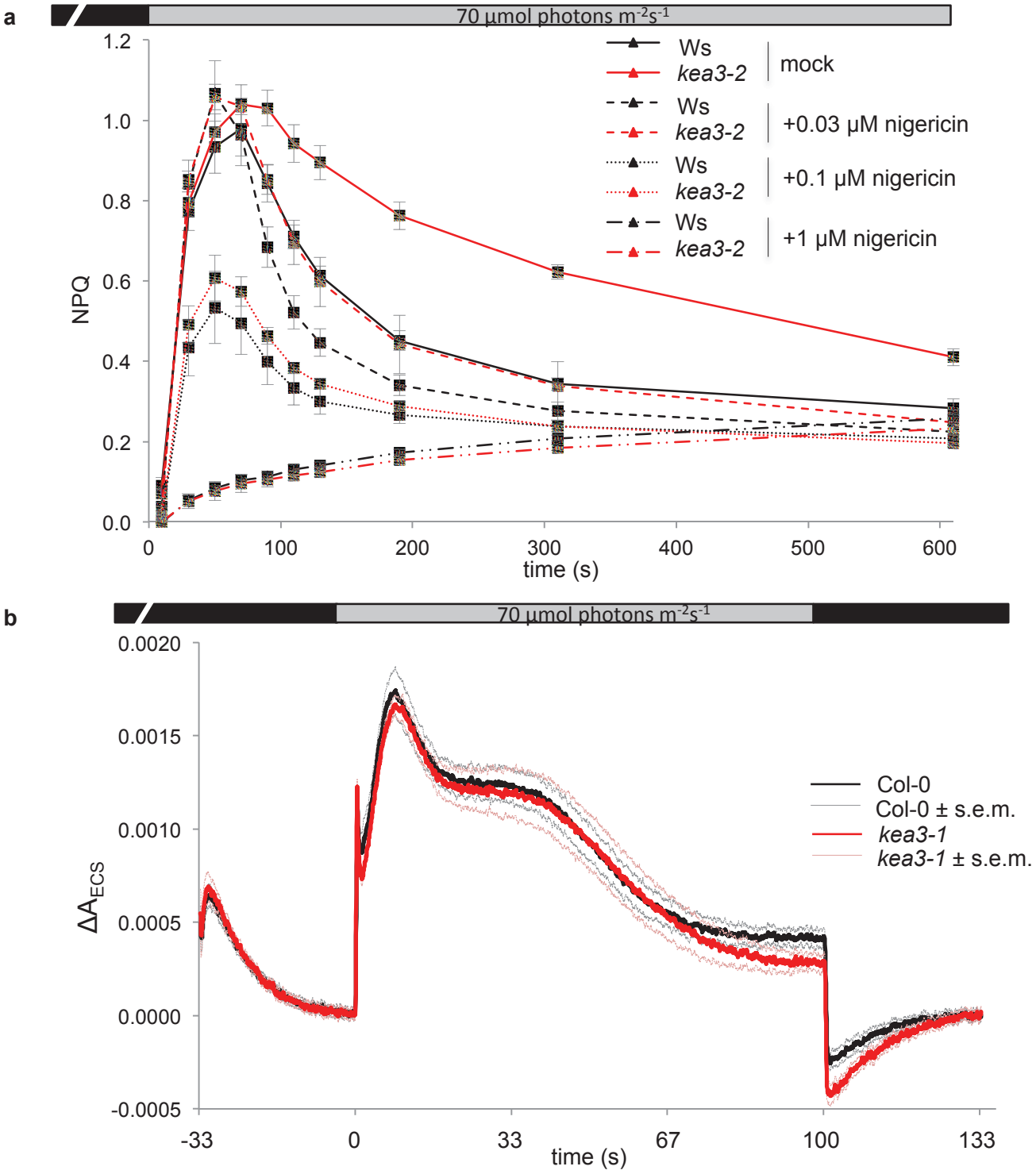

Supplementary Figure 8 | Nigericin rescues the *kea3* NPQ phenotype at low concentrations; and eliminates transient NPQ at high concentrations. After 100 s of low light, *kea3* mutants show increased ΔpH and decreased Δψ. a, NPQ induction upon transition from dark to 70 µmol photons m^{-2} s^{-1} light was measured in WT (Ws) and *kea3-2* leaves incubated in water (mock) or with indicated concentrations of nigericin. Error bars represent s.e.m. (n = 6). **b,** Plants were dark adapted for 30 min, and then illuminated for 100 s with 90 µmol m^{-2} s^{-1}. Then, the light was turned off and full ECS decay kinetics were recorded as absorption change at 520 nm (deconvolved by subtracting a baseline between 505 nm and 535 nm) to measure ΔpH and Δψ in WT (Col-0) and *kea3-1*. The average without and +/- s.e.m. of 6 independent measurements per genotype was plotted as a moving average with interval 5.

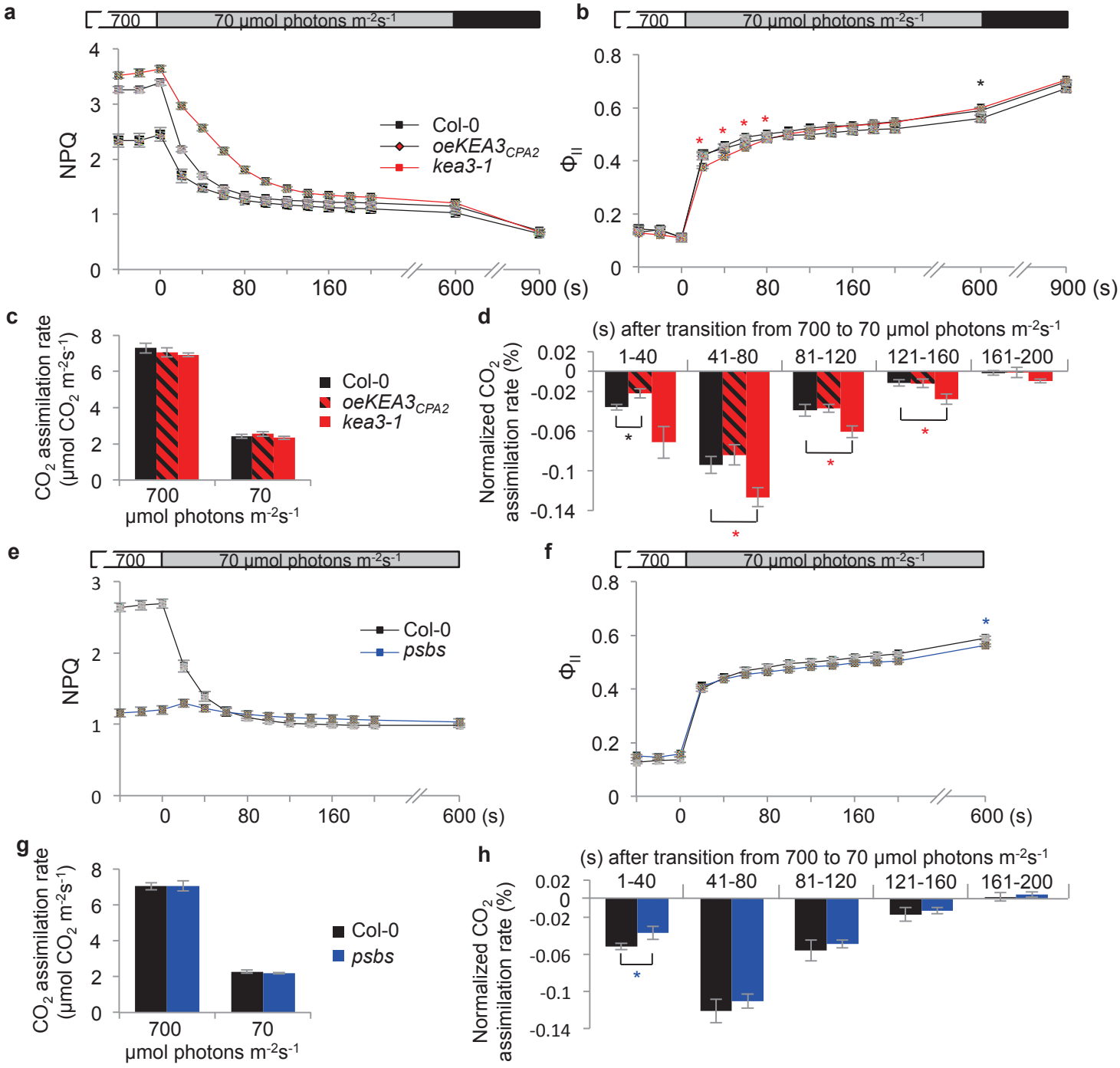

Supplementary Figure 9 | The relative CO2 assimilation rate after a shift from high to low light is increased in *oeKEA3*$_{CPA2}$ and *psbs* mutants. a, **e**, *oeKEA3*$_{CPA2}$ and *psbs* have lower NPQ in high light and upon transition to low light as compared to Col-0. **b**, **f**, Φ_{II} is decreased in low light in *oeKEA3*$_{CPA2}$ and *psbs* as compared to Col-0. Φ_{II} was calculated from the same measurement as in (a,e) respectively. **c, g,** *oeKEA3*$_{CPA}$ and *psbs* show similar CO_2 assimilation rates during steady state high (700 µmol photons $m^{-2}s^{-1}$) and low light (70 µmol photons $m^{-2}s^{-1}$) as compared to Col-0. **d**, **h**, The normalized CO_2 assimilation rate (as described in Fig. 4) is increased in *oeKEA3*$_{CPA2}$ and *psbs* in the first 40 s after the transition to low light, when NPQ is lower compared to Col-0. **a-d**, *kea3-1* behaves very similarly to *kea3-2* upon a transition from high to low light (Fig. 4) with slower NPQ relaxation kinetics, slower recovery of maximum Φ_{II} and a decrease in relative CO2 assimilation as compared to WT (Col-0). **a-h** Error bars represent s.e.m. (n = 6). **b, d, f, h,** Asterisks represent significantly lower Φ_{II} and normalized CO_2 assimilation rate in *oeKEA3*$_{CPA2}$ (black), *psbs* (blue), and *kea3-1* (red) as compared to Col-0 ($p < 0.04$).

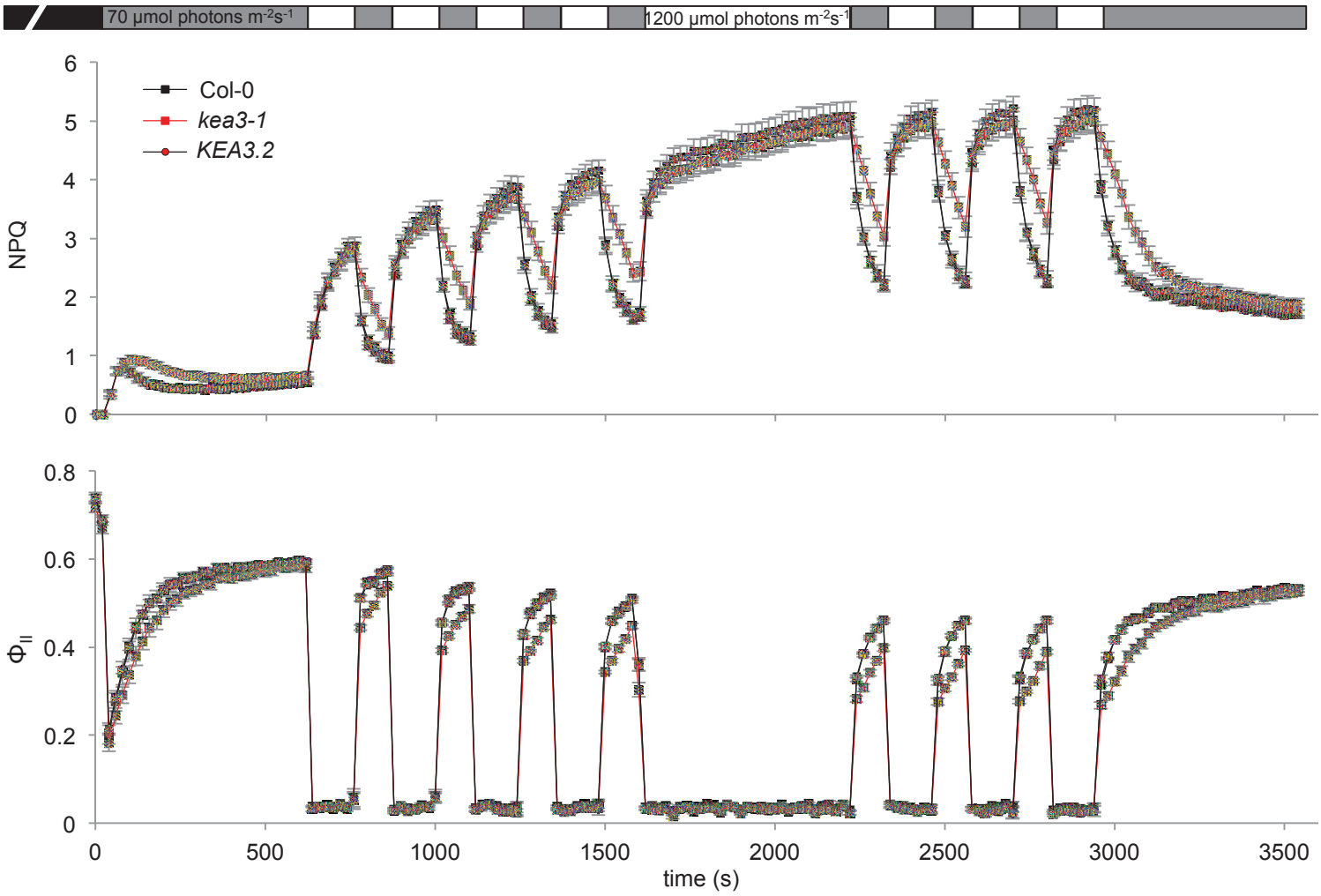

Supplementary Figure 10 | KEA3 regulates the dynamics of photosynthesis in fluctuating light . **a**, In fluctuating light, NPQ relaxation is delayed after each transition from high to low light in *kea3-1*. **g,** Φ_{II} is decreased in *kea3-2* during each transition from high to low light. Φ_{II} was calculated from the same measurement as in **f**. **a**, **b**, Expression of *KEA3.2-GFP* (*KEA3.2*) in *kea3-1* rescues fast NPQ relaxation and recovery of high Φ_{II} . Error bars represent s.e.m. (n = 6).

Gene	Forward primer	Reverse primer	Experiment(s)
KEA3	TAGGGTTTATGGGTGACAACAA	GTCAACTTCAGGAGTTTGCAC	Genotyping *kea3-1*
	AAGCTTTTGTGGCCCTTTGC	TTGGCATGGGACTAACTCAG	Genotyping *kea3-2* RT-PCR exon 10-12
	TTGGCATGGGACTAACTCAG	ACGGCCTCATCAATGCTTCT	RT-PCR exon 4-6
	ATGGCAATTAGTACTATGTTAGG	TTAATCTTGAGCTTTATCAGCTTT	RT-PCR full length
	GGGGACAAGTTTGTACAAAAAAG CAGGCTATGGCAATTAGTACTAT GTTAG	GGGGACCACTTTGTACAAGAAAGCT GGGTTATCTTGAGCTTTATCAGCTT TA	Cloning of *KEA3.2* into pDONR for expression in plants
	GGGGACAAGTTTGTACAAAAAAG CAGGCTATGGCAATTAGTACTAT GTTAG	GGGGACCACTTTGTACAAGAAAGCT GGGTTCATCTTCACCTCTCCGGGAT	Cloning of $KEA3_{CPA2}$ into pDONR for expression in plants
AT3G07480	CTCTTCAGAAACTCTCCTCTCAA	ATTCCTCTGCGATCTGAACCTC	RT-PCR control

Supplementary Table 1 | Primer combinations used in this work.

Author Contributions

L.P. performed Chl *a* fluorescence measurements and RP-HPLC-based pigment analyses. L.P. contributed to writing the methodology on relevant work performed and statistical analyses of resulting data towards the study.

4. Discussion

The present work examined the importance of the transthylakoid $\Delta\psi$ in early light activation of qE-type energy dissipation in the model C_3 land plants spinach and *Arabidopsis thaliana*. The application of channel-forming ionophores has enabled selective probing of the relative contribution of the $\Delta\psi$ in addition to the ΔpH to qE-type quenching and associated xanthophyll cycle conversion. While considerable efforts have been made to examine ΔpH-dependent regulation of qE in an array of photosynthetic organisms, including but not limited to the model systems *Chlamydomonas* and *Arabidopsis*, more comprehensive study of the role of light-induced $\Delta\psi$ formation in qE regulation has been comparatively limited thus far. This is particularly important in the context of qE regulation via changes in light-induced *pmf* partitioning into the $\Delta\psi$ and ΔpH, as proposed by Cruz *et al*. (2001).

Spectroscopic characterization of NPQ, with an emphasis on early light activation of photosynthesis and accompanying changes in linear and cyclic electron transport were characterized in Wt and mutant lines of *Arabidopsis*. Mutants defective in cyclic electron transport, PsbS, cytochrome b_6f, and xanthophyll cycle activities crucial to light harvesting and heat dissipatory reactions provide an overview of key well-known characteristics of NPQ and electron transport kinetics. Most importantly, these kinetics provided a starting point for analyses of previously uncharacterized dynamics of chloroplast *pmf* partitioning in Wt and mutant lines in relation to qE under limiting and more saturating light conditions. Finally, a comprehensive, recently published study of the role of *KEA3*-mediated potassium/proton antiport in qE regulation is presented in lieu of the importance of ion fluxes during the switch between photosynthesis and photoprotection.

4.1 The Role of $\Delta\psi$ in Regulation of Early qE Activation *in vitro*

4.1.1 NPQ in Isolated Spinach Thylakoids

Initial characterization of NPQ processes was performed in thylakoids isolated from intact dark-adapted spinach leaves to clarify the hypothesized role of the transmembrane $\Delta\psi$ during early light activation of qE. NPQ kinetics were monitored via quenching of maximal Chl fluorescence for 10 min of high light and 5 min of relaxation in the dark. Moderately high concentrations (2 μM) of nigericin and gramidicin and low nanomolar concentrations (10 nM) of valinomycin were added to thylakoids prior to and during continuous illumination, as

described in 3.1.1. Treatment of thylakoids with ΔpH-abolishing nigericin and gramicidin as positive controls led to clear reductions in maximal NPQ established in the light (Figure 3.3A). This underscores the overriding requirement of the ΔpH for downstream biochemical and photophysical changes that synergistically predicate rapidly inducible/reversible, short-term qE quenching. In contrast, valinomycin-treated thylakoids showed essentially indistinguishable NPQ kinetics from those of negative controls (Figure 3.3B). This suggests that selective collapse of the $\Delta\psi$ mediated by valinomycin supplemented with sufficient KCl has comparatively no impact on qE formation in saturating light. One would therefore expect a concomitant increase in the ΔpH component of the light-induced *pmf*, assuming that *pmf* partitioning in thylakoids is comparable to that under *in vivo* conditions. This should then stimulate early ΔpH-dependent NPQ, leading to increased qE at steady state under these conditions, which was not observed in the presence of low concentrations of valinomycin. Alternatively, minor increases in Chl fluorescence yield and thus reductions in quenching in the presence of low concentrations of valinomycin reflect well-known impacts of changes in transthylakoid ion gradients on fluorescence yield (Gross and Prasher, 1974; Krause, 1974; Mills *et al*., 1976; Ishijima *et al*., 2003) altered by uncouplers like valinomycin. Indeed, K^+ gradients, imposed by the ionic strength of the external reaction medium, are important for facilitating optimal $\Delta\psi$-collapsing transmembrane K^+-conductance selectively mediated by valinomycin at low concentrations.

Dark-adapted thylakoids treated prior to or during early illumination in saturating light with valinomycin at higher micromolar concentrations showed reduced maximal NPQ (data not shown). This is consistent with early work that underscores different modes of action of valinomycin at higher concentrations with respect to energy transduction at the level of the thylakoid membrane (i.e., Keister and Minton, 1970; Wraight and Crofts, 1970). Valinomycin at higher concentrations inhibits linear electron transport and coupled ATP formation via the ATP synthase as well as photophosphorylation irrespective of external supplied K^+ concentrations. Subsequent work using millisecond delayed light emission (ms-DLE), which is sensitive to such changes in electron transport, ATP synthesis, and phosphorylation, confirms previously reported impacts of high concentrations of valinomycin in isolated spinach chloroplasts (Telfer and Barber, 1974). High concentrations of valinomycin (> 1 μM) were shown to inhibit electron transport and coupled proton flux into the lumen at cytochrome b_6f and efflux via the ATP synthase by increasing the H^+ permeability of thylakoid membranes in a K^+-independent manner. This is facilitated by a

substantial transthylakoid ΔpH established upon illumination of chloroplasts, and the collapse of a ΔpH in addition to the $\Delta\psi$ is reflected by a reduction in qE *in vitro*. In contrast, low valinomycin concentrations (< 10 nM) did not inhibit electron transport and coupled ATP synthesis, but rather inhibited the fast component of ms-DLE induction, related specifically to light-induced $\Delta\psi$ formation, in a K^+-dependent manner.

It is therefore clear that reductions in maximal NPQ presently observed *in vitro* in the presence of high valinomycin concentrations may likewise be attributed to unspecific H^+-uncoupling effects of valinomycin at high concentrations. One can therefore conclude that the light-induced $\Delta\psi$ appears to have no major role in early antenna-based qE-type quenching, at least in saturating light under *in vitro* conditions. Going forward, it would be important to examine possible changes in proton conductance through the ATP synthase via changes in ATP synthesis in isolated thylakoids treated with low concentrations of valinomycin and sufficient KCl, which has not been carried out in the present work.

Measurements of 9-AA fluorescence quenching alongside Chl fluorescence probed by ΔpH- and/or $\Delta\psi$-abolishing ionophores confirm the action of applied ionophores on underlying changes in the lumen pH and thus the ΔpH under the same conditions used to study NPQ. Changes in the ΔpH have been extensively studied using the monovalent cation 9-AA, pKa ≈ 10, which diffuses freely across thylakoid membrane as a de-protonated base (Searle *et al*., 1977; Haraux and de Kouchkovsky, 1980; Grzesiek and Dencher, 1988; Schreiber and Klughammer, 2009). Use of 9-AA in directly measuring the lumen pH *in vitro* (Schuldiner *et al*., 1972) relies on early studies of acridines in monitoring changes in the state of membrane energization (Kraayenhof, 1970). However, the exact physical mechanism of 9-AA quenching remains unclear (Grzesiek *et al*., 1989; Schreiber and Klughammer, 2009).

Estimates of the ΔpH *in vitro* according Schuldiner *et al*. (1972) highlight a relative low lumen pH (~ 5) in isolated untreated thylakoids exposed to 10 min of saturating light, consistent with previous *in vitro* estimates (Kramer *et al*., 2003). This was demonstrated by rapid 9-AA quenching during the initial dark-light transition in controls (Figure 3.4A-B). Recovery of quenching during the light-dark transition was more rapid than initial 9-AA quenching during the dark-light transition. This respectively reflects more rapid proton efflux through the ATP synthase along the free energy gradient of ATP formation dictated by ΔG_{ATP} (Avenson *et al*., 2005) compared to rate-limiting proton uptake at cytochrome b_6f and water-oxidation at PSII that contribute to ΔpH formation and thus 9-AA quenching.

Treatment of thylakoids with nigericin exclusively collapsed the ΔpH and thus completely inhibited 9-AA quenching in the light (Figure 3.4A), which was not reflected by a commensurate decline in the estimated ΔpH. Similarly, a comparatively lower, near-complete reduction in 9-AA quenching in the presence of ΔpH-collapsing gramicidin is not linearly related to a decline in the derived ΔpH. As a large and bulky channel-forming molecule, gramicidin may thus be limited in its ability to fully abolish the ΔpH by virtue of its inability to fully infiltrate the thylakoid intramembrane space. Resulting overestimations of the ΔpH in the presence of nigericin and gramicidin further underscore the non-linear relationship between 9-AA quenching and the derived ΔpH. In contrast, nanomolar concentrations of valinoymcin did not significantly affect the kinetics of 9-AA quenching and recovery (Figure 3.4B). Minor reductions in 9-AA quenching in the presence of valinomycin within the standard deviation of averaged treatment curves may reflect differences in background flurorescence, which are assumed negligible in estimation of the ΔpH. Alternatively, abolishment of the $\Delta\psi$ will necessarily alter the surface charge density or potential of the thylakoid membrane, as is typically the case during light activation of transthylakoid ion fluxes under normal physiological conditions (Searle *et al*., 1977). Thus, valinomycin-induced re-equilibration of transmembrane K^+ gradients may facilitate binding of dissolved K^+ to negatively charged sites on the lumenal face of the thylakoid membrane. This would cause competitive displacement of 9-AA into the aqueous lumenal space and raise 9-AA fluorescence yield in a similar manner as that demonstrated with Chl fluorescence (Fiolet *et al*., 1974; Searle *et al*., 1977; Chow and Barber, 1980; Haraux and de Kouchkovsky, 1980).

Higher concentrations of valinomycin (2 μM) have been shown to drastically reduce 9-AA quenching in isolated thylakoids in saturating light (data not shown). This may be attributed to previously reported H^+-uncoupling effect of valinomycin at high micromolar concentrations. Valinomycin infiltration of the thylakoid membrane may facilitate H^+ in the aqueous lumenal space to competitively displace 9-AA bound to negatively charged sites on the lumenal side of the membrane into the aqueous lumenal space, leading to an increase in 9-AA fluorescence yield and concomitant reduction in 9-AA quenching. Grzesiek and Dencher (1988) also observed a reduction in quenching in the light by 93 % relative to dark baseline levels in the presence of micromolar concentrations of valinomycin and 100 mM KCl. Quenching was also considerably, but not fully abolished in the presence of 5 μM of carbonyl cyanide *m*-chlorophenyl hydrazone, an effective protonophore that abolishes the ΔpH. Thus, the effects of high valinomycin concentrations on 9-AA quenching mimic those

of ΔpH-abolishing uncouplers like nigericin and gramicidin, which may affect 9-AA quenching in a similar manner, and are unrelated to the Δψ-abolishing action of valinomycin in this context. Any accurate estimation of changes in the ΔpH based on 9-AA quenching according to Schuldiner *et al*. (1972) is limited by the extrinsic physical properties of isolated membranes and 9-AA as a cationic fluorescent indicator of changes in lumen pH *in vitro*. Nevertheless, the relative effects of applied uncouplers remain valid and confirm the expected ΔpH-abolishing action of nigericin and gramicidin not observed in the presence of valinomycin at low concentrations. These findings confirm the overriding importance of the ΔpH in early qE activation, while the collapse of the Δψ in the presence of valinomycin has no impact on lumen acidification underlying early light activation of qE.

4.1.2 Probing the Δψ Monitored via Absorbance Changes at 515 nm

The importance of the Δψ in regulating the energy balance of chloroplasts in mitochondria and chloroplasts according to Mitchell's hypothesis has prompted early pulse-poise spectroscopic measurements of absorbance changes at 515-520 nm, related to changes in light-induced Δψ formation. Absorbance changes at 515 nm induced by a single pulse of saturating light, which turns over each light reaction between the photosystems once, confirm the effectiveness of critically low concentrations of valinomycin in selectively collapsing the Δψ. This is supported by a marked reduction in the amplitude of the rapid rise in the flash-induced 515 nm absorbance signal in dark-adapted thylakoids in the presence of valinomycin (Figure 3.5B; Table 3.2), reflecting a reduction in the magnitude of the Δψ. This is attributed to increased Δψ-collapsing K^+-conductance across the thylakoid membrane along the free energy gradient of K^+ flux mediated by valinomycin at low concentrations during relaxation of the signal. Accordingly, an accelerated decline in the 515 nm signal was observed following a saturating flash applied to valinomycin-treated thylakoids (Figure 3.5B; Table 3.2). The reductive effect on the amplitude of the flash-induced absorbance increase and subsequent decay was substantially more pronounced in the presence of gramicidin (Figure 3.5A; Table 3.2). This reflects the ability of gramicidin to collapse the Δψ in addition to the ΔpH at a commensurately 200-fold higher concentration compared to that of valinomycin.

Early spectroscopic work corroborating the Δψ-abolishing effect of valinomycin highlights a rapid decline in the flash-induced 515 nm signal in isolated chloroplasts treated with ~ 10 nM valinomycin and 10 mM KCl (Junge and Schmid, 1971). This is attributed to reduced transthylakoid capacitance due to increased Δψ-collapsing K^+-conductance selectively

mediated by valinomycin at low concentrations. Direct measurements of $\Delta\psi$-generating membrane potential in large intact chloroplasts of *Peperomia metallica* following a brief pulse of white light showed increasingly accelerated potential decay with increasing KCl concentrations (1-100 mM) in the presence of 0.2 μM valinomycin (Bulychev and Vredenberg, 1976). Kinetics of potential decay are nearly identical to those of absorbance changes at 515 nm under comparable conditions and highlight the specificity of valinomycin for $\Delta\psi$ collapse in a K^+ concentration-dependent manner. Prolonged illumination of untreated chloroplasts incubated in 1 mM KCl accelerated decay following a saturating flash, as observed in the presence of valinomycin (Bulychev and Vredenberg, 1976). This is consistent with existing findings in pre-illuminated untreated spinach thylakoids (Figure 3.5B; Table 3.2) that underscore the involvement of light-activated transthylakoid ion fluxes in dissipating $\Delta\psi$, which is expedited by treatment with valinomycin.

4.1.3 Probing pH-Dependent Xanthophyll Cycle Activity

The importance of the lumen pH in activating V_XDE to convert V_X to Z_X via the intermediate A_X is most clearly revealed by monitoring the DEPS of the total VAZ pool. Uncoupler treatment of dark-adapted thylakoids exposed to 10 min of saturating light under the same *in vitro* conditions as before served to define the impacts of uncoupler-mediated ΔpH and/or $\Delta\psi$ collapse on underlying qE-related Z_X formation assessed in terms of DEPS *in vitro*.

RP-HPLC-based analyses of pigment data in general highlight clear changes in key xanthophyll cycle pigments in terms of DEPS and the VAZ pool (Table 3.3). Illumination of untreated control thylakoids expectedly increased DEPS due to significant pH-dependent Z_X formation and minor contributions from A_X formation in saturating light. Abolishment of the ΔpH by nigericin or gramicidin led to drastic reductions in DEPS, as the lumen pH increased well above ~ 5.8 under *in vitro* conditions (Kramer *et al*., 2003), leading to V_XDE inactivation, thus limiting Z_X formation. This underscores the importance of the lumen pH and thus ΔpH in qE-associated V_XDE-catalyzed Z_X formation.

A reduction in DEPS upon illumination following treatment with 10 nM valinomycin (Table 3.3) was unexpected, as there are no known reported direct or indirect effects of $\Delta\psi$ on the lumenal-side membrane-bound V_XDE in terms of its ability to catalyze Z_X formation. Rather, V_XDE activity is strictly regulated by the lumen pH and requires ascorbate as a co-factor (Eskling *et al*., 1997; Eskling and Åkerlund, 1998). As valinomycin at low concentrations

had no effect on NPQ and 9-AA quenching, one can assume that valinomycin does not affect early light-regulated processes to include lumen acidification involved in qE activation. Rather, a reduction in DEPS in the presence of valinomycin suggests that valinomycin may interact with V_XDE and reduce its binding capacity to the thylakoid membrane influenced by the $\Delta\psi$. Dissipation of $\Delta\psi$ by valinomycin may alter the charge properties of the membrane (i.e., surface charge density), influenced by the $\Delta\psi$, which in turn may affect V_XDE binding and Z_X formation. Reductive impacts of valinomycin on Z_X formation and thus DEPS without consequent reductions in NPQ in a manner similar to Z_X-independent quenching previously reported under *in vitro* as well as *in vivo* conditions, assuming a low enough lumen pH (Ruban *et al*., 2012). However, this cannot be confirmed on the basis of *in vitro* data presented here. Assuming the reproducibility of existing findings, the reductive effect of valinomycin on DEPS remains to be confirmed in future *in vitro* study.

4.2 The Role of $\Delta\psi$ in Regulation of Early qE Activation *in vivo*

4.2.1 NPQ and Electron Transport in *Arabidopsis* Wild-type

The role of $\Delta\psi$ in regulation of early qE-type quenching has been thus far examined using various spectroscopic approaches in isolated spinach thylakoids. A closer look at the role of the $\Delta\psi$ in early qE regulation *in vivo* resembling more normal physiological conditions is therefore warranted. It is known that light-induced linear electron transport at PSII establishes the *pmf* required for ATP synthesis and CO_2 fixation during photosynthesis in limiting light as well as coupled qE-type photoprotection in saturating light. Consequently, it is important to assess the kinetics of linear and cyclic electron transport and coupled NPQ over a wide range of intensities. High-resolution measurements of Chl fluorescence quenching were performed in real-time in detached leaves of Wt *Arabidopsis*, as described in 3.2.2.1. Derived kinetics of NPQ and linear as well as cyclic electron flux reveal key underlying regulatory components of qE and will be compared against the dynamics of *pmf* partitioning assessed over a comparable time period under the same light conditions. This will enable more detailed study of the dynamics of *pmf* partitioning in relation to qE regulation *in vivo*.

Measurements of NPQ in Wt exposed to low and higher intensities confirmed well-known intensity-dependent induction and relaxation of NPQ (Figure 3.6A-B). Dark-adapted Wt plants shifted to low light (~ 50 μmol quanta m^{-2} s^{-1}) showed peak transient NPQ formation after ~ 60 s of illumination (Figure 3.6B). Peak transient NPQ formation has been shown to

reach maximal levels within 100 μmol quanta m^{-2} s^{-1} (Kalituho *et al*., 2007). This transient NPQ phenomenon has been related to PSII core reactions (Finazzi *et al*., 2004) involving transient lumen acidification (ΔpH formation) driven by linear and cyclic electron flow (Munekage *et al*., 2002) and sensed by the PsbS (Finazzi *et al*., 2004). Kalituho *et al*. (2007) support the importance of the lumen pH and PsbS in the transient qE response, the extent of which is regulated by Z_X and argued to be mechanistically identical to stable qE responses. Linear electron transport increased rapidly upon low light illumination (Figure 3.6D), reflecting efficient reduction of PSII RC's, leading to stable steady-state electron transport at PSII in low light. Kinetics of linear electron transport do not correlate with transient NPQ induction kinetics in low light. In contrast, cyclic electron flow around PSI is transiently reduced in low light due to transiently increased limitation of PSI acceptor-side electron transfer (Klughammer and Schreiber, 2008) and ATP synthesis required for CO_2 fixation via the Calvin-Benson cycle (Avenson *et al*., 2005). This was reflected by a transient increase in P700 oxidation in low light (Figure 3.6F), consistent with transient lumen acidification and NPQ formation in low light. Relaxation of transient NPQ with prolonged illumination (Figure 3.6B) arises from dissipation of the ΔpH by light-activated consumption of NADPH and ATP in downstream CO_2 fixation reactions (Horton, 1983; Munekage *et al*., 2002; Kalituho *et al*., 2007). Thus, transient NPQ formation is believed to be an initial transitory state of energy dissipation that leads to stable qE, qT, or qI dictated by prevailing light and physiological conditions (Finazzi *et al*., 2004; Kalituho *et al*., 2007).

Higher, increasingly saturating intensities promote accumulation of H^+ in the lumen at rates that exceed those of H^+ consumption by the ATP synthase (Kalituho *et al*., 2007). Consequently, a stable transthylakoid ΔpH is rapidly formed, reflected by a rapid initial increase in NPQ (Figure 3.6B). In Wt *Arabidopsis* grown under ~ 100 μmol quanta m^{-2} s^{-1}, a near stable, steady-state NPQ, consisting largely of qE, was observed at steady state after 20 min at ~ 200 μmol quanta m^{-2} s^{-1} (Figure 3.6A). In addition to a stable ΔpH, PsbS-mediated conformation changes and longer-term Z_X formation in LHCII sustain NPQ at steady state. An increase in the rate of linear electron transport commensurate with increasing light intensity was clearly observed after 100 s of illumination (Figure 3.6D), leading to higher steady-state ETR (Figure 3.6C), consistent with previous estimates in *Arabidopsis* (i.e., Nilkens *et al*., 2010). Increasing saturation of linear electron transport was accompanied by increasing photoinhibition of the photosynthetic apparatus commensurate with increasing intensities above ~ 200 μmol quanta m^{-2} s^{-1}. This is reflected by an increasing qI component

of steady-state NPQ with increasing intensity (Figure 3.6A). Concomitantly, increasing donor-side limitation of PSI electron transfer at intensities above ~ 100 μmol quanta m^{-2} s^{-1} (Klughammer and Schreiber, 2008) contributes to rapid early and increased steady-state P700 oxidation at higher intensities (Figure 3.6E-F) reflecting reduced cyclic electron transport around PSI. Kinetics of ETR and NPQ induction are thus more strongly intercorrelated at higher intensities compared to P700 oxidation kinetics, which correlate more strongly with kinetics of NPQ formation in low light.

In examining the relationship between energy dissipation, electron transport, and xanthophyll conversion in terms of qE regulation, it is thus clear that rapid light-induced electron transport between PSII and PSI is critical to generating the ΔpH as a pre-requisite for downstream PsbS-mediated LHCII conformation changes and Z_X formation that synergistically give rise to qE. The role of $\Delta\psi$ in early qE activation has been traditionally assumed to be negligible. This is due in part to the long-held view that qE is essentially pH-dependent, and that light-activated transthylakoid ion fluxes rapidly dissipate a substantial rapidly-established $\Delta\psi$, as mentioned before, particularly at higher intensities. It is therefore important to examine NPQ and electron transport altered by defects in cyclic electron transport, PsbS, cytochrome b_6f, and xanthophyll cycle activity *in vivo*. In particular, low light conditions reveal early light-regulated processes critical to qE activation, to include possibly the $\Delta\psi$, which will be confirmed by examining the dynamics of *pmf* partitioning.

4.2.2 NPQ and Electron Transport in *Arabidopsis* Mutants

Defects in Fd-dependent cyclic electron transport, cytochrome b_6f, PsbS, and xanthophyll cycle activities further reveal the importance of underlying regulatory components and mechanisms of photosynthesis and NPQ, particularly during early light activation of qE. Changes in cyclic electron transport were generally well correlated with changes in NPQ, particularly in low light, in Wt and mutants alike (Figures 3.6E-F, 3.14A-D, and 3.15A-F). Thus, the *pgr5* and *pgrl1ab #273* cyclic electron transport-deficient mutants (Munekage *et al*., 2002; DalCorso *et al*., 2008) showed clear reductions in peak transient NPQ in low light in varying degrees (Figures 3.12B and 3.12D). The importance of cyclic electron transport in transient lumen acidification and transient NPQ formation in low light is reflected by increased, sustained P700 oxidation in low light in both mutants (Figures 3.14B and 3.14D). Impaired cyclic electron transport limits ATP/NADPH regeneration driven by the ΔpH, which is required for downstream CO_2 fixation, causing stromal over-reduction that depletes

$NADP^+$ at intensities well above ~ 100 μmol quanta m^{-2} s^{-1} (Munekage *et al*., 2002; DalCorso *et al*., 2008). This leads to a reduction in P700 oxidation via charge recombination and is consistent with reduced linear electron transport in high light (data not shown; Munekage *et al*., 2002; DalCorso *et al*., 2008), accompanied by reduced steady-state NPQ in high light in *pgr5* (Figures 3.12B) and *pgrl1ab #273* (Figures 3.12D). *PGR5* and *PGRL1* cooperatively mediate the switch between cyclic and linear electron transport to balance the ratio of ATP/NADPH via the ΔpH in response to prevailing metabolic and photoprotective demands (Munekage *et al*., 2002; DalCorso *et al*., 2008). As such, cyclic electron transport clearly contributes to transient ΔpH formation required for early activation of qE in low light.

The role of the ΔpH in NPQ in general is further underscored by the *pgr1* mutant, which has a point mutation in the *petC* gene encoding the Rieske iron-sulfur subunit of cytochrome b_6f and shows a reduced maximal ΔpH (Munekage *et al*., 2001; Jahns *et al*., 2002). This is due to an altered pH-dependence of linear electron transport (Kalituho *et al*., 2007). As such, *pgr1* showed markedly reduced peak transient NPQ in low light and maximal steady-state NPQ in high light (Figure 3.13B) compared to Wt, as observed previously (Munekage *et al*., 2001; Kalituho *et al*., 2007). The difference in the magnitude of peak transient NPQ formation in Wt and *pgr1* reflects the contribution of the ΔpH to transient NPQ formation in low light. Reduced peak transient and steady-state NPQ in low and high light, respectively, in *pgr1* reflects pronounced limitation of light-induced linear electron transport prior to complete activation of qE limited by impaired cytochrome b_6f oxidation (Munekage *et al*., 2001). Reduced linear electron transport increases the reduction level of Q_A and in turn the oxidation level of P700 in low and to some extent in high light (Figure 3.15B) as PSI is depleted of electrons in *pgr1* (Munekage *et al*., 2001). Limited ΔpH formation in *pgr1* may not necessarily translate into a reduction in the relative contribution of the ΔpH to the light-induced *pmf* or conversely increase the $\Delta\psi$ fraction of the *pmf*. This will be assessed in more detail in terms of the dynamics of *pmf* partitioning *in vivo* in *pgr1* under these conditions.

Overexpression of PsbS in *L17* (Li *et al*., 2002) led to enhanced peak transient NPQ formation in low light as well as maximal steady-state NPQ in high light compared to Wt (Figure 3.13C), as shown previously (i.e., Kalituho *et al*., 2007). This correlates with a minor increase in peak transient and steady-state P700 oxidation in low and high light, respectively, in *L17* (Figure 3.15C), arising from a minor increase in PSI acceptor- and donor-side limitation, respectively. Enhanced PsbS relative to maximal V_XDE activity may require a less

acidic lumen to activate qE. A higher lumen pH and thus reduced ΔpH would reduce the burden on and allow for increased linear electron transport, as shown previously at steady state in high light in *L17* (data not shown; Nilkens *et al*., 2010). Increased peak and steady-state P700 oxidation may indicate a reduced contribution of cyclic to linear electron transport-dependent ΔpH formation in low and high light in *L17*. It is therefore important to examine the contribution of the ΔpH (and $\Delta\psi$) to the *pmf* established during early qE activation in low and high light to confirm the requirement for a lower ΔpH and increased $\Delta\psi$ contribution to activation of PsbS-dominated qE quenching.

Conversely, a frameshift mutation in the *psbS* gene of *Arabidopsis* leading to a lack of PsbS expression and accumulation (Graßes *et al*., 2002) is characterized by a lack of transient NPQ formation in low light and a severely delayed increase in and reduced steady-state NPQ in high light *in npq4* (Figure 3.13D), as shown previously (Li *et al*., 2000; Kalituho *et al*., 2007). This is consistent with reduced peak transient P700 oxidation in low light in *npq4* (Figure 3.15D), reflecting transiently reduced PSI acceptor-side limitation of electron transfer. This may point to an increased contribution of cyclic to linear electron transport-dependent ΔpH formation to compensate for impaired PsbS activity. In contrast, increased steady-state P700 oxidation in high light in *npq4* (Figure 3.15D) may reflect increased PSI donor-side limitation of electron transfer. This may arise from increased photoinhibition and over-reduction of the electron transport chain as steady-state linear electron transport is increased in high light in *npq4* (Nilkens *et al*., 2010). This fits with reduced NPQ in high light (Figure 3.13D) when quenching capacity is limited by impaired PsbS activity. Indeed, linear electron transport is mediated by the redox state of the PSII acceptor side in *npq4* in high light when NPQ capacity is reduced (Peterson and Havir, 2004). Deficient PsbS activity may be offset by more pronounced lumen acidification and thus ΔpH formation required for qE activation. However, lumen acidification alone in the absence of PsbS is not sufficient to give rise to maximal transient and steady-state NPQ in low and high, respectively.

Sustained accumulation of Z_X due to impaired Z_XE activity in *npq2* (Niyogi *et al*., 1998) contributes to increased peak transient NPQ formation in low light in *npq2* (Figure 3.13E). Rapid initial NPQ induction in high light in *npq2* (Figure 3.13E) reflects the contribution of early ΔpH formation and PsbS-protonation to qE activation in the presence of excess Z_X. The accumulation of Z_X *in vivo* is approximately proportional to photosynthetic electron transport (Demmig-Adams and Adams 1992). As such, changes in the rate of electron transport should

be reflected in changes in Z_X levels and vice versa. This is confirmed by a reduction in cyclic electron transport, inferred from a sustained increase in P700 oxidation in low light in *npq2* (Figure 3.15E), due to increased PSI acceptor-side limitation and is consistent with reduced early linear electron transport in low light in *npq2* (Nilkens *et al*., 2010). Enhanced Z_X-dominated quenching in low light in the presence of excess Z_X in *npq2* may pose a burden on early electron transport activity. In high light however, higher steady-state P700 oxidation in *npq2* (Figure 3.15E) is consistent with increased steady-state linear electron transport (data not shown; Nilkens *et al*., 2010), as the contribution of cyclic to linear electron transport-dependent ΔpH formation is reduced in high light in *npq2*. It has been argued that a lower Z_XE relative to maximal V_XDE activity would necessitate a less acidic lumen than ordinarily needed to activate qE when excess Z_X is present (Takizawa *et al*., 2007), which may facilitate a higher capacity for linear electron transport. This is based on the notion that Z_XE-mediated Z_X reconversion in saturating light affects the pH sensitivity of qE activation, whereby the apparent pK_a for V_XDE-mediated Z_X and A_X accumulation will be shifted from the pK_a for V_XDE activation in proportion to the ratio of Z_XE to maximal V_XDE activities. Alternatively, Z_X formation may be determined by the inaccessibility of V_X for V_XDE, which should not be a limiting factor in Z_X formation in *npq2* as no V_X is formed in the presence of excess Z_X. In Wt, inaccessibility of V_X for V_XDE would limit the activity of V_XDE, the activation of which is dependent on thioredoxin-dependent electron transfer from PSI to V_XDE (Nikkanen and Rintamäki, 2014). Increased steady-state linear electron transport in high light in *npq2* may thus simply arise from a lack of limitation of V_XDE activation in saturating light. Regardless, changes in electron transport in response to changes in Z_X accumulation, as demonstrated in *npq2*, are important to understanding the regulation of qE in low and high light.

The importance of, but not exclusive dependence on Z_X in relation to electron transport in qE regulation is also demonstrated by *npq1*. The V_XDE-deficient *npq1* mutant (Niyogi *et al*., 1998) showed reduced peak transient and steady-state NPQ formation in low and high light, respectively (Figure 3.13F). Rapid induction of NPQ in high light in *npq1*, as in *npq2*, reflects initial ΔpH- and PsbS-dominated quenching in the absence of Z_X. Reduced peak transient NPQ is correlated with reduced peak transient P700 oxidation in low light in *npq1* (Figure 3.15F). This reflects increased cyclic electron transport, which may be attributed to slightly enhanced initial linear electron transport in low light in *npq1* (Kalituho *et al*., 2007), possibly due to reduced limitation of PSI acceptor-side electron transfer in the absence of Z_X. Minor reductions in steady-state linear electron transport in high light in *npq1* (data not

shown) reflect a lower reduction state of Q_A at steady state in high light (Niyogi *et al*., 1998). This may contribute to slightly enhanced steady-state P700 oxidation in high light in *npq1* (Figure 3.15F), reflecting increased PSI donor-side limitation of electron transfer. As electron transfer from PSI activates V_XDE in a thioredoxin-dependent manner (Nikkanen and Rintamäki, 2014), impaired V_XDE activation may limit linear electron transport in high light in *npq1* by exacerbating PSI donor-side limitation. This may be due to reduced electron transfer from PSI to V_XDE via thioredoxin required for initial V_XDE activation in high light.

4.3 Probing Changes in the Transthylakoid ΔpH and Δ*ψ in vivo*

Light-regulated Δ*ψ* and ΔpH formation probed by uncouplers like valinomycin has been examined thus far under *in vitro* conditions in spinach. However, characterization of Δ*ψ* formation *in vitro* is limited by a number of crucial factors to include inactivity of nearly all (~ 99%) valinomycin molecules reversibly bound to the thylakoid membrane (Schmid and Junge, 1975). This limits accurate determination of *in vitro* valinomycin concentrations. Moreover, isolated thylakoids stripped of their outer envelope and resuspended in media often containing high salt concentrations (Kramer *et al*., 2003) are far from the native complexity of dynamic interdependent membrane systems that affect whole plant responses to photo-oxidative stress. It is therefore important to examine the dynamics of Δ*ψ* and ΔpH partitioning of the *pmf* in relation to critical changes in NPQ and coupled electron transport *in vivo* in Wt and mutant lines of *Arabidopsis* under limiting and more saturating light conditions. This will clarify the role of Δ*ψ* in early light-dependent regulation of qE.

4.3.1 Regulation of qE via *pmf* Partitioning in *Arabidopsis* Wild-type

Taking advantage of the electrochromic properties of thylakoid membranes, more accurate indirect measurements of changes in Δ*ψ* in response to proton flux in intact leaves based on the ECS peaking at 515 nm were performed in *Arabidopsis* Wt, as described in 3.2.2.2. It is clear that light reactions and downstream biochemical processes are tightly integrated to balance photochemical efficiency, while minimizing or preventing photo-oxidative damage. It is also clear that the *pmf* is a central ephemeral intermediate of photosynthesis that links the light, dark, and photoprotective reactions (Avenson *et al*., 2005; Takizawa *et al*., 2007). Probing it *in vivo* is critical because quantitative extrapolation from *in vitro* studies is problematic, as demonstrated by early work in *Peperomia* and other systems that pointed to an all ΔpH-stored transthylakoid *pmf* due in large part to Δ*ψ*-dissipating counterion

movement. In contrast, bacterial and mitochondrial membranes possess a low ionic permeability and ΔpH (~ 0.5), resulting in a *pmf* largely consisting of the Δψ. The Δψ is a more effective component of the mitochondrial *pmf* in maintaining catalytic turnover and preventing inactivation of pH-sensitive enzymes (Mitchell, 1966; Cruz *et al*., 2001). A relatively large ΔpH implies a very acidic thylakoid lumen compartment (Kramer *et al*., 2003; Avenson *et al*., 2005; Johnson and Ruban, 2014). This is not compatible with the biochemical properties of the photosynthetic apparatus because a low pH would negatively impact the integrity and function of key pH-sensitive protein complexes and co-factors involved in the light reactions (Kramer *et al*., 2003; Avenson *et al*., 2005; Takizawa *et al*., 2007). As such, further study of changes in the *pmf* partitioning *in vivo* with respect to qE regulation is critical to better understanding the role of Δψ during early light activation of qE.

DIRK ECS analysis *in vivo* in Wt highlights a transient early increase and subsequent decline in the extent of the light-induced *pmf*, estimated from ECS_t (Figure 3.8A). This was observed most clearly in low light (Figure 3.8B). Transient *pmf* formation, peaking after ~ 30-40 s in low light, correlates with transient NPQ formation in low light. A strong reduction in ECS_t during prolonged illumination in low light is consistent with a reduction in transient NPQ (Figure 3.6B) as well as P700 oxidation (Figure 3.6F) after ~ 50 s in low light. In contrast, a less pronounced reduction in ECS_t was observed as NPQ continued to increase after 60 s at intensities above ~ 200 μmol quanta m^{-2} s^{-1}. Although changes in ECS_t do not correlate as clearly with NPQ induction kinetics at higher intensities compared to low light, it is clear that ECS_t may be a crucial parameter in regulating the extent of qE formation, particularly during early light activation of photosynthesis in limiting light. This is because a stable NPQ persists during prolonged illumination at higher intensities when the magnitude of the *pmf* is likely above a certain critical threshold. A decline in transient NPQ accompanying a strong reduction in the *pmf* during prolonged illumination in low light supports downregulation of qE when the *pmf* is below the threshold required for sustained activation of qE.

Further analysis of the dynamics of *pmf* partitioning *in vivo* highlight a rapid transient-like increase in the relative ΔpH contribution to the *pmf*, estimated from ECS_{inv} in relation to ECS_t, peaking after 30 s at all intensities (Figure 3.8D). This corresponds to a rapid transient decline in the derived lumen pH, particularly at 1287 μmol quanta m^{-2} s^{-1} (Figure 3.9B) as well as a transient increase in early *pmf* formation. Unlike *pmf* formation however, this transient response of *pmf* partitioning, which may be a normal phenomenon, is short-lived.

This is indicated by a continued increase in the relative ΔpH contribution to the *pmf* with prolonged illumination at low and higher intensities to at least ~ 60 % at steady state (Figure 3.8C). Lumen acidification continues to increase to a maximal level at steady state under these conditions (Figure 3.9A). An increasing ΔpH fraction of the *pmf* arising from increasing lumen acidification would facilitate a sustained increase in ΔpH-dependent NPQ, leading to stable steady-state NPQ at higher intensities (Figure 3.6A). This suggests that the dynamics of *pmf* partitioning compared to the dynamics of *pmf* formation are a generally good indicator of qE formation in more saturating light. However, comparable lumen acidification and *pmf* partitioning after 180 s at 53-660 μmol quanta m^{-2} s^{-1} contrasts with differences in the extent of NPQ formation under these conditions. Clearly, NPQ continues to increase at higher intensities, but continues to decline to negligible levels by steady state after peaking at 60 s in low light (Figure 3.6B). This reduced pH-dependence of early NPQ formation supports the involvement of other regulatory factors aside from the lumen pH in early qE activation. This may include a large $\Delta\psi$ fraction of the *pmf* (~ 50-60 % on average) established within 60-180 s at 53-660 μmol quanta m^{-2} s^{-1} (Figure 3.8D). Alternatively, despite an increasing contribution of the ΔpH to the *pmf* during prolonged illumination in low light, the lumen pH and thus ΔpH may be below the minimum threshold required to maintain stable qE in limiting light. This suggests that the dynamics of *pmf* partitioning and derived lumen acidification in contrast to the dynamics of *pmf* formation give a less clear indication of qE formation in limiting light. Otherwise, more pronounced intensity-dependent partitioning of the *pmf* and lumen acidification would have been observed. Existing analyses of *pmf* partitioning and lumen acidification *in vivo* thus indicate that early lumen acidification alone is not sufficient to activate and sustain qE. Rather, a large $\Delta\psi$ fraction of the *pmf* formed during early light activation of photosynthesis may contribute to early qE regulation when the total *pmf* is above the threshold for early qE activation.

A growing number of studies relying on analyses of the DIRK ECS signal support the notion that as much as half of the chloroplast *pmf* can be stored as $\Delta\psi$ over a range of steady-state conditions in terrestrial C_3 plants and the marine alga *Chlamydomonas* (Cruz *et al*., 2001; Kramer *et al*., 2003; Avenson *et al*., 2004; Johnson and Ruban, 2014). Indeed, a substantial fraction of the *pmf* consisting of the $\Delta\psi$ can persist indefinitely under continuous illumination if the stromal concentration and thus $\Delta\psi$-dissipating flux of key permeable ions like K^+ is low and the lumen proton buffering capacity is high (Cruz *et al*., 2001). Reductions in the ECS_{inv} (ΔpH) fraction *in vitro* are possible if the rate of proton efflux is slower compared to

counterion flux (Cruz *et al*., 2001; Avenson *et al*., 2005). Although internal chloroplast concentrations of permeable ions are high in intact leaves (i.e., ~ 20-80 mM K^+), a considerable fraction of K^+ may be sequestered in the inner chloroplast envelope, thus limiting transthylakoid K^+ fluxes (Cruz *et al*., 2001). Indeed, ECS measurements for 65 s of illumination in intact spinach leaves showed that ~ 50 % of the light-induced *pmf* consisted of $\Delta\psi$, enabling use of ECS_{ss} or alternatively ECS_{inv} as reliable probes of $\Delta\psi$ or ΔpH, respectively, *in vivo*. Regulation of qE via changes in *pmf* partitioning brought about by changes in the stromal ionic balance and proton buffering capacity of the lumen is therefore particularly important in terms of flexible short-term responses to photo-oxidation. The contribution of $\Delta\psi$ to the transthylakoid *pmf* along with the ΔpH can also be modified by light-driven ATP-dependent H^+ pumps in the inner envelope, which induce counterion movement and raise the stromal pH (Avenson *et al*., 2005). Thus, regulation of ionic strength and balance possibly at the level of the inner envelope may also play a key role in modulating *pmf* partitioning into the $\Delta\psi$ and ΔpH.

ECS measurements of detached leaves incubated in varying concentrations of valinomycin and KCl would aid in confirming the contribution of $\Delta\psi$ to *pmf* partitioning during brief and prolonged illumination at limiting and more saturating intensities. Complementary measurements of NPQ and electron transport *in vivo* probed by $\Delta\psi$-abolishing valinomycin under the same conditions would clarify the role of $\Delta\psi$ in electron transport-coupled qE activation, particularly in limiting light. However, extensive previous work involving valinomycin treatment of detached leaves of *Arabidopsis* further underscores the difficulties of valinomycin-assisted probing of light-induced $\Delta\psi$ formation *in vivo* in terms of NPQ. For instance, varying micromolar concentrations of valinomycin (0.03-50 μM) in the presence of 50 mM KCl have been shown to reduce peak NPQ in low light in varying, inconsistent degrees (data not shown). ECS measurements under the same conditions showed that the valinomycin did not fully abolish, if at all, the rapidly increasing and relaxing phases of the ECS signal during the dark-light and light-dark transitions, respectively. These phases are related to light-induced $\Delta\psi$ formation. Thus, clear $\Delta\psi$-abolishing effects of valinomycin *in vivo* were not observed and the contribution of $\Delta\psi$ to early qE activation *in vivo* cannot be confirmed to date. Such *in vivo* approaches are further affected by varying leaf optical properties as well as gradients of photoinhibition between abaxial and adaxial surfaces complicated by differences in chloroplast structure (Krause and Jahns, 2003). Retention of uncouplers like valinomycin in outer membrane systems like the outer chloroplast envelope

limits homogenous ionophore uptake and activity at the level of the thylakoid membrane *in vivo*. Such limitations must be considered in future *in vivo* study of $\Delta\psi$-related qE regulation.

An increasing *pmf* fraction stored as the ΔpH during prolonged illumination over a range of intensities suggests a fine-tuned regulatory response related to light activation of qE. The extent of this observed increase in the ΔpH fraction of the *pmf*, particularly at steady state, might vary, depending on the prevailing physiological and experimental conditions. Existing intensity-dependent estimates of the steady-state ΔpH contribution to the *pmf* ($\geq \sim 60$ %) suggest a highly acidic lumen compartment (i.e., < 6). This is supported by derived estimates of a low steady-state lumen pH (< 6) only at the highest saturating intensity (Figure 3.9A), but not at lower intensities (~ 50-700 μmol quanta m^{-2} s^{-1}). Such a highly acidic lumen at steady state is expected to inactivate key pH-sensitive enzymes (Avenson *et al*., 2005; Takizawa *et al*., 2007) as part of an efficient pH-dependent photoprotective feedback system. Previous work however stresses a considerably lower steady-state ΔpH fraction of the *pmf*, ranging from ~ 10 % at 50 μmol quanta m^{-2} s^{-1} to ~ 50 % at ~ 800 μmol quanta m^{-2} s^{-1}, and thus a higher steady-state lumen pH under these conditions in ambient air (Takizawa *et al*., 2007). This discrepancy in steady-state estimates of the relative ΔpH fraction and derived lumen pH in the present and previous work may in part be explained by CO_2 availability. Detached leaves in enclosed cuvettes may be increasingly limited by CO_2 availability during prolonged ECS measurements. More pronounced lumen acidification accompanying partitioning into a larger ΔpH fraction *in vivo* observed in low ambient CO_2 is attributed to reduced proton conductance through the ATP synthase (Takizawa *et al*., 2007). This causes excess H^+ accumulation in the lumen that contributes to increased ΔpH formation as the lumen pH declines in an intensity-dependent manner. Concomitantly, low CO_2 availability contributes to enhanced *pmf* formation at steady state, particularly at higher intensities, facilitated by Fd-dependent cyclic electron transport. Cyclic electron transport contributes to ΔpH formation by promotion linear electron transport-coupled H^+ influx at cytochrome b_6f in the absence of H^+ efflux via the ATP synthase (Avenson *et al*., 2005). This highlights the importance of cyclic electron transport to *pmf* formation under low CO_2 conditions and would explain somewhat higher estimates of steady-state ECS_t at 53-216 μmol quanta m^{-2} s^{-1} (Figure 3.8A), as reported previously at comparable intensities in low CO_2 (Takizawa *et al*., 2007).

Estimates of *pmf* partitioning and lumen pH can also be significantly affected by ECS signal stability, which is influenced by prevailing physiological and experimental conditions

(Schreiber and Klughammer, 2008). For the purposes of DIRK ECS analyses, reduced signal stability is manifested by severe non-linearity or 'drift' in the decaying DIRK ECS signal away from the x-axis. Light-scattering processes to include Z_X formation, assessed as absorbance changes at 505 nm (Takizawa *et al*., 2007), have been shown to predominate during prolonged illumination, particularly at higher intensities. Indeed, measurements of absorbance changes at 535 nm, related to pH-dependent light-scattering processes, confirm increasing contributions of light-scattering effects to the ECS signal after 1-3 min at intensities above 200 μmol quanta m^{-2} s^{-1} (data not shown). These overlapping absorbance changes will necessarily affect the kinetics of the ECS signal. Thus, estimates of ECS_{inv} in relation to ECS_t, critical to quantifying *pmf* partitioning and lumen acidification, can vary from sample to sample depending on the direction and degree of drift. Overlapping absorbance changes can thus limit accurate estimates of *pmf* partitioning and in turn the lumen pH *in vivo* in the absence of overlapping signal de-convolution (Avenson *et al*., 2004). Normalization of DIRK ECS amplitudes to the magnitude of the rapid absorbance change at 515 nm following a single saturating pulse of white light can minimize ECS-related differences in sample-specific optical properties and physiological conditions manifested over short time scales (Sacksteder *et al*., 2000; Avenson *et al*., 2004). However, this approach cannot sufficiently control for confounding effects of pronounced light-scattering processes manifested as overlapping absorbance changes over longer time scales.

More direct measurements of the lumen pH *in vivo* using GFP-tagged fluorescent probes expressed in stably transformed plant lines (Choi *et al*., 2012) would provide a clearer overview of lumenal processes in early qE regulation over a range of physiological and light conditions. Modification of the native protein of GFP chromophores has enabled the development of fluorescence protein-based pH sensors (Choi *et al*., 2012). Tagging pH-sensing proteins to proteins targeted to inner chloroplast compartments like the thylakoid lumen would enable quantification of dynamic changes in the lumen pH *in vivo*. However, certain limitations of this approach must be taken into account. Assuming tagged proteins are stably expressed without being downregulated by native regulatory defence systems to include RNA silencing (Meister and Tuschl, 2004), the pH sensitivity and responsiveness of the sensor can vary depending on the nature of the sensor. Certain GFP-based sensors like pHluorins are more sensitive to changes in pH over a more restricted pH range compared to others like Pt-GFP, which show lower pH sensitivity over a broader pH range (Schulte *et al*., 2006; Choi *et al*., 2012). Changes in pH can be quantified using spectral analysis of changes

in the excitation ratio of so-called ratiometric sensors like pHluorins and Pt-GFP. The development of ratiometric pH sensors has eliminated confounding effects like changes in indicator concentration on spectral-based derivation of pH (Schulte *et al*., 2006).

Proton conductance mediated largely by the ATP synthase (Kanazawa and Kramer, 2002) was assessed *in vivo* in Wt to examine the impacts of changes in the ΔpH, assessed in terms of *pmf* partitioning, on g_H^+ in terms of qE regulation. This is based on the notion that light-induced lumen acidification and thus ΔpH formation across the thylakoid membrane enables proton efflux through the ATP synthase. ECS analyses of g_H^+ over a range of intensities highlight a higher g_H^+ at steady state in low compared to higher intensities (Figure 3.10A), as shown previously over a comparable range of intensities *in vivo* in ambient air (Kanazawa and Kramer, 2002). This highlights downregulation of the ATP synthase, while the electron transport chain is increasingly over-reduced at higher intensities. Under these conditions, reduced proton efflux leading to downregulation of the ATP synthase, while excess H^+ accumulating in the lumen would contribute to rapid downregulation of photosynthesis and activation of sustained qE. This is supported by existing ECS data that show an increasing ΔpH contribution to the *pmf* (Figure 3.8C) and thus lumen acidification (Figure 3.9A) during prolonged illumination at higher intensities. However, no strong intensity-dependent differences in g_H^+ were observed at higher intensities, particularly at steady state, despite clear differences in the extent of NPQ formation at higher intensities. This suggests that proton conductance may already be limited at less saturating intensities, possibly even during early light activation of qE under these conditions.

Reductions in proton conductance are further exacerbated by low ambient CO_2 levels (Kanazawa and Kramer, 2002). Indeed, more pronounced changes in proton conductance activity have been shown to predominantly regulate qE responses under varying atmospheric CO_2 conditions (Avenson *et al*., 2005). For instance, g_H^+ has been shown to decline by 5-fold as qE increased 5-fold in tobacco plants exposed to CO_2-free air compared to 2000 ppm CO_2 and ambient O_2 conditions (Kanazawa and Kramer, 2002; Avenson *et al*., 2005). This was accompanied by a clear reduction in linear electron transport in the absence of added cyclic electron transport around PSI. While large fluctuations in light intensity are typical of various natural environments, such fluctuations in atmospheric CO_2 are more likely in aquatic rather than terrestrial environments (Avenson *et al*., 2004). Although CO_2 availability may have been a limiting factor to some extent during prolonged ECS measurements, comparison of

existing estimates of proton conductance with previously reported data gives no indication of significant impacts of CO_2 availability on proton conductance. Regardless, conditions that inhibit downstream carbon fixation via Calvin-Benson cycle (i.e., high light, low CO_2) will lead to an accumulation of phosphorylated intermediates in the stroma (Avenson *et al*., 2005). These intermediates will consume free P_i required for ATP synthesis and thus ATP synthase activity (Kanazawa and Kramer, 2002; Avenson *et al*., 2004; Avenson *et al*., 2005). The availability of free P_i could allosterically limit substrate binding at the ATP synthase, leading to a reduction in the effective rate constant for ATP synthesis and g_H^+. This is consistent with the view that stromal P_i sequestration influences both the light and carbon assimilating reactions of photosynthesis (Kanazawa and Kramer, 2002).

In contrast to saturating light conditions, proton conductance is delayed during the initial ~ 90 s of illumination in low light and increases rapidly thereafter (Figure 3.10B), approaching saturation towards steady state (Figure 3.10A). This delayed g_H^+ response follows an early transient increase in NPQ, which declines after 60 s with prolonged illumination in low light (Figure 3.6A). Increasing g_H^+ with prolonged illumination in low light would dissipate the *pmf* to a certain extent, as supported by a reduction in ECS_t (Figure 3.8A), by reducing the ΔpH. This parallels a decline in transient NPQ over the same period under these conditions (Figure 3.6A). However, an increasing ΔpH fraction of the *pmf* (Figure 3.8C) accompanying lumen acidification (Figure 3.9A) in spite of a decline in transient NPQ formation during prolonged illumination in low light suggests an increasing ΔpH. This may be reconciled by the notion that the ΔpH may below a certain threshold for sustained qE activation in limiting light. The extent of this ΔpH would be regulated by proton efflux via the ATP synthase balanced by proton influx via the Q cycle at cytochrome b_6f (Avenson *et al*., 2005). Taken together, existing data thus support the idea that changes in g_H^+ can clearly impact pH-dependent qE responses over a range of environmental conditions.

4.3.2 Xanthophyll Cycle Activity in Regulation of qE in *Arabidopsis* Wild-type

Lumen acidification as a pre-requisite for qE activation not only facilitates proton efflux through the ATP synthase, but also Z_X formation mediated by V_XDE. Changes in xanthophyll conversion were assessed in terms of the DEPS of the VAZ pool monitored *in vivo* in Wt over a range of light intensities, as described in 3.2.2.3. Analysis of DEPS underscores the importance of Z_X formation in qE responses. A delayed increase in DEPS during early illumination in low light (Figure 3.11) reflects delayed activation of V_XDE and thus Z_X

formation when the lumen pH is not low enough (above the pK_a) for V_XDE protonation *in vivo* (Takizawa *et al*., 2007). This is consistent with existing estimates of a relatively high lumen pH during early illumination in low light (Figure 3.9B). In contrast, the rapid early increase in DEPS in more saturating light, particularly at 1287 μmol quanta m^{-2} s^{-1} (Figure 3.11), reflects rapid V_XDE activation catalyzing Z_X (and minor A_X) formation when the lumen pH is low enough to activate V_XDE. This rapid early increase in DEPS in more saturating compared to limiting light contrasts with the comparable degree of NPQ formation during the initial 60 s of illumination at all intensities (Figure 3.6B). DEPS analyses thus underscore differences in V_XDE activation as an indication of differences in intensity-dependent lumen acidification. Activation of qE is therefore delayed in response to changes in the lumen pH. Alternatively, qE not only responds to the lumen pH during early activation of photosynthesis, particularly in low light, but also to other regulatory factors. This includes the $\Delta\psi$ as the predominant parameter of early *pmf* formation in low and more saturating light.

Previous work supports delayed activation of qE in response to lumen acidification, estimated from ECS_{inv} (Takizawa *et al*., 2007), as the pre-requisite for PsbS and V_XDE protonation in their interaction to synergistically give rise to qE. This delayed response of qE holds true even under varying light and CO_2 conditions, which impact lumen acidification. Delayed activation of qE allows fine-tuning of the pH response of the xanthophyll cycle, such that the onset of qE occurs at a higher lumen pH, particularly in low light, than the apparent pK_a for plastoquinol oxidation at cytochrome b_6f. According to the Takizawa *et al*. (2007), increasing actinic intensity reduces the lumen pH to ~ 6.3-6.7, approximately consistent with the apparent pK_a for cytochrome b_6f oxidation. Thus, half-activation of qE in high light occurs at a pH of ~ 6.5 above that which reduces linear electron transport limited by plastoquinol oxidation at cytochrome b_6f and leads to accumulation of photo-oxidative Q_A^-. As such, delayed activation of qE facilitates efficient light harvesting at a higher lumen pH in limiting light. Rapid activation of V_XDE accompanies a rapid induction of qE below a lumen pH of ~ 7 as part of a precise transition between light-harvesting and photoprotective states. Saturation of qE below a lumen pH of ~ 6 thus enables acclimation to high light and/or low CO_2 conditions. However, such a high lumen pH of ~ 7, below which V_XDE activation rapidly follows that of qE, may be questionable on the basis of previous *in vitro* estimates of a lower range of pH (< 6.5) regulating V_XDE activation (Kramer *et al*., 2003).

4.3.3 Regulation of qE via *pmf* Partitioning in *Arabidopsis* Mutants

Variable partitioning of the *pmf* in chloroplasts thus contends against the traditional view of *pmf* partitioning into a largely ΔpH component that marginalizes the contribution of $\Delta\psi$ under both *in vitro* and *in vivo* conditions. Nevertheless, changes in the ΔpH contribution to the *pmf* against an energetically opposing $\Delta\psi$ fraction can thus significantly contribute to regulating pH-dependent qE activity over a range of conditions to include high light and low CO_2, all else equal (Cruz *et al*., 2001; Avenson *et al*., 2004; Avenson *et al*., 2005). ECS measurements in *Arabidopsis* support the notion of variable partitioning of the *pmf* into a significant $\Delta\psi$ fraction *in vivo* in Wt (Figure 3.4E-F) as well as in *kea3* (see Armbruster *et al*., 2014), which may contribute to early light activation of qE, at least under limiting light conditions. ECS analyses in *Arabidopsis* mutants defective in cyclic electron transport, cytochrome b_6f, PsbS, and xanthophyll cycle activities offer further insight into the impacts of energy dissipation, linear and cyclic electron transport, and xanthophyll cycle activity on *pmf* partitioning in terms of qE regulation. This will clarify the proposed role of $\Delta\psi$ in early qE activation influenced by changes in *pmf* partitioning.

The impacts of defects in Fd-dependent cyclic electron transport in *pgr5* and *pgrl1ab #273* on the dynamics of *pmf* partitioning with respect to qE regulation were characterized *in vivo*. More pronounced reductions in the light-induced *pmf* (ECS_t) were observed early on in low light in *pgrl1ab #273* (Figure 3.17D) and to a lesser extent in *pgr5* (Figure 3.17B) when compared to Wt. This corresponds to reductions in peak transient NPQ in *pgr5* (Figure 3.12B) and *pgrl1ab #273* (Figure 3.12D) as well as increased P700 oxidation in low light in *pgr5* (Figure 3.14B) and *pgrl1ab #273* (Figure 3.14D). A reduced early *pmf* in low light in *pgr5* is characterized by a reduced ΔpH fraction of the *pmf* in low light in *pgr5* (Figure 3.19B). This further supports the importance of *PGR5*-dependent cyclic electron transport-mediated *pmf* formation to early transient ΔpH-dependent NPQ formation in low light. Reductions in the steady-state *pmf* in high light in *pgr5* (Figure 3.17B) and to a lesser extent in *pgrl1ab #273* (Figure 3.17D) are consistent with a reduced steady-state NPQ in high light in *pgr5* (Figure 3.12B) and *pgrl1ab #273* (Figure 3.12D). Dissipation of the light-induced *pmf* in *pgr5* and *pgrl1ab #273* is mediated by ΔpH-consuming proton efflux through the ATP synthase in the absence of *PGR5*- and *PGRL1*-dependent cyclic electron transport-mediated proton influx at cytochrome b_6f, as reported previously in *pgr5* (Avenson *et al*., 2005; Shikanai, 2014). Impaired cyclic electron transport causes a minor imbalance (decrease) in

the output ratio of ATP/NADPH and thus depletion of $NADP^+$ due to stromal over-reduction at intensities above ~ 100 μmol quanta m^{-2} s^{-1} (Munekage *et al*., 2002; DalCorso *et al*., 2008). This leads to a reduction in linear electron transport at PSII, as shown previously in *pgr5* and *pgrl1ab* (DalCorso *et al*., 2008), and coupled *pmf* formation. Reduced linear electron transport is accompanied by a reduction in P700 oxidation in high light, as shown in *pgr5* (Figure 3.14B) and *pgrl1ab #273* (Figure 3.14D). As such, maximal steady-state NPQ is reduced in high light (DalCorso *et al*., 2008), as observed in *pgr5* and *pgrl1ab #273*. In contrast, comparable *pmf* partitioning at steady state in high light is demonstrated by *pgr5*, *pgrl1ab #273*, and Wt, despite a larger ΔpH fraction of *pmf* established early on in high light in *pgrl1ab #273* (Figure 3.19D) compared to Wt. This suggests that known impacts of impaired cyclic electron transport on the ΔpH and in turn NPQ do not necessarily impact *pmf* partitioning, particularly in high light. Taken together, the above findings underscore the importance of the contribution of cyclic electron transport to linear electron transport-coupled *pmf* formation. Close correlation between reduced early *pmf* and NPQ formation, particularly in low light, further supports the importance of the total *pmf* in regulating the extent of qE responses during early light activation of photosynthesis.

Partitioning of the *pmf* altered by impaired cytochrome b_6f activity in *pgr1* modulates qE responses. Indeed, a rapid reduction in ECS_t and thus the *pmf* established during early illumination in low light was observed in *pgr1* (Figure 3.18B) compared to Wt (Figure 3.18A). The *pmf* was also markedly reduced early on and at steady state in high light in *pgr1*. Attenuation of linear electron transport at cytochrome b_6f observed previously during early illumination in low light in *pgr1* (Kalituho *et al*., 2007) would limit early *pmf* formation in low light. This is consistent with reduced peak transient NPQ formation in low light in *pgr1* (Figure 3.13B). Reduced steady-state linear electron transport and enhanced P700 oxidation accompanying enhanced Q_A reduction in high light in *pgr1* (Munekage *et al*., 2001) would also limit *pmf* formation. This is consistent with reduced steady-state NPQ in high light in *pgr1* (Figure 3.13B). A rapid decline in the *pmf* in low and high light in *pgr1* is accompanied by *pmf* partitioning into a rapidly increasing ΔpH fraction (Figure 3.20B) and lumen acidification (Figure 3.22B) in *pgr1* compared to Wt. Despite an increasing ΔpH contribution to the *pmf* and lumen acidification, NPQ formation is reduced in low and high light due to limited ΔpH formation in *pgr1*. The dynamics of *pmf* partitioning thus give no clear indication of changes in the absolute ΔpH, which may not be accurately inferred from changes in the estimated lumen pH in *pgr1*. This is because ECS-based estimates of the

lumen pH *in vivo* rely in part on estimates of ECS_{inv} in relation to ECS_t (ΔpH) assuming steady-state conditions in the light are reached (Takizawa *et al*., 2007). Such assumptions may not be met during more brief periods of illumination in general, which may limit the accuracy of estimates of the lumen pH under these conditions. Nevertheless, existing analyses of *pmf* partitioning in *pgr1* further support the importance of the total light-induced *pmf* in regulating early activation of qE.

PsbS overexpression in *L17* and V_XDE-deficiency in *npq1* impacts the dynamics of *pmf* partitioning *in vivo* and gives key insight into early qE regulation. Increased early light-induced *pmf* formation in low and high light, peaking after 60 s of illumination in high light, was sustained with prolonged illumination towards steady state in *L17* (Figure 3.18C) compared to Wt (Figure 3.18A). Similarly, increased *pmf* formation, particularly during the initial 60-180 s of illumination in high light was observed in *npq1* (Figure 3.18F). Increased early *pmf* formation in low and high light in *L17* corroborates enhanced peak transient and rapid induction of NPQ in low and high light, respectively, in *L17* (Figure 3.13C). Enhanced PsbS relative to maximal V_XDE activity may necessitate a less acidic lumen needed to activate qE. This is supported by a reduction in the relative ΔpH contribution to the *pmf* established after 60 s of illumination in high light in *L17* (Figure 3.20C), accompanied by delayed lumen acidification during the initial 60-180 s of illumination in high light in *L17* (Figure 3.22C). A higher lumen pH and thus reduced ΔpH would reduce the burden on and allow for increased steady-state linear electron transport in high light (Nilkens *et al*., 2010), which would facilitate increased *pmf* formation in high light. The relative ΔpH contribution to the *pmf* was also reduced after 60 s of illumination in high light in *npq1* (Figure 3.20F), accompanied by delayed lumen acidification under these conditions in *npq1* (Figure 3.22F), but to a lesser extent than in *L17*. This contrasts with rapid early NPQ formation in high light in *npq1* (Figure 3.13F), which may necessitate a more acidic lumen offset by a lack of Z_X to activate qE. However, as this was not observed in *npq1* early on in high light in terms of the dynamics of *pmf* partitioning and lumen acidification, the PsbS may instead largely control rapid early NPQ formation in high light in *npq1*. This is supported by comparable dynamics of early *pmf* partitioning in high light in *L17* and *npq1*. Delayed early *pmf* partitioning and lumen acidification in *L17* and *npq1* in high light is consistent with delayed relaxation of the DIRK ECS signal characterized by a truncated ECS_{inv} fraction after 60 s of illumination in high light in *L17* (Figure 3.16B) in *npq1* (Figure 3.16C). Comparatively more rapid recovery of the ECS signal leading to an increase in ECS_{inv} was observed after 3 min of illumination in

high light in *L17* (Figure 3.16B). This indicates that this relatively rapid transition in the rate of DIRK ECS relaxation following brief high light illumination appears to be governed by the PsbS. The PsbS is the predominant regulatory factor influencing the activation and extent of qE responses when excess PsbS is present in *L17* and Z_X is absent in *npq1*. Under these conditions, quenching largely attributed to the PsbS is argued to originate from the Q1 site in the major LHCII complexes, which detach from the native PSII/RC supercomplex in a PsbS-dependent manner to give rise to quenching (Holzwarth *et al*., 2009).

Delayed early *pmf* partitioning and lumen acidification, particularly in *L17*, allows the formation of a large $\Delta\psi$ contribution to the early light-induced *pmf* that may contribute to early light activation of qE. This is supported by early measurements of membrane potential using microcapillary glass electrodes inserted into large isolated chloroplasts of *Peperomia*. Indeed, delayed relaxation of the transthylakoid potential extending transiently below the dark baseline was observed following prolonged illumination on the order of at least hundreds of milliseconds (Vredenberg and Tonk, 1975; Vredenberg and Bulychev, 1976; Bulychev *et al*., 1980). The magnitude of this transient undershoot is dependent on light intensity and duration and has been related to re-equilibration of the transthylakoid ion (i.e., H^+, K^+) diffusion potential coupled to light-induced electron transport. Application of DCCD, which inhibits ATP synthase activity, abolished the formation of this undershoot driven by continued proton efflux through the ATP synthase in the dark (Bulychev *et al*., 1980). In contrast, valinomycin supplemented by millimolar concentrations of KCl accelerated the relaxation of membrane potential and thus re-equilibration of K^+ (Vredenberg and Bulychev, 1976) in a similar manner as that observed in *L17* and *npq1* after 3 min of illumination in high light. One can therefore argue that PsbS-dependent quenching dominating in *L17* and *npq1* may somehow regulate the extent and kinetics of acceleration of transthylakoid K^+ fluxes during early activation of photosynthesis in high light. Although such fluxes would dissipate a non-trivial light-induced $\Delta\psi$ established during early light activation of qE, clearly quenching depending largely on the PsbS delays dissipation of this substantial $\Delta\psi$ component during the initial 3 min in high light. As such, the $\Delta\psi$ may contribute to PsbS-dependent regulation of early light activation of qE. However, this remains to be confirmed in subsequent *in vivo* studies of NPQ and *pmf* partitioning in *L17* and *npq1* probed by $\Delta\psi$-collapsing valinomycin supplemented with KCl under low and high light conditions.

Regulation of qE-type quenching influenced by changes in *pmf* partitioning limited by PsbS- and Z_XE-deficiency in *npq4* and *npq2*, respectively, was also examined *in vivo*. The PsbS-deficient *npq4* mutant showed an increased *pmf* established during early and prolonged illumination in low as well as high light (Figure 3.18D) compared to Wt (Figure 3.18A). Concomitantly, the relative ΔpH contribution to early *pmf* formation in low and high light was increased in *npq4* (Figure 3.20D), consistent with more rapid early lumen acidification in low and high light in *npq4* (Figure 3.22D), possibly to compensate for a lack of PsbS activity. Enhanced cyclic electron transport, inferred from reduced peak transient P700 oxidation in *npq4* (Figure 3.15D) might contribute to increased early *pmf* formation consisting largely of the ΔpH in low light in *npq4*. Similarly, an increased *pmf* stored largely as the ΔpH in high light, particularly at steady state, may be attributed to an increased rate of linear electron transport during prolonged high light illumination in *npq4* (Nilkens *et al*., 2010). An increased early *pmf* stored largely as the ΔpH and a low lumen pH in the absence of PsbS, which overrides any pH or *pmf* effects, stresses the importance of the PsbS in addition to the ΔpH in qE activation in low and high light.

In contrast to the other mutant lines like *L17*, *npq1*, and *npq4*, the Z_XE-deficient *npq2* mutant is characterized by a more rapid reduction in the *pmf* established early on in low light (Figure 3.18E) compared to Wt (Figure 3.18A). This corresponds to increased peak transient NPQ formation (Figure 3.13E) as well as increased initial *pmf*-generating linear electron transport in low light in *npq2* (Kalituho *et al*., 2007). The extent of the light-induced *pmf* also declined more rapidly during early illumination in high light in *npq2* (Figure 3.18E) compared to Wt. Concomitantly, the relative contribution of the ΔpH to the light-induced *pmf* increased rapidly, peaking after 60-180 s of high light illumination in *npq2* (Figure 3.20E). This was accompanied by a more pronounced reduction in the lumen pH in *npq2* under these conditions (Figure 3.22E), but to a lesser extent than in *npq4* (Figure 3.22D). More pronounced lumen acidification might contribute to rapid early NPQ formation in high light in *npq2* (Figure 3.13E). However, this contradicts with the predicted requirement of a less acidic lumen than otherwise required for qE activation facilitated by higher maximal V_XDE activity relative to that of Z_XE in the presence of excess Z_X in *npq2*, as discussed previously according to Takizawa *et al*. (2007). Existing *pmf* partitioning data in *npq2* thus indicate that the pH-dependence of qE activation in saturating light may not be influenced by the reconversion of Z_X. In contrast to high light, a slower rate of increase in the ΔpH contribution to the *pmf* during the initial 60-180 s in low light allows a substantial $\Delta\psi$ contribution (≥ 50

%) to a reduced total *pmf* (Figure 3.18E) established within 60-180 s in low light in *npq2*. Delayed lumen acidification and a slower rate of decline in increased peak transient NPQ giving rise to a higher qE response active over a longer period in low light in *npq2* supports a possible role of the $\Delta\psi$ during early qE activation influenced by sustained excess Z_X levels.

5. Summary

All photosynthetic organisms periodically absorb more light than can be used efficiently during photosynthesis. The 'energy'-dependent qE component of non-photochemical quenching (NPQ) is the predominant and most effective means of photoprotection during major short-term light fluxes. NPQ is largely controlled by the thylakoid lumen pH and thus transthylakoid proton gradient (ΔpH) according to an unknown photo-physical mechanism requiring PsbS-mediated LHCII conformational changes and zeaxanthin (Z_X) formation. The ΔpH in contrast to electric field ($\Delta\psi$) component of the proton motive force (*pmf)* is known to play a central regulatory role in both photochemical and non-photochemical reactions. It is hypothesized that the $\Delta\psi$ may play a role in early light activation of qE.

Characterization of NPQ based on Chl fluorescence quenching in isolated spinach thylakoids treated with ΔpH-abolishing nigericin or gramicidin underscored the importance of the ΔpH in qE formation in saturating light. This was confirmed by *in vitro* estimates of the ΔpH via measurements of 9-AA fluorescence quenching and abolishment of lumen pH-regulated Z_X formation under the same conditions. However, low concentrations of $\Delta\psi$-abolishing valinomycin with 50 mM KCl had no impact on NPQ formation. As such, there is no support for a hypothesized role of $\Delta\psi$ in early qE activation *in vitro*.

Analyses of *pmf* partitioning *in vivo* in wild-type *A. thaliana* indicate that the total light-induced *pmf* within a defined range regulates the extent of NPQ responses at various intensities, particularly during early activation of qE in limiting light. Chiefly, the *pmf* early on in low and high light is stored largely as the $\Delta\psi$ (~ 60 %), which may contribute to early light activation of qE when the *pmf* is above a certain critical threshold for qE activation. This is supported by differential early NPQ induction at low and higher intensities despite comparable *pmf* partitioning and lumen acidification. The extent of early qE responses is thus not only regulated by the lumen pH within a defined range, but also by other factors to include possibly the $\Delta\psi$. Regulation of qE is also mediated by changes in proton efflux (g_{H^+}) via the ATP synthase, as shown in high light and low CO_2 conditions. This g_{H^+}-dependent regulation of qE is governed by changes in stromal P_i availability. Comparison of early violaxanthin de-epoxidation to Z_X at low and higher intensities underscores a delayed response of pH-dependent qE activation in relation to lumen acidification. Alternatively, qE responds not only to early lumen acidification, particularly in low light, but also to other regulatory factors to include the $\Delta\psi$, largely contributing to early *pmf* formation.

Analysis of *pmf* partitioning in *Arabidopsis* mutant lines underscores a substantial $\Delta\psi$ contribution to the light-induced *pmf* under certain conditions. This was observed after 1-3 min in low light in *npq2* and in particular after 1-3 min of illumination in high light in *L17* and to a lesser extent in *npq1*. The proposed role of $\Delta\psi$ in early qE activation in these mutant lines will be further discussed in more detailed analyses of mutant-specific differences in the dynamics of *pmf* partitioning in low and high light.

5. Zusammenfassung

Alle photosyntetisch aktiven Lebewesen absorbieren regelmäßig mehr Energie als sie effektiv für die Photosynthese nutzen können. Der „Energie“-abhängige qE Mechanismus der nicht-photochemischen Energie-Löschung (engl. non-photochemical quenching, NPQ) ist der wichtigste und dominierende Schritt der Photoprotektion während sich schnell ändernder Lichtbedingungen. NPQ Prozesse sind hauptsächlich durch den Lumen pH kontrolliert. Mit dem Aufbau eines pH Gradienten (ΔpH) werden, nach bisher unbekanntem Mechanismus, PsbS-Protein abhängige Konformationsänderungen in den Lichtsammelkomplexen des Photosystem II (engl. light-harvesting-complex, LHCII) durchgeführt. Zusätzlich wird die pH abhängige Bildung des Zeaxanthin (Z_X) aktiviert. Beide Mechanismen basieren auf dem Aufbau eines pH Gradienten, welcher eine zentrale Rolle in der photochemischen und nicht-photochemischen Energielöschung spielt. Im Gegensatz dazu steht die andere Komponente der Protonen motorischen Kraft (engl. proton motive force, *pmf*): das elektrische Feld ($\Delta\psi$). Vermutlich ist $\Delta\psi$ in den frühen Prozessen der lichtabhängigen qE Aktivierung wichtig.

Schätzungen des ΔpH mit Hilfe von 9-AA, Messungen zur Löschung der Chlorophyll Fluoreszenz und das Ausbleiben der pH-abhängigen Umwandlung von Z_X *in vitro* bestätigten die Relevanz des ΔpH für die Ausbildung des qE Mechanismus unter sättigen Lichtbedingungen. Dafür wurde das NPQ unter sättigenden Lichtbedingungen und der Zugabe von Nigericin und Gramicidin, welche beide den ΔpH abbauen, charakterisiert. Im Gegensatz dazu hatte die Zugabe von niedrig konzentriertem Valinomycin, welches das $\Delta\psi$ abbaut, in Kombination mit 50 mM KCl keinen Effekt auf den Aufbau des NPQ. Daraus resultierend konnte der zuvor angenommene Einfluss des $\Delta\psi$ auf die frühe Ausbildung des qE *in vitro* nicht bestätigt werden.

In vivo Analysen zur *pmf* Partitionierung in Wildtyp *A. thaliaana* Pflanzen zeigten, dass innerhalb eines bestimmten Bereiches das Ausmaß des NPQ von der Licht-induzierten gesamt-*pmf* reguliert wird, insbesondere die frühe Aktivierung des qE Mechanismus unter limitierenden Lichtbedingungen. Unter Schwach- und Starklichtbedingungen ist die initiale *pmf* hauptsächlich als $\Delta\psi$ gespeichert (~ 60%), welches möglicherweise zu der frühen Aktivierung des qE beiträgt, allerdings nur wenn die *pmf* einen bestimmten Schwellenwert überschreitet. Unterstütz wird diese Annahme dadurch, dass Stark- und Schwachlicht unterschiedlich hohes NPQ induzieren, die *pmf* Partitionierung und Ansäuerung des Lumens unter den Bedingungen jedoch vergleichbar sind. Das Ausmaß der frühen qE Antwort kann

innerhalb eines bestimmten Bereiches deshalb nicht nur durch den Lumen pH reguliert sein, sondern durch weitere Faktoren, wie möglicherweise das $\Delta\psi$. Unter Starklicht oder niedrigen CO_2 Bedingungen wird qE auch durch Änderungen im Protonen Efflux durch die ATP Synthase (g_H^+) beeinflusst. Diese g_H^+- abhängige Regulation hängt von Veränderungen der stromalen P_i Verfügbarkeit ab. Anhand des Vergleiches der frühe Deepoxidationphase von Violaxanthin zu Z_X unter Schwach- und Starklichtbedingungen wird deutlich, dass die Reaktion des pH abhängigen qE Mechanismus im Vergleich zu der Ansäuerung des Lumens verzögert ist. Daraus resultierend ist die qE Antwort, speziell in Schwachlicht, nicht nur von der anfänglichen Ansäuerung des Lumens abhängig, sondern auch von anderen, regulierenden Faktoren, wie das $\Delta\psi$, welches einen hohen Beitrag zur anfänglichen Ausbildung der *pmf* leistet.

Analysen der *pmf* Partitionierung in *Arabidopsis* Mutanten unter bestimmten Bedingungen unterstrichen die Bedeutung des $\Delta\psi$ an der Licht-induzierten *pmf*. Gezeigt wurde dies in *npq2* Mutanten unter Schwachlicht Bedingungen nach 1-3 Min, sowie nach 1-3 Min Belichtung mit Starklicht in *L17* und *npq1*, in letzterem in geringerem Ausmaß. Des Weiteren wurden Mutanten-spezifische Unterschiede in der Dynamik der *pmf* Partitionierung unter Schwach- und Starklicht Bedingungen sowie die mögliche Rolle des $\Delta\psi$ an der anfänglichen Aktivierung des qE detaillierter diskutiert.

6. References

Ahn, T.K., Avenson, T.J., Ballottari, M., Cheng, Y.C., Niyogi, K.K., Bassi, R., Fleming, G.R. (2008) Architecture of a charge-transfer state regulating light harvesting in a plant antenna protein. *Science* 320: 794-797.

Allen, J.F., Bennett, J., Steinback, K.E., Arntzen, C.J. (1981) Chloroplast protein phosphorylation couples plastoquinone redox state to distribution of excitation energy between photosystems. *Nature* 291: 25-29.

Andersson, J., Walters R.G., Horton, P. (2001) Antisense inhibition of the photosynthetic antenna proteins CP29 and CP26: Implications for the mechanism of protective energy dissipation. *Plant Cell* 13: 1193-1204.

Andersson, J., Wentworth, M., Walters, R.G., Howard, C.A., Ruban, A.V., Horton, P., Jansson, S. (2003) Absence of the Lhcb1 and Lhcb2 proteins of the light-harvesting complex of photosystem II - effects on photosynthesis, grana stacking and fitness. *Plant J.* 35: 350-361.

Apel, K., Hirt, H. (2004) Reactive oxygen species: Metabolism, oxidative stress, and signal transduction. *Annu. Rev. Plant Biol.* 55: 373-399.

Armbruster, U., Carrillo, L.R., Venema, K., Pavlovic, L., Schmidtmann, E., Kornfeld, A., Jahns, P., Berry, J.A., Kramer, D.M., Jonikas, M.C. (2014) Ion antiport accelerates photosynthetic acclimation in fluctuating light environments. *Nat. Commun.* 5: 5439.

Arnon, D.I. (1949) Copper enzymes in isolated chloroplasts. Polyphenoloxidase in *Beta vulgaris*. *Plant Physiol.* 24: 1-15.

Aro, E-M., Kettunen, R., Tyystjärvi, E. (1992) ATP and light regulate D1 protein modification and degradation. Role of D1* in photoinhibition. *FEBS Lett.* 297: 29-33.

Asada, K. (2006) Production and scavenging of reactive oxygen species in chloroplasts and their functions. *Plant Physiol.* 141: 391-396.

Avenson, T.J., Cruz, J.A., Kramer, D.M. (2004) Modulation of energy-dependent quenching of excitons in antennae of higher plants. *Proc. Natl. Acad. Sci. USA* 101: 5530-5535.

Avenson, T.J., Kanazawa, A., Cruz, J.A., Takizawa, K., Ettinger, W.E., Kramer, D.M. (2005) Integrating the proton circuit into photosynthesis: Progress and challenges. *Plant, Cell and Environ.* 28: 97-109.

Baier, M., Dietz, K.J. (2005) Chloroplasts as source and target of cellular redox regulation: a discussion on chloroplast redox signals in the context of plant physiology *J. Exp. Bot.* 56: 1449-1462.

Baker, N.R., Harbinson, J., Kramer, D.M. (2007) Determining the limitations and regulation of photosynthetic energy transduction in leaves. *Plant Cell Environ.* 30: 1107-1125.

Bennett, J., Steinback, K.E., Arntzen, C.J. (1980) Chloroplast phosphoproteins: regulation of excitation energy transfer by phosphorylation of thylakoid membrane polypeptides. *Proc. Natl. Acad. Sci. USA* 77: 5253-5257.

Biaudet, P., Haraux, F. (1987) ΔpH-dependent activation of chloroplast coupling factors and external pH effects on 9-aminoacridine response in lettuce and spinach thylakoids. *Biochim. Biophys. Acta* 893: 544-556.

Bulychev, A.A., Vredenberg, W.J. (1976) The effect of cations and membrane permeability modifying agents on the dark kinetics of the photoelectric response in isolated chloroplasts. *Biochim. Biophys. Acta* 423: 548-556.

Bulychev, A.A., Andrianov, V.K., Kurella, G.A. (1980) Effect of dicyclohexylcarbodiimide on the proton conductance of thylakoid membranes in intact chloroplast. *Biochim. Biophys. Acta* 590: 300-308.

Burkhart, B.M., Gassman, R.M., Langs, D.A., Pangborn, W.A., Duax, W.L., Pletnev, V. (1999) Gramicidin D conformation, dynamics and membrane ion transport. *Biopolymers* 51: 129-144.

Cammann, K. (1985) Ion-selective bulk membranes as models for biomembranes. *Top. Curr. Chem.* 128: 219-259.

Carraretto, L., Formentin, E., Teardo, E., Checchetto, V., Tomizioli, M., Morosinotto, T., Giacometti, G.M., Finazzi, G., Szabó, I. (2013) A thylakoid-located two-pore K^+ channel controls photosynthetic light utilization in plants. *Science* 342: 114-118.

Choi, W-G., Swanson, S.J., Gilroy, S. (2012) High-resolution imaging of Ca^{2+}, redox status, ROS and pH using GFP biosensors. *Plant J.* 70: 118-128.

Chow, W.S., Barber, J. (1980) 9-aminoacridine fluorescence changes as a measure of surface charge density of the thylakoid membrane. *Biochim. Biophys. Acta* 589: 346-352.

Cruz, J.A., Sacksteder, C.A., Kanazawa, A., Kramer, D.M. (2001) Contribution of electric field ($\Delta\psi$) to steady-state transthylakoid proton motive force (*pmf*) *in vitro* and *in vivo*. Control of *pmf* parsing into $\Delta\psi$ and ΔpH by ionic strength. *Biochem.* 40: 1226-1237.

DalCorso, G., Pesaresi, P., Masiero, S., Aseeva, E., Schünemann, D., Finazzi, G., Joliot, P., Barbato, R., Leister, D. (2008) A complex containing PGRL1 and PGR5 is involved in the switch between linear and cyclic electron flow in *Arabidopsis*. *Cell* 132: 273-285.

Dau, H., Zaharieva, I. (2009) Principles, efficiency, and blueprint character of solar-energy conversion in photosynthetic water oxidation. *Accts. Chem. Res.* 42: 1861-1870.

Delrieu, M.J., Rosengard, F. (1993) Events near the reaction center in O_2 evolving PSII enriched thylakoid membranes: The presence of an electric field during the S_2 state in a population of centers. *Photosynth. Res.* 37: 205-215.

Demmig, B., Björkman, O. (1987) Comparison of the effect of excessive light on chlorophyll fluorescence (77K) and photon yield of O_2 evolution in leaves of higher plants. *Planta* 171: 171-84.

Demmig-Adams, B., Adams III, W.W., Heber, U., Neimanis, S., Winter, K., Krüger, A., Czygan, F-C., Bilger, W., Björkman, O. (1990) Inhibition of zeaxanthin formation and of

rapid changes in radiationless energy dissipation by dithiothreitol in spinach leaves and chloroplasts. *Plant Physiol.* 92: 293-301.

Demmig-Adams, B., Adams III, W.W. (1992) Photoprotection and other responses of plants to high light stress. *Annu. Rev. Plant Phvsiol. Plant Mol. Biol.* 43: 599-626.

Elrad, D., Niyogi, K.K., Grossman, A.R. (2002) A major light-harvesting polypeptide of photosystem II functions in thermal dissipation. *Plant Cell* 14: 1801-1816.

Eskling, M., Arvidsson, P-O., Åkerlund, H-E. (1997) The xanthophyll cycle, its regulation and components. *Physiol. Planta.* 100: 806-816.

Eskling, M., Åkerlund, H-E. (1998) Changes in the quantities of violaxanthin de-epoxidase, xanthophylls and ascorbate in spinach upon shift from low to high light. *Photosynth. Res.* 57: 41-50.

Falkowski, P.G., Kolber, Z. (1995) Variations in chlorophyll fluorescence yields in phytoplankton in the world oceans. *Aust. J. Plant Physiol.* 22: 341-355.

Färber, A., Young, A.J., Ruban, A.V., Horton, P., Jahns, P. (1997) Dynamics of xanthophyll-cycle activity in different antenna subcomplexes in the photosynthetic membranes of higher plants. *Plant Physiol.* 115: 1609-1618.

Finazzi, G., Johnson, G.N., Dall'Osto, L., Joliot, P., Wollman, F.A., Bassi, R. (2004) A zeaxanthin-independent nonphotochemical quenching mechanism localized in the photosystem II core complex. *Proc. Natl. Acad. Sci. USA* 101: 12375-12380.

Fiolet, J.W.T., Bakker, E.P., van Dam, K. (1974) The fluorescent properties of acridines in the presence of chloroplasts or liposomes. On the quantitative relationship between fluorescence quenching and the transmembrane proton gradient. *Biochim. Biophys. Acta* 368: 432-445.

Frank, H.A., Cua, A., Chynwat, V., Young, A., Gosztola, D., Wasielewski, M.R. (1994) Photophysics of the carotenoids associated with the xanthophyll cycle in photosynthesis. *Photosynth. Res.* 41: 389-395.

Frommolt, R., Goss, R., Wilhelm, C. (2001) The de-epoxidase and epoxidase reactions of *Mantioniella squamata* (Prasinophyceae) exhibit different substrate-specific reaction kinetics compared to spinach. *Planta* 213: 446-456.

Genty, B., Briantais, J-M., Baker, N.R. (1989) The relationship between the quantum yield of photosynthetic electron transport and quenching of chlorophyll fluorescence. *Biochim. Biophys. Acta* 990: 87-92.

Gilmore, A.M., Yamamoto, H.Y. (1991) Resolution of lutein and zeaxanthin using a non-endcapped, lightly carbon loaded C_{18} high-performance liquid chromatographic column. *J. Chromatgr. A* 543: 137-145.

Gilmore, A.M. (1997) Mechanistic aspects of xanthophyll cycle-dependent photoprotection in higher plant chloroplasts and leaves. *Physiol. Plant* 99: 197-209.

Gilmore, A.M., Yamamoto, H.Y. (2001) Time-resolution of the antheraxanthin- and ΔpH-dependent chlorophyll a fluorescence components associated with photosystem II energy dissipation in *Mantoniella squamata*. *Photochem. Photobiol.* 74: 391-402.

Goss, R., Bohme, K., Wilhelm, C. (1998) The xanthophyll cycle of *Mantoniella squamata* converts violaxanthin into antheraxanthin but not to zeaxanthin: consequences for the mechanism of enhanced non-photochemical energy dissipation. *Planta* 205: 613-621.

Govorunova, E.G., Jung, K.H., Sineshchekov, O.A., Spudich, J.L. (2004) *Chlamydomonas* sensory Rhodopsins A and B: Cellular content and role in photophobic responses. *Biophys. J.* 86: 2342-2349.

Graßes, T., Pesaresi, P., Schiavon, F., Varotto, C., Salamini, F., Jahns, P., Leister, D. (2002) The role of ΔpH-dependent dissipation of excitation energy in protecting photosystem II against light-induced damage in *Arabidopsis thaliana*. *Plant Physiol. Biochem.* 40: 41-49.

Graven, S.N., Estrada-O, S., Lardy, H.A. (1966) Alkali metal cation release and respiratory inhibition induced by nigericin in rat liver mitochondria. *Proc. Natl. Acad. Sci. USA* 56: 654-658.

De Grooth, B.G., van Gorkom, H.J., Meiburg, R.F. (1980) Electrochromic absorbance changes in spinach chloroplasts induced by an external electrical field. *Biochim. Biophys. Acta* 589: 299-314.

Gross, E.L., Prasher, S.H. (1974) Correlation between monovalent cation-induced decreases in chlorophyll *a* fluorescence and chloroplast structural changes. *Arch. Biochem. Biophys.* 164: 460-468.

Grzesiek, S., Dencher, N.A. (1988) The 'ΔpH'-probe 9-aminoacridine: response time, binding behaviour and dimerization at the membrane. *Biochim. Biophys. Acta* 938: 411-424.

Grzesiek, S., Otto, H., Dencher, N.A. (1989) ΔpH-induced fluorescence quenching of 9-aminoacridine in lipid vesicles is due to excimer formation at the membrane. *Biophys. J.* 55: 1101-1109.

Haraux, F., de Kouchkovsky, Y. (1980) Measurement of chloroplast internal protons with 9-aminoacridine. Probe binding, dark proton gradient, and salt effects. *Biochim. Biophys. Acta* 592: 153-168.

Hendrickson, L., Furbank, R.T., Chow, W.S. (2004) A simple alternative approach to assessing the fate of absorbed light energy using chlorophyll fluorescence. *Photosynth. Res.* 82: 73-81.

Hibberd, J.M., Sheehy, J.E., Langdale, J.A. (2008) Using C_4 photosynthesis to increase the yield of rice – rationale and feasibility *Curr. Opin. Plant Biol.* 11: 228-231.

Holt, N.E., Zigmantas, D., Valkunas, L., Li, X.P., Niyogi, K.K., Fleming, G.R. (2005) Carotenoid cation formation and the regulation of photosynthetic light harvesting. *Science* 307: 433-436.

Holzwarth, A.R., Miloslavina, Y., Nilkens, M., Jahns, P. (2009) Identification of two quenching sites active in the regulation of photosynthetic light-harvesting studied by time-resolved fluorescence. *Chem. Phys. Lett.* 483: 262-267.

Horton, P., Ruban, A.V. (1992) Regulation of photosystem II. *Photosynth. Res.* 34: 375-385.

Horton, P., Ruban, A.V., Young, A.J. (1999) Regulation of the structure and function of the light-harvesting complexes of photosystem II by the xanthophyll cycle. *In Frank, H.A., Young, A.J., Britton, G., Cogdell, R.J. (eds.): The Photochemistry of Carotenoids, Springer, Dordrecht, the Netherlands,* pp. 271-291.

Horton, P., Ruban, A.V., Wentworth, M. (2000) Allosteric regulation of the light-harvesting system of photosystem II. *Phil. Trans. R. Soc. Lond. B* 355: 1361-1370.

Horton, P. (1983) Effects of changes in the capacity for photosynthetic electron transfer and photophosphorylation on the kinetics of fluorescence induction in isolated chloroplasts. *Biochim. Biophys. Acta* 724: 404-410.

Horváth, G., Niemi, H.A., Droppa, M., Faludi-Dániel, A. (1979) Characteristics of the flash-induced 515 nanometer absorbance change of intact isolated chloroplasts. *Plant Physiol.* 63: 778-782.

Hosler, J.P., Yocum, C.F. (1987) Regulation of cyclic photophosphorylation during ferredoxin-mediated electron transport. *Plant Physiol.* 83: 965-969.

Huber, S.C., Edwards, G.E. (1976) Studies on the pathway of cyclic electron flow in mesophyll chloroplasts of a C_4 plant. *Biochim. Biophys. Acta* 449: 420-433.

Ishijima, S., Uchibori, A., Takagi, H., Maki, R., Ohnishi, M. (2003) Light-induced increase in free Mg^{2+} concentration in spinach chloroplasts: Measurement of free Mg^{2+} by using a fluorescent probe and necessity of stromal alkalinization. *Arch. Biochem. Biophys.* 412: 126-132.

Jahns, P., Junge, W. (1990) Dicyclohexylcarbodiimide-binding proteins related to the short circuit of the proton-pumping activity of photosystem II: Identified as light-harvesting chlorophyll-*a*/*b*-binding proteins. *Eur. J. Biochem.* 193: 731-736.

Jahns, P., Depka, B., Trebst, A. (2000) Xanthophyll cycle mutants from *Chlamydomonas reinhardtii* indicate a role for zeaxanthin in the D1 protein turnover. *Plant Physiol. Biochem.* 38: 371-376.

Jahns, P., Graf, M., Munekage, Y., Shikanai, T. (2002) Single point mutation in the Rieske iron-sulfur subunit of cytochrome b_6/f leads to an altered pH dependence of plastoquinol oxidation in *Arabidopsis*. *FEBS Lett.* 519: 99-102.

Jahns, P., Holzwarth, A.R. (2012) The role of the xanthophyll cycle and of lutein in photoprotection of photosystem II. *Biochim. Biophys. Acta* 1817: 182-193.

Johnson, M.P., Pérez-Bueno, M.L., Zia, A., Horton, P., Ruban, A.V. (2009) The zeaxanthin-independent and zeaxanthin-dependent qE components of nonphotochemical quenching involve common conformational changes within the photosystem II antenna in *Arabidopsis*. *Plant Physiol.* 149: 1061-1075.

Johnson, M.P., Ruban, A.V. (2014) Rethinking the existence of a steady-state $\Delta\psi$ component of the proton motive force across plant thylakoid membranes. *Photosynth. Res.* 119: 233-242.

Joliot, P., Joliot, A. (2005) Quantification of cyclic and linear flows in plants *Proc. Natl. Acad. Sci. USA* 102: 4913-18.

Junge, W., Schmid, R. (1971) The mechanism of action of valinomycin on the thylakoid membrane. *J. Membrane Biol.* 4: 179-192.

Kalituho, L., Beran, K.C., Jahns, P. (2007) The transiently generated nonphotochemical quenching of excitation energy in *Arabidopsis* leaves is modulated by zeaxanthin. *Plant Physiol.* 143: 1861-1870.

Kanazawa, A., Kramer, D.M. (2002) *In vivo* modulation of nonphotochemical exciton quenching (NPQ) by regulation of the chloroplast ATP synthase. *Proc. Natl. Acad. Sci. USA* 99: 12789-12794.

Keister, D.L., Minton, N.J. (1970) K+-independent effects of valinomycin in photosynthetic systems. *Bioenergetics* 1: 367-377.

Klughammer, C., Schreiber, U. (2008) Saturation Pulse method for the assessment of energy conversion in PSI. *PAN* 1: 11-14.

Kovacs, L., Damkjaer, J., Kereiche, S., Ilioaia, C., Ruban, A.V., Boekema, E.J., Jansson, S., Horton, P. (2006) Lack of the light-harvesting complex CP24 affects the structure and function of the grana membranes of higher plant chloroplasts. *Plant Cell* 18: 3106-3120.

Koziol, A.G., Borza, T., Ishida, K-I., Keeling, P., Lee, R.W., Durnford, D.G. (2007) Tracing the evolution of the light-harvesting antennae in chlorophyll *a*/*b*- containing organisms. *Plant Phys.* 143: 1802-1816.

Kraayenhof, R. (1970) Quenching of uncoupler fluorescence in relation on the "energized state' in chloroplasts. *FEBS Lett.* 6: 161-165.

Kramer, D.M., Sacksteder, C.A., Cruz, J.A. (1999) How acidic is the lumen? *Photosynth. Res.* 60: 151-163.

Kramer, D.M., Cruz, J.A., Kanazawa, A. (2003) Balancing the central roles of the thylakoid proton gradient. *Trends Plant Sci.* 8: 27-32.

Kramer, D.M., Johnson, G., Kiirats, O., Edwards, G.E. (2004) New fluorescence parameters for the determination of Q_A redox state and excitation energy fluxes. *Photosynth. Res.* 79: 209-218.

Krause, G.H. (1973) The high-energy state of the thylakoid system as indicated by chlorophyll fluorescence and chloroplast shrinkage. *Biochim. Biophys. Acta* 292: 715-728.

Krause, G.H. (1974) Changes in chlorophyll fluorescence in relation to light-dependent cation transfer across thylakoid membranes. *Biochim. Biophys. Acta* 333: 301-313.

Krause, G.H., Vernotte, C., Briantais, J.M. (1982) Photoinduced quenching of chlorophyll fluorescence in intact chloroplasts and algae. Resolution into two components. *Biochim. Biophys. Acta* 679: 116-124.

Krause, G.H., Virgo, A., Winter, K. (1995) High susceptibility to photoinhibition of young leaves of tropical forest trees. *Planta* 197: 583-591.

Krause, G.H., Jahns, P. (2003) Pulse amplitude modulated chlorophyll fluorometry and its application in plant science. *In Green, B.R., Parson, W.W. (eds): Light-Harvesting Antennas in Photosynthesis, Springer, Dordrecht, the Netherlands,* pp. 373-399.

Krause, G.H., Jahns, P. (2004) Non-photochemical energy dissipation determined by chlorophyll fluorescence quenching. Characterization and function. *In Papageorgiou, G.C., Govindjee (eds.): Chlorophyll Fluorescence: A Signature of Photosynthesis, Springer, Dordrecht, the Netherlands,* pp. 463-495.

Kunz, H-H., Gierth, M., Herdean, A., Satoh-Cruz, M., Kramer., D.M., Spetea, C., Schroeder, J.I. (2014) Plastidial transporters KEA1, -2, and -3 are essential for chloroplast osmoregulation, integrity, and pH regulation in Arabidopsis. *Proc. Natl. Acad. Sci. USA* 111: 7480-7485.

Leitsch, J., Schnettger, B., Critchley, C., Krause, G.H. (1994) Two mechanisms of recovery from photoinhibition *in vivo*: Reactivation of photosystem II related and unrelated D1-protein turnover. *Planta* 194: 15-21.

Li, X-P., Björkman, O., Shih, C., Grossman, A.R., Rosenquist, M., Jansson, S., Niyogi, K.K. (2000) A pigment-binding protein essential for regulation of photosynthetic light harvesting. *Nature* 403: 391-395.

Li, X-P., Müller-Moule, P., Gilmore, A.M., Niyogi, K.K. (2002) PsbS-dependent enhancement of feedback de-excitation protects photosystem II from photoinhibition. *Proc. Natl. Acad. Sci. USA* 99: 15222-15227.

Li, Z., Wakao, S., Fischer, B.B., Niyogi, K.K. (2009) Sensing and responding to excess light. *Annu. Rev. Plant Biol.* 60: 239-260.

Marmagne, A., Vinauger-Douard, M.,Monachello, D., de Longevialle, A.F., Charon, C., Allot, M., Rappaport, F., Wollman, F-A., Barbier-Brygoo, H., Ephritikhine, G. (2007) Two members of the *Arabidopsis* CLC (chloride channel) family, AtCLCe and AtCLCf, are associated with thylakoid and Golgi membranes, respectively. *J. Exp. Bot.* 58: 3385-3393.

Mäser, P., Thomine, S., Schroeder, J.I., Ward, J.M., Hirschi, K., Sze, H., Talke, I.N., Amtmann, A., Maathius, F.J.M., Sanders, D., Harper, J.F., Tchieu, J., Gribskov, M., Persans, M.W., Salt, D.E., Kim, S.A., Guerinot, M.L. (2001) Phylogenetic relationships within cation transporter families of *Arabidopsis*. *Plant Phys.* 126: 1646-1667.

Meister, G., Tuschl, T. (2004) Mechanisms of gene silencing by double-stranded RNA. *Nature* 431: 343-349.

Mettler, T., Mühlhaus, T., Hemme, D., Schöttler, M.A., Rupprecht, J., Idoine, A., Veyel, D., Pal, S.K., Yaneva-Roder, L., Winck, F.V., Sommer, F., Vosloh, D., Seiwert, B., Erban, A., Burgos, A., Arvidsson, S., Schönfelder, S., Arnold, A., Günther, M., Krause, U., Lohse, M., Kopka, J., Nikoloski, Z., Mueller-Roeber, B., Willmitzer, L., Bock, R., Schroda, M., Stitt, M. (2014) Systems analysis of the response of photosynthesis, metabolism, and growth to an increase in irradiance in the photosynthetic model organism *Chlamydomonas reinhardtii*. *Plant Cell* 26: 2310-2350.

Metz, J.G, Pakrasi, H.B., Seibert, M., Arntzen, C.J. (1986) Evidence for a dual function of the herbicide-binding D1 protein in photosystem II. *FEBS Lett.* 205: 269-274.

Miller, R., Wu, G., Deshpande, R.R., Vieler, A., Gärtner, K., Li, X., Moellering, E.R., Zäuner, S., Cornish, A.J., Liu, B., Bullard, B., Sears, B.B., Kuo, M-H., Hegg, E.L., Shachar-Hill, Y., Shiu, S-H., Benning, C. (2010) Changes in transcript abundance in

Chlamydomonas reinhardtii following nitrogen deprivation predict diversion of metabolism. *Plant Phys.* 154: 1737-1752.

Mills, J.D., Telfer, A., Barber, J. (1976) Cation control of chlorophyll *a* fluorescence yield in chloroplasts. Location of cation sensitive sites. *Biochim. Biophys. Acta* 440: 495-505.

Mitchell, P. (1961) Coupling of phosphorylation to electron and hydrogen transfer by a chemi-osmotic type of mechanism. *Nature* 191: 144-148.

Mitchell, P. (1966) Chemiosmotic coupling in oxidative and photosynthetic phosphorylation. *Biol. Rev.* 41: 445-502.

Munekage, Y., Takeda, S., Endo, T., Jahns, P., Hashimoto, T., Shikanai, T. (2001) Cytochrome b_6f mutation specifically affects thermal dissipation of absorbed light energy in *Arabidopsis*. *Plant J.* 28: 351-359.

Munekage, Y., Hojo, M., Meurer, J., Endo, T., Tasaka, M., Shikanai, T. (2002) PGR5 is involved in cyclic electron flow around photosystem I and is essential for photoprotection in *Arabidopsis. Cell* 110: 361-371.

Murata, N. (1969) Control of excitation transfer in photosynthesis. II. Magnesium ion-dependent distribution of excitation energy between two pigment systems in spinach chloroplasts. *Biochim. Biophys. Acta* 189: 171-181.

Murata, N., Tashiro, H., Takamiya, A. (1970) Effects of divalent metal ions on chlorophyll *a* fluorescence in isolated spinach chloroplasts. *Biochim. Biophys. Acta* 197: 250-256.

Nilkens, M., Kress, E., Lambrev, P., Miloslavina, Y., Müller, M., Holzwarth, A.R., Jahns, P. (2010) Identification of a slowly inducible zeaxanthin-dependent component of non-photochemical quenching of chlorophyll fluorescence generated under steady-state conditions in *Arabidopsis*. *Biochim. Biophys. Acta, Bioenerg.* 1797: 466-475.

Niyogi, K.K., Björkman, O., Grossman, A.R. (1997) *Chlamydomonas* xanthophyll cycle mutants identified by video imaging of chlorophyll fluorescence quenching. *Plant Cell* 9: 1369-1380.

Niyogi, K.K., Grossman, A.R., Björkman, O. (1998) *Arabidopsis* mutants define a central role for the xanthophyll cycle in the regulation of photosynthetic energy conversion. *Plant Cell* 10: 1121-1134.

Noctor, G., Rees, D., Young, A., Horton, P. (1991) The relationship between zeaxanthin, energy-dependent quenching of chlorophyll fluorescence, and trans-thylakoid pH gradient in isolated chloroplasts. *Biochim. Biophys. Acta* 1057: 320-330.

Oelze, M-L., Kandlbinder, A., Dietz, K-J. (2008) Redox regulation and overreduction control in the photosynthesizing cell: Complexity in redox regulatory networks. *Biochim. Biophys. Acta* 1780: 1261-1272.

Okegawa, Y., Tsuyama, M., Kobayashi, Y., Shikanai, T. (2005) The *pgr1* mutation in the Rieske subunit of the cytochrome b_6f complex does not affect PGR5-dependent cyclic electron transport around photosystem I. *J. Biol. Chem.* 280: 28332-28336.

Owens, T.G. (1994) Excitation energy transfer between chlorophylls and carotenoids. A proposed mechanism for non-photochemical quenching. *In Baker, N.R., Bowyer, J.R. (eds.): Photoinhibition of Photosynthesis. From Molecular Mechanisms to the Field*, pp. 95-109.

Oxborough, K., Lee, P., Horton, P. (1987) Regulation of thylakoid protein phosphorylation by high-energy-state quenching. *FEBS Lett.* 221: 211-214.

Papageorgiou, G., Govindjee. (1968a) Light-induced changes in fluorescence yield of chlorophyll *α in vivo*. I. *Anacystis nidulans*. *Biophys. J.* 8: 1299-1315.

Papageorgiou, G., Govindjee. (1968b) Light-induced changes in fluorescence yield of chlorophyll *α in vivo*. I. *Chlorella pyrenoidosa*. *Biophys. J.* 8: 1316-1328.

Passarini, F., Wientjes, E., Hienerwadel, R., Croce, R. (2009) Molecular basis of light harvesting and photoprotection in CP24: Unique feature of the most recent antenna complex. *J. Biol. Chem.* 284: 29536-29546.

Pearcy, R.W. (1990) Sunflecks and photosynthesis in plant canopies. *Annu. Rev. Plant Physiol. Plant Mol. Biol.* 41, 421–453.

Peters, R.L.A., van Kooten, O., Vredenburg, W.J. (1984) The effect of uncouplers (F)CCCP and NH_4Cl on the kinetics of the flash-induced P515 electrochromic bandshift in spinach chloroplasts. *FEBS Lett.* 177: 11-16.

Peterson, R.B., Havir, E.A. (2004) The multiphasic nature of nonphotochemical quenching: implications for assessment of photosynthetic electron transport based on chlorophyll fluorescence. *Photosynth. Res.* 82: 95-107.

Pogson, B., McDonald, K.A., Truong, M., Britton, G., DellaPenna, D. (1996) *Arabidopsis* carotenoid mutants demonstrate that lutein is not essential for photosynthesis in higher plants. *Plant Cell* 8: 1627-1639.

Reinhard, K., Smith, W.K., Carter, G.A. (2010) Clouds and cloud immersion alter photosynthetic light quality in a temperate mountain cloud forest. *Bot.* 88: 462-470.

Rose, L., Jenkins, A.T.A. (2007) The effect of the ionophore valinomycin on biomimetic solid supported lipid DPPTE/EPC membranes. *Bioelectrochem.* 70: 387-393.

Ruban, A.V., Walters, R.G., Horton, P. (1992) The molecular mechanism of the control of excitation energy dissipation in chloroplast membranes. Inhibition of ΔpH-dependent quenching of chlorophyll fluorescence by dicyclohexylcarbodiimide. *FEBS Lett.* 309: 175-179.

Ruban, A.V., Berera, R., Ilioaia, C., van Stokkum, I.H.M., Kennis, J.T.M., Pascal, A.A., van Amerongen, H., Robert, B., Horton, P., van Grondelle, R. (2007) Identification of a mechanism of photoprotective energy dissipation in higher plants. *Nature* 450: 575-578.

Ruban, A.V., Johnson, M.P., Duffy, C.D.P. (2012) The photoprotective molecular switch in the photosystem II antenna. *Biochim. Biophys. Acta* 1817: 167-181.

Sacksteder, C.A., Kanazawa, A., Jacoby, M.E., Kramer, D.M. (2000) The proton to electron stoichiometry of steady-state photosynthesis in living plants: A proton-pumping Q cycle is continuously engaged. *Proc. Natl. Acad. Sci. USA* 97: 14283-14288.

Sacksteder, C.A., Kramer, D.M. (2000) Dark-interval relaxation kinetics (DIRK) of absorbance changes as a quantitative probe of steady-state electron transfer. *Photosynth. Res.* 66: 145-158.

Sage, R.F. (2004) The evolution of C_4 photosynthesis. *New Phyt.* 161: 341-370.

Schmid, R., Junge, W. (1975) Current-voltage studies on the thylakoid membrane in the presence of ionophores. *Biochim. Biophys. Acta* 394: 76-92.

Schreiber, U., Schliwa, U., Bilger, W. (1986) Continuous recording of photochemical and non-photochemical chlorophyll fluorescence quenching with a new type of modulation fluorometer. *Photosynth. Res.* 10: 51-62.

Schreiber, U. (2004) Pulse-amplitude-modulation (PAM) fluorometry and saturation pulse method: An overview. *In Papageorgiou G, Govindjee (eds.): Chlorophyll a Fluorescence: A Signature of Photosynthesis. Springer, Dordrecht, the Netherlands*, pp. 279-319.

Schreiber, U., Klughammer, C. (2008) Non-photochemical fluorescence quenching and quantum yields in PS I and PS II: Analysis of heat-induced limitations using Maxi-Imaging-PAM and DUAL-PAM-100. *PAN* 1: 15-18.

Schreiber, U., Klughammer, C. (2009) New NADPH/9-AA module for the DUAL-PAM-100: Description, operation and examples of application. *PAN* 2: 1-13.

Schuldiner, S., Rottenberg, H., Avron, M. (1972) Determination of ΔpH in chloroplasts 2. Fluorescent amines as a probe for the determination of ΔpH in chloroplasts. *Eur. J. Biochem.* 25: 64-70.

Schulte, A., Lorenzen, I., Böttcher, M., Plieth, C. (2006) A novel fluorescent pH probe for expression in plants. *Plant Methods* 2: 7.

Searle, G.F.W., Barber, J., Mills, J.D. (1977) 9-amino-acridine as a probe of the electrical double layer associated with the chloroplast thylakoid membranes. *Biochim. Biophys. Acta* 461: 413-425.

Shikanai, T. (2014) Central role of cyclic electron transport around photosystem I in the regulation of photosynthesis. *Curr. Opin. Biotech.* 26: 25-30.

Shimizu, M., Nishimura, M. (1977) Formation of electrical field accompanying temperature jump in isolated spinach chloroplasts. *Biochim. Biophys. Acta* 459: 412-417.

Strasser, R.J., Srivastava, A., Govindjee (1995) Polyphasic chlorophyll *α* fluorescence transient in plants and cyanobacteria. *Photochem. Photobiol.* 61: 32-42.

Streb, P., Feierabend, J., Bligny, R. (1997) Resistance to photoinhibition of photosystem II and catalase and antioxidative protection in high mountain plants. *Plant Cell Environ.* 20: 1030-1040.

Suetsugu, N., Mittmann, F., Wagner, G., Hughes, J., Wada, M. (2005) A chimeric photoreceptor gene, *NEOCHROME*, has arisen twice during plant evolution. *Proc. Natl. Acad. Sci. USA* 102: 13705-13709.

Taiz, L., Zeiger, E. (2002) Chapter 7. Photosynthesis: The Light Reactions. *In Taiz, L., Zeiger, E. (eds.): Plant Physiology, Third Edition. Sinauer Associates, Sunderland, MA, USA.,* pp. 126.

Takizawa, K., Cruz, J.A., Kanazawa, A., Kramer, D.M. (2007) The thylakoid proton motive force *in vivo*. Quantitative, non-invasive probes, energetics, and regulatory consequences of light-induced *pmf*. *Biochim. Biophys. Acta* 1767: 1233-1244.

Takizawa, K., Kanazawa, A., Kramer, D.M. (2008) Depletion of stromal P_i induces high 'energy-dependent' antenna exciton quenching (q_E) by decreasing proton conductivity at CF_O-CF_1 ATP synthase. *Plant Cell Environ.* 31: 235-243.

Thiele, A., Krause, G.H. (1994) Xanthophyll cycle and thermal energy dissipation in photosystem II: Relationship between zeaxanthin formation, energy-dependent fluorescence quenching and photoinhibition *J. Plant Physiol.* 144: 324-332.

Thiele, A., Schirwitz, K., Winter, K., Krause, G.H. (1996) Increased xanthophyll cycle activity and reduced D1 protein inactivation related to photoinhibition in two plant systems acclimated to excess light. *Plant Sci.* 115: 237-250.

Telfer, A., Barber, J. (1974) Twofold effect of valinomycin on isolated spinach chloroplasts: Uncoupling and inhibition of electron transport. *Biochim. Biophys. Acta* 333: 343-352.

Vredenberg, W.J., Tonk, W.J.M. (1975) On the steady-state electrical potential difference across the thylakoid membranes of chloroplasts in illuminated plant cells. *Biochim. Biophys. Acta* 387: 580-587.

Vredenberg, W.J., Bulychev, A.A. (1976) Changes in the electrical potential across the thylakoid membranes of illuminated intact chloroplasts in the presence of membrane-modifying agents. *Plant Sci. Lett.* 7: 101-107.

Wada, M., Kagawa, T., Sato, Y. (2003) Chloroplast movement. *Annu. Rev. Plant Biol.* 54: 455-468.

Walters, R.G., Horton, P. (1991) Resolution of components of non-photochemical chlorophyll fluorescence quenching in barley leaves. *Photosynth. Res.* 27: 121-133.

Walters, R.G., Horton, P. (1993) Theoretical assessment of alternative mechanisms for non-photochemical quenching of PS II fluorescence in barley leaves. *Photosynth. Res.* 36: 119-139.

Walters, R.G., Ruban, A.V., Horton, P. (1996) Identification of proton-active residues in a higher plant light-harvesting complex. *Proc. Natl. Acad. Sci. USA* 93: 14204-14209.

Witt, H.T. (1971) Coupling of quanta, electrons, fields, ions and phosphorylation in the functional membrane of photosynthesis. Results by pulse spectroscopic methods. *Q. Rev. Biophys.* 4: 365-477.

Witt, H.T. (1979) Energy conversion in the functional membrane of photosynthesis. Analysis by light pulse and electric pulse methods: The central role of the electric field. *Biochm. Biophy. Act.* 505: 355-427.

Wraight, C., Crofts, A.R. (1970) Energy-dependent quenching of chlorophyll alpha fluorescence in isolated chloroplasts. *Eur. J. Biochem.* 17: 319-327.

7. Appendix

7.1 Abbreviations

9-AA	9-aminoacridine
AL	Actinic light
ATP	Adenosine triphosphate
CAB	Chlorophyll *a*/*b* binding
Chl	Chlorophyll
CO_2	Carbon dioxide
Col-0	Columbia
DCCD	*N,N´*-dicyclohexylcarbodiimide
DEPS	De-epoxidation state
DIRK	Dark-interval relaxation kinetics
DNA	Deoxyribonucleic acid
$\Delta\psi$	Transthylakoid electric field
ΔpH	Transthylakoid proton gradient
ECS	Electrochromic shift
ECS_{inv}	Amplitude of the inverse portion of the decaying DIRK ECS signal
ECS_t	Amplitude of the rapidly decaying DIRK ECS signal
EDTA	Ethylenediaminetetraacetic acid
EGTA	Ethyleneglycoltetraacetic acid
EL	Excess light
ETR	Electron transport rate at PSII
Fd	Ferredoxin
F	Measurement fluorescence
F_0	Ground fluorescence
F_M	Maximal fluorescence
F_V	Variable fluorescence
H^+	Proton
HEPES	4-(2-hydroxyethyl)-1-piperazineethanesulfonic acid
GFP	Green fluorescence protein
Gra	Gramicidin
g_H^+	Proton conductance through the ATP synthase
K^+	Potassium ion
KCl	Potassium chloride
LHC(I/II)	Light-harvesting antenna complex (I/II)
Mg^{2+}	Magnesium ion
$MgCl_2$	Magnesium chloride
$NADP(^+)(H)$	Nicotinamide diphosphate (oxidized)(reduced)
Nig	Nigericin
NPQ	Non-photochemical quenching
n.s.	Not significant
$^1O_2{}^*$	Superoxide radical
PAM	Pulse-amplitude-modulation
PAR	Photosynthetically active radiation
PC	Plastocyanin
pmf	Proton motive force
PQ	Plastoquinone

PSI/II	Photosystem I/II
Q_A	Primary (electron acceptor) quinone A
qE	Energy-dependent quenching
qI	Photoinhibitory quenching
qP	Photochemical quenching
qT	State-transition quenching
qZ	Zeaxanthin-dependent quenching
RC	Reaction centre
RNA	Ribonucleic acid
ROS	Reactive oxygen species
RP-HPLC	Reversed-phase high-performance liquid chromatography
SD	Standard deviation
Val	Valinomycin
VAZ	Total violaxanthin, antheraxanthin, and zeaxanthin pool
V_X	Violaxanthin
V_XDE	Violaxanthin de-epoxidase
Ws	Wassilewskija
Wt	Wild-type
Z_X	Zeaxanthin
Z_XE	Zeaxanthin epoxidase

7.2 Acknowledgements

I would like to acknowledge the invaluable financial support of the iGRAD-Plant program, particularly during the early years of my doctoral studies at the University of Düsseldorf. I am also very grateful to the Natural Sciences and Engineering Research Council of Canada for the invaluable financial support over the past four years of my studies through the Post-Graduate Scholarship program at the Master's and Doctoral levels.

I would like especially thank my chief supervisor, Prof. Dr. Peter Jahns, for all his kind support, understanding and professionalism on several occasions throughout the course of my work. I am very grateful to my co-supervisor, Prof. Dr. Laura Rose, for her kind support and guidance at annual committee meetings and beyond. It has been an unforgettable experience over the years working and interacting with all members of iGRAD-Plant and AG Jahns, both in and outside of the laboratory in Germany and greater Europe. A very special thanks to all the doctoral students in the group, Tobias, Viviana, and Nadine and the kindest, motherly house technician with the most infectious laugh of all, Maria, for invaluable support in all shapes and forms over the years! From iGRAD-Plant, I would like to especially thank Prof. Dr. Andreas Weber and Dr. Sigrun Wegener-Feldbrügge for their unending kindness, support, advice, and utmost professionalism since my arrival in Düsseldorf.

Most importantly, I would like to thank my parents, my sister, and closer family and friends for their unwavering and boundless, unconditional love, support, and guidance over the years! Без вас не бих био човек у кога сам се уз вашу безусловну љубав, подршку, велико стрпљење и разум развио. Са завршетком овог рада посвећено вама, прекреће се страница новог погљавља нашег заједницког зивота у непрестајном унапређењу у сваком смислу, најбољем здрављу и слози у име и част господа Бога.

7.3 Statement of Declaration

I, Lazar Pavlovic, hereby declare that I have fully and independently written the submitted dissertation without additional unauthorized support and consultation beyond that permitted and specified in the dissertation to include the necessary and appropriate cited literary resources. The dissertation in its present or similar form has not been previously submitted under the same or otherwise specified institution and department name. Previous unsuccessful oral examinations have not been registered or attempted.

Düsseldorf, 29.04.2015.